EXPERIMENTAL AND ANALYTICAL EVALUATION OF MULTI-HAZARD DUCTILE FAÇADE CONNECTORS

By

LAURA E. RENDOS

Submitted in partial fulfillment of the requirements of the degree of

Master of Science

Department of Civil Engineering

CASE WESTERN RESERVE UNIVERSITY

January 2018

Case Western Reserve University

School of Graduate Studies

We hereby approve the thesis of:

Laura E. Rendos

Candidate for the Master of Science degree*

Dr. Michael Pollino

(Chair of the Committee)

Dr. Dario Gasparini

Dr. Yue Li

Date 12/04/2017

*We also certify that written approval has been obtained for any proprietary material contained therein.

Table of Contents

List of Tables

List of Figures

Experimental and Analytical Evaluation of Multi-Hazard Ductile Façade Connectors

Abstract

By

LAURA E. RENDOS

A building envelope (or façade) participates structurally during service and high-hazard loading. The design of the facade and its connections to structural framing requires strength and deformation standards for in-plane and out-of-plane loading. This study examines three multi-hazard ductile façade connectors (MDCs) designed for performance objectives under loading including dead load, thermal/moisture movement, wind, seismic, blast, tornado wind, and projectile impact. The MDC designs resist loading elastically, accommodate thermal/moisture or seismic drift deformations with limited force transfer, and plastically deform during low-probability hazardous loading to protect the facade or enhance the building resistance. Quasi-static experiments, which created forces or deformations to simulate loading, were conducted on the three MDCs. The experiments examined each MDC's behavior during its respective critical hazardous loading and validated finite element models. The experimental and analytical results of this study had similar force-deformation behavior and reasonably matched the design-basis performance objectives.

1. Introduction and Problem Statement

During many hazardous loading events, the building envelope or façade of a structure experiences large forces and potentially plastic deformations associated with the loading. This is true of loading such as earthquakes, high winds, impacts and blasts. The hazardous loading then follows the load path from the façade to the structural frame. The connections between the façade and the structural frame are critical structural elements during such loading events. Facade connections are prime locations along the load path for forcing predictable plastic deformations to occur during hazardous loading events. Controlled plastic deformations along the load path will reduce the energy and loading transmitted to the structural frame during the hazardous loading event. It will also limit the damage done to the façade and structural frame. In many hazardous loading situations, it is impossible to completely avoid damaging the structure. By forcing plastic deformations at multi-hazard ductile façade connections (MDCs), the building damage from the hazardous loading is concentrated in localized, repairable areas. These damaged connections are relatively easy to replace when compared to replacing or repairing the façade or structural frame. This study seeks to understand the force-deformation and energy absorbing behavior of three selected MDC designs during the controlling loading hazardous loading scenario for each design. To investigate the behavior of select MDC designs, experimental methods and finite element analyses were employed.

A quasi-static experimental setup was designed and constructed in the Case Western Reserve University Structural Engineering Laboratory (CSEL). This setup was capable of simulating the appropriate translations, rotations, and gravity loading on two MDC designs by the façade panel during the controlling loading scenario. Additionally,

a 220-kip MTS compression testing machine was utilized to test one of the MDC designs. The experimental results from the three MDC types, as well as a previous experiment, were used to calibrate and refine a finite element model for each MDC design. The experimental test results, finite element analysis results, and theoretical design-basis criteria are compared for each MDC type.

2. Literature Review

2.1. Overview of Façade Connections

The building envelope (or façade) is a critical component that must resist various types of hazardous loading which may be applied as pressures, often on the exterior of the façade, or contact resulting from inter-story building deformations. The façade encloses the interior building spaces from the outside environment and its failure can result in further building performance issues (moisture penetration, thermal, etc). The connection between the building façade to the building frame must transfer forces (façade dead load, wind forces, seismic inertia forces), accommodate differential movement of the structure under serviceability conditions (temperature and moisture expansion and contraction), allow for construction tolerances, and also accommodate the seismic drift in the plane of the panel such that lateral force is not resisted by the façade. Furthermore, for defense critical structures or those near high-energy sources, air-blast and projectile impact loading on the façade might also be considered in the façade design. All of these connection functions must be accomplished in a space only a few inches wide between the LFRS and the structural frame. The design of such connectors requires large elastic load carrying capacity in some directions and nonlinear force-deformation behavior in other directions to achieve acceptable performance under all conditions. The type of façade and utilization of the floor slab overhanging the spandrel beam tend to control the connection design rather than the discussed connection functions (Parker, 2008).

When façade connections are designed, the type of façade is a controlling component of the design. Some of the most common types of facades include brick veneer, precast concrete panels, and aluminum curtain walls. All of these façade types

require different quantities, thicknesses, and tolerances of membranes, backup walls, and other components between the building frame and the façade. Additionally, the façade type can control or limit the connection hinge location (Figure 2-1). If the façade connection can be embedded into the façade, the connection can directly bear on the floor slab. This type of façade connection may be applicable to a precast concrete panel that allows the connection to be cast into the concrete. However, this type of connection may not be feasible for all facades, such as curtain walls. Facades connections may need to be attached to the back of the façade, which creates eccentric forces on the connection. The type of connections required for a type of façade will cause the loading and eccentricity to vary, which affects the size and shape of the connection (Parker, 2008).

Just as the façade type is crucial to the connection design, the floor slabs also play a role in façade connection design. The location the facade relative to the steel frame, the amount of slab overhanging the spandrel beam, the strength of the slab, and the degree that the slab edge is similar throughout the structural frame all affect the façade connection design. The façade connection design normally occurs after these aspects of the structure have been designed, so the slab design must anticipate necessary accommodations required for the façade connection design. The connection can apply the façade load directly to the slab overhanging the spandrel beam, or it can transmit load through a steel assembly to the slab. Transmitting the load directly to the slab is the most economical approach to connection design, but transmitting it though a steel assembly creates a connection more adaptable to the slab design. Although both the type of façade and the slab design affect the façade connection, connection designs are at the discretion of the structural engineer and can vary widely across structures (Parker, 2008).

2.2. Overview of Energy Absorbing Devices

Within current structural engineering design, many types of loads (wind, seismic, ice, etc.) and loading scenarios must be considered during the building design process. However, seismic loading, extreme wind loading, and blast loading are unique loading scenarios that are special design considerations. These loading scenarios require a structure to absorb the kinetic energy associated with the loading. This energy absorption can be accomplished with an energy-absorbing device that plastically deforms to absorb the loading energy (Alghamdi, 2001). A variety of devices that vary in shape, size, and material properties were studied in this review for their energy dissipating properties. Yet, no energy-dissipating device has undergone a multi-hazard assessment to determine its ability to satisfy design objectives for two or more extreme-loading events. This review will examine previous studies of metallic energy dissipating connectors in order to determine which dissipaters are most suitable for acting as a façade connection that experiences a multi-hazard loading assessment.

Within the metallic energy absorbing devices, there are a variety of metals, shapes, and sizes used. Metallic energy absorbing devices are commonly studied for both structural engineering purposes and crashworthiness for vehicles. This review focused on steel, aluminum, and brass energy dissipaters. The review focuses on circular tubes, square tubes, corrugated tubes, stiffened tubes, multicellular tubes, and frusta.

In the mid-1980s, Mamalis, Johnson, and Viegalahn (1984) studied the plastic deformation of thin-walled, steel frusta under axial loading. One experimental study found that the thickness of the steel frusta dictated the mode with which the frusta collapsed under axial compression (Figure 2-2). When the wall frusta wall thickness

increased, the peak and post-buckling load increased. The researchers also found that increasing the semi-apical angle of the frusta increases the peak and post-buckling load (Mamalis, Johnson, & Viegelahn, 1984). A second experimental study in 1986 concluded that the wall thickness/diameter ratio played a key role in the deformation mode of aluminum and steel frusta. The narrow ends of frusta with a large thickness/diameter ratio deformed in circumferential rings, while the larger ends with a smaller thickness/diameter ratio deformed as lobes (Mamalis, Manolakos, Saigal, Viegelahn, & Johnson, 1986).

In 2000, Hanssen, Langseth, and Hopperstad studied the static and dynamic crushing of square and circular aluminum extrusions filled with aluminum foam. The square extrusion experiments focused on the effects of wall thickness and the density of the aluminum foam for energy absorption. The researchers found that foam-filled extrusions deformed less and were capable of withstanding higher loads than the same aluminum extrusions without foam. The force capacity of the foam filled extrusion also increased as the foam density increased (Hanssen, Langseth, & Hopperstad, 2000). Similar results were determined from the circular extrusion experiments. Additionally, both sets of experiments found that the force capacity of the foam filled extrusions were higher than the combined force capacity of the separate extrusion and foam (Figure 2-3 and Figure 2-4). An interaction between the extrusion and foam contributes to the higher load capacity (Hanssen et al., 2000).

Afterwards, in 2002, Kim investigated the properties of multi-cell aluminum extrusions under axial crushing using finite element modeling. The study modeled a variety of square extrusions that contained smaller cell extrusions within the square. It

also investigated a square extrusion with circular cell extrusions inside the corners (Figure 2-5). The multi-cell extrusions were found to have higher energy absorption and weight efficiency than a single cell aluminum square extrusion (Figure 2-6). This increased energy absorption is due to the more complex mode of deformation for the multi-cell extrusions (Kim, 2002).

After the 2002 study by Kim, Saleghaffari, Rais-Rohani, and Najafi studied the axial crushing of externally stiffened tubes in 2011. The geometric properties of the stiffeners located on the outside of the tube determined the crushing stability, energy absorption, and peak crushing force for the tube. The stiffener spacing/tube thickness ratio determined if the crushing was unstable or stable (Figure 2-7). The stiffened tubes were deemed more efficient than circular tubes at energy absorption (Salehghaffari, Rais-Rohani, & Najafi, 2011).

Lavarnway tested the radial energy absorbing capacity of steel tubes under building blast conditions in 2013. The tubes were welded radially between two plates, which simulated the façade and the structural frame of a building. The tubes were expected to act as a typical connection between the façade and frame before dissipating energy from the blast. During experiments in which the tubes were loaded radially, the tubes successfully dissipated high blast forces with large deformations (Figure 2-8). It was determined that the use of a tube shaped section as a façade connection would significantly improve the blast resistance of a structure by absorbing the energy of the blast (Lavarnway, 2013).

During 2014, research projects occurred that tested the energy absorption of a variety of shapes. Zhang performed one such project, which tested the absorption

capacity of multi-cell circular extrusions made of aluminum. Single, double, triple, and quadruple cell circular tubes were investigated. The multi-cell extrusions had a higher energy absorption capacity than the single cell extrusions (Figure 2-9). The double cell tube also had a different deformation mode than the triple or quadruple cell (Zhang & Zhang, 2014).

Additionally, Evyazian, Habibi, Hamouda, and Hedayati tested the crushing and energy absorption of corrugated tubes in 2014. The corrugations in the tube caused the tube to plastically deform at predetermined locations. Some tubes that were tested had the corrugations parallel to the force, while others had corrugations that were perpendicular to the force. The study found that the mean load of the corrugated tubes was less than that of a straight walled tube (Figure 2-10), but that the corrugated tube has a load uniformity during deformation (Eyvazian, K. Habibi, Hamouda, & Hedayati, 2014).

Alavi Nia and Parsapour studied the energy absorption of many different triangular, square, hexagonal, and octagonal thin-walled, aluminum sections during 2014. Each type of specimen has a simple, single cell section tested for that shape. Two multi-cell modifications of each shape were also tested. The multi-cell modifications had a higher mean load than the single cell of each shape (Figure 2-11). The modifications also had a higher energy absorption than their single cell counterparts (Alavi Nia & Parsapour, 2014).

2.3. Overview of A500 Hollow Structural Steel Material Properties

The Seismic Provisions for Structural Steel Buildings (AISC 341-10) include guidance to evaluate the expected material yield and tensile strengths of common

structural grade steels in order to better estimate the true strength of materials (not minimum nominal). The provisions use factors that can be applied to the nominal yield and tensile strengths to estimate the expected yield and tensile strengths of a section (Figure 2-12). The yield strength is multiplied by the R_y factor and the tensile strength is multiplied by the R_t factor (AISC 2010b).

Fadden (2013) studied hollow structural steel (HSS) sections to determine if the sections could improve seismic moment resisting frames. An intensive study into the material properties of A500 Grade B HSS was conducted as part of this research. Fadden tested 114 tensile coupons from locations throughout the cross sections of 11 different rectangular HSS (Figure 2-13). Many of the coupons were from the side-walls of the rectangular HSS, but coupons were also taken from the rounded corners and the welded seam of the sections. Coupons were tested from many areas of the HSS cross section to evaluate the variation of material properties across the cross section. The rolling process and welding used to create HSS shapes leaves residual stresses in the sections, which affects its material properties. Fadden determined that while material properties of the HSS side-walls were not affected by the rolling process, the material properties of the rounded corners and welded seams had significantly different stress-strain characteristics as seen in Figure 2-14. The rounded corners and welded seams were less ductile and had slightly lower R_y and R_t ratios than recommended in the Seismic Provisions for Structural Steel Buildings. The changes in the material properties were localized to the corner and weld locations (Fadden, 2013).

The combination of test data from Fadden (2013) and the AISC Seismic Provisions (2010b) are used in the finite element modeling section to help establish the material models used in the analysis.

2.4. Overview of Multi-hazard Ductile Connector (MDC) Design

The three MDC designs investigated in this study were developed by Slovenec (2016). Appendix 1 contains a full report on the design development and objectives for the various loading scenarios considered. The MDCs were designed and evaluated in this study were based on a prototype, 3-story building located in Los Angeles, CA with reinforced pre-cast concrete façade panels. Wind, seismic, and blast loadings were considered to determine the controlling load scenario for each design. The edge façade panels of a building contact each other during seismic drift, which was critical in the design of the MDCs against seismic hazards. Three blast-loading scenarios of varying blast intensity were also considered for the MDC design. Three different connection types are evaluated as part of this study and referred to as MDC1, MDC2, and MDC3. While each connection attaches to the same prototype panel and participates in many of the loading scenarios considered, they are evaluated for what was deemed as the most critical loading scenario for each MDC type. The fabrication drawings for each MDC type is provided in Appendix 2.

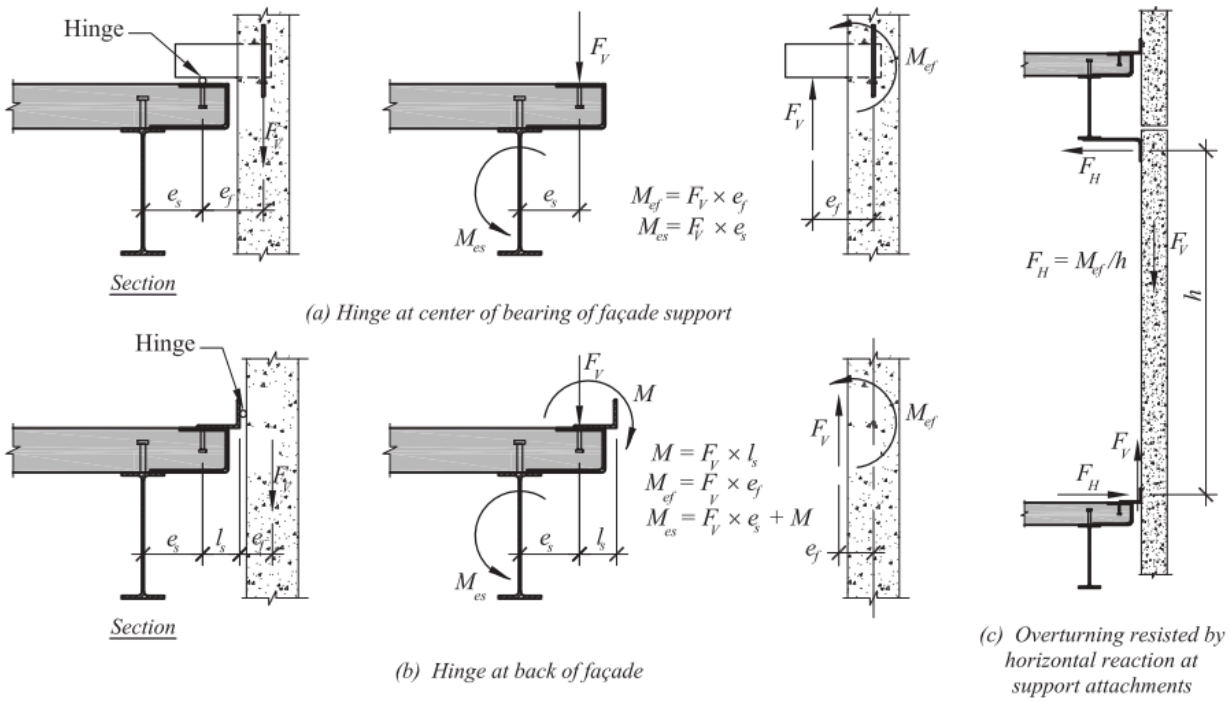

Figure 2- 1 Examples of eccentricity and connection type (Parker, 2008)

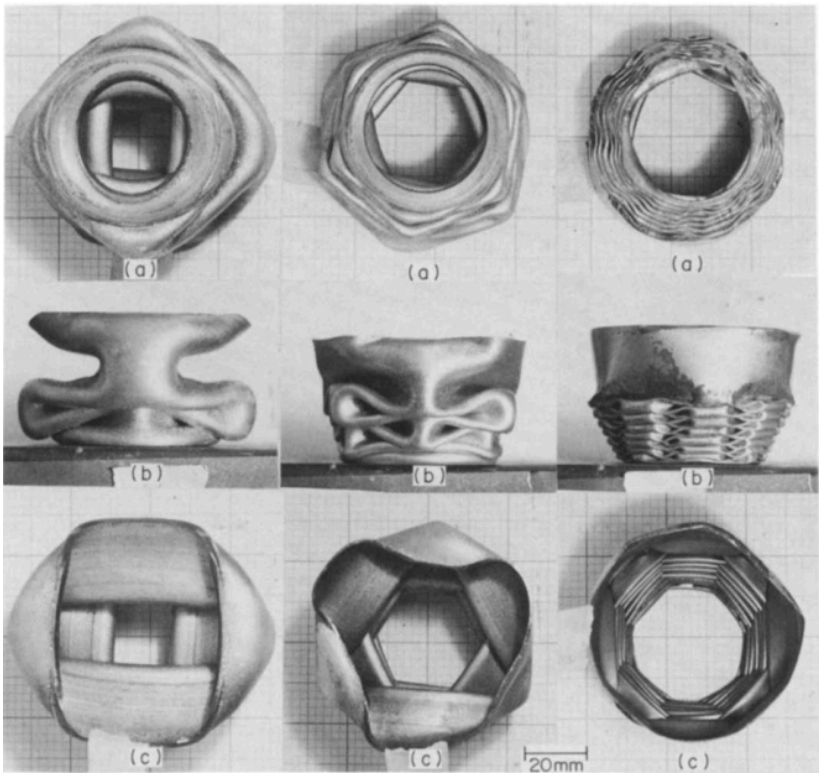

Figure 2- 2 Deformation modes of different thicknesses of frusta (Mamalis, Johnson, & Viegelahn, 1984)

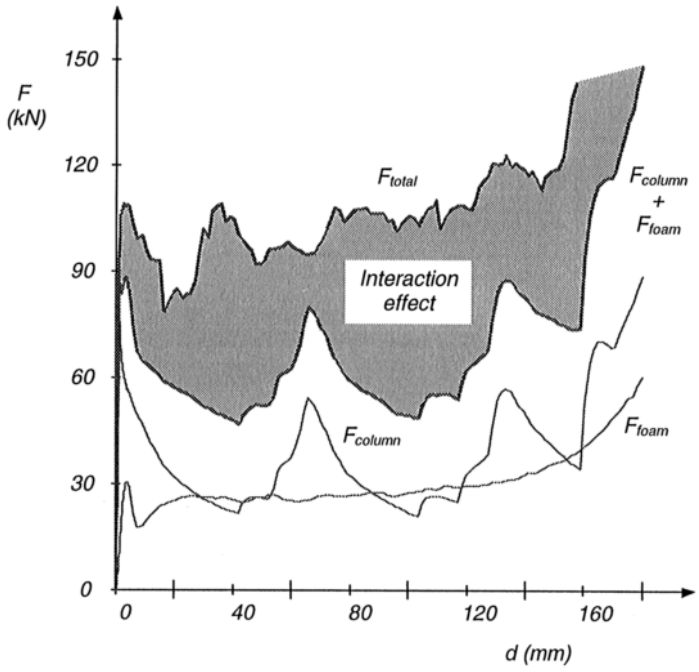

Figure 2- 3 Force-deformation relationship for square aluminum extrusions filled with aluminum foam. (Hanssen et al., 2000)

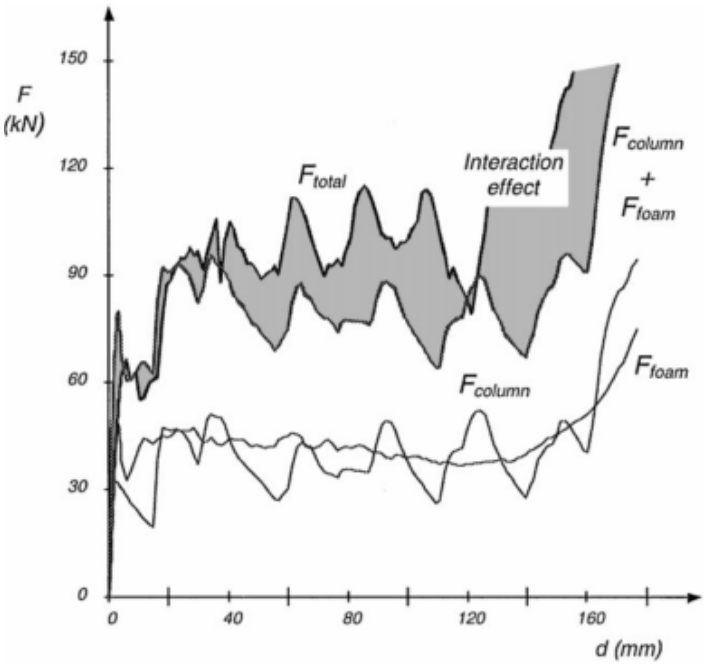

Figure 2- 4 Force-deformation relationship for circular aluminum extrusions filled with aluminum foam (Hanssen et al., 2000)

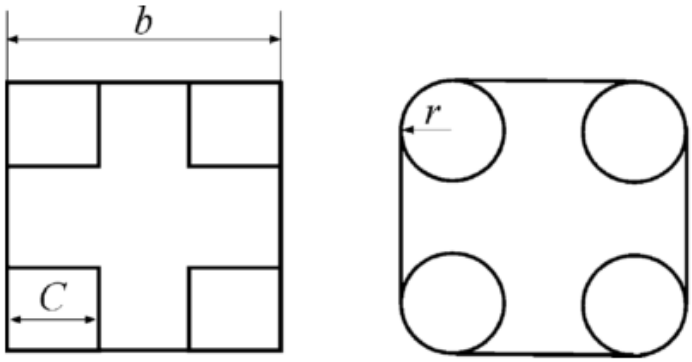

Figure 2- 5 Two of five multi-cell cross sections tested in the study by Kim (Kim, 2002)

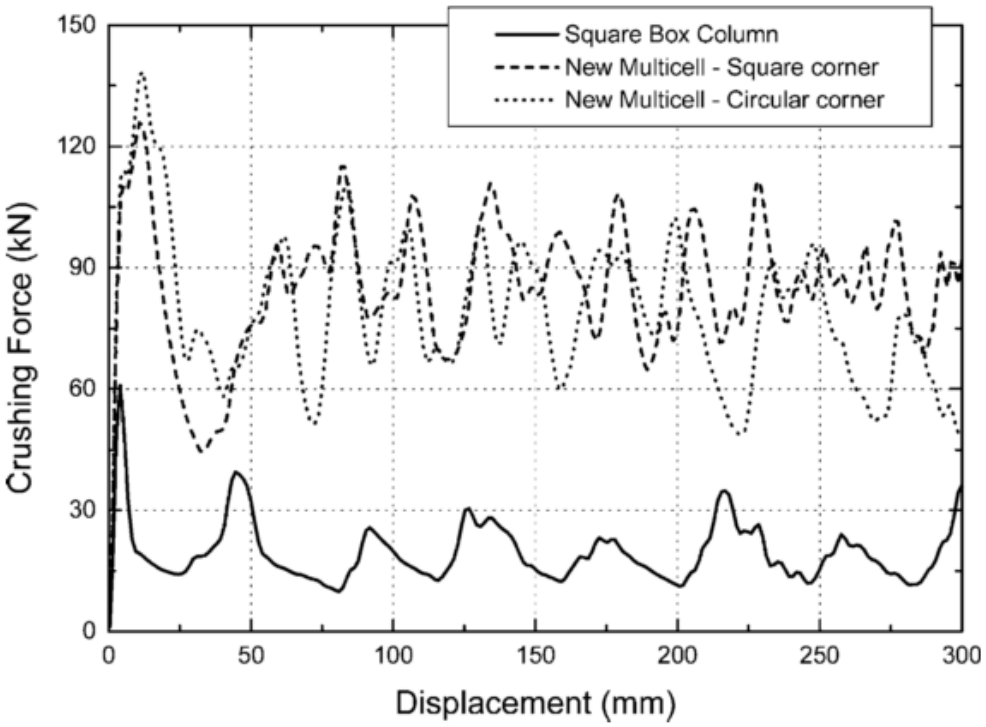

Figure 2- 6 Force-displacement relationship for a square column and two multi-cell columns with the cross sections pictured in Figure 4 (Kim, 2002)

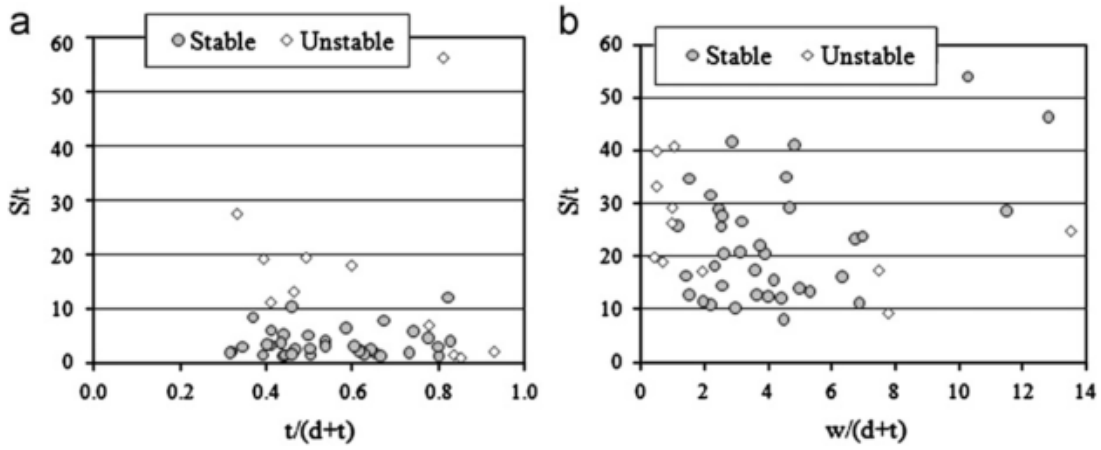

Figure 2- 7 Stable and unstable specimens plotted with geometric data. S is the spacing between stiffeners, t is the tube wall thickness, d is the stiffener thickness, and w is the height of one stiffener (Salehghaffari et al., 2011)

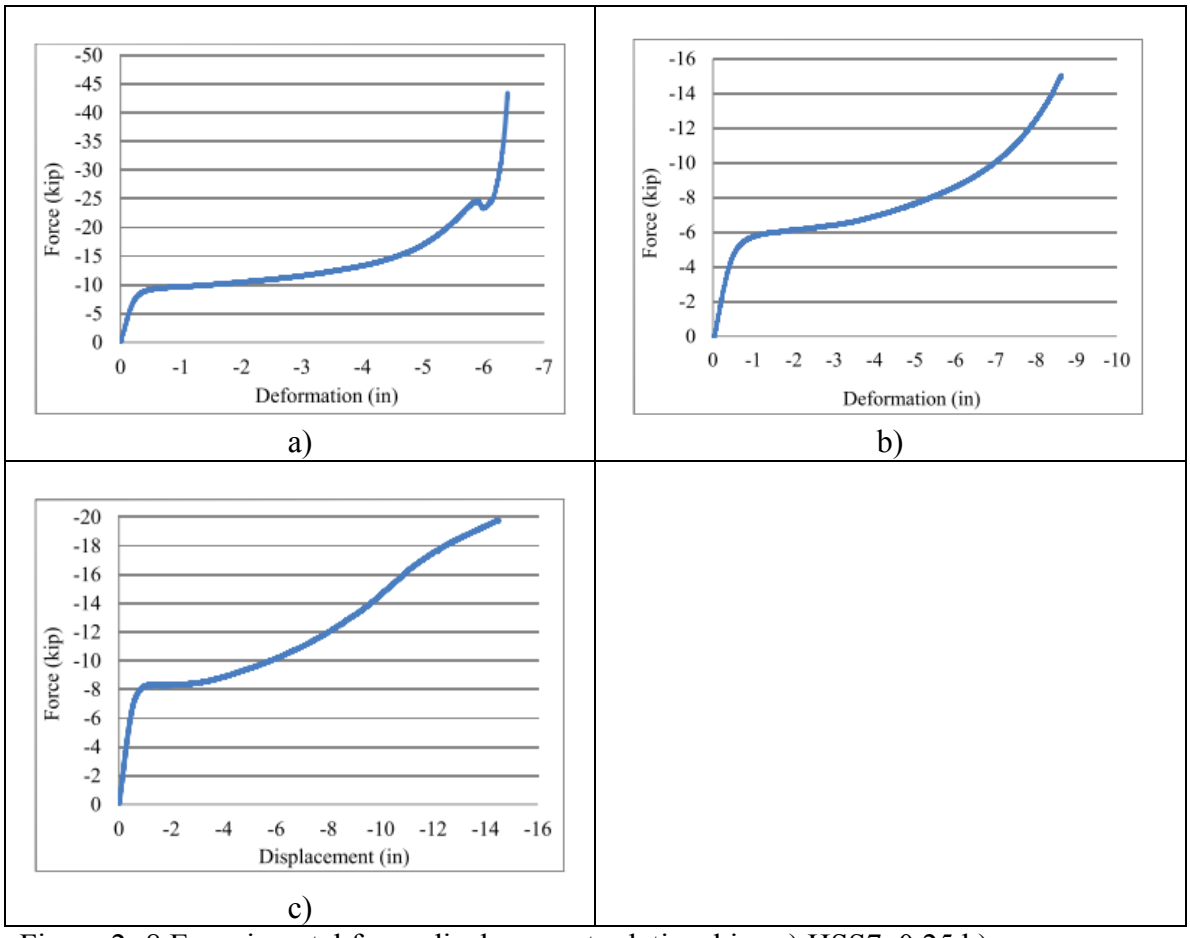

Figure 2- 8 Experimental force-displacement relationships a) HSS7x0.25 b) HSS10.75x0.25 c) HSS16x0.375 (Lavarnway, 2013)

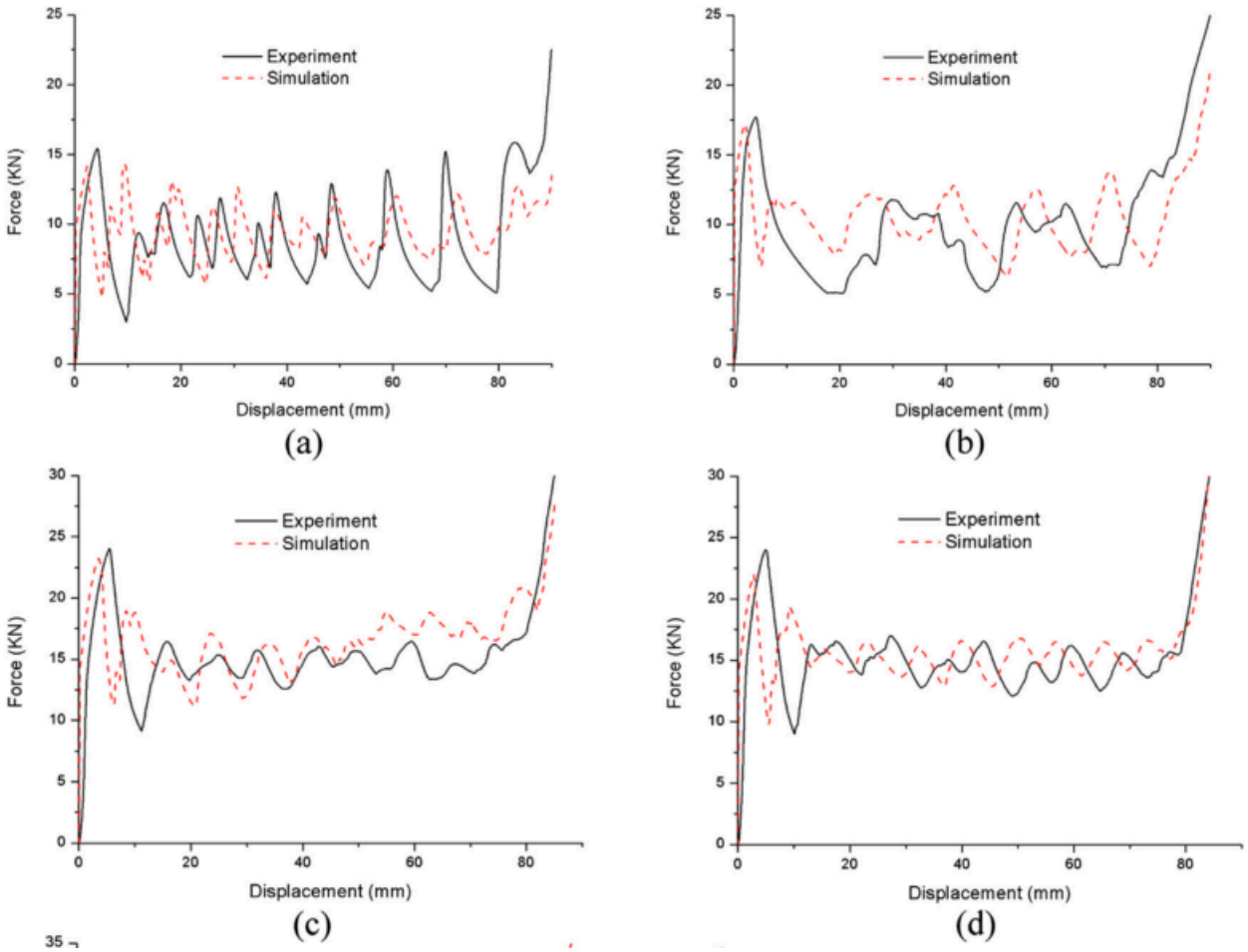

Figure 2- 9 Force-displacement relationships for four of seven specimens a) single cell section b) double cell section c) triple cell section d) triple cell section (Zhang & Zhang, 2014)

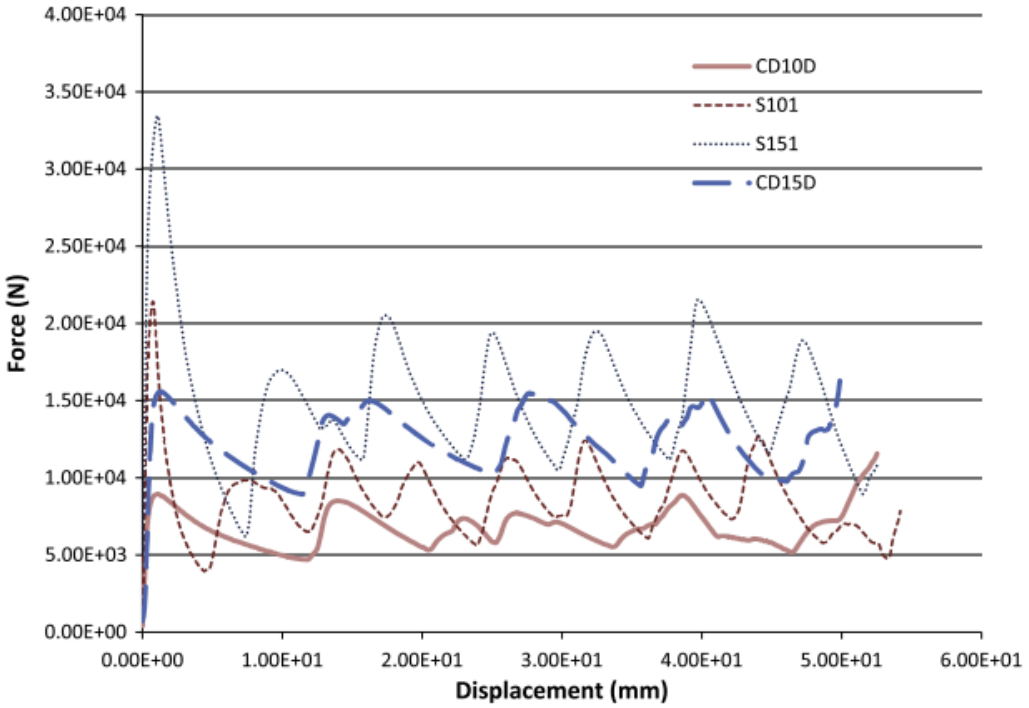

Figure 2- 10 Force-displacement relationship for four of fourteen specimens; the "S" specimens represent straight tube and the "CD" tube represents corrugated specimens; S101 and CD10D have the same diameter, thickness, and length, as do S151 and CD15D (Eyvazian et al., 2014)

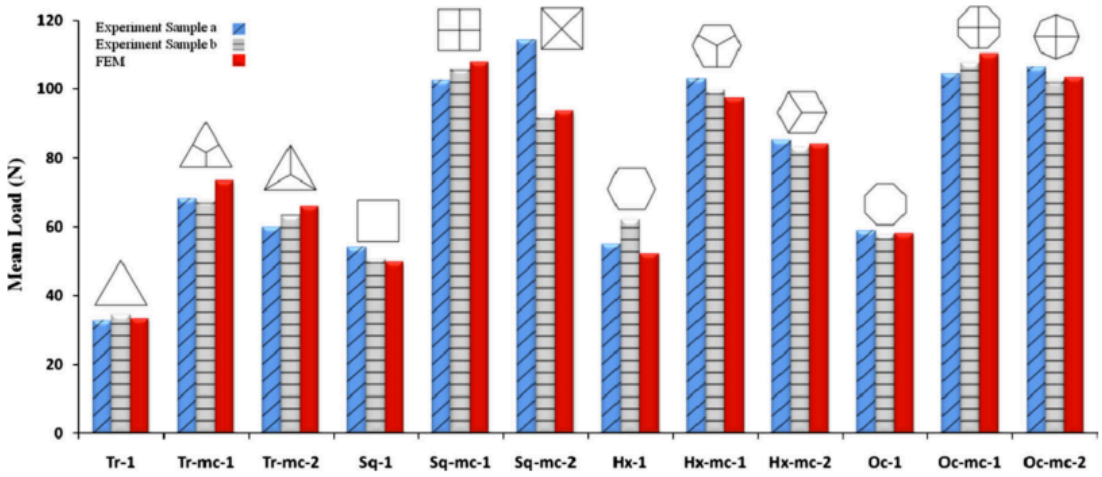

Figure 2- 11 Mean load for the study specimens (Alavi Nia & Parsapour, 2014)

TABLE A3.1
R_y and R_t Values for Steel and Steel Reinforcement Materials

Application	R_y	R_t
Hot-rolled structural shapes and bars:		
• ASTM A36/A36M	1.5	1.2
• ASTM A1043/1043M Gr. 36 (250)	1.3	1.1
• ASTM A572/572M Gr. 50 (345) or 55 (380), ASTM A913/A913M Gr. 50 (345), 60 (415), or 65 (450), ASTM A588/A588M, ASTM A992/A992M	1.1	1.1
• ASTM A1043/A1043M Gr. 50 (345)	1.2	1.1
• ASTM A529 Gr. 50 (345)	1.2	1.2
• ASTM A529 Gr. 55 (380)	1.1	1.2
Hollow structural sections (HSS):		
• ASTM A500/A500M (Gr. B or C), ASTM A501	1.4	1.3
Pipe:		
• ASTM A53/A53M	1.6	1.2
Plates, Strips and Sheets:		
• ASTM A36/A36M	1.3	1.2
• ASTM A1043/1043M Gr. 36 (250)	1.3	1.1
• A1011/A1011M HSLAS Gr. 55 (380)	1.1	1.1
• ASTM A572/A572M Gr. 42 (290)	1.3	1.0
• ASTM A572/A572M Gr. 50 (345), Gr. 55 (380), ASTM A588/A588M	1.1	1.2
• ASTM 1043/1043M Gr. 50 (345)	1.2	1.1
Steel Reinforcement:		
• ASTM A615, ASTM A706	1.25	1.25

Figure 2- 12 Ry and R_t values for standard steel sections and reinforcing (AISC 2010b)

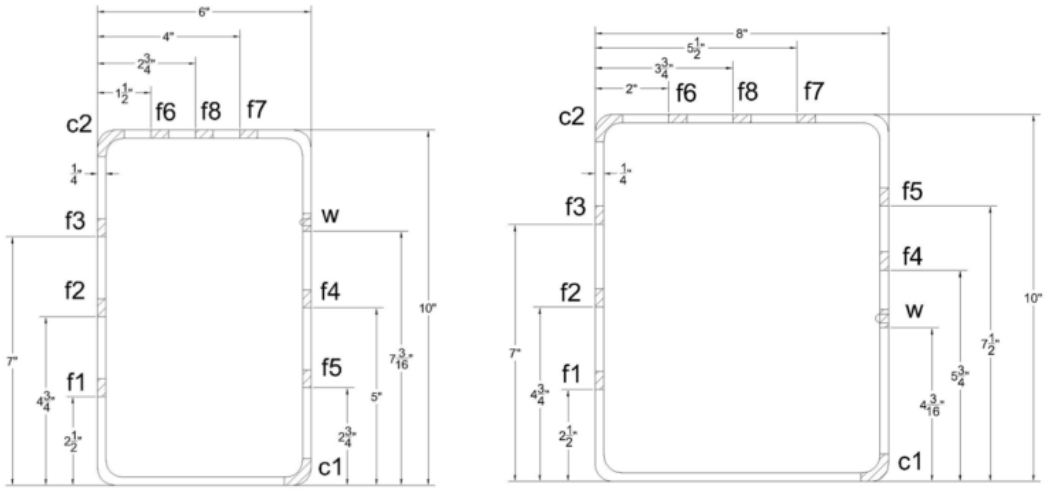

Figure 2- 13 Tensile coupon locations throughout the cross section of HSS10x6x1/4 (right) and HSS10x8x1/4 (left) (Fadden, 2013)

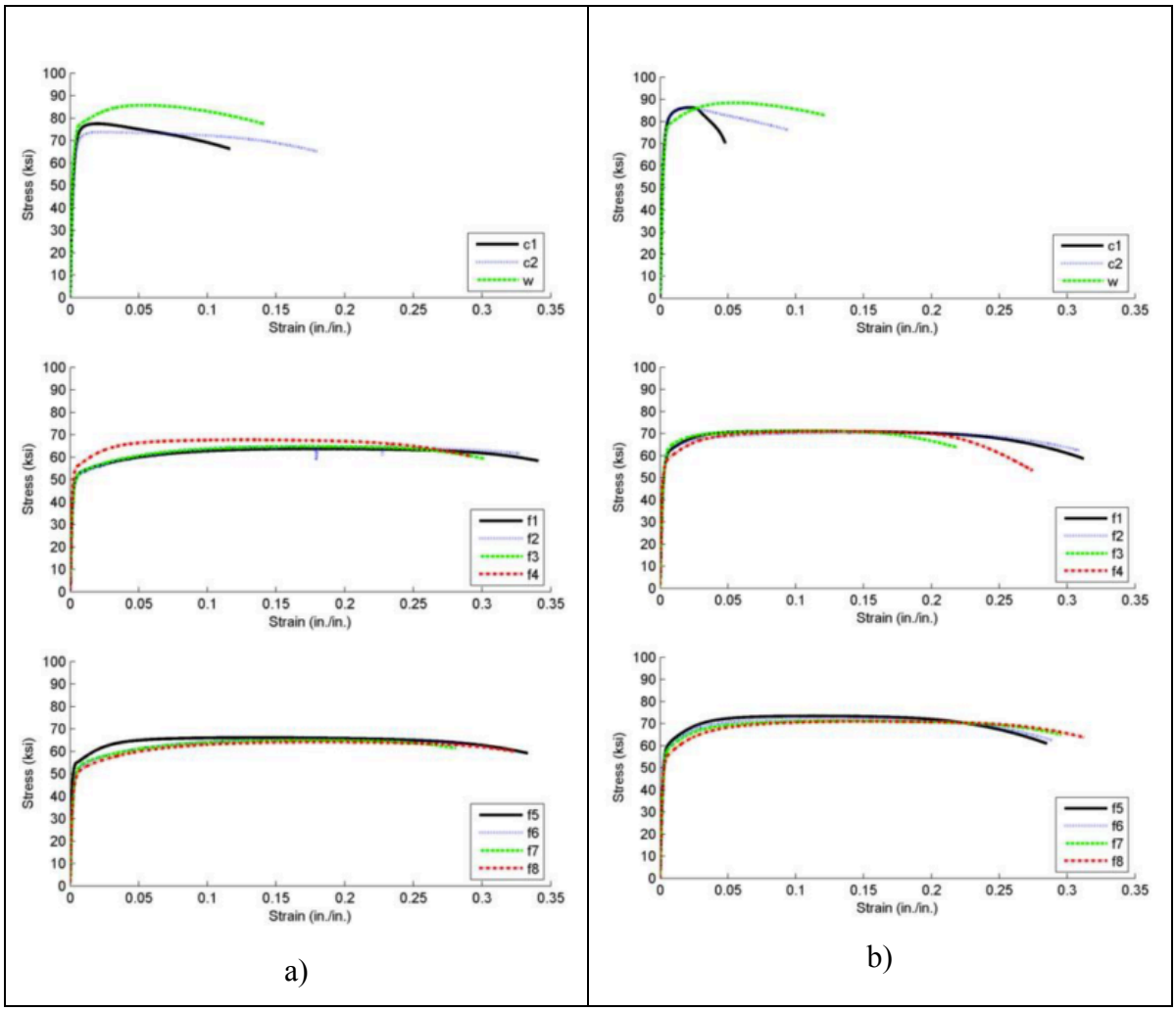

Figure 2- 14 Tensile coupon results a) HSS10x6x1/4 b) HSS10x8x1/4 (Fadden, 2013)

3. Experimental Testing of Multi-Hazard Ductile Connectors

3.1 Introduction

The multi-hazard ductile connector (MDC) designs for the prototype building/panel (Appendix 1) were tested quasi-statically in a setup that was capable of applying the critical façade panel gravity loads, deformations, and rotations to each of the MDC specimens. The testing was intended to physically evaluate the designs and provide critical data for the calibration and validation of the MDC finite element analysis model (Section 4). Three specimens were tested representing MDCs connected at different locations on the prototype building panel as illustrated in Figure 3-1. The MDCs are oriented differently with respect to the panel in order to allow for vertical and horizontal in-plane panel load resistance (Y- and Z-directions) while also having end plate details accommodate panel deformations due to thermal/moisture expansion and seismic drift. Each MDC design is controlled by different hazard loading scenarios as follows (Appendix 1):

1) MDC Type 1 (MDC1): Tested for outward seismic drift compatibility expected for corner façade panels, which includes outward (tensile, $+x_L$) translation and rotation about horizontal ($+\theta_{zL}$).
2) MDC Type 2 (MDC2): Tested with constant façade panel gravity loading ($-z_L$ direction) and quasi-static blast deformation history including inward (compressive, $-x_L$) translation, outward (tensile, $+x_L$) translation, and rotation (about horizontal, $+/-\theta_{yL}$).

3) MDC Type 3 (MDC3): Tested to determine maximum load carrying capacity along MDC longitudinal axis (z_L). Critical MDC to carry lateral seismic inertia and contact forces (for corner façade panel).

3.2 Specimens

The MDC specimens were designed based on the prototype building considered in Appendix 1. The critical dimensions of the HSS and MDC end plates are provided in Table 3-1. The MDCs require a nearly identical gap between the façade and steel frame (MDC3 used slightly thicker end plates). In an actual application, the space between the façade panel and structural frame needs to remain consistent because all MDC types are attached to the same façade panel to protect against multiple hazards. The HSS length was a critical dimension of the design that was altered to appropriately withstand the controlling hazard for each MDC (Table 3-1). Additionally, the end plate bolt hole details are significantly different for each MDC type. Each type needs to accommodate moisture, thermal, or seismic drift deformations in different directions (vertical Y or horizontal Z). Drawings of each MDC design are provided in Appendix 2 and annotated pictures of each MDC specimen are shown in Figure 3-2, Figure 3-3, and Figure 3-4. The annotated pictures note end plate details and local coordinate systems corresponding to Figure 3-1. The steel grade of the HSS was ASTM A500 grade C and the MDC end plates were fabricated from ASTM A36 steel.

Tensile test coupons were taken from the same section of HSS tube used for all MDC types and the end plates for MDC1. The HSS coupon specimens possessed the tube curvature across its width. The MDC1 end plate coupon specimens were machined from the ¾” thick plates into 3/8” thick plates to fit the end grips available within the

Case Western Reserve University's Structural Engineering Laboratory (CSEL) test setup. The coupon dimensions and tension test procedure were based on ASTM standard A370-12 (ASTM 2012). These coupons were used to determine the stress-strain behavior of the steel used to fabricate the MDCs.

3.3 MDC1 and MDC2 Experiments

3.3.1 Testing Setup

The experiments were performed in the CSEL. An illustration of the test setup arranged in the CSEL is shown in Figure 3-5 and the full design calculations are available in Appendix 3. The key components of the facility used for the experiments include the strong floor, L-shaped strong wall, a 55-kip actuator with 6 inch total stroke (+-3"), and (2) uni-directional shake tables (run quasi-statically in these experiments). Each shake table had a 22-kip force capacity and 10 inch total stroke (+-5") and was attached to the strong floor or strong wall W1 in the positions shown in Figure 3-5.

A reaction frame was designed and installed in the laboratory to resist loading from the 55-kip actuator. The reaction frame consisted of a vertical column (Reaction Frame, RF Column) to which the actuator was attached, a foundation beam (attached to the laboratory strong floor), and a diagonal brace between the RF column and foundation beam. The RF column and foundation beam were used in prior experiments in the lab and had adequate capacity for the MDC tests. Minor fabrication was performed on the RF column and foundation beam at connection points. The frame diagonal and lateral bracing were designed as part of this test setup. Due to errors in the diagonal brace fabrication, it did not completely bear on the foundation beam. A mortar pad was made

to allow the base of the diagonal brace to fully bear on the foundation beam. The mortar pad was 1" thick at its highest location.

The specimen was installed between the vertical table (attached to strong wall W1) and a vertical column. The vertical column (Rocker Bearing, RB column) was supported at its base on a rocker bearing attached to the floor table. The top of the RB column was attached to the 55-kip actuator. The movements of the 55-kip actuator and the floor table allowed both translation and rotation of the RB column, which was then imposed on one end plate of the MDC specimen. In the MDC1 test, the 55-kip actuator was directly attached to the RB column using high-strength threaded rods with some "spacing" nuts. However, in the MDC2 experiment, there was a steel spacer section between the RB column and the actuator.

The entire setup was designed to the force limits of the equipment rather than the expected force demands from the specimens. Early MDC designs suggested that (2) 55-kip actuators would be necessary to supply appropriate force to deform and rotate the MDC specimens. All connections and the reaction frame were designed to remain within the elastic range under the application of a maximum lateral force of 132 kips (2*55 kip + 22 kip) and a maximum vertical force of 22 kips to the MDC specimen. Final MDC specimen designs only required (1) 55kip actuator. The setup used in the experiments could apply a maximum lateral force of 77 kips (55kip + 22kip) and a maximum vertical force of 22 kips.

The floor table and actuator were capable of imposing translation and/or rotation to the RB column to apply an inward panel (-X, $-x_L$) translation, outward panel (+X, $+x_L$) translation, and/or rotation on one end plate of the MDC1 and MDC2 specimens. The

differential movement between the floor table and the actuator created the rotation of the MDC specimen. The vertical table attached to the W1 strong wall provided a constant gravity load (panel vertical in-plane, -Y) for the MDC2 test and held a constant position (Y) for the MDC1 test.

Lateral bracing was provided to both the RB column, which translated and rotated significantly during the tests, and to the RF column, which remained essentially stationary during the tests. The RB column had a lateral bracing system consisting of two anchors attached to the strong wall W2 and HSS sections spanning between the two anchors. The RB column was installed between the HSS sections, and a low-friction plastic was placed between the RB column and HSS sections to reduce the friction between the two components during test movements. This lateral bracing system allowed the RB column to move and rotate in the direction of the MDC specimen deformations, but stopped out-of-plane movement. The RF column also had a lateral bracing system that directly attached to the strong wall W2. It consisted of two plates, two threaded rods, and two diwydag bars cantilevered from the strong wall and attached to the RF column. This bracing system ensured that the RF column did not move out of plane during the testing. The lateral bracing systems were designed based on the requirements of the AISC Specifications (AISC 2010b) Appendix 6.

A four channel MTS Flextest 60 controller, with a model number of 494.06, was used during all experiments. This controller utilized the MTS software model 793.10 MultiPurpose TestWare Version 5.6 to run all of the equipment and record all experimental data.

3.3.2 Loading Protocols

The design of each of the MDC types (1-3) considered the various hazardous load scenarios to the prototype building envelope panel. As discussed in Appendix 1, all MDCs participate in each of the loading scenarios. However the design of each MDC tends to be controlled by a specific load scenario. The experimental program was established for what is believed to be the most critical loading conditions for each MDC type. For instance, MDC1 participates in the blast resistance of the panel but is also critical for the seismic drift compatibility scenario for corner panels (Appendix 1). The MDC1 specimen was tested to simulate the seismic drift compatibility requirements for a façade corner panel where contact between panels from two perpendicular sides of the building is expected to occur. The load protocol requires application of a radially outward (tensile) deformation of the HSS tube of 3.1 inches ($+x_L$ direction) while simultaneously applying a rotation (about the horizontal) of 0.025 radians (about z_L axis). These deformations are based on basic deformation compatibility requirements of this connector when the building is at an inter-story drift of 2.5%. However, the test was run to deformations and rotations exceeding these design-basis deformations and to the stroke limits of the testing equipment as discussed in the Section 3.3.1. The deformation protocol for each of the controlled experimental channels and the intended resulting MDC1 deformations and rotations are illustrated in Figure 3-6.

The MDC2 specimen test simulated the tributary façade panel gravity load to the MDC and the deformations and rotations resulting from the critical blast loading scenario (Appendix 1). The wall shake table represented the building frame side and the RB column was the façade panel side of the MDC. This configuration allowed the maximum MDC deformations and rotations to be applied to the specimen. It fully utilized the

stroke of the floor table while maintaining the gravity loading and rotation consistent with the loading and movement of the façade panel during the critical blast load scenario. The vertical shake table applied the tributary gravity load to a single MDC2 which was equal to 15.08 kips in z_L direction of MDC2. The gravity load was held constant on the single MDC2 over the entire test. This loading was applied vertically upward by the wall table, which represented the vertical support reaction provided on the building frame side. The design blast deformation required applying a radially inward (compressive) deformation on the HSS of -4 inches ($-x_L$ direction) followed by a rotation (about the horizontal) of 0.105 radians (about y_L axis). The actual rotation of the specimen was limited to a slightly smaller value of 0.097 rad due to the stroke limits of the 55-kip actuator and floor table. The max translation applied in the experiment was reduced to -3 inches due to contact between the HSS and plate nuts. The translation was reduced to limit the influence of contact between the HSS and plate nuts in the experiment. Contact with the nuts is not considered in the design and was a design oversight. The HSS/nut contact could have been avoided by moving the connection hardware further from the HSS on the end plates. The -3 inch translation and 0.097 radians of rotation was followed by reversing the deformations to a radial translation of -0.945 inches (x_L direction) and rotation of +0.037 radians (about y_L axis) relative to the undeformed MDC shape. The simulated blast deformation history is based on nonlinear dynamic blast analyses in Appendix 1. The loading protocol for each of the controlled experimental channels and the intended resulting MDC2 deformations are illustrated in Figure 3-7.

The MTS controller separately operated each piece of equipment in either a force or deformation-controlled mode. During the MDC2 experiment, the shake table on

strong wall W1 was operated in force control mode to simulate the tributary façade panel gravity loading to MCD2. The wall shake table was run in displacement controlled mode with a zero relative displacement during the MDC1 experiment because MDC1 does not support any of the façade panel gravity load. Both the floor shake table and 55kip actuator operated in deformation control in the MDC1 and MDC2 experiments. The deformation control mode of these pieces of equipment simulated the translation and rotation imposed on the MDCs by the façade panel under the relevant loading scenario.

3.3.3 Instrumentation

The instrumentation layout for the MDC1 and MDC 2 experiments is shown in Figure 3-8. The following instruments were used to collect the raw experimental results:

- Strain gauges (SG1, SG2, SG3, SG4): Four Micro-Measurement EA-06-250BG-120/L strain gauges were attached to the RB column below the MDC. Two strain gauges were attached to each flange of the RB column, which is a W12x58 section. The readings from these gauges were used to determine the internal shear force and bending moment in the RB column. These RB column forces were then used to calculate lateral force and moment acting on the MDC.
- String potentiometers (SPot1, SPot2, SPot3, SPot4): Four Unimeasure HX-PB-10 string potentiometers were used to record the movement of the MDC during the test. Each string potentiometer had a 10 inch (+/-5") total range. SPot1 and SPot2 were set up to record the radial (x_L) movement of the MDC to obtain the MDC translation and rotation. The

other two sting potentiometers were placed to record vertical MDC movement and differential movement between the MDC plates.

- Actuator Load Cells (F_{Act}, F_{HT}, F_{VT}) of the 55-kip Actuator, Horizontal (Floor) and Vertical (Wall) Shake Tables: All of the actuator and table load cell data was recorded during the experiments. The 55-kip actuator uses an MTS 661.22C-01 load cell. The 22-kip actuators in the horizontal and vertical tables utilize MTS 661.20E-03 load cells. The actuator and the vertical wall table load cell data were used to calculate MDC loads. Although the horizontal floor table load cell data was recorded, it was not used in the MDC calculations.
- Actuator LVDTs (δ_{Act}, δ_{HT}, δ_{VT}): The movement of the 55-kip actuator and tables were recorded using the standard LVDTs for the MTS 244.22 and 244.31 actuators. This data was not used in the MDC deformation calculations because these LVDT measurements included elastic deformations of the test setup components and any slippage within connections of the experimental setup.
- Camera (δ_{HSS_1}, δ_{PP_1}, δ_{FP_1}): Both MDC1 and MDC2 experiments were recorded with a Panasonic HC-V700 video camera. Still shots of the video were used to estimate the relative deformations of the MDC1 HSS, panel plate, and frame plate at critical states during the tests.

Measuring the strains, displacements, and forces allowed for calculation of the following desired quantities: lateral force applied to MDC (F_{MDC_Lat}), vertical force applied to MDC (F_{MDC_Vert}), moment applied to MDC (M_{MDC}), total centerline

displacement of MDC (δ_{MDC}), rotation of MDC (θ_{MDC}), and the local deformations across MDC1 (δ_{HSS_1}, δ_{PP_1}, δ_{FP_1}). All of these desired quantities are calculated from the measured instrument quantities except the local deformations across MDC1, which were estimated using video recordings of the test for each component of the MDC (end plates and HSS). The relevant dimensions between the strain gauges, string potentiometers, MDC, and equipment relevant to the MDC calculations are shown in Figure 3-5 and Figure 3-8. The lateral force applied to the MDC (F_{MDC_Lat}) is equal to the sum of the 55 kip actuator load cell measurement (F_{Act}) and shear force in the RB column (obtained from the strain gauges):

$$F_{MDC\_Lat} = F_{Act} + \frac{\frac{E_{steel} \cdot I_{x,RBC}}{d_{RBC}} \cdot (\varepsilon_{SG1} - \varepsilon_{SG2})}{H_{SG1}} \quad \text{Eq. 3-1}$$

The vertical force on the MDC (F_{MDC_Vert}) was determined from the vertical wall table load cell:

$$F_{MDC\_Vert} = F_{VT} \quad \text{Eq. 3-2}$$

The moment applied to the MDC (M_{MDC}) is determined from the 55 kip actuator load cell and moment in the RB column (obtained from the strain gauges) and can be determined using the equation:

$$M_{MDC} = \frac{E_{steel} \cdot I_{x,RBC}}{d_{RBC}} \cdot (\varepsilon_{SG1} - \varepsilon_{SG2}) - F_{Act} \cdot (H_{Act} - H_{MDC}) - F_{MDC\_Vert} \cdot e_{RBC} \quad \text{Eq. 3-3}$$

The deformation applied to the MDC (δ_{MDC}) is determined from the string pots lateral movement measurement and calculated from the following:

$$\delta_{MDC} = \delta_{SPot2} + \frac{D_{MDC}}{D_{SPot}} \cdot (\delta_{SPot1} - \delta_{SPot2}) \quad \text{Eq. 3-4}$$

The rotation applied to the MDC (θ_{MDC}) is also determined from the string pots lateral movement measurement and can be calculated using the following equation:

$$\theta_{MDC} = \tan^{-1}\left(\frac{(\delta_{SPot1} - \delta_{SPot2})}{D_{SPot}}\right) \quad \text{Eq. 3-5}$$

3.4 MDC3 Experiment

3.4.1 Test Setup

While MDC1 and MDC2 required a specially designed and constructed experimental setup to simulate the critical hazardous loading scenarios, MDC3 utilized a self-reacting MTS 220-kip compression machine in the CSEL. The MTS 220-kip compression machine has a total stroke of 5.8 inches (+/-2.9”). A critical design loading scenario for MDC3 occurs during seismic loading and requires this MDC to carry the entire lateral seismic inertia force and the lateral force imposed during contact of the building corner panels (Appendix 1). This MDC is intended to remain elastic under this loading scenario. The test’s primary objective was to evaluate the maximum load carrying capacity of this MDC design. Therefore, this MDC is subjected to a large lateral shear force in the longitudinal HSS direction (z_L direction). Because the MDC3 end plates experienced fixed end conditions imposed by the building façade panel and connection to the perimeter frame, the MDC experiences equal and opposite end moments in addition to the applied shear. In the experiment, MDC3 was attached to loading arms and placed inside the compression machine load frame (Figure 3-9). The loading arms allowed a compression force to be applied by the machine concentrically

through the HSS centerline, which resulted in a shear force and equal and opposite moments on the two plates of the MDC. A cylindrical steel member was placed between the bottom load arm and the bottom of the loading frame to act as a roller bearing. At the top loading arm, the spring head of the actuator also acted as a bearing. These bearings ensured that only a concentric compressive force was applied to the loading arms during the experiment.

3.4.2 Loading Protocol

The controller applied a slowly ramped deformation history to the MDC3 specimen until it ran out of actuator stroke or the operator stopped the test. Translation was applied to the MDC at a rate of 0.00235 in/sec.

3.4.3 Instrumentation

The MTS 220kip compression machine was run using the same MTS 494.06 Flextest controller and 793.10 MultiPurpose TestWare Version 5.6 software as in the previously described MDC1 and MCD2 experimental setup.

The instrumentation used in this test is shown in Figure 3-9. The following instruments were used to collect the raw experimental results:

- String potentiometers (SPot1_3 and SPot2_3): Two Unimeasure HX-PB-10 string potentiometers were used to record the movement of the MDC during the test. Each string potentiometer had a 10 in (+/-5") total range. One string pot was attached to each of the two MDC plates to record the vertical movement of each plate separately.
- Actuator LVDT (δ_{Act_3}): The deformation of the 220-kip actuator was recorded using the standard LVDT for the MTS 244.51 actuator.

Although this data was recorded, it was not used to calculate relevant MDC3 data.

- Actuator Load Cell (F_{Act_3}): The 220-kip actuator in the compression frame uses a 661.31A-02 load cell to record the force it applies. The load cell force is equal to the applied longitudinal shear force on MDC3.
- Camera: The MDC3 experiment was recorded with a Panasonic HC-V700 video camera.
- Vic-3D V7 Digital Image Correlation (DIC) System (ε_{HSS} contours): Two cameras and software for the Vic-3D V7 system from Correlated Solutions were used to map the MDC HSS strain contours over the test. A white background with a black speckle pattern was painted onto one side of the MDC HSS. The dots in the speckle pattern were tracked by the DIC system throughout the test. The software analyzed the speckle pattern movement, which created strain contours on the HSS over the experiment length.

Measuring the displacements and forces allowed for calculation of the following desired quantities: shear force applied to MDC (F_{MDC_Shear}) and total differential displacement of MDC plates (δ_{MDC}). The vertical force that was applied to the MDC was determined using the actuator load cell:

$$F_{MDC\_Shear} = F_{Act\_3} \quad \text{Eq. 3-6}$$

The differential movement between the MDC plates was calculated using the data from the string potentiometers. The actuator LVDT was not used because it recorded

both the deformations in the MDC specimen and the deformations in the entire setup (loading arms, rocker bearings, bolted connections, etc.). The differential shearing movement between the MDC3 end plates is:

$$\delta_{MDC\_3} = \delta_{SPot1\_3} - \delta_{SPot2\_3} \quad \text{Eq. 3-7}$$

3.5 Experimental Test Results

3.5.1 Material Coupon Tension Test Results

A total of four tensile coupons were tested to examine the material properties of the MDC components. Two coupons were tested for both the MDC1 end plate material (specified as ASTM A36) and the HSS material (specified as ASTM A500 Gr. C). The results from these tests were intended to develop material stress-strain curves for the FEA models of the MDCs (Section 4).

The resulting stress-strain curves for the MDC1 end plate coupons are provided in Figure 3-10. The yield stress of the MDC1 plate coupons was approximately 50 ksi. The measured plate yield stress met the criteria of A36 steel (36 ksi minimum). MDC1 was designed assuming that the plates would have a yield stress of $1.3*F_y$ (46.8 ksi), which is the expected yield stress (R_yF_y) for A36 steel based on the AISC Seismic Provisions (AISC 2010a). During the hardening phase, the MDC1 plate strain hardened from 50 ksi to approximately 70 ksi. The expected tensile stress (R_tF_u) from AISC (2010a) is equal to 1.2*58 ksi (69.6 ksi) and is consistent with the observed measurements. Overall, the MDC1 plate material behaved as expected. The coupon stress-strain data for the MDC1 end plates was used in the finite element models in the following section (Section 4).

The HSS expected yield stress (R_yF_y) and expected tensile stress (R_tF_u) were also determined using the AISC Seismic Provisions (AISC 2010a). The yield strength of the two HSS tensile coupons varied greatly. Coupon 1 had a yield stress of 52 ksi and coupon 2 had a yield stress of 36 ksi, which are significantly lower than the expected yield stress (R_yF_y) of 64 ksi (Figure 3-11). Additionally, the coupons also had a tensile stress (R_tF_u) that was lower than the expected value of 80.6ksi. These discrepancies may be due to the machining of the coupon and subsequent modifications required to adjust the coupon.

The HSS coupons were cut out of the HSS tube section that was used in the MDC fabrication such that the long side of the coupon was cut from the longitudinal dimension of the tube. The coupons possessed the HSS curvature across its width. Extracting these coupons from the tube is a more difficult and involved process than machining a coupon from plate. As a result, the dimensions of HSS coupons were more variable than those of the plate coupons. In order to allow the grips of the testing machine to sufficiently grip an appropriate area of the coupon ends, the curvature of the coupon ends needed to be reduced. The coupon ends were placed between two pieces of wood and flattened with an actuator applying a force of approximately 30 kips to the coupon ends. However, even after this flattening process, the coupon ends were too curved and slipped in the machine grips. The coupon ends were then ground down to a flatter surface using a surface grinder. This created a flattened surface on the coupon ends that could be appropriately gripped by the machine for tensile testing. Although the grip ends of the coupon were flattened before the tensile tests, the reduced section of both the coupons maintained the HSS tube curvature. During the tensile tests, the curvature of the reduced

sections also flattened. This flattening visibly occurred very early in the coupon 2 test, but was not observed in the coupon 1 test until near the end of the test. Ultimately, the HSS coupon test results were deemed unreliable and are not used as the basis for the material model of the finite element analysis of Section 4.

3.5.2 MDC1 Specimen Test Results

During this experiment, MDC1 was deformed to +4.53 inches in the tensile direction ($+x_L$) while simultaneously rotated (about z_L axis) +0.0357 radians. This deformation and rotation was beyond the design-basis deformations of +3.1 inches and +0.025 rad. These deformations were limited by the equipment stroke limits. Figure 3-12 a shows the deformation and rotation of the MDC throughout the experiment. MDC1 was designed to allow yielding of both the HSS and its end plates in order to accommodate the seismic drift compatibility requirements. Forcing all of the deformation onto the HSS alone would have resulted in an increase in force due to the large deformation stiffening of the HSS. The MDC component contributions to the total deformation are shown in Figure 3-12 b. The MDC plates began deforming approximately at +0.2 inches and a rotation of +.0025 radians. At +3.1 inches of translation and +0.025 radians of rotation, the HSS deformed approximately +1.8 inches, the panel plate deformed about +0.6 inches, and the frame plate also deformed about +0.7 inches. At the maximum MDC displacement of +4.53 inches, the HSS deformed +2.2 inches, the panel plate approximately deformed +1.3 inches, and the frame plate deformed +1.0 inch. The MDC experienced a maximum force of 59 kips of tension and a maximum moment of 58 kip-ft, which both occurred at a +4.23 inches of deformation (Figure 3-12 c-d).

3.5.3 MDC2 Specimen Test Results

Initially, a gravity load of 15.08 kips was applied to MDC2, which was held constant throughout the experiment (Figure 3-13 b). Then, a deformation of -2.75 inches (compression) was applied to the MDC. That deformation was maintained while a rotation of -.087 radians was applied. Then, a compressive deformation of -0.96 inches and a rotation of +0.031 radians (both relative to the original MDC position) were applied to the MDC. All of the deformations and rotations throughout the experiment are available in Figure 3-13 a. As with MDC1, the prescribed movement of the tables and actuators were intended to create the desired MDC deformation and rotations described above. However, the experimental setup components between the actuators and the MDC also deformed, reduced the deformation and rotation applied at the MDC location. MDC 2 experienced a maximum force of 23.3 kips of compression and a maximum moment of 43 kip-ft. Both of these maximum values occurred when the MDC was deformed to -2.75 inches and rotated to -.087 radians. The nuts that attached at the MDC2 end plates to attach to the test equipment contacted the HSS at about -0.75 inches of compression ($-x_L$) and any further compression. The resulting HSS deformation at a nut location is pictured in Figure 3-13 f. MDC2 absorbed approximately 43 kip-inches of energy throughout the entire experiment. The design energy absorption was 42.4 kip-in. This energy absorption was determined using the trapezoidal rule for the area under the force-deformation curve in Figure 3-13 c from the undeformed position at 0 inches to the maximum displacement of -2.78 inches:

$$energy = area = \Delta x \cdot (\frac{y_0}{2} + y_1 + y_2 + \ldots + \frac{y_n}{2}) \qquad \text{Eq. 3-8}$$

After the initial experiment, MDC2 was deformed in three further experiments. Experiment 2 applied nearly the same deformations and rotations as experiment 1. Experiment 3 and 4 applied -4.0 inches of compression ($-x_L$) to MDC2 and did not apply any rotation (Figure 3-14 a). All four of the experiments applied the 15.08 kip tributary gravity load to MDC2 (z_L direction) (Figure 3-14 b). Over the course of the experiments, the maximum force on MCD2 increased (Figure 3-14 c). Ultimately, at the end of Experiment 4, MDC2 failed. The HSS fractured outside the plate weld locations on both the frame and panel plate. The HSS entirely separated from the frame plate and partially separated from the panel plate (Figure 3-14 d).

3.5.4 MDC3 Specimen Test Results

The resulting force-deformation plot for the MDC3 specimen is shown in Figure 3-15 b. The data recorded by the instrumentation had a noticeable variance throughout the experiment. The data was modified by finding a linear approximation from 0 inches to 0.075 inches and 0.75 inches to 0.22 inches of MDC translation. This linear modification created a smoother force-deformation curve. The specimen behaved linear-elastically to a loading of approximately 140 kips, which was the design elastic strength. At its limit, MDC3 experienced approximately 0.27 inches of differential movement between the MDC plates and a maximum force of 172 kips. After about 0.27 inches of deformation, the loading arms began to rotate out-of-plane and the force applied to the MDC began to decrease. Tearing of the HSS just outside the weld bar (connected into the end plate) was observed as seen in Figure 3-15 d and is believed to have triggered an asymmetric failure mode resulting in torsion and twisting of the specimen. The test was stopped due to the out-of-plane rotation of the loading arms. In Figure 3-15 c, a clear

yield line is visible on the HSS in the picture at the ultimate displacement. This yield line began developing about half way through the experiment and continued to propagate until the full yield line appeared.

The Vic-3D DIC software and cameras recorded the HSS speckle pattern movement throughout the experiment. The first principal strain contours at points throughout the experiment, including the design loading of 135 kips, are available in Figure 3-16. The cameras and software did not recognize small areas within the speckle pattern, so there are small areas on the HSS that do not have principal strain data available. The DIC recorded principal strain contours that were roughly symmetric about the center (z-direction) of the HSS.

3.6 Summary

All of the MDC designs and tensile coupons were experimentally tested in the CSEL. Four tensile coupons were tested for the MDC materials, including two plate coupons and two HSS coupons. The plate coupons produced results close to the expected stress-strain curves for A36 steel. However, the HSS coupon results were drastically different form the expected stress-strain curves for A500 grade C steel. This discrepancy may be due to the machining and flattening of the coupon. The plate coupon data was used in the following finite element models, but the HSS coupon data was not utilized for the models.

The MDC1 and MDC2 designs were tested in a custom experimental setup designed to apply gravity loads, lateral translations, and rotations. MDC3 was tested in an MTS 220-kip compression frame that applied a shear deformation to the MDC. Each MDC was tested using a loading protocol based on its controlling hazardous loading

condition. All raw strains, deformations, and forces were recorded from the equipment and through additional instrumentation as applicable for each experiment. This raw data was used to create force-deformation curves for each MDC, which confirmed each MDC design and will be used to validate the finite element models described in Section 4. A comparison of the design objectives and the recorded experimental values are available in Table 3-2. The MDC1 experimental results showed that the maximum tensile force was within about 11% of the design maximum tensile force. In the experiment, the MDC1 HSS translated more than expected from the design while the MDC1 plates translated less than expected. MDC2 dissipated 1.5% more energy than anticipated in the design. MDC2 had a higher maximum compressive force than the design maximum compressive force. MDC3 remained elastic up to the 140 kips design elastic strength. It experienced an ultimate strength of 172 kips.

Specimen Design	HSS Diameter	HSS Wall Thickness	HSS Length	MDC End (Panel/Frame) Plate Thickness
MDC1	6.0in	0.25in	8.0in	0.75in
MDC2	6.0in	0.25in	13.5in	0.75in
MDC3	6.0in	0.25in	16.5in	1.0in

Table 3- 1 Nominal Dimensions of MDC Specimen Components

	Maximum Tensile Force (kips)		Maximum HSS Translation (in)	
	Design	Exp.	Design	Exp.
MDC 1	45.9	50.7	1.6	1.95
	Maximum Panel Plate Translation (in)		Maximum Frame Plate Translation (in)	
	Design	Exp.	Design	Exp.
	0.75	0.58	0.75	0.58

	Energy Dissipation (kip-in)		Maximum Compressive Force (kips)	
MDC2	Design	Exp.	Design	Exp.
	42.4	43.0	19.1	23.3

	Elastic Strength (kips)		Ultimate Strength (kips)	
MDC3	Design	Exp.	Design	Exp.
	135	140	N/A	172.2

Table 3- 2 Comparison of MDC experimental results to design values

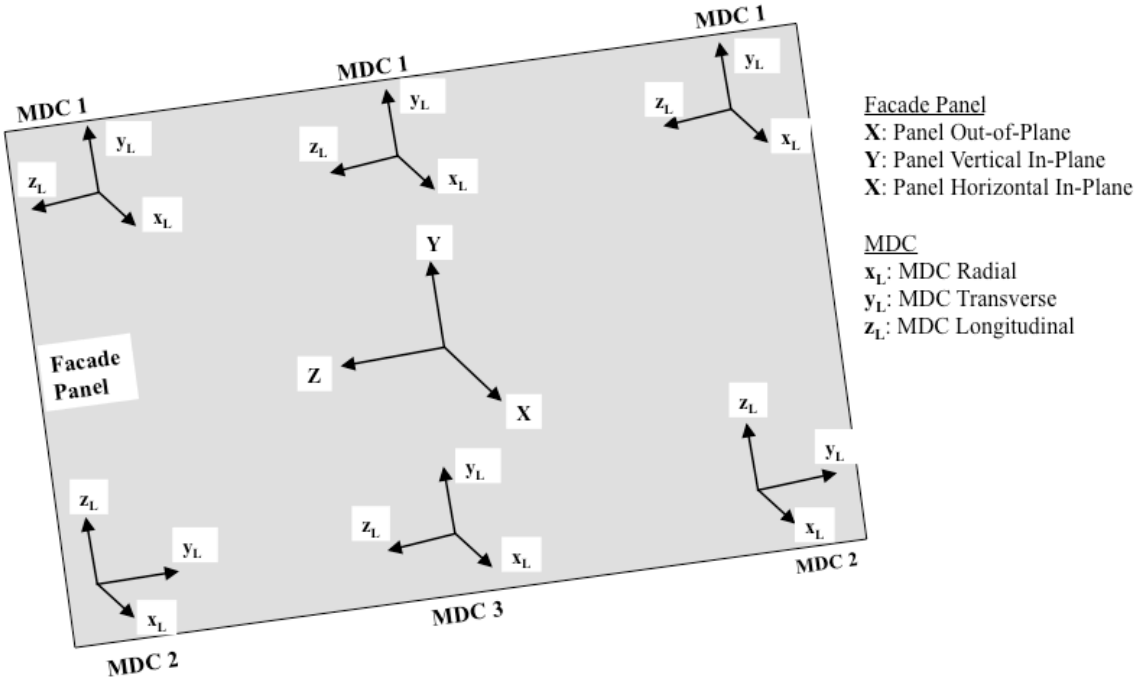

Figure 3- 1 Façade panel and MDC axes

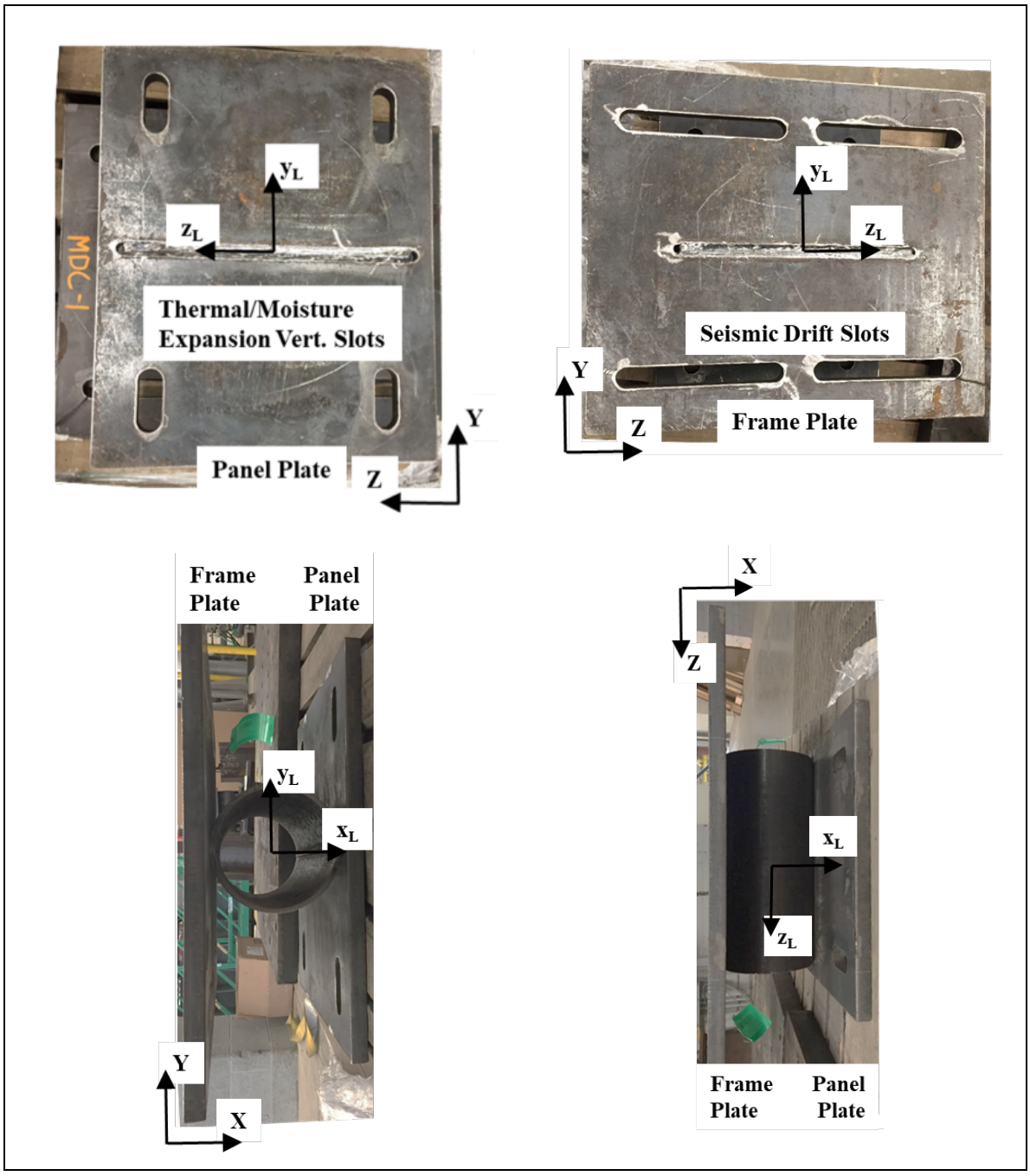

Figure 3- 2 MDC type 1 axes and details

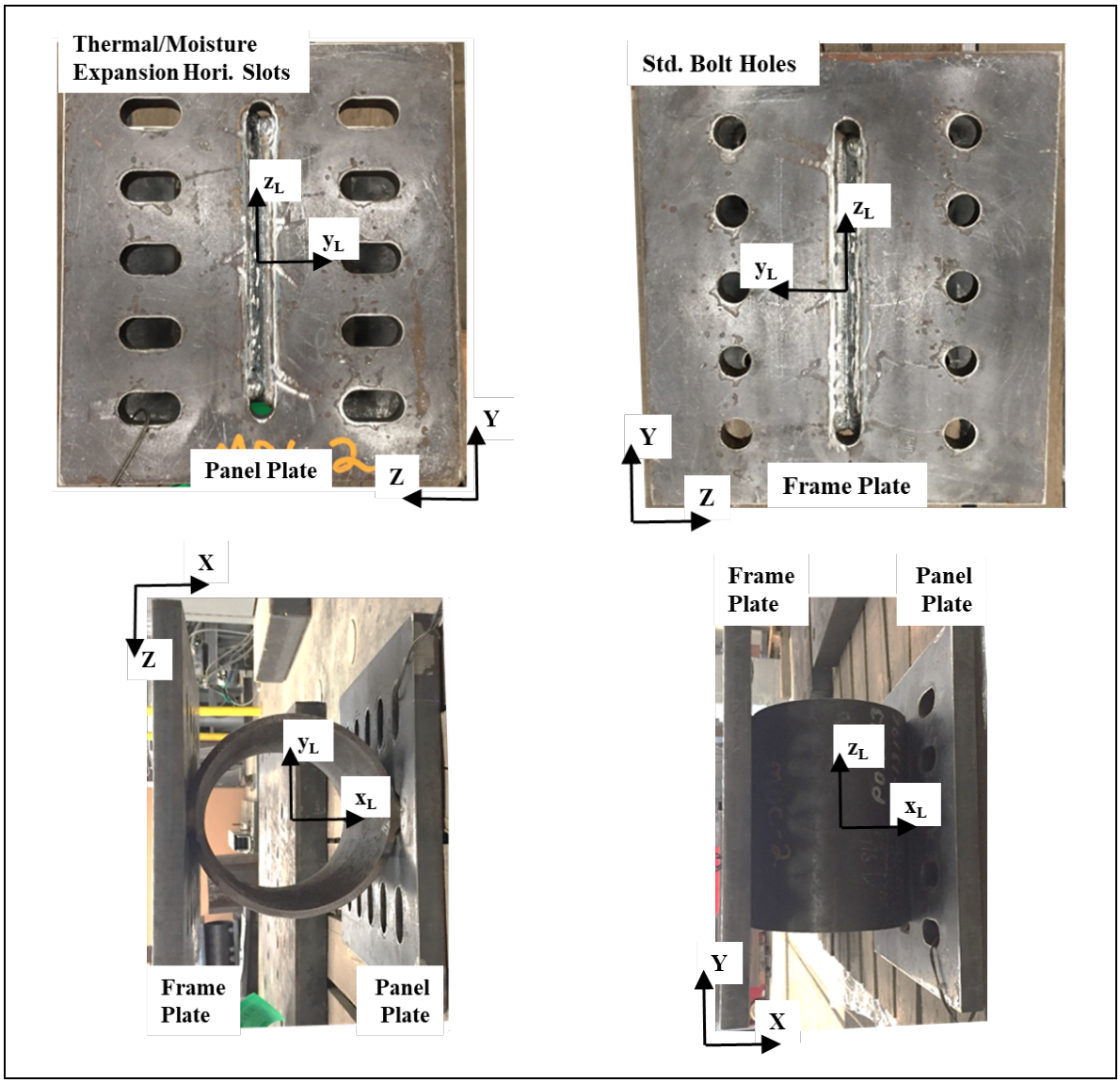

Figure 3- 3 MDC type 2 axes and details

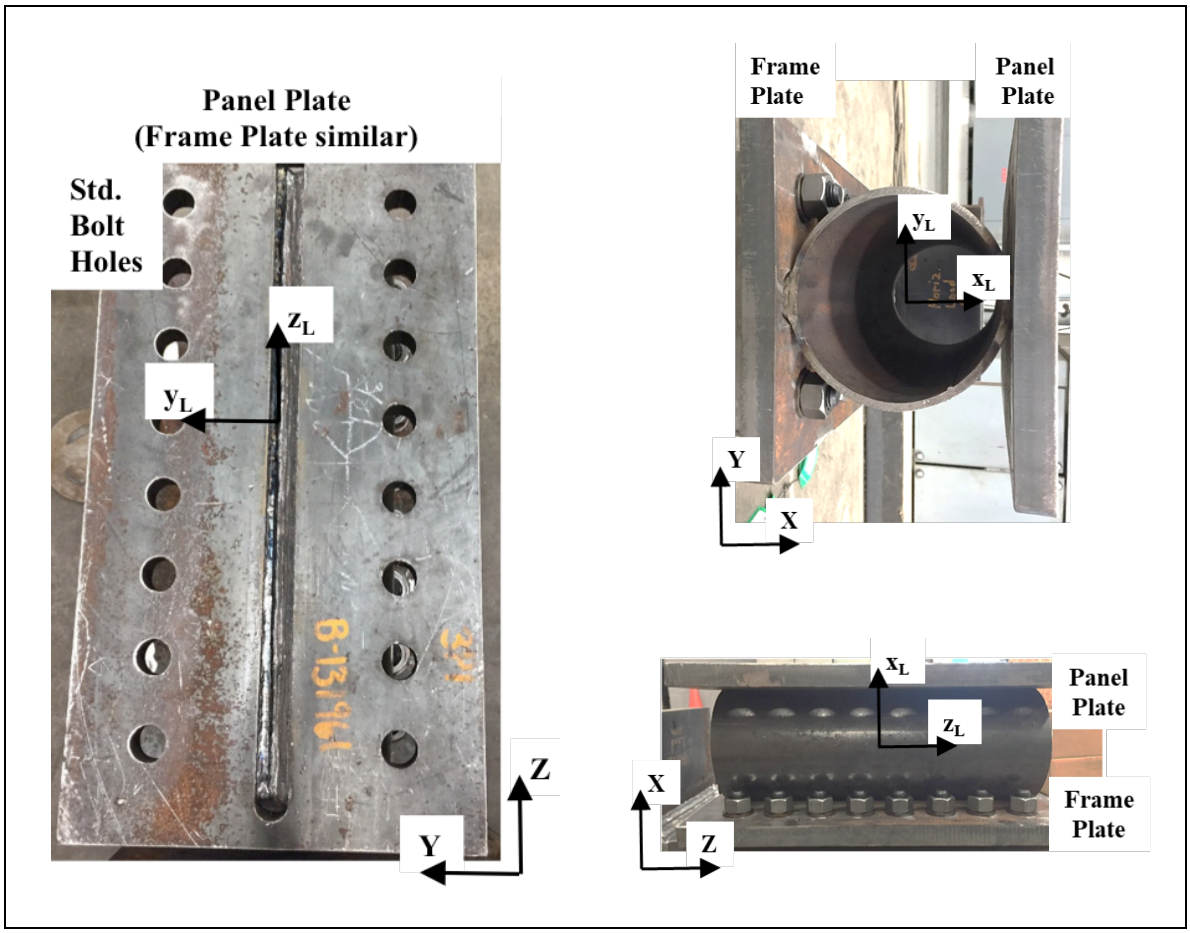

Figure 3- 4 MDC type 3 axes and details

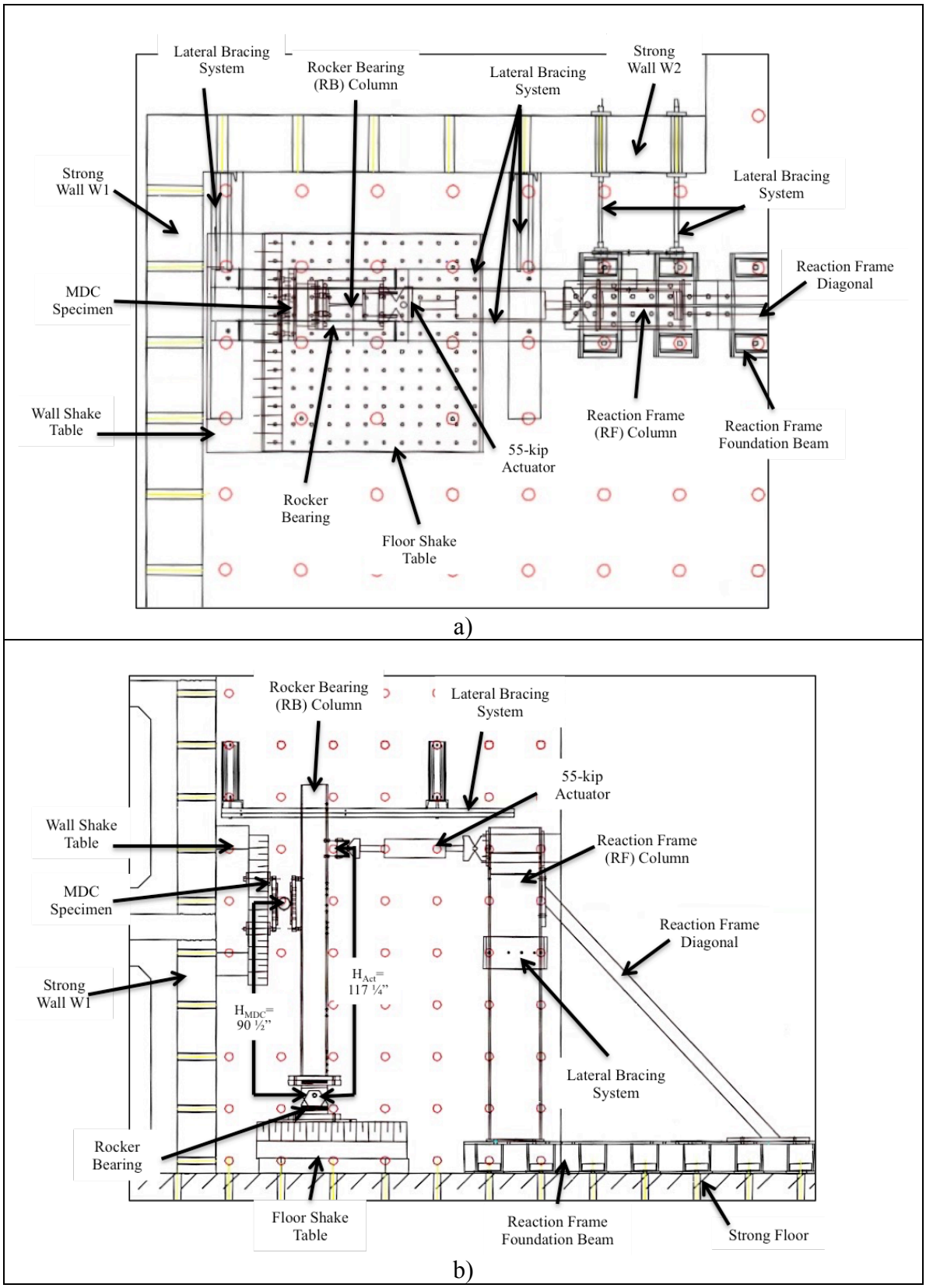

Figure 3- 5 Experimental Setup a) Plan view of the laboratory with test equipment b) Elevation view of the laboratory with test equipment

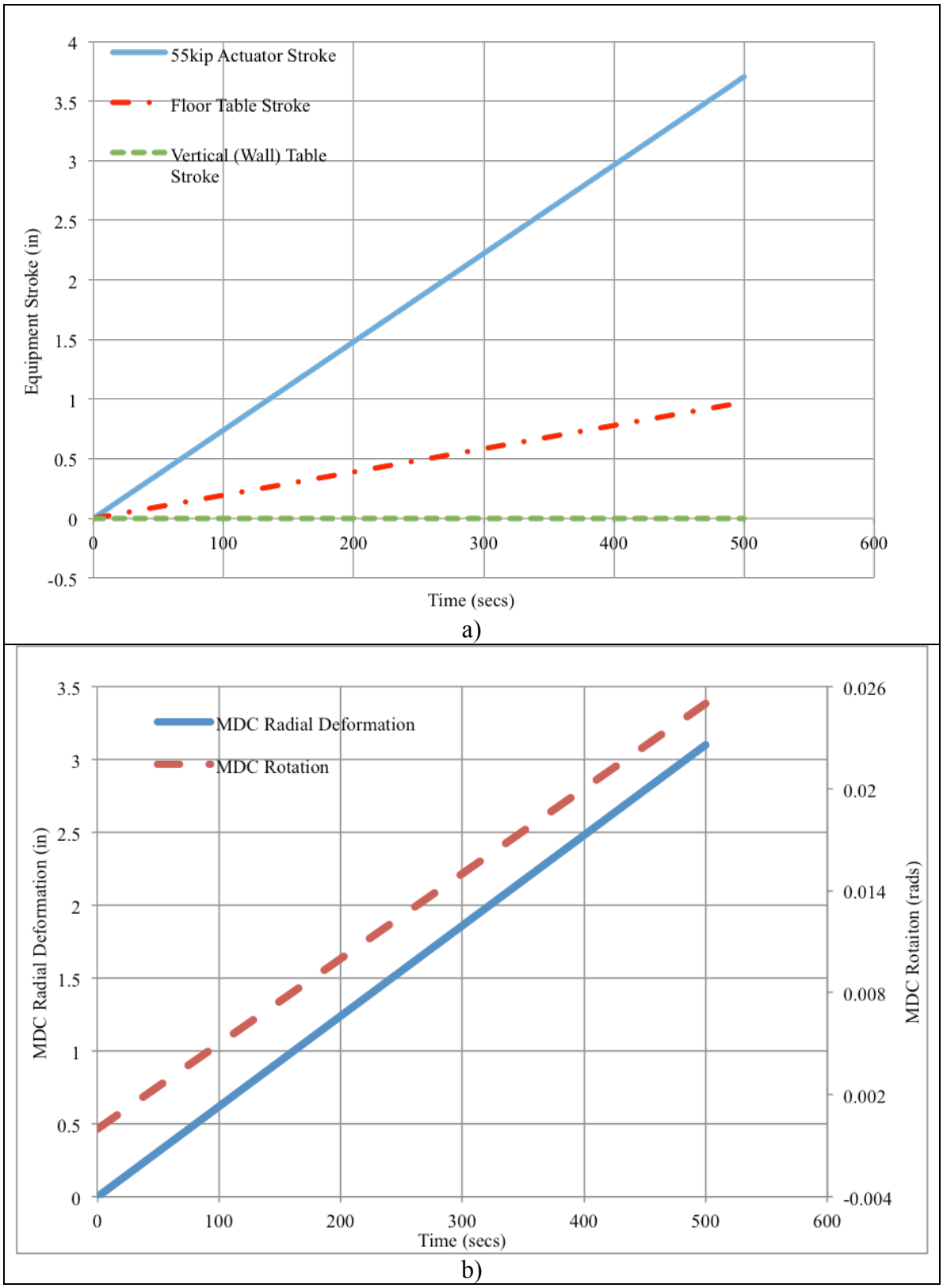

Figure 3- 6 MDC1 experimental loading protocol a) 55-kip actuator, floor table, and wall table deformation protocol b) Resulting MDC translation and rotation

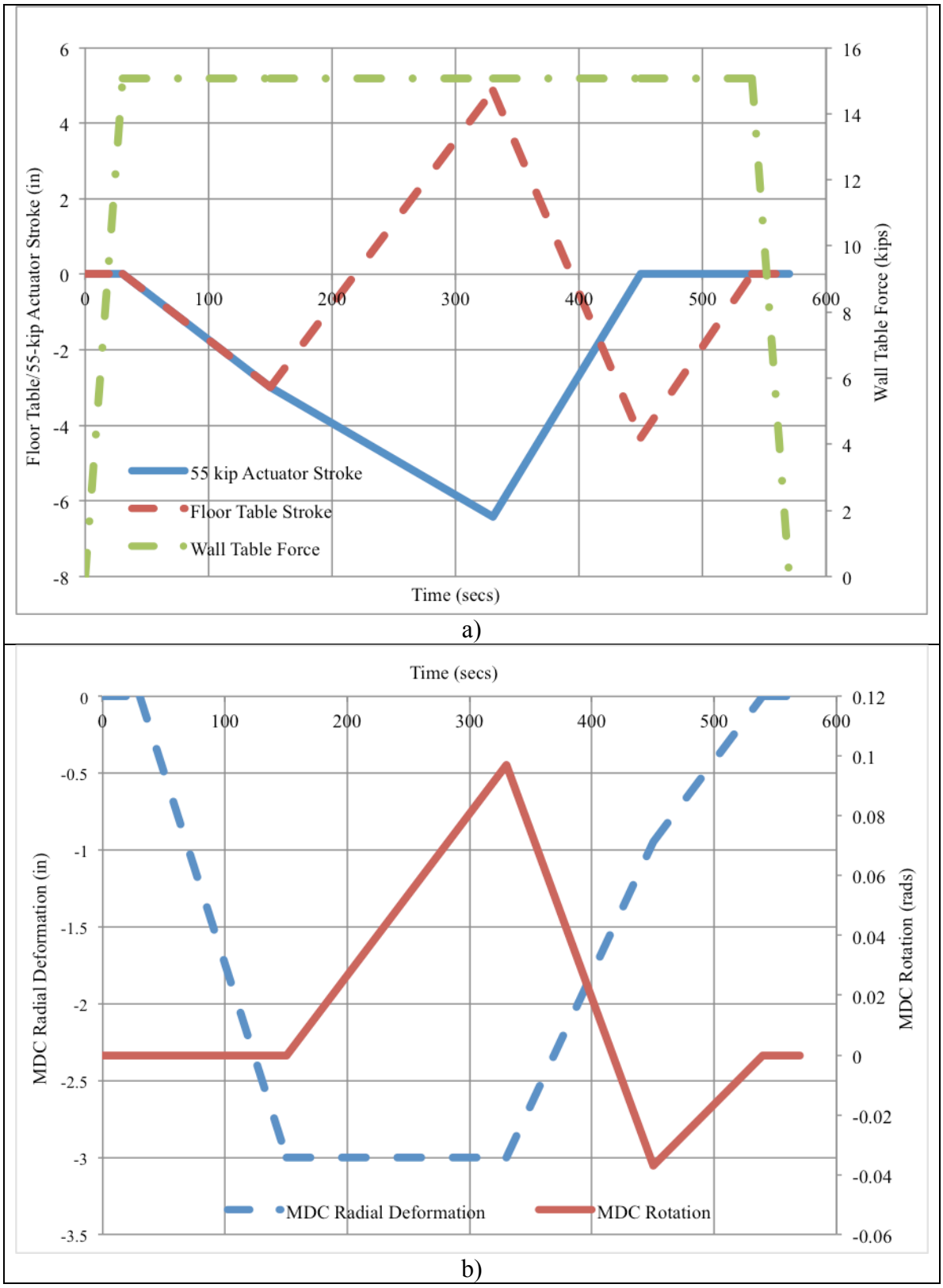

Figure 3- 7 MDC2 experimental loading protocol a) 55-kip actuator and floor table deformation protocol and wall table loading protocol b) Resulting MDC translation and rotation

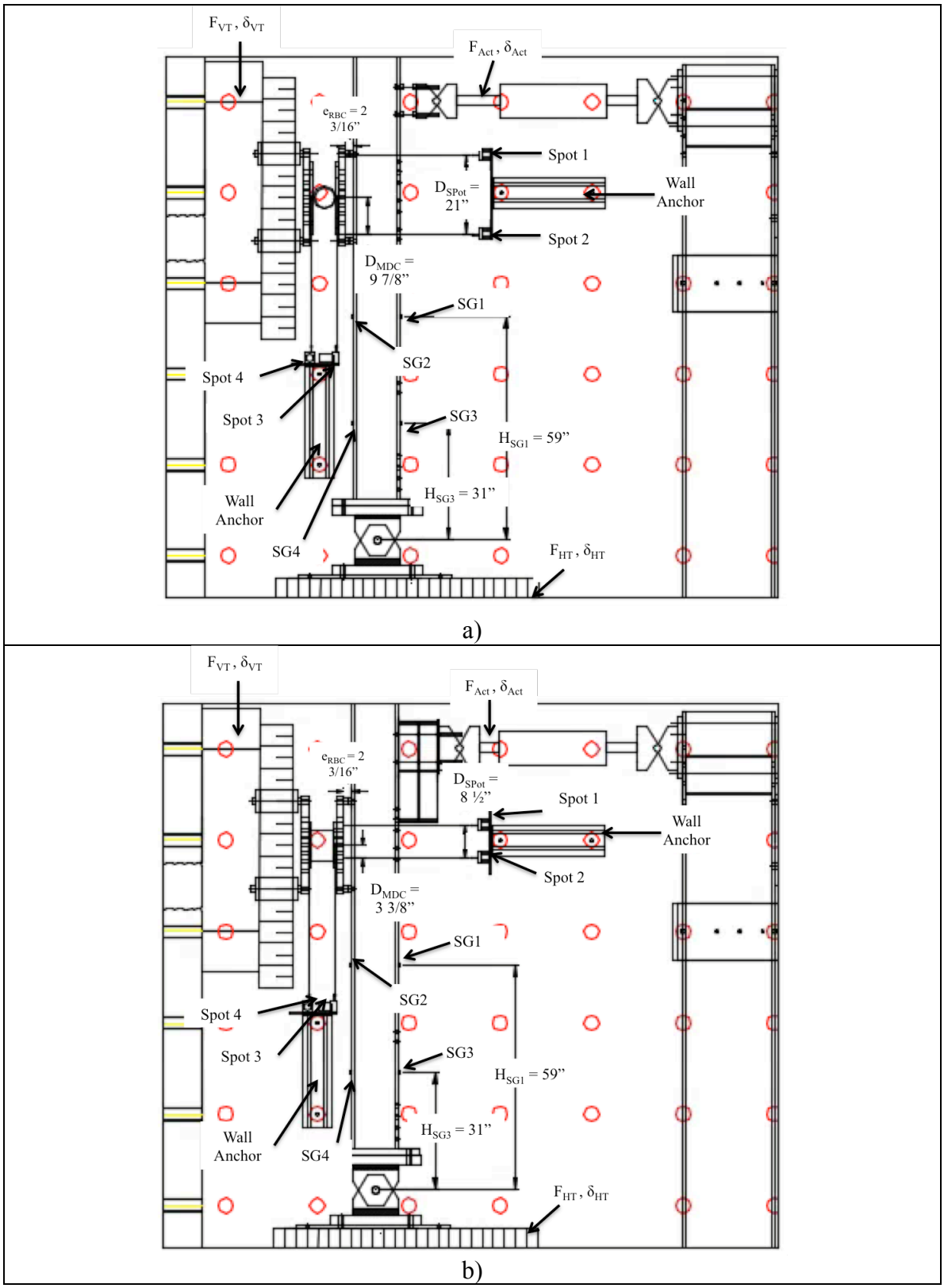

Figure 3-8 Instrumentation Layouts a) Instrumentation layout for the MDC1 experiment b) Instrumentation layout for MDC2 experiment

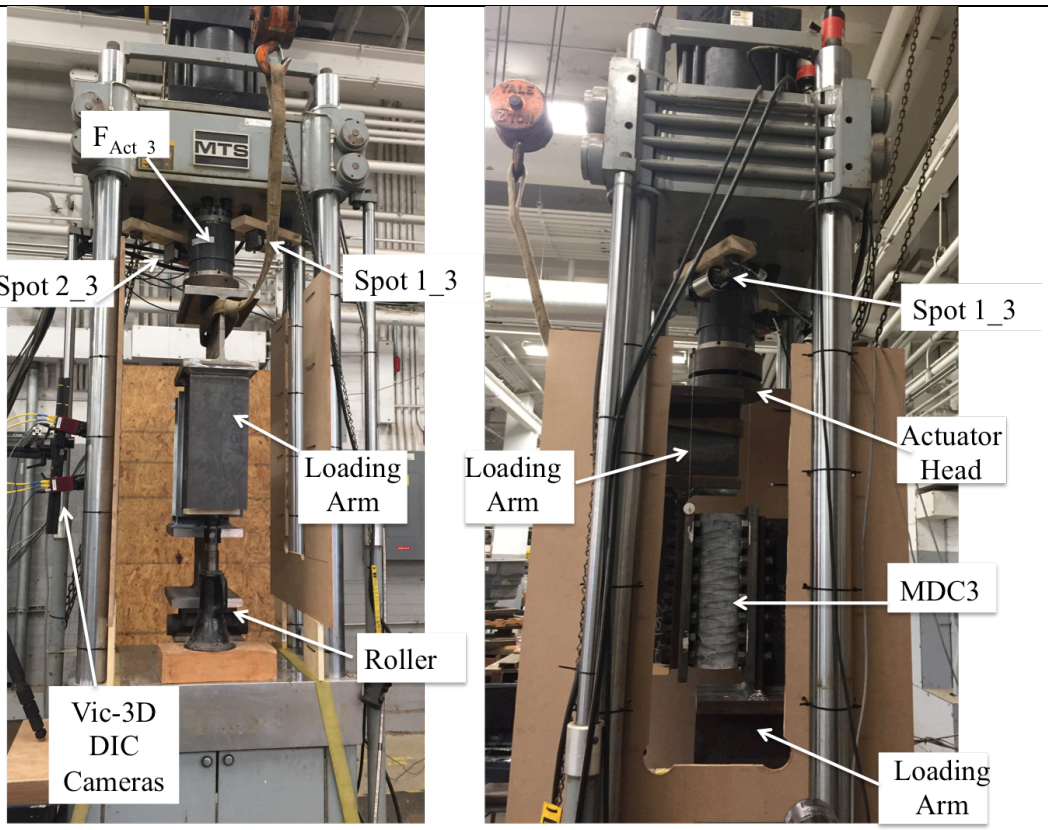

a)

b)

Figure 3- 9 MDC3 Experiment Setup a) Equipment and instrumentation in 220kip machine b)Vic 3-D DIC speck pattern on the HSS

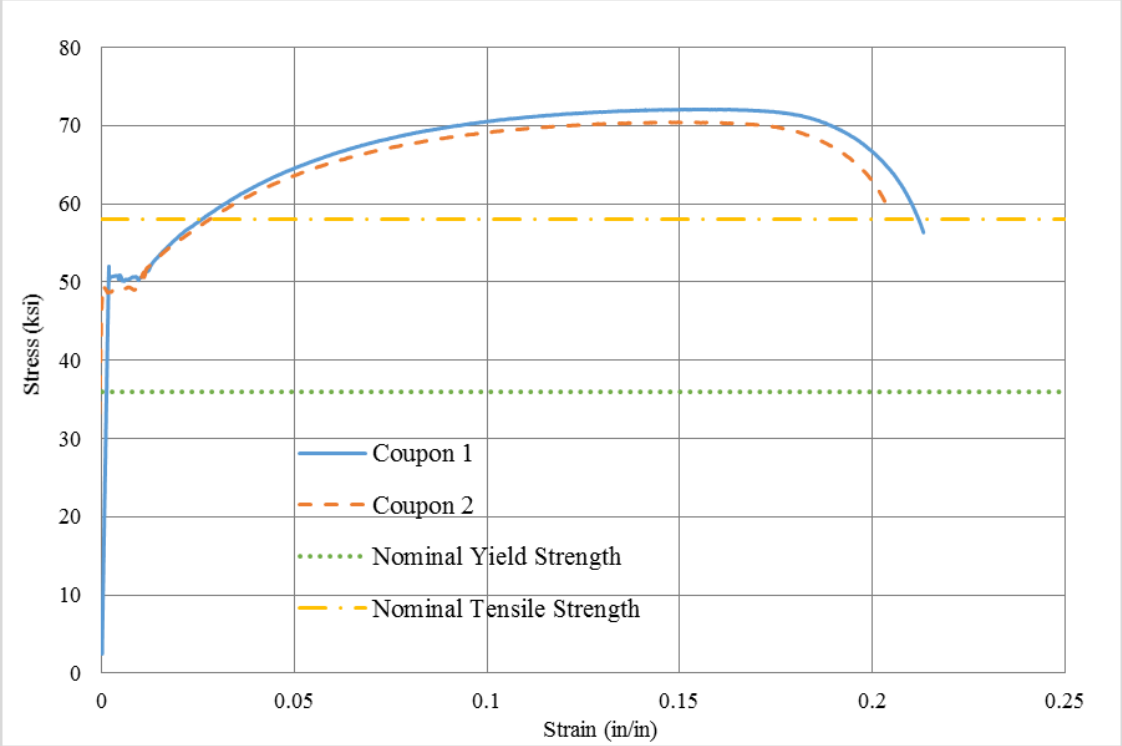

Figure 3- 10 MDC1 plate stress-strain curves from two tensile coupons and the nominal yield strength and tensile strength for ASTM A36 steel

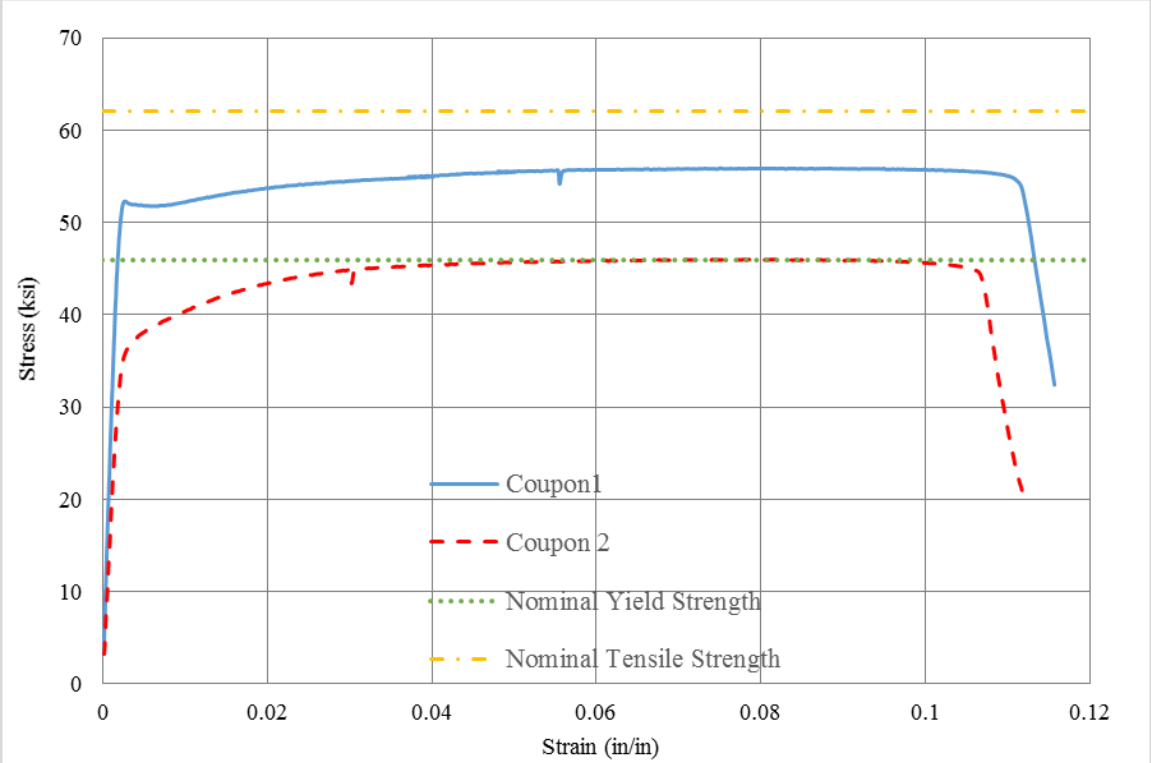

Figure 3- 11 HSS stress-strain curves from two tensile coupons and the nominal yield strength and tensile strength for ASTM A500 Grade C steel

Figure 3- 12 MDC1 Experiment Results a) Applied radial deformation $+x_L$ and rotation (about $+z_L$) b) Approximate deformations of the MDC components c) Force-Deformation curve d) Moment-Rotation curve e) Deformation of the MDC at various times

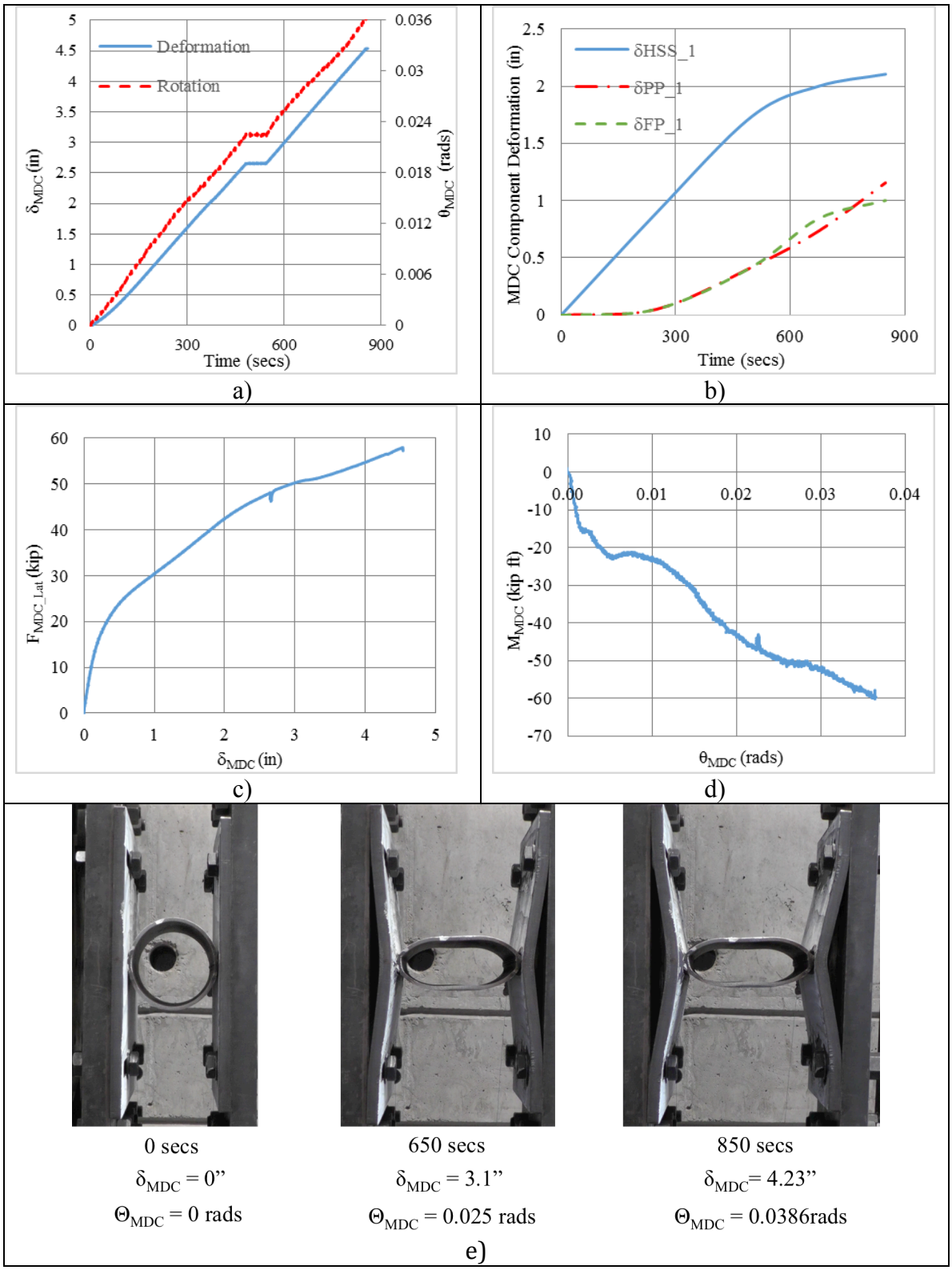

Figure 3- 13 MDC2 Experiment 1 Results a) Applied radial deformation $-x_L$ and applied rotation (about y_L) b) Applied gravity load $+z_L$ c) Force-Deformation curve d) Moment-Rotation curve e) Deformation of the MDC at times throughout the loading protocol f) Nut contact with the HSS at times throughout the loading protocol

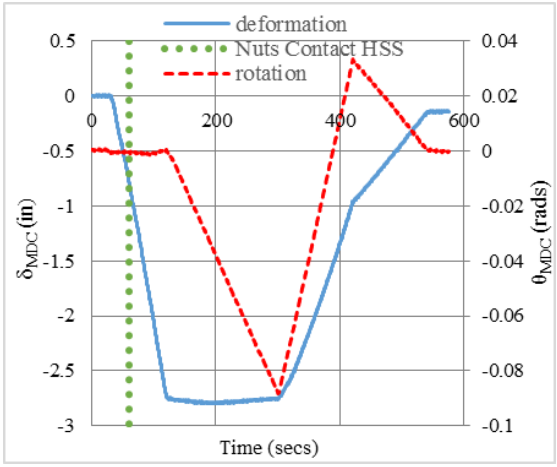

a)

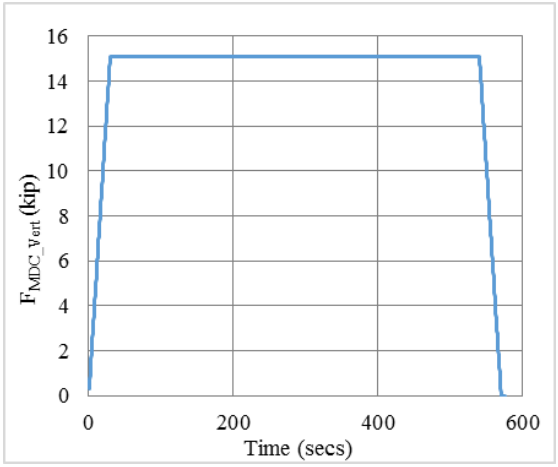

b)

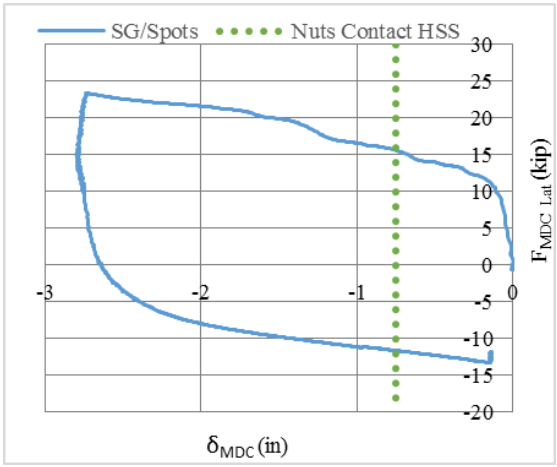

c)

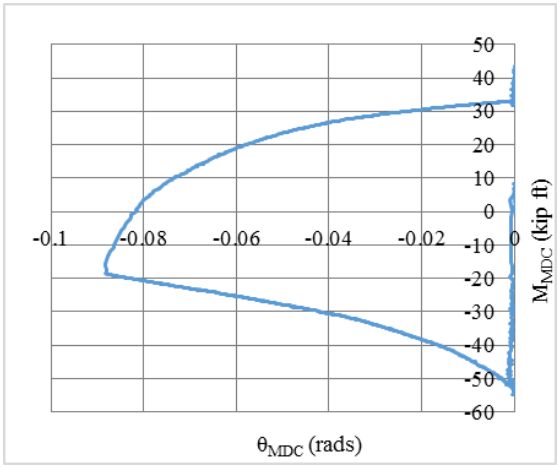

d)

30 secs	125 secs	300 secs	430 secs	550 secs
δ_{MDC} = 0”	δ_{MDC} = -2.78”	δ_{MDC} = -2.78”	δ_{MDC} = -0.97”	δ_{MDC} = 0”
Θ_{MDC} = 0 rads	Θ_{MDC} = 0 rads	Θ_{MDC} = -0.087 rads	Θ_{MDC} = 0.033 rads	Θ_{MDC}= 0 rads

e)

60 secs	90 secs	125 secs
δ_{MDC} = -0.75”	δ_{MDC} = -1.75”	δ_{MDC} = -2.78”
Θ_{MDC} = 0 rads	Θ_{MDC} = 0 rads	Θ_{MDC} = 0 rads

f)

Figure 3- 14 MDC 2 Experimental 1-4 Results a) Applied radial deformations $-x_L$ and applied rotations (about y_L) for four consecutive experiments b) Applied gravity loads $+z_L$ for four consecutive experiments c) Force-Deformation curves for four consecutive experiments d) Final fracture surfaces at the end of MDC2 Experiment 4 on panel plate (left) and frame plate (right)

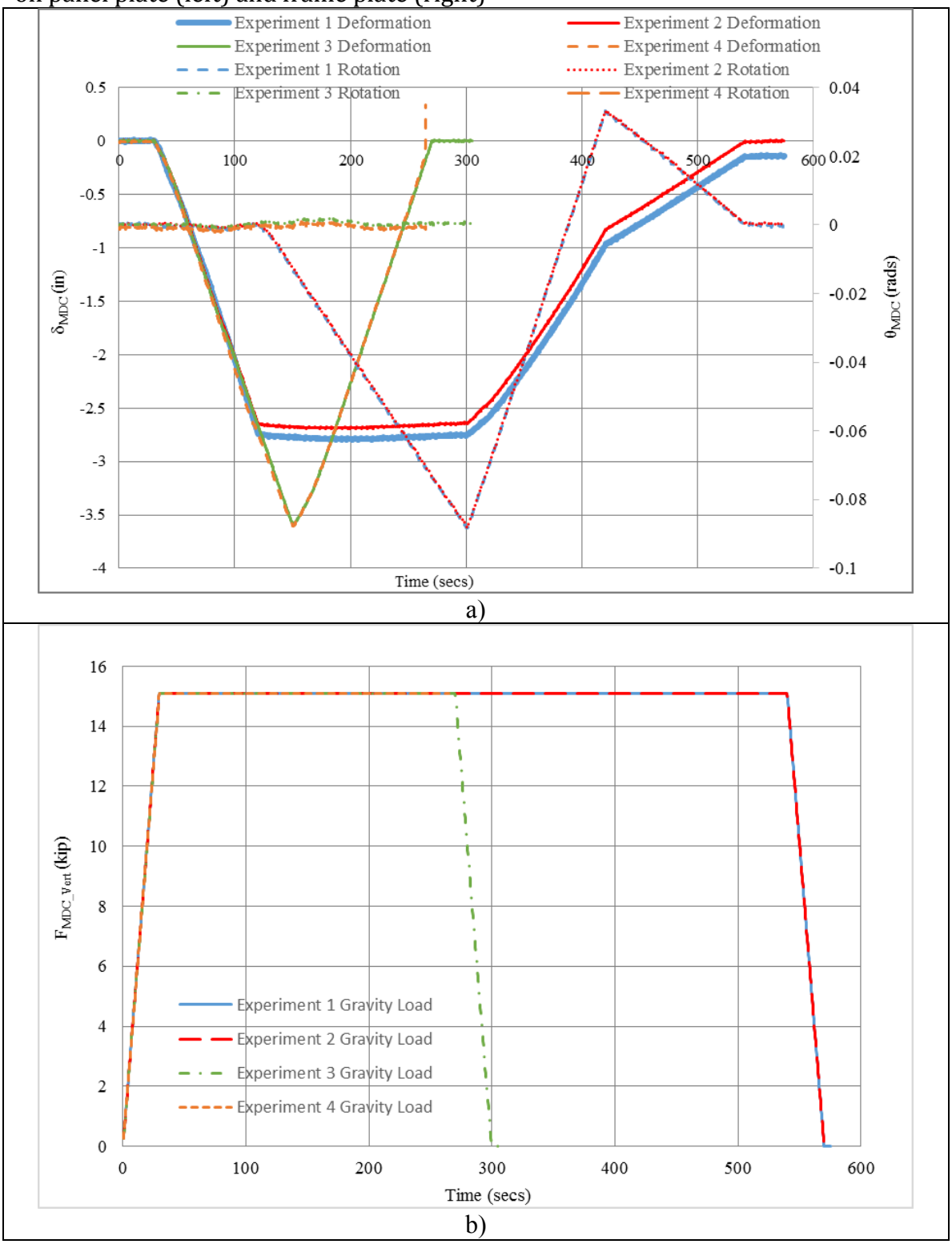

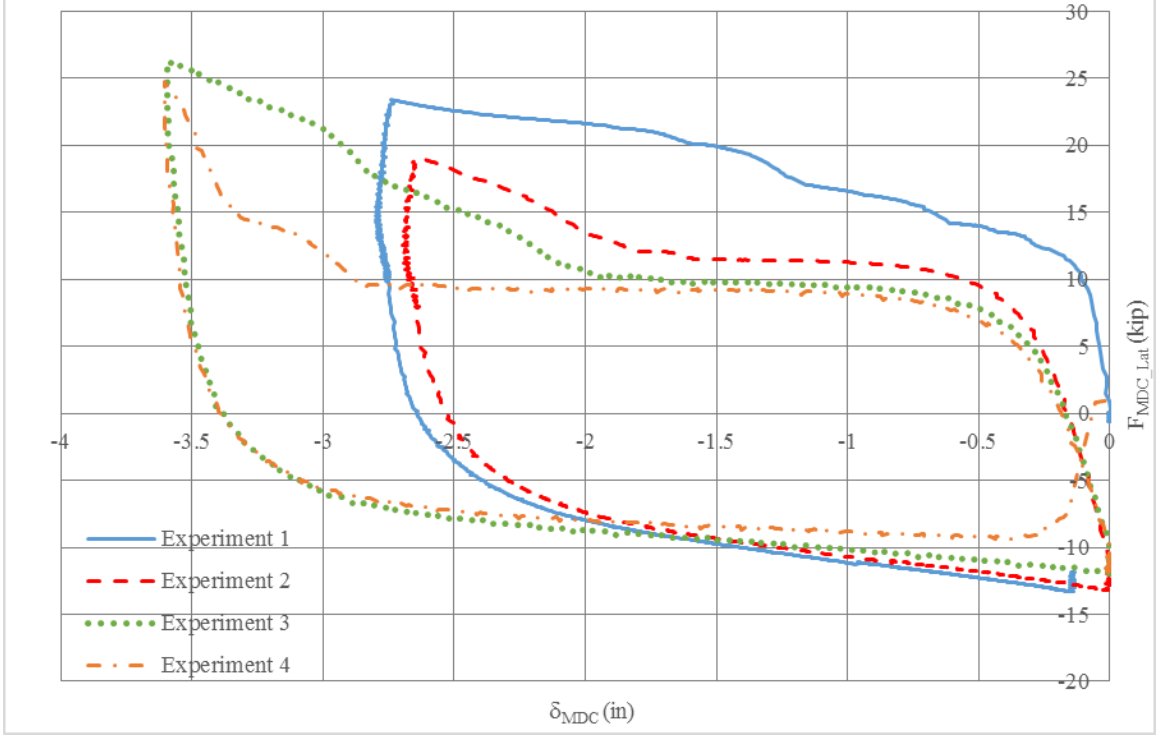
30
25
20
15
10
5
0
-5
-10
-15
-20
-4
-3.5
-3
-2.5
-2
-1.5
-1
-0.5
0
Experiment 1
Experiment 2
Experiment 3
Experiment 4
δ_{MDC} (in)
F_{MDC_Lat} (kip)

c)

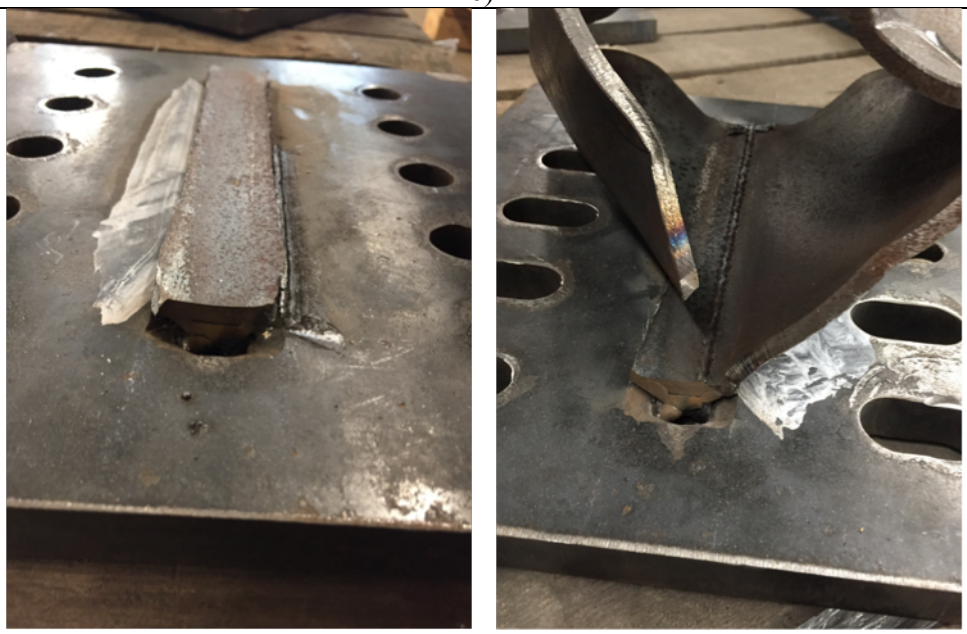

d)

Figure 3- 15 MDC3 Experiment Results a) The shearing deformation imposed between the MDC plates in z_L b) Force-Deformation curve c) Deformation of the MDC d) Failure surface of MDC3 (left) and failure locations (right)

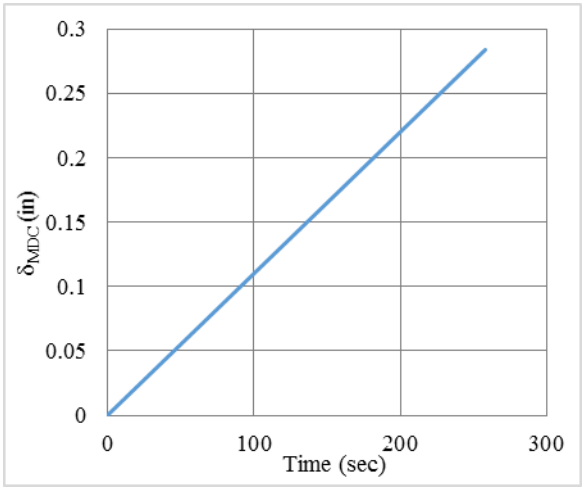

a)

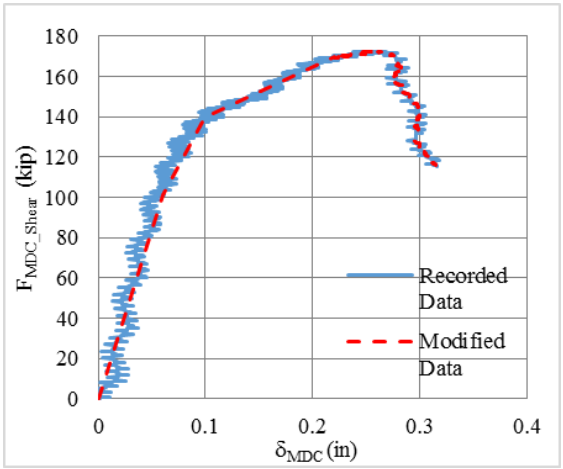

b)

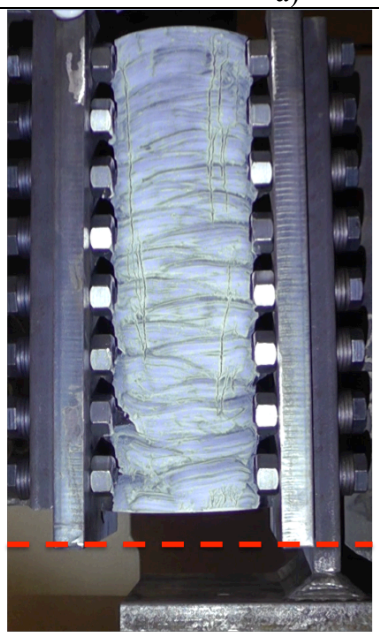

0 secs

δ_{MDC} = 0”

F_{MDC_Shear} = 0 kip

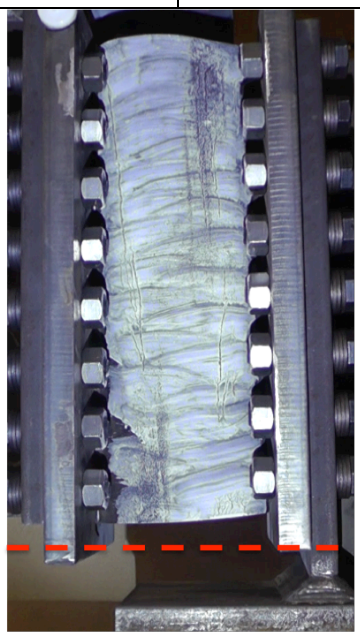

125 secs

δ_{MDC} = 0.1”

F_{MDC_Shear} = 140 kip

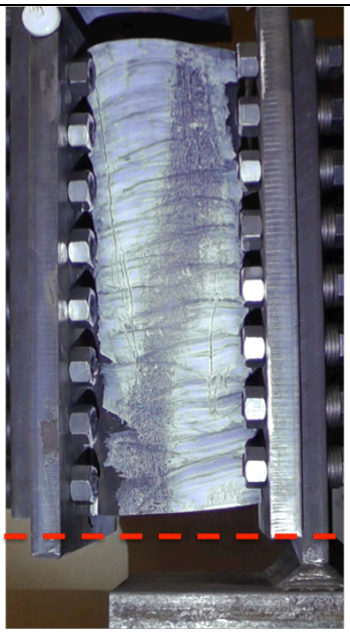

250 secs

δ_{MDC} = 0.3”

F_{MDC_Shear} = 120 kip

c)

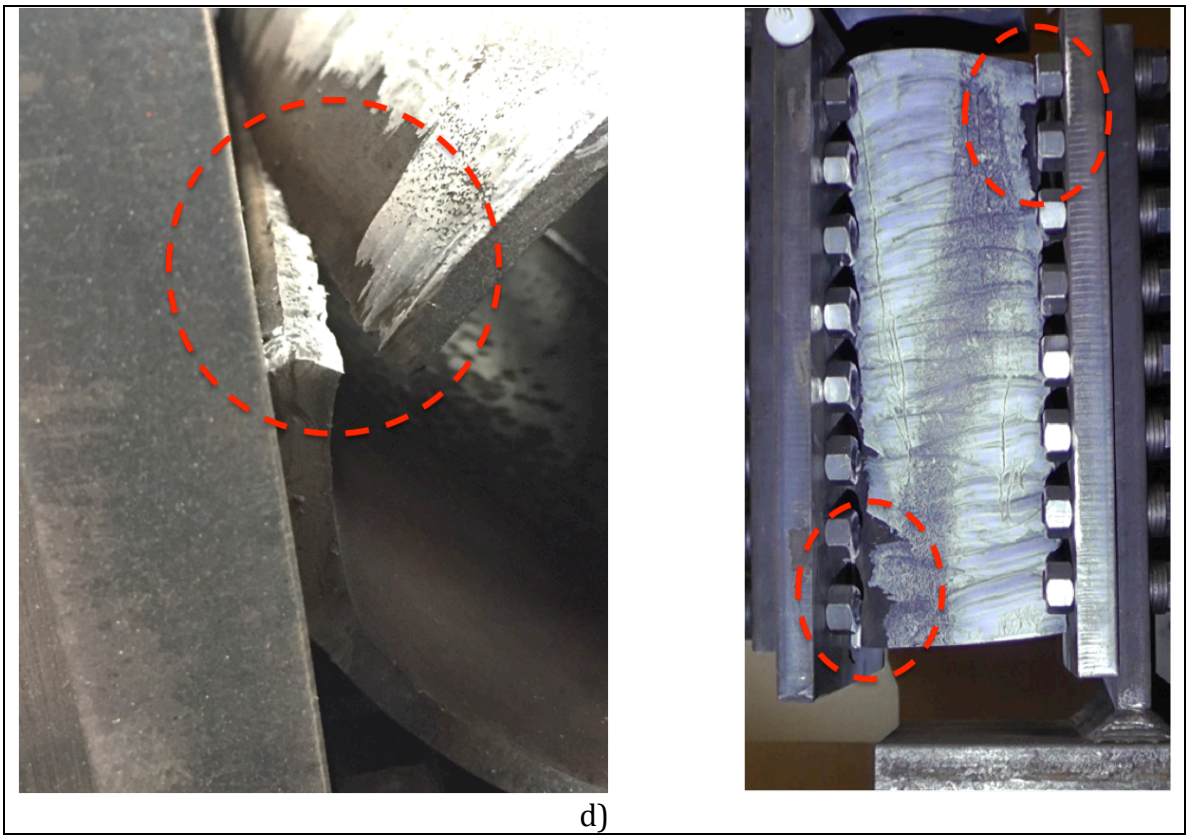

d)

Figure 3- 16 MDC3 Vic-3D DIC first principal strain results

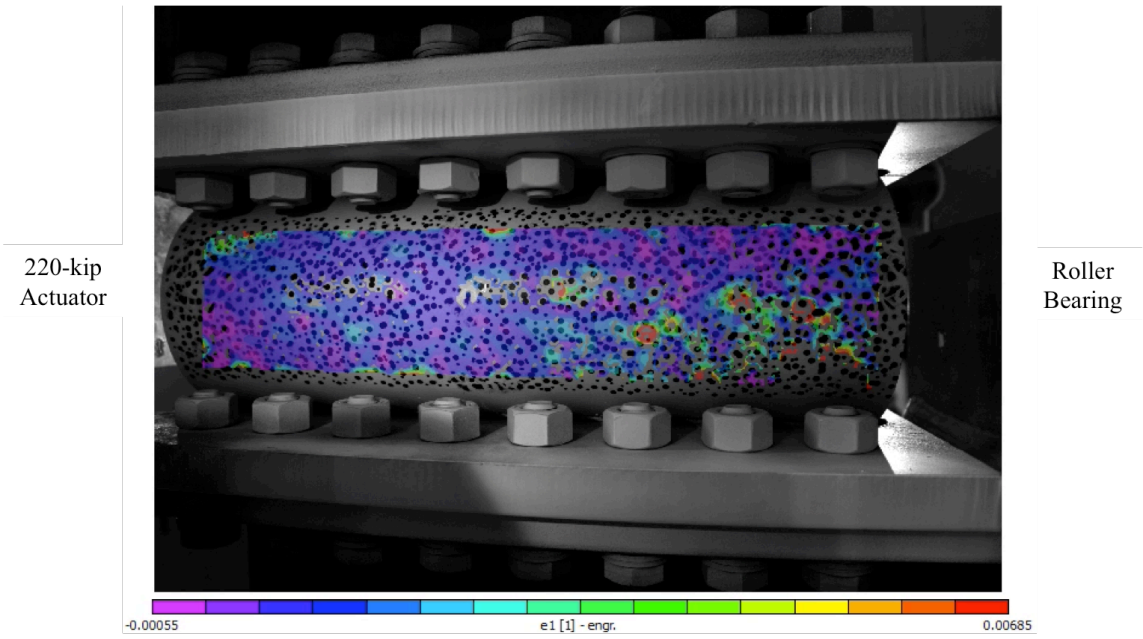

45 secs δ_{MDC} = 0.043" F_{MDC_Shear} = 70.4 kips

220-kip Actuator

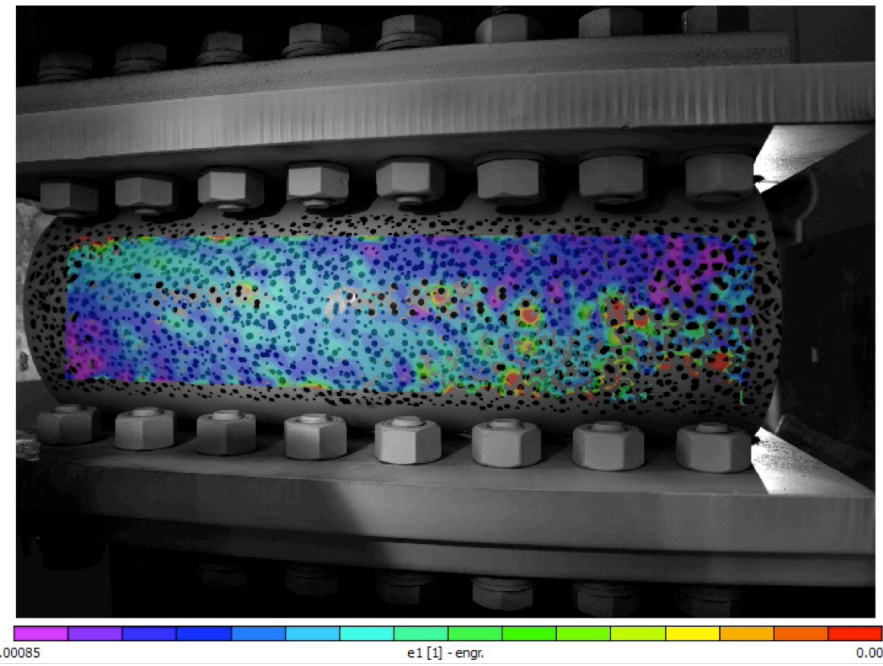

Roller Bearing

90 secs $\delta_{MDC} = 0.072$” $F_{MDC\_Shear} = 135$ kips

220-kip Actuator

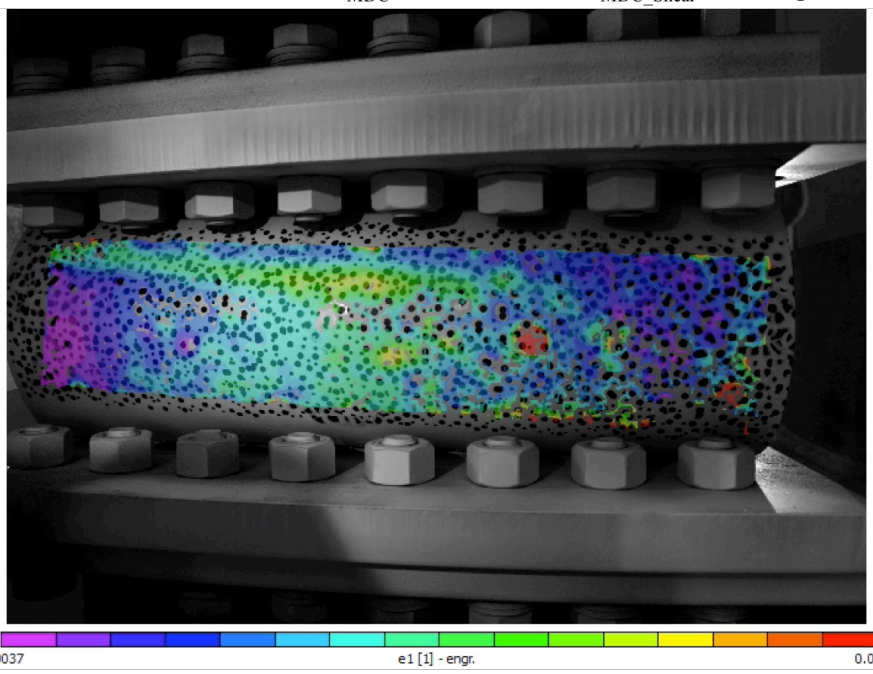

Roller Bearing

260 secs $\delta_{MDC} = 0.315$” $F_{MDC\_Shear} = 116$ kips

4. Finite Element Model of Multi-hazard Ductile Connectors

4.1 Introduction

Computational model of the experimentally tested multi-hazard ductile connector (MDC) designs were developed using finite element analysis (FEA) to simulate the static, nonlinear behavior of the MDC under various forms of loading expected from each hazard. The particular MDC considered was that proposed by Lavarnway (2013), which consisted of a circular, steel hollow structural shape (HSS) connected between two flat steel plates. Initial baseline MDC models were analyzed and its results were compared with the experimental test results from Lavarnway (2013). This study was chosen as the baseline analysis due to the simpler loading protocol compared to that of this project. These analyses will be referred to as "baseline" or "base" models. Once the base model reasonably matched the Lavarnway (2013) results, the MDC model was adapted to the three current MDC designs and analyzed for the loading scenarios that occurred in the experiments as described in Section 3. This section provides a description and validation of the base model, development of a more comprehensive MDC model, and comparison of the FEA model results with design criteria.

4.2 Base Model

4.2.1 Model Description

All finite element analysis was performed using ANSYS Mechanical, Academic Research Version17.2 (ANSYS Inc., 2016). The MDC considered by Lavarnway consists of three components, an HSS circular tube between two flat steel plates. A local coordinate system was used for all the FEA models as shown in Figure 4-1. The end plates are connected to either the façade panel or the building frame and are assumed to

be parallel to one another. The MDC was modeled using shell elements (ANSYS Shell 181), which are four-noded elements with six degrees of freedom per node (ANSYS Inc., 2016). The structural behavior of both the HSS and end plate components of the model are defined by the shell elements. The HSS and plate shell elements are assigned a plasticity material model that includes kinematic and isotropic hardening with a Von-Mises yield criterion (ANSYS Multi-linear Isotropic Hardening Model), and is defined by a series of stress-strain points. The stress-strain data for the baseline models and the MDC models are presented in their respective sections.

Contact between the HSS and end plates was simulated because the MDC is expected to undergo large deformations during high hazard loading events such as blast and impact loading. Large radial deformations to the HSS will cause it to contact the plates. Contact elements (ANSYS Conta 173) were used around the centerline of the HSS with a mesh matching the shell element mesh. These elements sit on the centerline of shell elements and are part of a pair of elements used to represent contact between 3D surfaces. Target elements (ANSYS Targe 170) are applied to the end plates. The target element mesh matches the shell element mesh of the flat plates. The contact and target elements identify the potential contact surfaces that may occur due to the HSS deformation during the analysis. However, these elements do not contribute to the modeled structural behavior, such as stiffness and strength.

The nodes in each flat plate are coupled together to behave as a rigid plane (ANSYS Cerig) to simulate the relatively rigid bodies to which the MDC end plates are attached. One plate represents the building frame and acts as a fixed connection that will not allow movement. The fixed plate is constrained in all directions. The opposite plate

is then assigned the translational and/or rotational displacements of the façade panel during the high hazard loading event.

4.2.2 Verification of Base Model Results

Two baseline MDCs, consisting of HSS16x0.375 and HSS10.75x0.25, were modeled and verified with the results from the Lavarnway (2013) experiments. An HSS7x.025 MDC was also tested in the Lavarnway (2013) experiments, but that size HSS was not considered for this verification. Since tensile coupon data was not available for this size HSS, its material properties were unknown. The stress-strain values considered in the FEA base model for the HSS16x0.375 and HSS10.75x0.25 are available in Figure 4-2. These curves were developed from the tensile coupon tests performed as part of the Lavarnway (2013) experiments. The stress-strain data plots from these tensile tests are available in Appendix 4. Both the HSS16x0.375 and HSS10.75x0.25 models were compressed 6 inches radially inward (x-direction). These deformations were performed to match the Lavarnway (2013) experiment deformations. Both the HSS16x0.375 and HSS10x0.25 FEA results closely matched with the Lavarnway (2013) experimental results as seen in Figure 4-3 and Figure 4-4. HSS10.75x0.25 FEA yield strength is about 5.8 kips and the FEA strength at 6 inches of deformation (x-direction) is 8.6 kips. Both of these strengths closely match the Lavarnway (2013) experimental strengths in Figure 4-3 a. Some difference was observed in the initial elastic strength, but the post-elastic strength and material strain hardening was well captured. In Figure 4-4 a, the FEA yield strength of the HSS16x0.375 is 7.8 kips and FEA strength at 6 inches (x-direction) is 10.9 kips. The Lavarnway (2013) experimental yield strength is 8.2 kips and the strength at 6 inches of deformation is 10.1

kips (Figure 4-4 a). The HSS16x0.375 FEA model experienced slightly more strain hardening than the experiment, but there was not a significant difference between the FEA Lavarnway (2013) experimental results in the hardened region. Despite the small differences between the FEA and Lavarnway (2013) experimental results, both of the force-deformation curves produced by the FEA models were deemed acceptably close to those of the experimental results. Reasonable deformed shapes were created in the FEA base model throughout the loading procedure (Figure 4-3 b and Figure 4-4 b). The equivalent plastic strain diagrams for both of the FEA models show plastic hinge yield lines are developing (Figure 4-3 d and Figure 4-4 d). The plastic hinges occurred in expected areas of the HSS where large changes in the HSS curvature are occurring. The maximum plastic strain in these diagrams show both models are experiencing likely acceptable levels of plastic strain. The Von-Mises stress diagrams in Figure 4-3 c and Figure 4-4 c show areas of high stress where the plastic hinges are forming corresponding to the strain levels and specified material model. Again, the maximum stress values available on these contour diagrams show reasonable values.

4.3 MDC Models of Experimental Specimens

4.3.1 Introduction

Once the base model results were verified against the Lavarnway (2013) experimental data, the model was adapted to the designs of the different types of MDCs considered in this research (MDC1, MDC2, and MDC3). The three MDC designs still consisted of a circular HSS attached between two parallel plates. The plates were ASTM A36 steel and the HSS were ASTM 500 Gr. C steel. All of the HSS tubes in the MDC designs were various lengths HSS6x0.25. The MDC plates included standard, short-

slotted, or long-slotted bolt holes for attaching to the facade panel or building frame. Although the MDC design models were constructed from the base model, the geometries, material properties, contact surfaces, supports, and loading of the three designs varied from the base model. The FEA axis directions remained consistent with those of the base model as seen in Figure 4-1.

4.3.2 MDC Material Models

The multi-linear plasticity material models for the HSS and plates with stress-strain properties for each MDC component are shown in Figure 4-5. The material model of the A36 plates was developed from the tensile coupon data presented in Section 3. Due to the issues testing the HSS coupons discussed in Section 3, the HSS material model was developed from a combination of the expected stresses from AISC 341-10 Seismic Provisions for Structural Steel Buildings (AISC, 2010a) and the material tests in Fadden (2013). The HSS material model yield stress was specified as R_y*F_y and the tensile stress as R_t*F_u. A value of 1.3 was used for R_y and a value of 1.2 was used for R_t per AISC 341-10. The model between the yield stress and tensile stress was developed based on the tests from Fadden (2013). The model was developed using the Fadden (2013) data from side-wall coupon tests from 0.25 inch thick HSS, the same HSS thickness used in this study. The coupons from the HSS corners were not used because the corner curvature is too large to be representative of the circular HSS. The corner areas experience significantly more strain hardening during the HSS fabrication process compared to the rest of the cross section. The weld seam coupon data was also not used because it is not representative of the average material properties over the HSS cross-section.

4.3.3 MDC Type 1 Model (MDC1)

4.3.3.1 Model Descriptions

The drawings of MDC1 are available in Appendix 2. The long bolt slots on the frame plate allow relative lateral movement to accommodate seismic drift and those on the panel plate allow relative vertical movement between the façade panel and connector for thermal expansion. The MDC type 1 (MDC1) was designed to simultaneously undergo 3.1 inches of outward radial translation (x-direction) and .025rads of rotation about the lateral in-plane panel axis (z-axis) (Figure 4-6 a). These deformations were determined from the critical loading scenario of out-of-plane seismic forces acting on a façade edge panel (Appendix 1).

Two MDC1 models were considered, which are referred to as Model 1 and Model 2. Each model had different boundary conditions to simulate bounds of potential initial bolt-hole bearing contact (Figure 4-6 c). Neither of the MDC1 models utilized any contact/target planes because the deformed HSS will not contact the plates during tensile MDC deformation. Like the base model, the structure of the HSS and plates consisted of shell181 elements in both MDC1 models. The MDC welded connection at the end plate was modeled by coupling nodes at the weld slots between the plates and HSS using the ANSYS Cerig constraint equation.

Boundary conditions were the only difference between the two MDC1 models. Model 1 applied boundary conditions only to areas of the plates that would experience bearing on the façade panel or building frame. These areas were on the top and bottom of both plates (y-direction) from the center of the bolt slot to the outside of the plate where plate prying will occur. These areas on each plate in Model 1 were coupled together using the "cerig" command. The top and bottom edges (y-direction) of the plates act as a rigid

body while the centers of the plates allowed deformation. For both plates in Model 1, the boundary conditions were applied assuming that the bolt was in the center of the bolt slot. The panel plate was a fixed boundary while the frame plate experienced the translations (x-axis) and rotation (about z-axis) imposed on the MDC. Model 2 had these same plate boundary conditions on the panel plate plus additional boundary conditions on the frame plate. The moving frame plate changed slightly in Model 2 to account for the bolts on the panel plate. On this frame plate, the nodes around the bolt locations were assumed to be stationary and could not move in the z or y directions. They were free to move in the x direction with the prescribed movement of the rest of the plate. For both Model 1 and Model 2, the HSS and the plates in MDC1 are designed to yield to provide the necessary behavior and create boundary conditions consistent with the connection details. To determine the appropriate plate thicknesses for MDC1, analyses were performed for various plate thicknesses including 1in, 0.75in, and 0.50in. Ultimately, a plate thickness of 0.75in was chosen for MDC1 and used in the experiment. The same plate thicknesses were applied to MDC2 and MDC3 to maintain the same MDC thickness.

4.3.3.2 Convergence Study

Convergence studies were performed on Model 1 to determine appropriate mesh size for both MDC1 models. The same final mesh size was applied to both models because these models are fundamentally the same and differ only in their boundary conditions. Force- deformation, Von-Mises stress, Von-Mises elastic strain, and equivalent plastic strain were studied for convergence at four points (P1, P2, P3, P4) on the MDC cross section (Figure 4-6 b). All of the points were studied near the center of the MDC length (z-direction). Once the change in the force-deformation, stress, and

strain was below 3% between each mesh size, these criteria were considered adequately converged. The average mesh size for each MDC component used in the convergence study is available in Table 4-1. The force-deformation curve for MDC1 (Figure 4-6 d) converged before most of the stress and strain at localized points. The force-deformation data was converged by mesh size 3. The stress and strain generally converged at the same mesh size at each point. For P1 located on an HSS hinge area, the Von-Mises stress and equivalent plastic strain converged at mesh size 4 (Figure 4-6 e). The stress and strain at point P2, located between the HSS hinge locations, was near convergence (10%) by mesh size 6. However, the values did not reach below the 3% convergence threshold (Figure 4-6 f). The Von-Mises stress and elastic strain on frame plate point P3 converged by mesh size 5 (Figure 4-6 g). The Von-Mises stress and elastic strain on panel plate point P4 both achieved convergence at mesh 3 (Figure 4-6 h). After the convergence study was performed, mesh size 6 was used in Model 1 and Model 2 to accurately obtain force, stress, and strain data.

4.3.3.3 Results

The force-deformation curves of MDC1 Model 1 and Model 2 are shown in Figure 4-7 a with the MDC1 experimental curve. Model 1 matches the experimental curve better than Model 2 at low deformations. However, the Model 2 force-deformation curve matches the experimental results better at high deformations. Due to these force-deformation curves, it can be determined that the boundary conditions in the MDC1 experiment were a combination of the Model 1 and Model 2 boundary conditions. During the experiment, the frame plate bolts engaged at higher deformations, which stopped the frame plate from moving in the y-direction at the bolt locations. The force-deformation plots for each

MDC component in Model 1, Model 2, and the MDC1 experiment is available in Figure 4-7 b. Overall, both models underestimated the deformation of the HSS while overestimating the deformations of the panel and frame plates. Noticeable differences between the Model 1 and Model 2 deformed shapes occurred at the design deformations of 3.1in of translation (x-direction) and design rotation of 0.025 rads (about z-axis) (Figure 4-7 c). In Model 1, both the panel and frame plates show similar amounts of deformation at the MDC design deformation and rotation. However, in Model 2,the frame plate clearly shows more deformation than the panel plate. These differences in deformed shape were due to the different boundary conditions applied in the models. The true deformed shape at the design deformation and rotation is closer to that of Model 2 because this model better represents MDC1 at higher deformations. Although the deformed shapes of Model 1 and Model 2 vary slightly, there were no significant differences in the Von-Mises stress and equivalent plastic strain plots at the design deformation and rotation (Figure 4-8 a-d). In Figure 4-8 c-d, the there are areas of significantly high plastic strains (40%-50%) in localized areas near the HSS weld connection to the plates. Such high plastic strains are not realistic and are due to the highly restrained mesh in these areas. The mesh refinement may also be locally inadequate in this area of the model. The average strains within the plastic hinge regions are on the order of 5-10% strain at the design deformation.

4.3.4 MDC Type 2 Model (MDC2)

4.3.4.1 Model Description

The MDC type 2 (MDC2) must withstand the tributary gravity load imposed on it by the façade panel in addition to the high hazard loading. The MDC2 drawings are

available in Appendix 2. The controlling out-of-plane loading for this connector is due to air-blast effects on the prototype system considered (Appendix 1). The gravity load applied to each MDC2 on the considered panel connection configuration is 15.08kips (Figure 4-9 b). After the gravity load is applied, MDC2 was compressed by -2.78 in of translation (x-direction) then rotated by .087 rads about the horizontal in-plane façade panel axis (about y-axis). After this compression and rotation, a rebound phase occurs that creates an inward translation to -0.96 in (x-direction) and the rotation of -0.031 rads (about y-axis) relative to the original position (Figure 4-9 a). Lastly, MDC2 is brought back to its zero position (Figure 4-9 a).

Both the HSS and plates utilized the shell181 elements from the base model. When the MDC was compressed, the walls of the HSS contact the plates as the HSS deforms. Therefore, the model needed the contact/target elements from the base model. The ANSYS "target" elements were copied from the shell plate mesh to ensure they exactly overlapped. The plate shell nodes, plate target nodes, and the HSS nodes near the plate weld line were coupled together using the ANSYS "cerig" command to simulate the welded connection between the HSS and plates. The boundary conditions were then applied to each of these rigid areas using a master node. The standard holes on the frame plate and the short slotted holes on the panel plate were not modeled due to the plates behaving rigidly and not contributing to the MDC deformation. The frame plate was held fixed in all directions while the panel plate experienced the translation (x-direction) and rotation (about the y-axis) imposed by the hazard loading as well as the gravity load (z-direction) (Figure 4-9 c). The panel plate was also constrained from rotating about the z-axis. The plates for MDC2 were made into rigid components because the plates do not

deform or yield to absorb any of the loading energy. Only the circular HSS deforms to absorb the blast loading that MDC2 experiences (Appendix 1).

4.3.4.2 Convergence Study

Convergence studies were conducted to determine an appropriate mesh size for the model force-deformation, stress, and strain data. The average mesh sizes of the MDC2 components are available in Table 4-1. Convergence studies were conducted at two points on the HSS cross section and no points on the rigid plates (Figure 4-9 d). Both of these HSS cross section points were analyzed at approximately the center of the HSS (z-direction). Point P1 is at a hinge location on the HSS and point P2 is between the HSS hinge locations. The convergence studies were conducted at the two design-level translations and rotations. The first design-level deformations occurred at load step 20 has -2.78 in of translation (x-direction) and 0.087 radians of rotation (about y-axis) and the second design-level deformations occurred at load step 29 has -0.96 in of translation (x-direction) and -0.031 radians of deformation (about y-axis). The mesh size was reduced until the changes of force-deformation, stress, and strain change by 3% or less between the mesh sizes. The force-deformation curve converged by mesh size 3 (Figure 4-9 e), which was before most of the Von-Mises stress, Von-Mises elastic strain, or equivalent plastic strain converged. At P1, the Von-Mises stress converged at mesh size 4 during step 20 and 29. The P1 equivalent plastic strain converged at mesh size 5 during step 20 and mesh size 4 during step 29 (Figure 4-9 f). The Von-Mises stress and elastic strain at P2 converged with mesh size 2 at step 29 and mesh size 5 at step 20 (Figure 4-9 g). Point P1 required a finer mesh to converge because there is a large stress and strain

gradient at the HSS hinge. Mesh size 5 was the required mesh size for the convergence of all relevant FEA data and was used in the final MDC2 model.

4.3.4.3 Results

The MDC2 force-deformation FEA results reasonably represent experimental results until approximately -0.75 inches of inward radial translation (x-direction) (Figure 4-10 a). The nuts holding the frame and panel plates to the experimental setup begin contacting the MDC HSS around this deformation, which is not represented in the model. The experimental results from -0.75 inches to -2.87 inches of compressed translation (x-direction) show a larger increase in force than during 0 inches to -0.75 inches of translation. This is expected because in the experiment the HSS had to deform around the nuts after contacting them. As the MDC is pulled back out (x-direction) to its original position, less force is also required to overcome the additional strain hardening caused by the nut contact. The energy that the MDC absorbed during the FEA was determined by numerical integration of the area under the resulting force-deformation curve. From 0 inches to -2.78 inches of translation (x-direction), MDC2 absorbed approximately 35.7 kip-in of energy. The FEA reasonably approximated the energy absorption, which was 43 kip-in in the MDC2 experiment. The FEA produced deformed shapes, Von-Mises stress contour plots, and equivalent plastic strain contour plots (Figure 4-10 b-c). The maximum plastic strains (Figure 4-10 d) were very high (25%-50%) in a few elements near the weld of the HSS to the plates. The maximum plastic strain outside these weld areas were 20-25%. The plates did not experience stress, strain, or deformation during the FEA loading because they were assumed to be rigid during the analysis.

4.3.5 MDC Type 3 Model (MDC3)

4.3.5.1 Model Description

The MDC drawings are available in Appendix 2. The MDC type 3 (MDC3) must withstand all of the lateral in-plane forces applied to the façade panels and is designed to have elastic behavior throughout its loading. The analysis applied a 0.315 inch translation (z-direction) on the MDC3 to determine its elastic strength and ultimate strength (Figure 4-11 a). Seismic loading controls the critical forces for design of MDC3 (Appendix 1).

Both the HSS and plates utilized the shell181 elements from the base model. When the deformation is applied to MDC3, the walls of the HSS contact the plates as the HSS deforms. Therefore, this model also required the contact/target elements from the base model. MDC3 also has weld slots and standard bolt holes on the plates. Each plate has a total of sixteen bolt holes, with eight holes above and eight below (y-direction) the weld slot. It is assumed that no relative movement can occur within these bolt holes. The contact planes, and end plate constraints were created similar to previous MDC models. Both the HSS contact elements and target plate elements had the same mesh as the respective shell elements. Both of the plates were made rigid using the "cerig" command and each had a master node to control plate movement. The deformation was applied by holding one plate fixed in all directions while the other was translated laterally in-plane (z-direction) (Figure 4-11 c). This moving plate was also constrained from moving out of plane in the x and y directions.

4.3.5.2 Convergence Study

A convergence study was conducted to evaluate an appropriate mesh size for MDC3. Average mesh sizes for each MDC component used in the study are available in Table 4-1. The force-deformation, Von-Mises stress, Von-Mises elastic strain, and equivalent plastic strain were evaluated for convergence. Convergence occurred when the difference between force-deformation, stress, and strain values were less than 3% between mesh sizes. Two points on the HSS cross-section were studied for convergence, both of which were located near the center of the HSS (z-direction) (Figure 4-11 b). The force-deformation curve converged at mesh size 3 (Figure 4-11 d). The Von-Mises stress and equivalent plastic strain at P1 also converged at mesh size 3 (Figure 4-11 e). At the location of P2, the Von-Mises stress and elastic strain converged at mesh size 4 (Figure 4-11 f). Because most of the desired quantities had converged by or before mesh size 5, this mesh size was used in the final MDC3 model.

4.3.5.3 Results

The MDC3 model force-deformation curve is compared with the experimental force-deformation data in Figure 4-12 a. Beyond 0.2 inches of translation, the experiment specimen began moving out-of-plane. This out-of-plane accounts movement is believed to cause the large difference between the curves at 0.2-0.315 inches of deformation. It is observed that the FEA slightly overestimates the MDC elastic stiffness and strength while the model underestimates its material hardening. The FEA created deformed shapes and Von-Mises stress contours (Figure 4-12 b-c). In the plastic strain contours in Figure 4-12 d, small areas of extremely high strain are found at the HSS connection to the plates. The high plastic strains (50%-60%) in these regions are

unreasonable and are likely due to the way the HSS was rigidly connected to the plates within the model. It may also be due to inadequate mesh refinement in these localized areas. The plate/HSS connection likely caused only a few elements to experience high strains, while the other element plastic strains are reasonable (1%-5%).

4.4 Summary

An FEA model was created and first validated against the experimental data from Lavarnway (2013). Following this validation, the model was adapted to three current MDC designs subjected to more complex loading protocols consistent with the hazardous loading considered. The MDC models also included more realistic fabrication details.

All three of the MDC designs deformed as expected in the analyses. Under radial compression (x), the circular HSS of MDC2 initially created four plastic yield lines and then six yield lines as contact between the HSS and end plates occurred. Under radial tension, the HSS in MDC1 formed four plastic hinges. The 0.75in thick end plates of the MDC1 was also designed to yield and form a plastic mechanism to accommodate the large radially outward deformations and absorb a portion of the energy from the loading scenario. The design intent of MDC3 was to resist the prescribed loads in an elastic manner however the analysis performed determined the ultimate force deformation behavior of the MDC in addition to confirming the intended elastic strength. Overall, the analysis of the three MDC designs provided force-deformation behavior, deformed shapes, stress, and plastic strains consistent with the MDCs design intent. Some of the models experienced very large plastic strains. However, these high strains occurred on very few elements in the models in regions where the mesh refinement was likely inadequate to capture the large strain gradient.

When compared to the design calculations, the FEA models performed as expected in terms of critical force, deformation, or energy absorption criteria for each MDC type (Table 4-2). The maximum tensile force of MDC1 FEA model was 51 kips, which is near the expected max force of 45.9 kips from the design calculations. However, the individual components of MDC1 behaved differently in the FEA model than in the design. The HSS was responsible for less than its design deformation, while the maximum plate deformation varied from their design deformation. Both plates were anticipated to deform the same about, and they did do so in MDC1 Model 1. However, the frame plate deformed more than the panel plate in MDC1 Model 2. MDC2 absorbed 35.7 kip-in of energy, which is 15% loxwer the design energy absorption. MDC2 also experienced approximately the same compressive force in the FEA as expected in the design (19 kips). Lastly, the MDC3 model showed the MDC remains elastic up to the design elastic load of 120 kips. MDC3 had an ultimate strength of 151 kips in the model. The calculations assumed that the shear capacity of the MDC3 tube was dependent on the center cross section of the HSS. The failure of the HSS in MCD3 may move from outside the center to the center, which would cause a lower maximum force.

	MDC Component	Mesh 1	Mesh 2	Mesh 3	Mesh 4	Mesh 5	**Mesh 6**
MDC1	HSS	1.89 in	0.94 in	0.63 in	0.47 in	0.31 in	**0.24 in**
	Frame Plate	0.70 in	0.53 in	0.42 in	0.35 in	0.26 in	**0.21 in**
	Panel Plate	1.16 in	0.70 in	0.50 in	0.39 in	0.27 in	**0.20 in**

	MDC Component	Mesh 1	Mesh 2	Mesh 3	Mesh 4	**Mesh 5**
MDC2	HSS	1.35 in	0.79 in	0.41 in	0.29 in	**0.25 in**
	Frame Plate	1.04 in	0.72 in	0.38 in	0.28 in	**0.24 in**
	Panel Plate	1.04 in	0.72 in	0.38 in	0.28 in	**0.24 in**

	MDC Component	Mesh 1	Mesh 2	Mesh 3	Mesh 4	**Mesh 5**
MDC3	HSS	1.57 in	0.67 in	0.41 in	0.30 in	**0.24 in**
	Frame Plate	1.58 in	0.70 in	0.42 in	0.32 in	**0.24 in**
	Panel Plate	1.91 in	0.84 in	0.51 in	0.38 in	**0.30 in**

Table 4- 1 Convergence study mesh sizes for each MDC component. Final mesh size for each MDC model is bold.

	Maximum Tensile Force (kips)			Maximum HSS Translation (in)		
	Design	FEA Model 1	FEA Model 2	Design	FEA Model 1	FEA Model 2
MDC1	45.9	47.5	50.9	1.6	1.44	1.55
	Maximum Panel Plate Translation (in)			Maximum Frame Plate Translation (in)		
	Design	FEA Model 1	FEA Model 2	Design	FEA Model 1	FEA Model 2
	0.75	0.86	1.17	0.75	0.80	0.38

	Energy Dissipation (kip-in)		Maximum Compressive Force (kips)	
MDC2	Design	FEA	Design	FEA
	30.9	35.7	36.2	19.0

	Elastic Strength (kips)		Ultimate Strength (kips)	
MDC3	Design	FEA	Design	FEA
	135	120	N/A	151.4

Table 4- 2 Comparison of the FEA results to the desired design values for each MDC

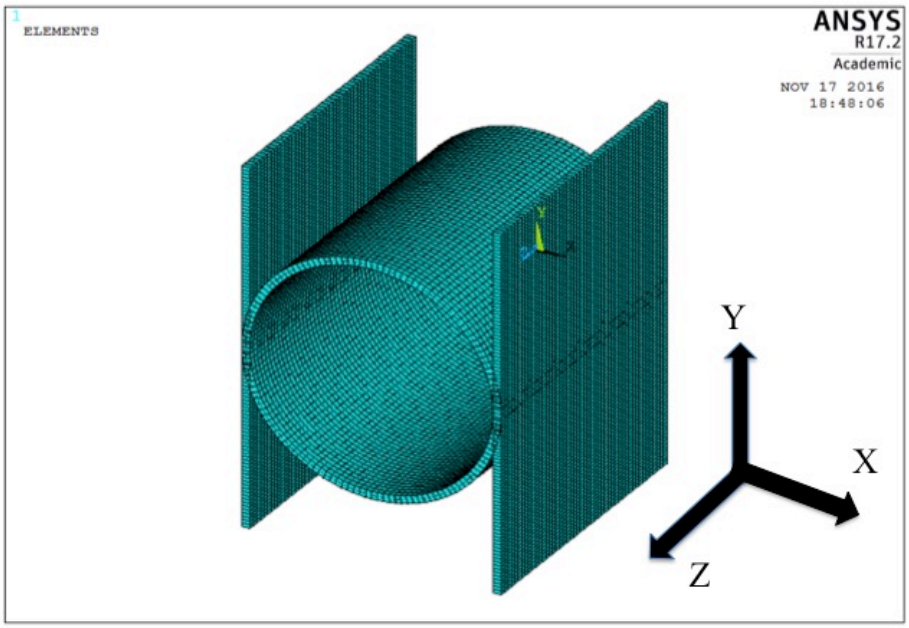

Figure 4-1 An example base model showing the coordinate system for all of the base and MDC models

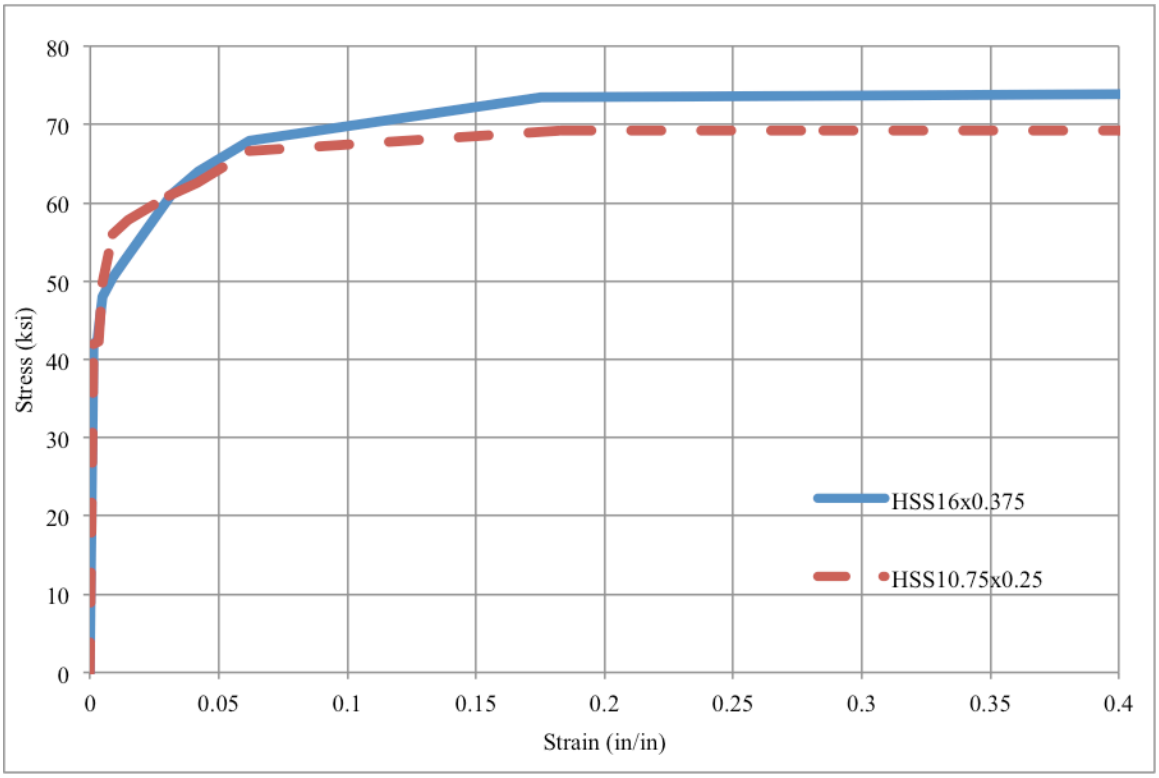

Figure 4-2 Stress-strain curves input into the base FEA models for HSS16x0.375 and HSS10.75x0.25. Based on tensile coupon data from Lavarnway (2013) experiments

Figure 4-3 HSS10.75x0.25 Base Model FEA Results a) Force-deformation response including comparison between FEA and Lavarnway (2013) experiment b) Deformed shapes of HSS10.75x0.25 c) Von-Mises stress of the HSS10x0.25 at δ_{HSS}=6". Stress in units of ksi. d) Plastic strain of the HSS10x0.25 at δ_{HSS}=6"

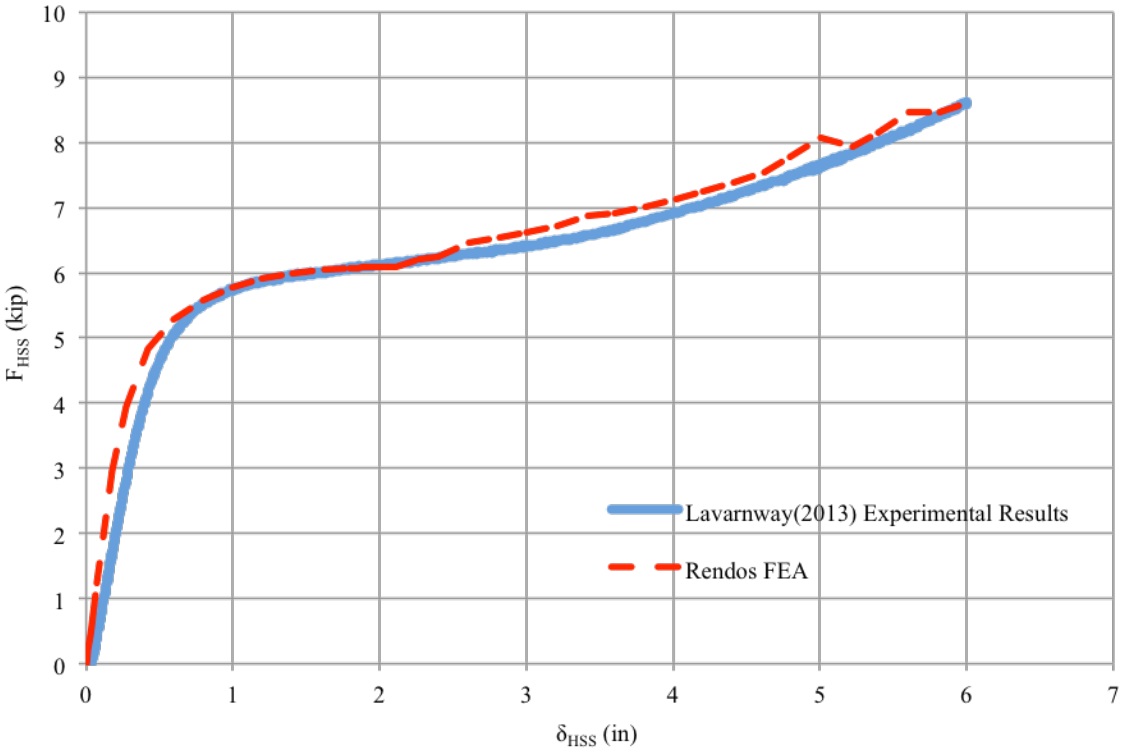

a)

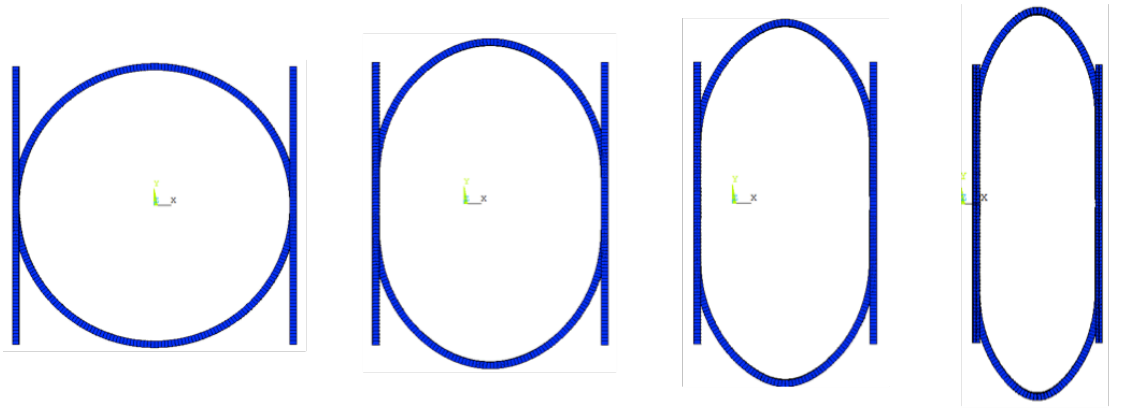

δ_{HSS}= 0" δ_{HSS}= 2" δ_{HSS}= 4" δ_{HSS}= 6"

b)

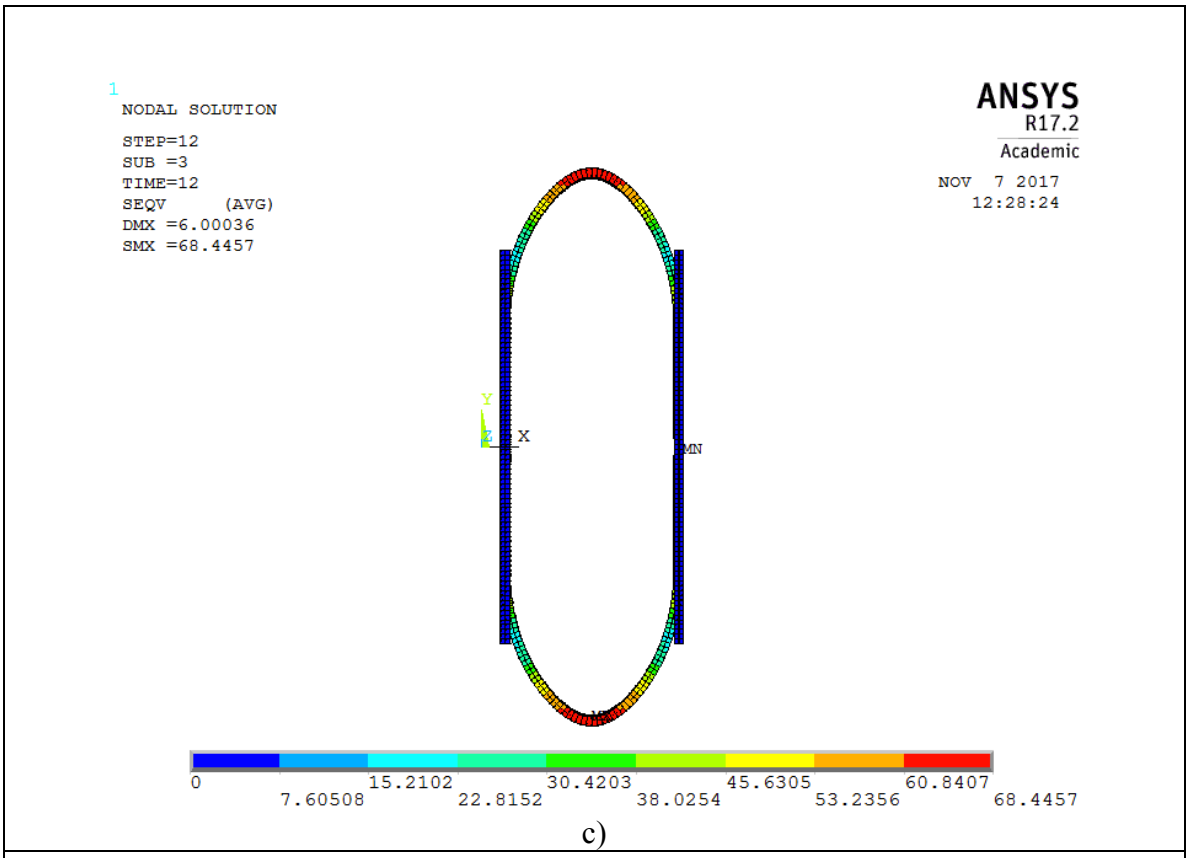
1
NODAL SOLUTION
STEP=12
SUB =3
TIME=12
SEQV (AVG)
DMX =6.00036
SMX =68.4457
ANSYS
R17.2
Academic
NOV 7 2017
12:28:24
Y
Z X
MN
MX
0
7.60508
15.2102
22.8152
30.4203
38.0254
45.6305
53.2356
60.8407
68.4457

c)

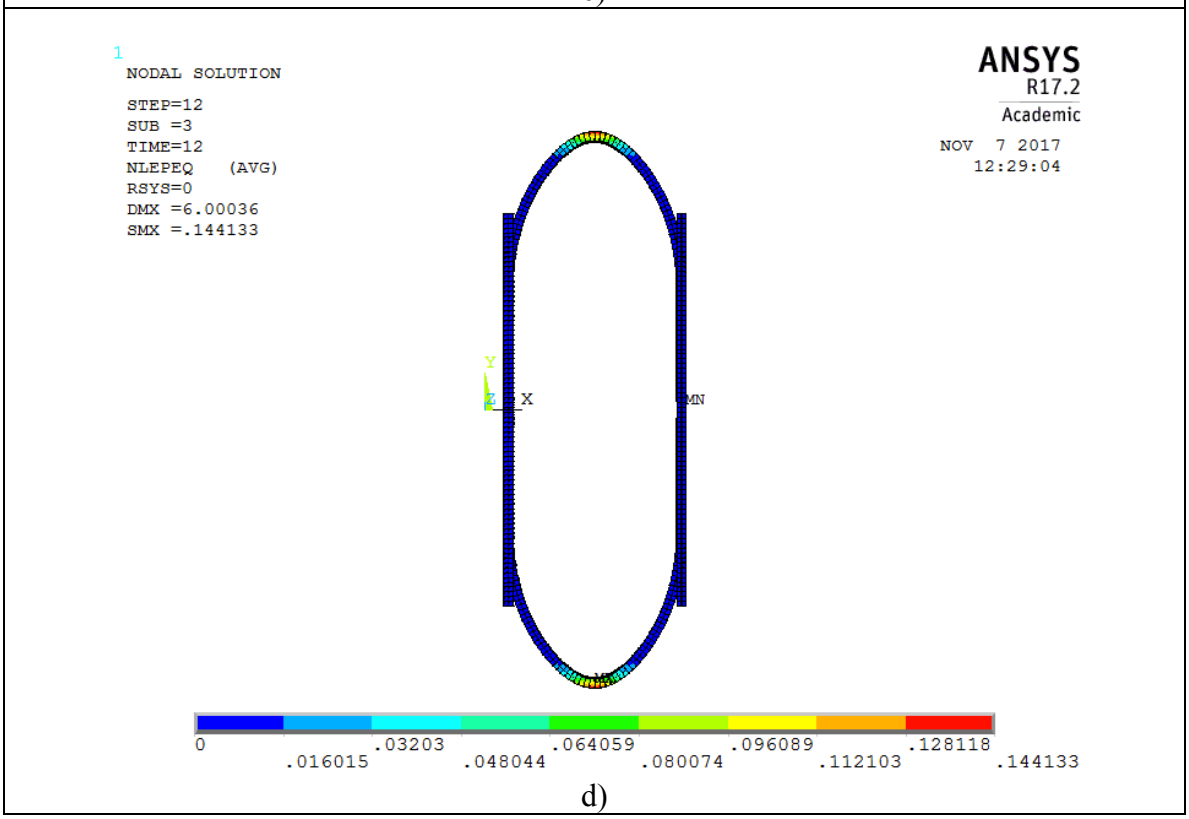
1
NODAL SOLUTION
STEP=12
SUB =3
TIME=12
NLEPEQ (AVG)
RSYS=0
DMX =6.00036
SMX =.144133
ANSYS
R17.2
Academic
NOV 7 2017
12:29:04
Y
Z X
MN
MX
0
.016015
.03203
.048044
.064059
.080074
.096089
.112103
.128118
.144133

d)

Figure 4-4 HSS16x0.375 Base Model FEA Results a) Force-deformation response including comparison between FEA and Lavarnway (2013) experiment b) Deformed shapes of HSS16x0.375 c) Von-Mises stress of the HSS16x0.375 at δ_{HSS}=6". Stress in units of ksi. d) Plastic strain of the HSS16x0.375 at δ_{HSS}=6"

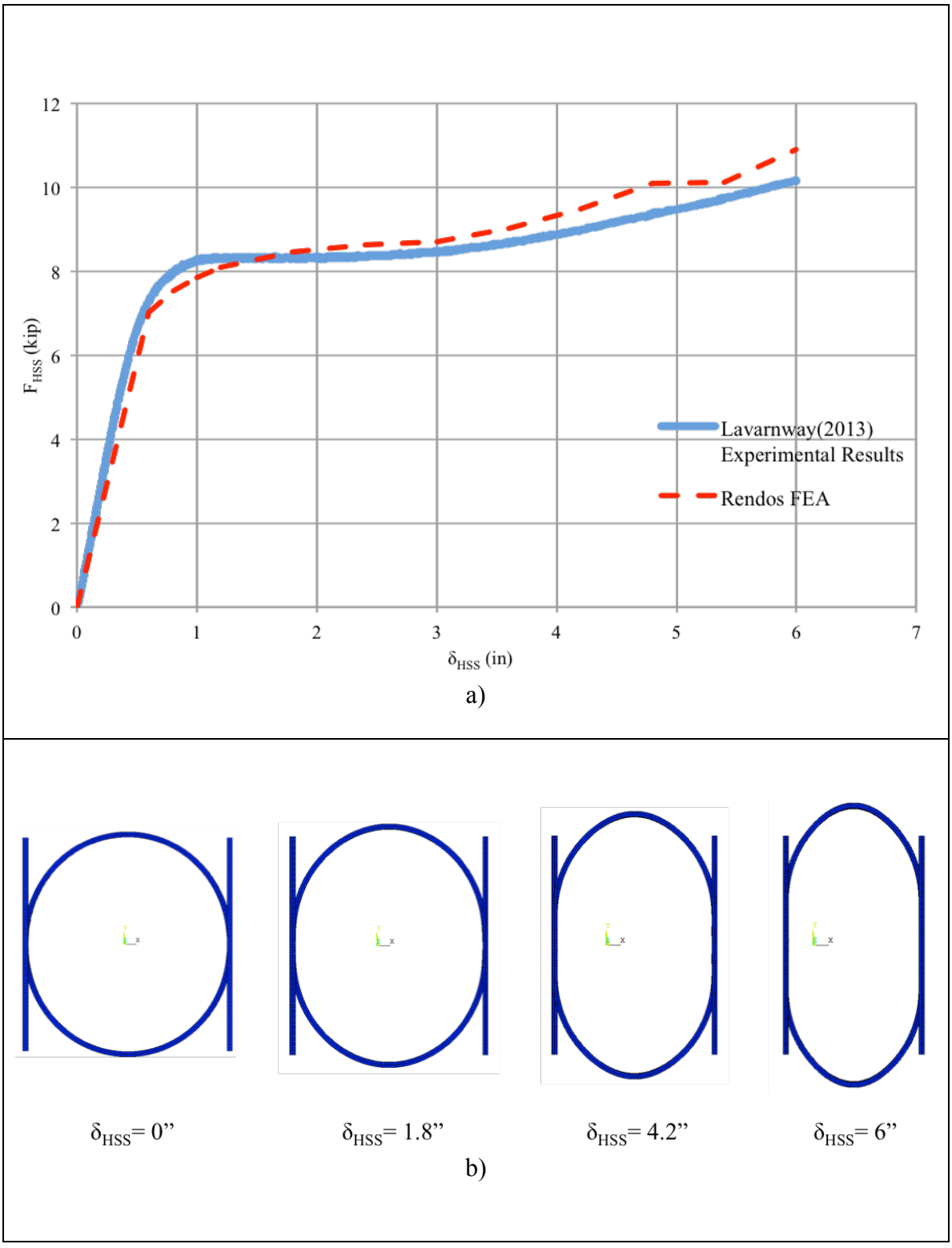

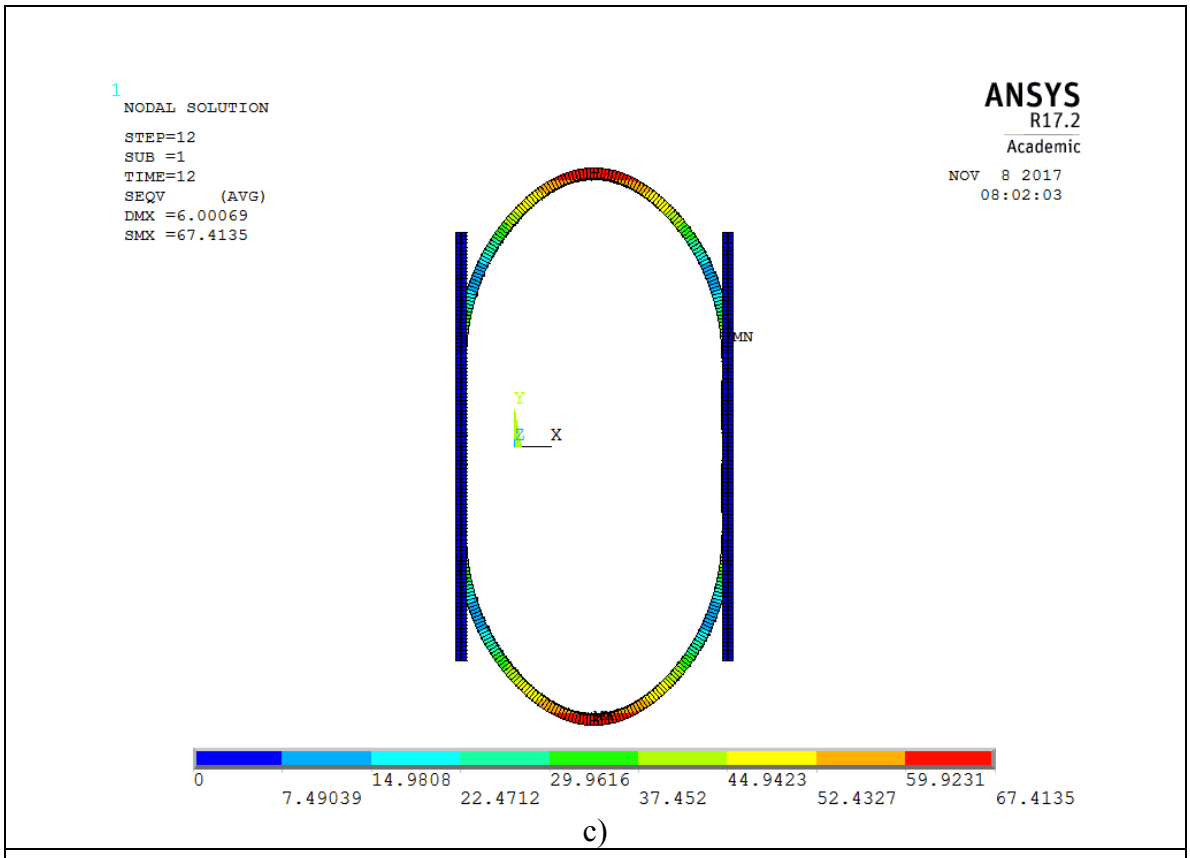
1
NODAL SOLUTION
STEP=12
SUB =1
TIME=12
SEQV (AVG)
DMX =6.00069
SMX =67.4135
ANSYS
R17.2
Academic
NOV 8 2017
08:02:03
MN
Y
Z X
0
7.49039
14.9808
22.4712
29.9616
37.452
44.9423
52.4327
59.9231
67.4135

c)

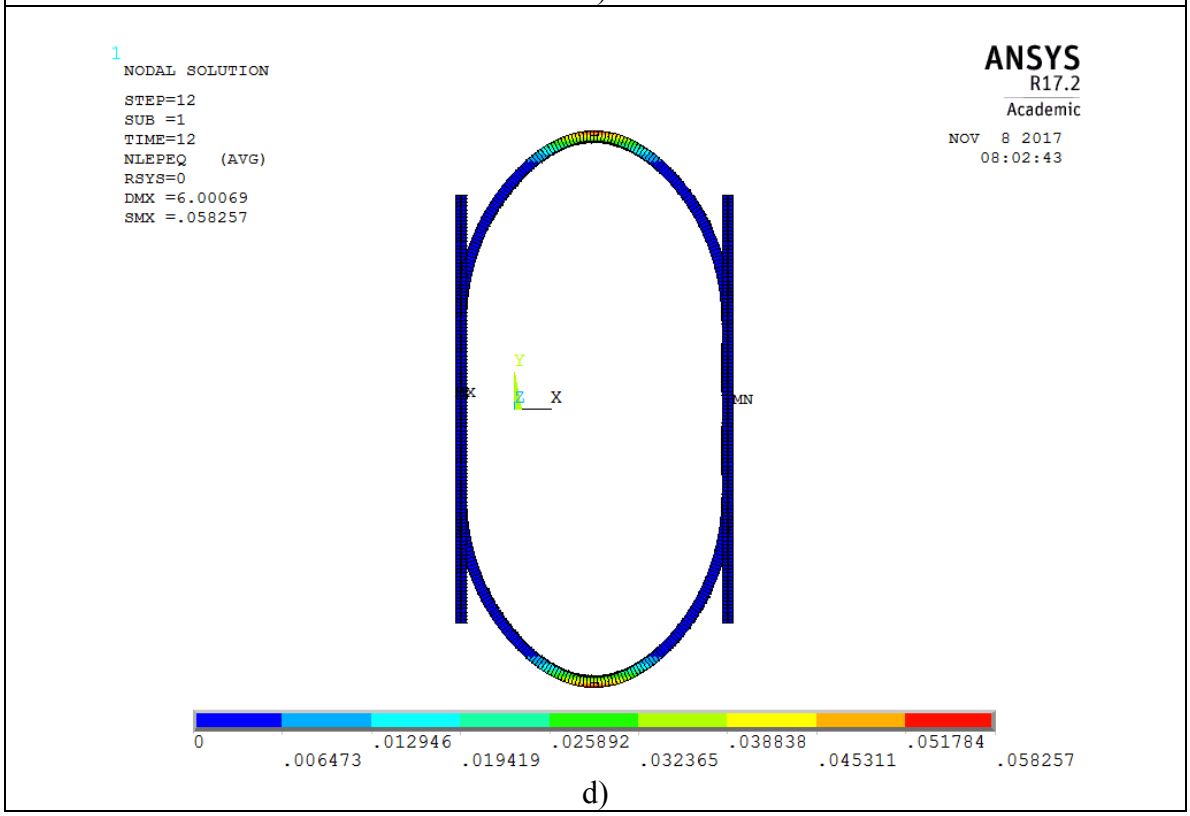
1
NODAL SOLUTION
STEP=12
SUB =1
TIME=12
NLEPEQ (AVG)
RSYS=0
DMX =6.00069
SMX =.058257
ANSYS
R17.2
Academic
NOV 8 2017
08:02:43
MN
Y
Z X
0
.006473
.012946
.019419
.025892
.032365
.038838
.045311
.051784
.058257

d)

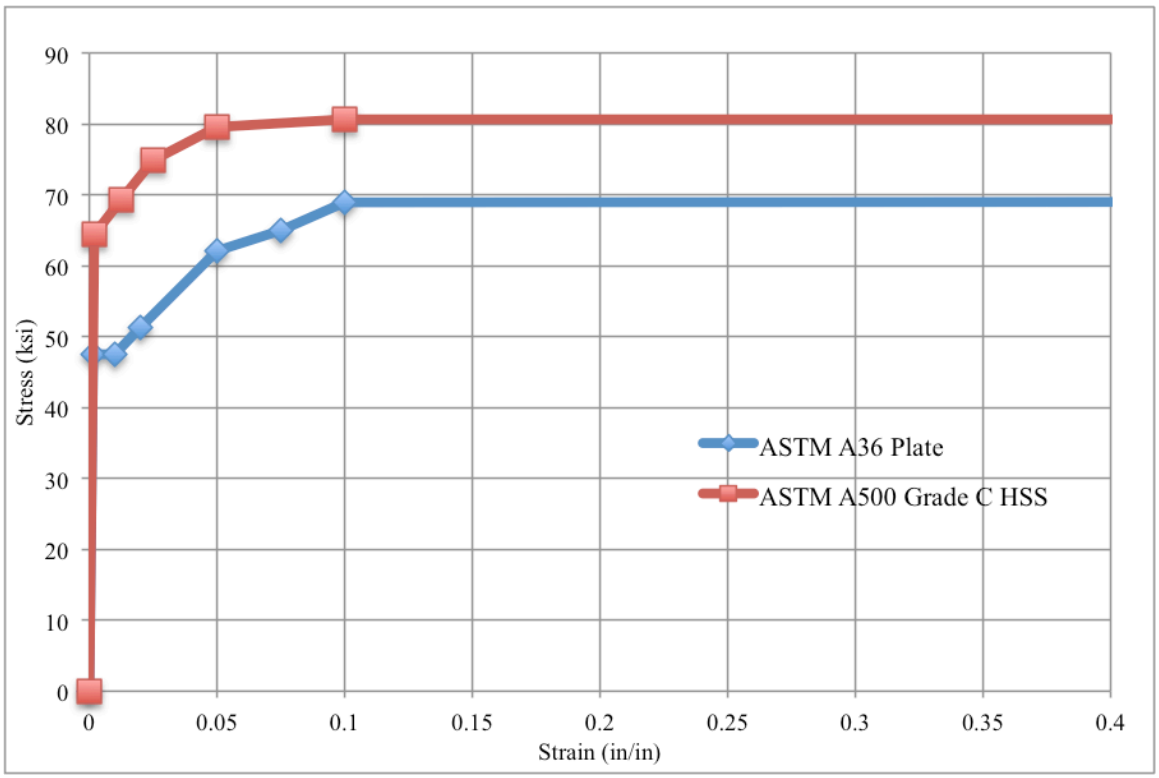

Figure 4-5 Stress-Strain data defining MDC material models for A36 plate and A500 Grade C HSS used in the FEA

Figure 4-6 MDC1 Convergence study at design basis of 3.1in translation and 0.025 rads rotation a) Deformation (x-direction) and rotation (about z- axis) applied in the FEA b) Approximate point locations on MDC1 cross section analyzed for convergence study c) Model 1 and Model 2 boundary conditions d) Force-Deformation results e) Convergence results of P1 on HSS f) Convergence results of P2 on HSS g) Convergence results of P3 on frame plate h) Convergence results of P4 on panel plate

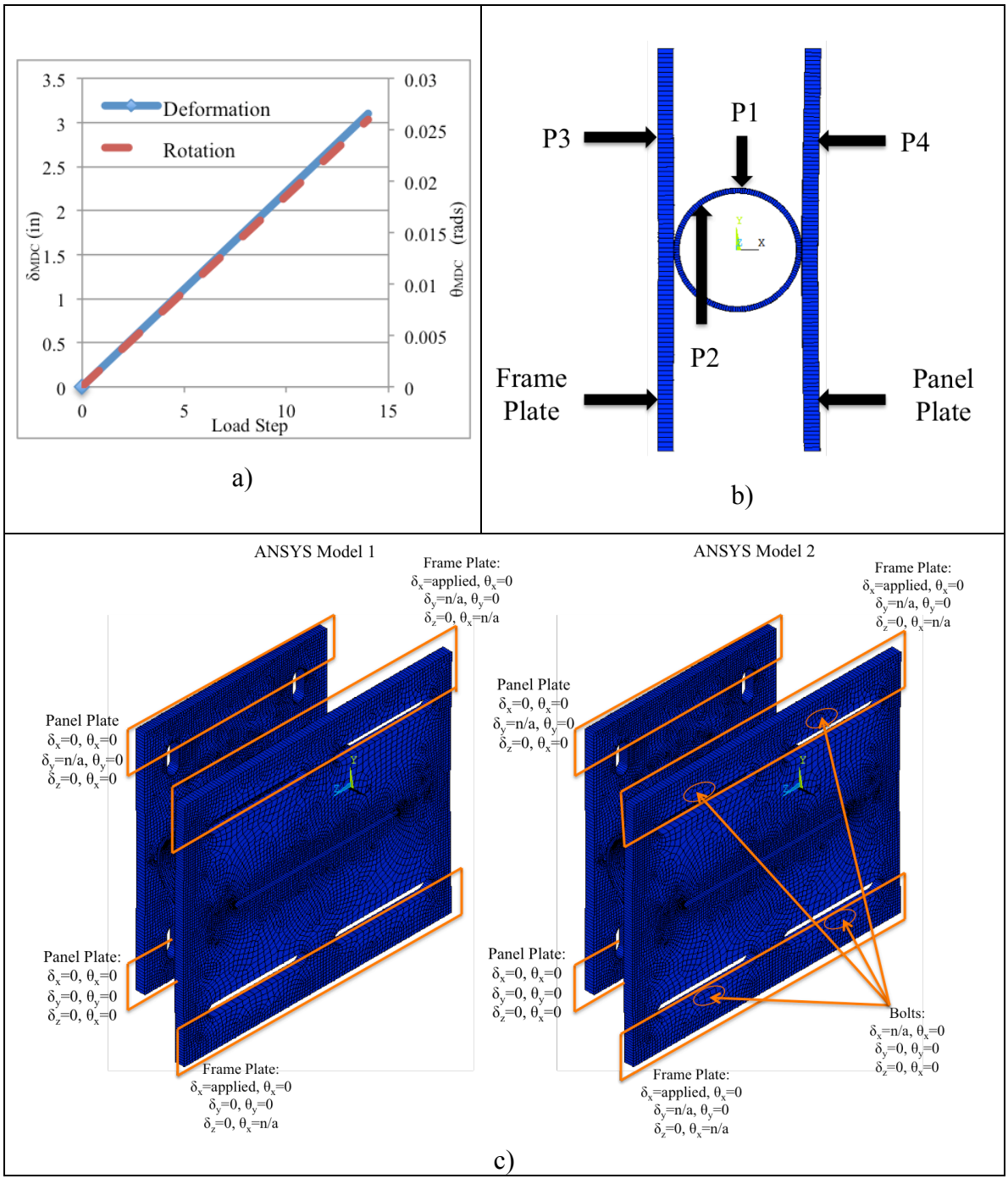

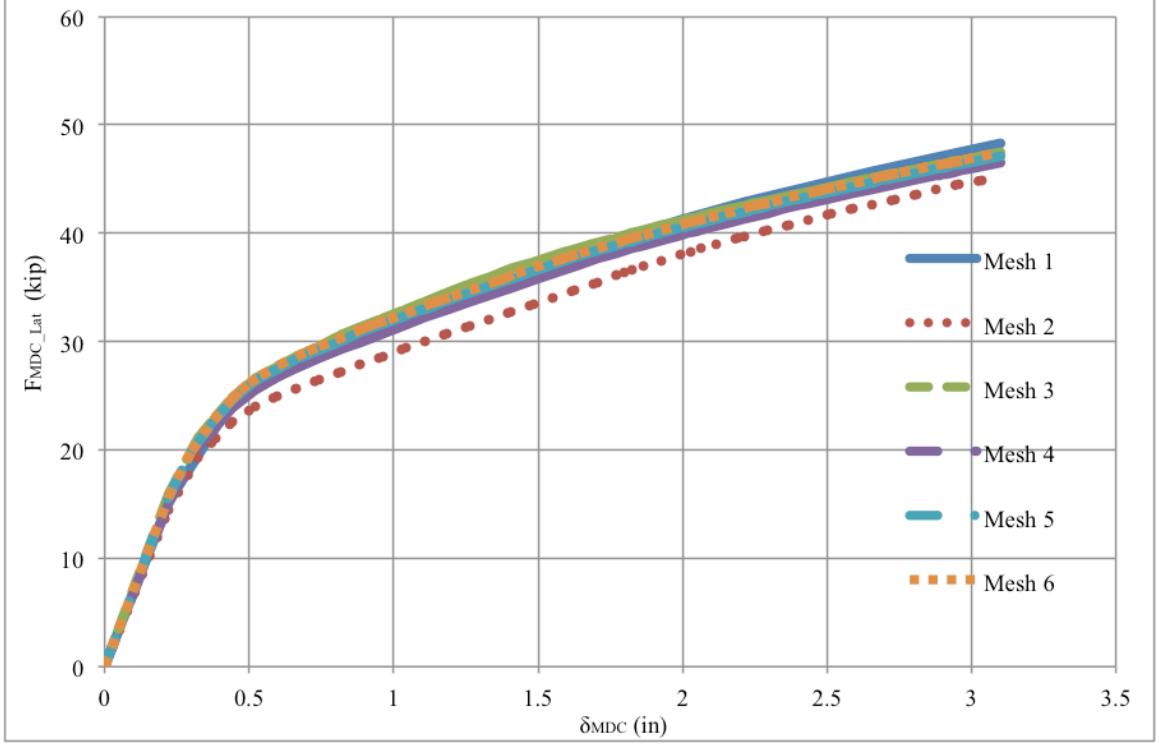
60
50
40
30
20
10
0
0
0.5
1
1.5
2
2.5
3
3.5
FMDC_Lat (kip)
δMDC (in)
Mesh 1
Mesh 2
Mesh 3
Mesh 4
Mesh 5
Mesh 6

d)

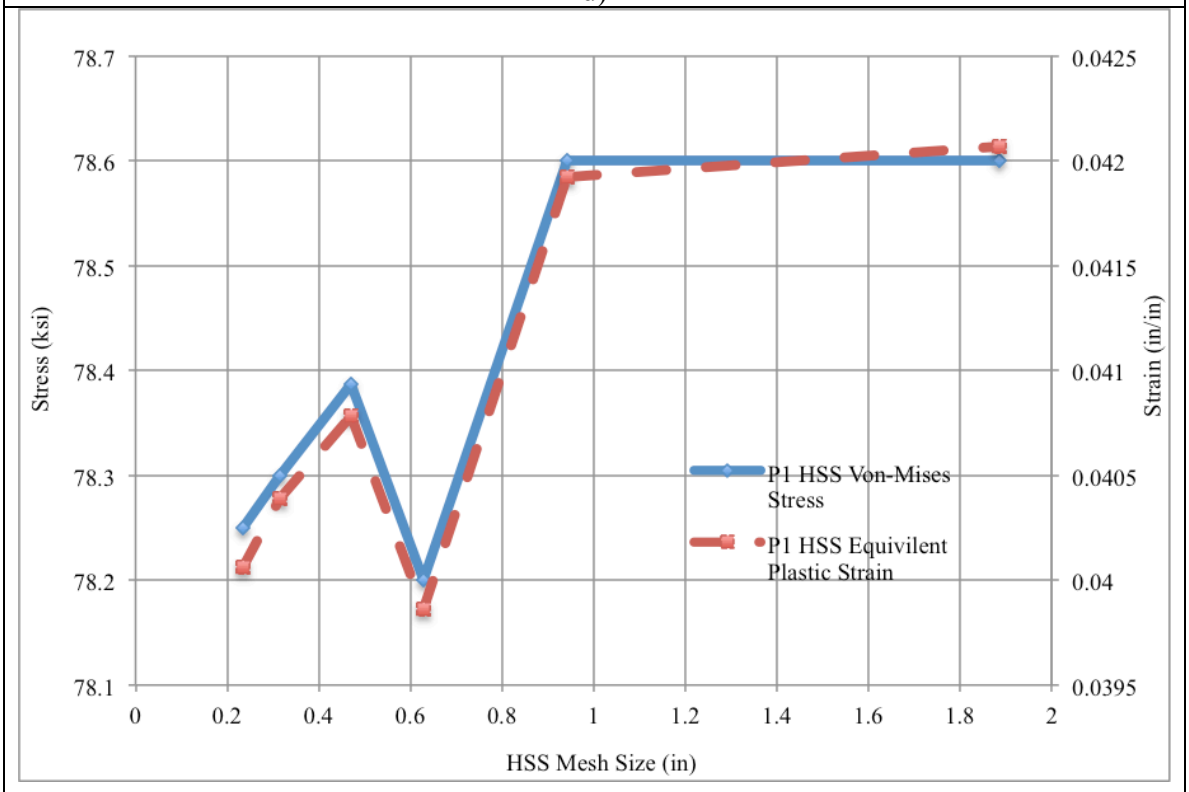
78.7
78.6
78.5
78.4
78.3
78.2
78.1
0.0425
0.042
0.0415
0.041
0.0405
0.04
0.0395
0
0.2
0.4
0.6
0.8
1
1.2
1.4
1.6
1.8
2
Stress (ksi)
Strain (in/in)
HSS Mesh Size (in)
P1 HSS Von-Mises Stress
P1 HSS Equivilent Plastic Strain

e)

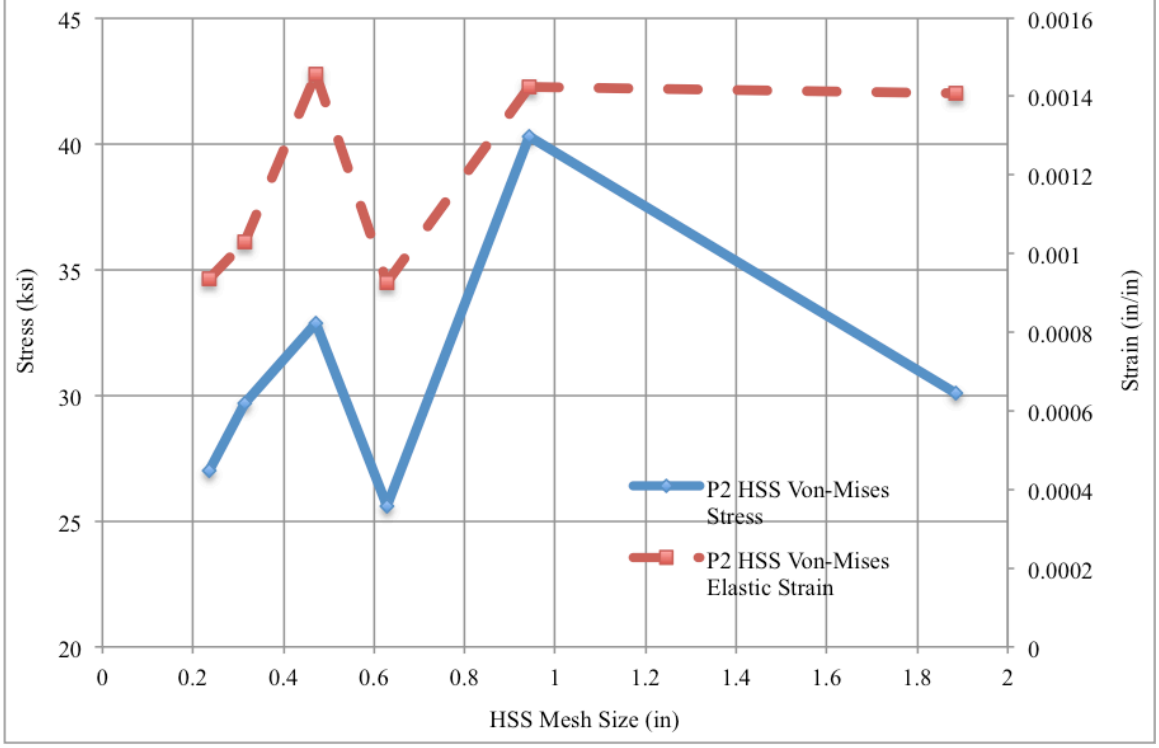
45
40
35
30
25
20
Stress (ksi)
0.0016
0.0014
0.0012
0.001
0.0008
0.0006
0.0004
0.0002
0
Strain (in/in)
0
0.2
0.4
0.6
0.8
1
1.2
1.4
1.6
1.8
2
HSS Mesh Size (in)
P2 HSS Von-Mises Stress
P2 HSS Von-Mises Elastic Strain

f)

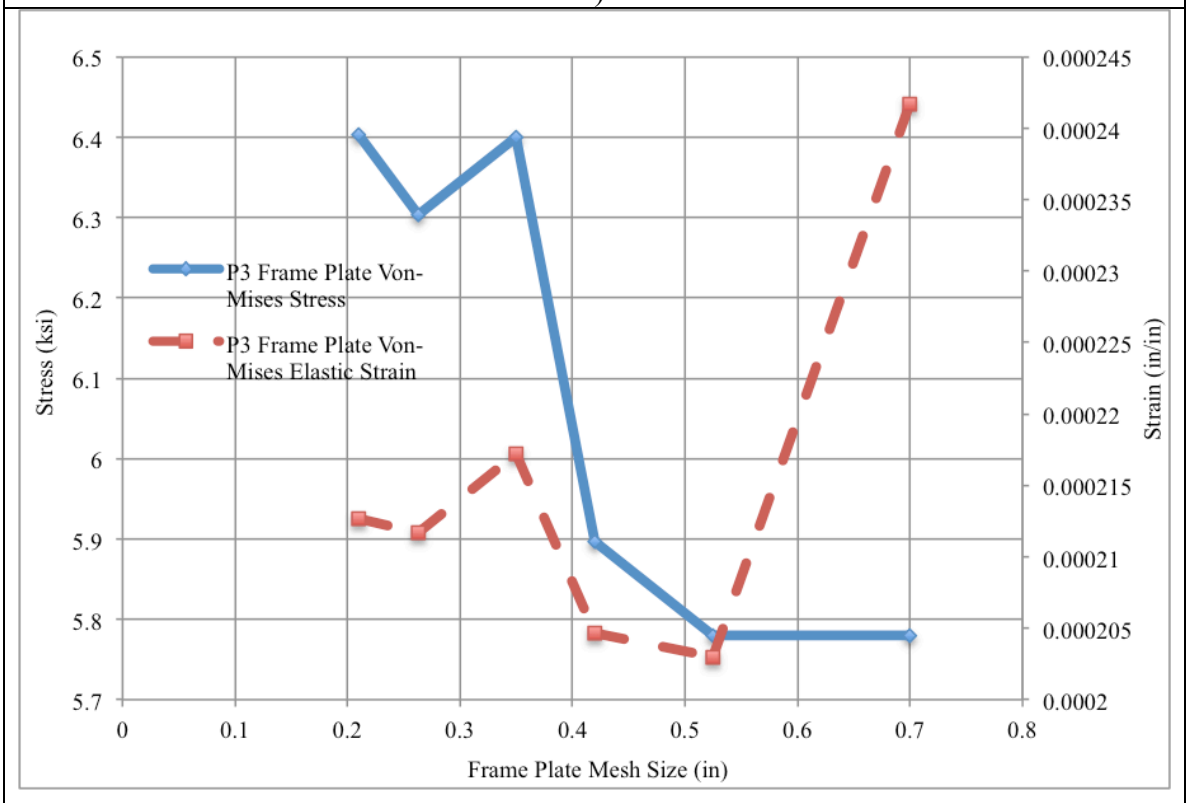
6.5
6.4
6.3
6.2
6.1
6
5.9
5.8
5.7
Stress (ksi)
0.000245
0.00024
0.000235
0.00023
0.000225
0.00022
0.000215
0.00021
0.000205
0.0002
Strain (in/in)
0
0.1
0.2
0.3
0.4
0.5
0.6
0.7
0.8
Frame Plate Mesh Size (in)
P3 Frame Plate Von-Mises Stress
P3 Frame Plate Von-Mises Elastic Strain

g)

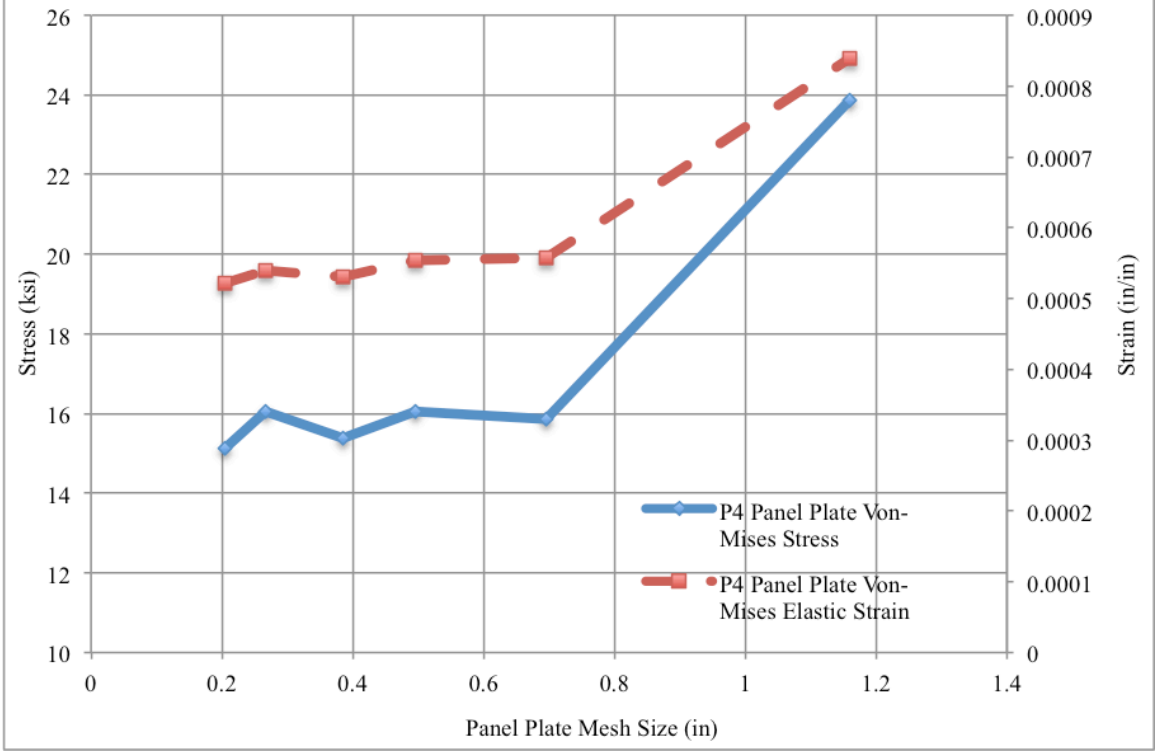
26
24
22
20
18
16
14
12
10
Stress (ksi)
0.0009
0.0008
0.0007
0.0006
0.0005
0.0004
0.0003
0.0002
0.0001
0
Strain (in/in)
0
0.2
0.4
0.6
0.8
1
1.2
1.4
Panel Plate Mesh Size (in)
P4 Panel Plate Von-Mises Stress
P4 Panel Plate Von-Mises Elastic Strain

h)

Figure 4-7 FEA Results of MDC1 a) Force-deformation curves of the FEA and MDC1 experiment b) Force-deformation curves of the MDC components from the FEA and MDC1 experiment c) Deformed shapes throughout the FEA

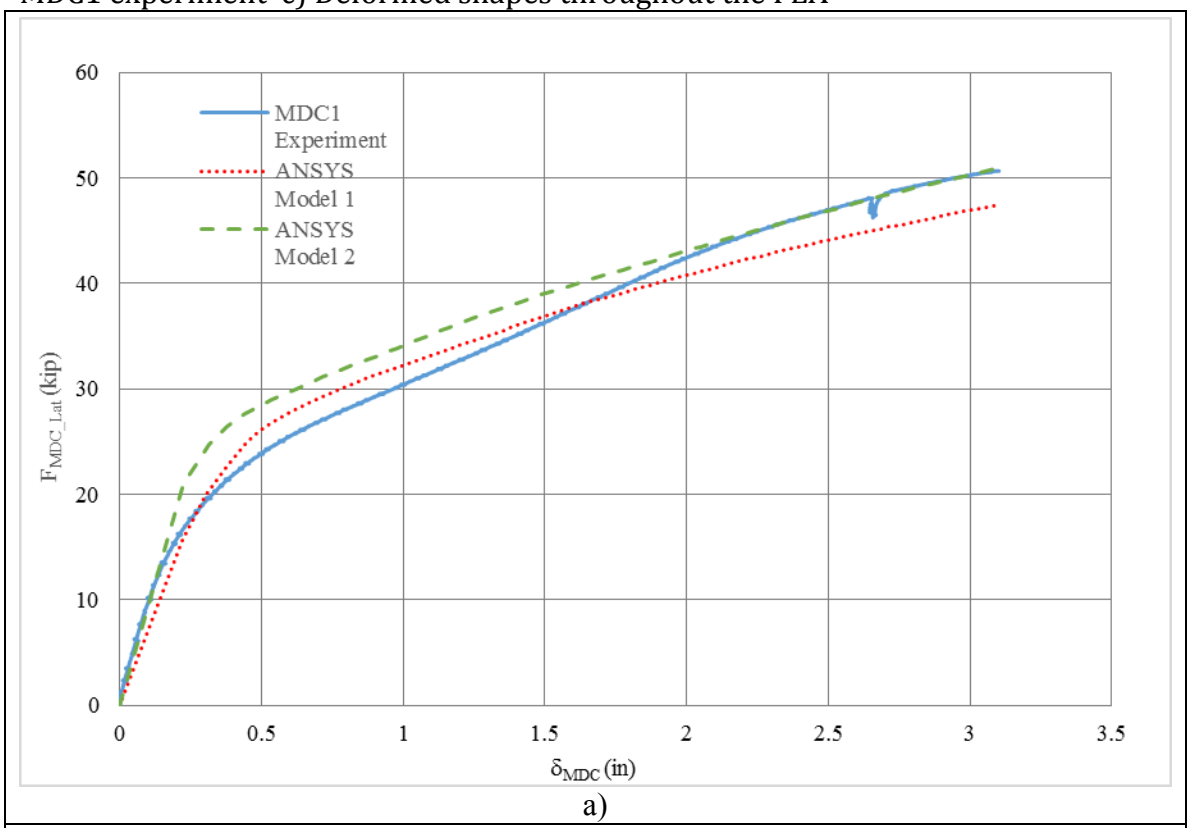

a)

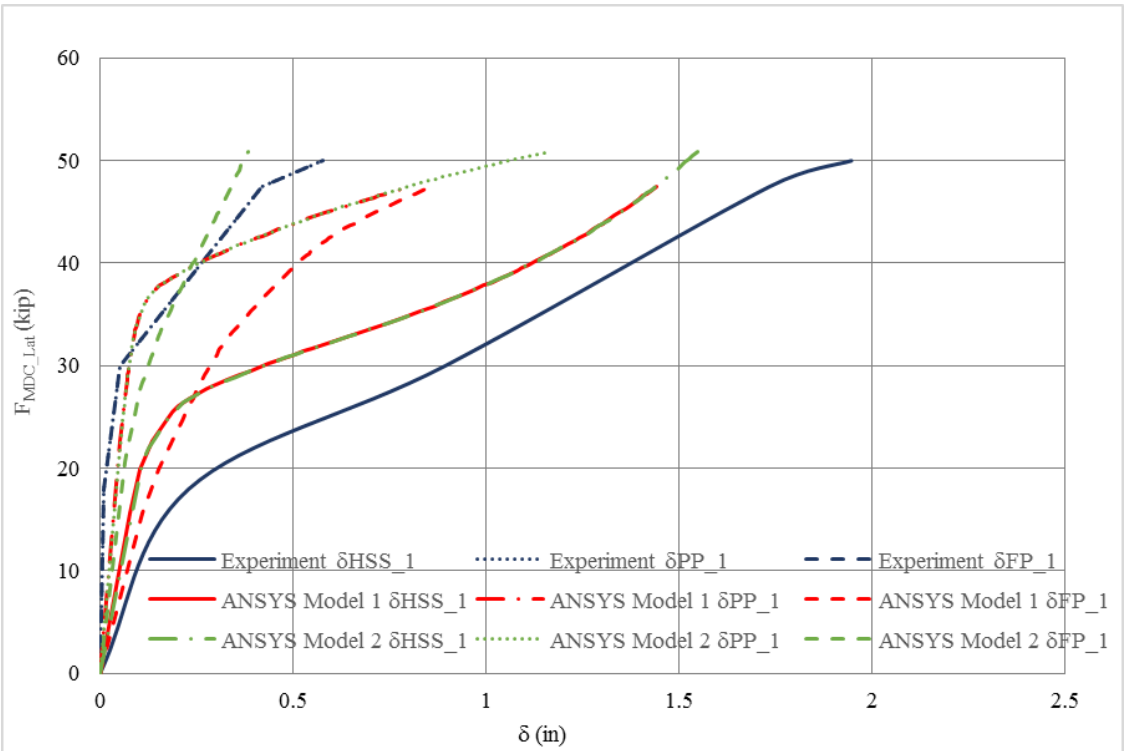

b)

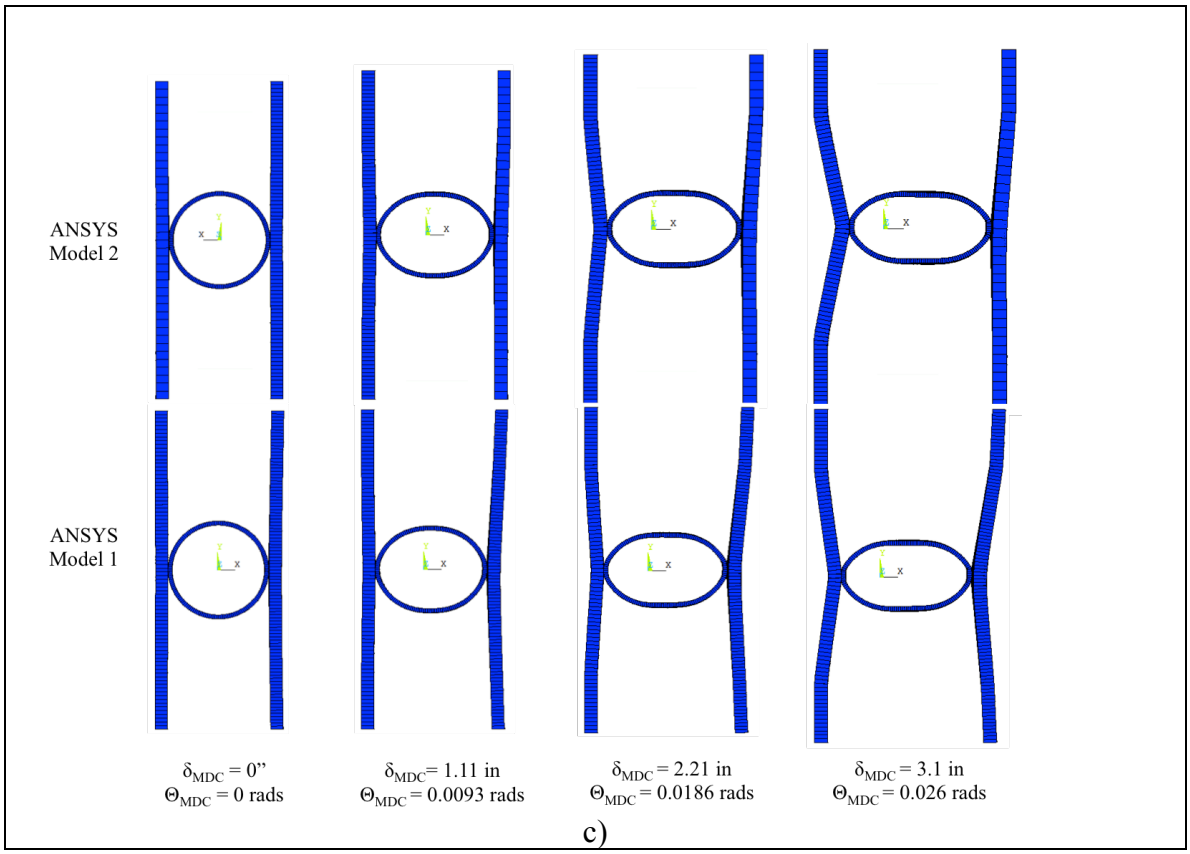
ANSYS
Model 2
ANSYS
Model 1
δMDC = 0”
ΘMDC = 0 rads
δMDC= 1.11 in
ΘMDC = 0.0093 rads
δMDC = 2.21 in
ΘMDC = 0.0186 rads
δMDC = 3.1 in
ΘMDC = 0.026 rads

c)

Figure 4-8 FEA MDC1 Stress and Strain Contours a) Model 1 Von-Mises stress (ksi) contours at the design deformation and rotation b) Model 2 Von-Mises stress (ksi) contours at the design deformation and rotation c) Model 1 Equivalent plastic strain contours at the design deformation and rotation d) Model 2 Equivalent plastic strain contours at the design deformation and rotation

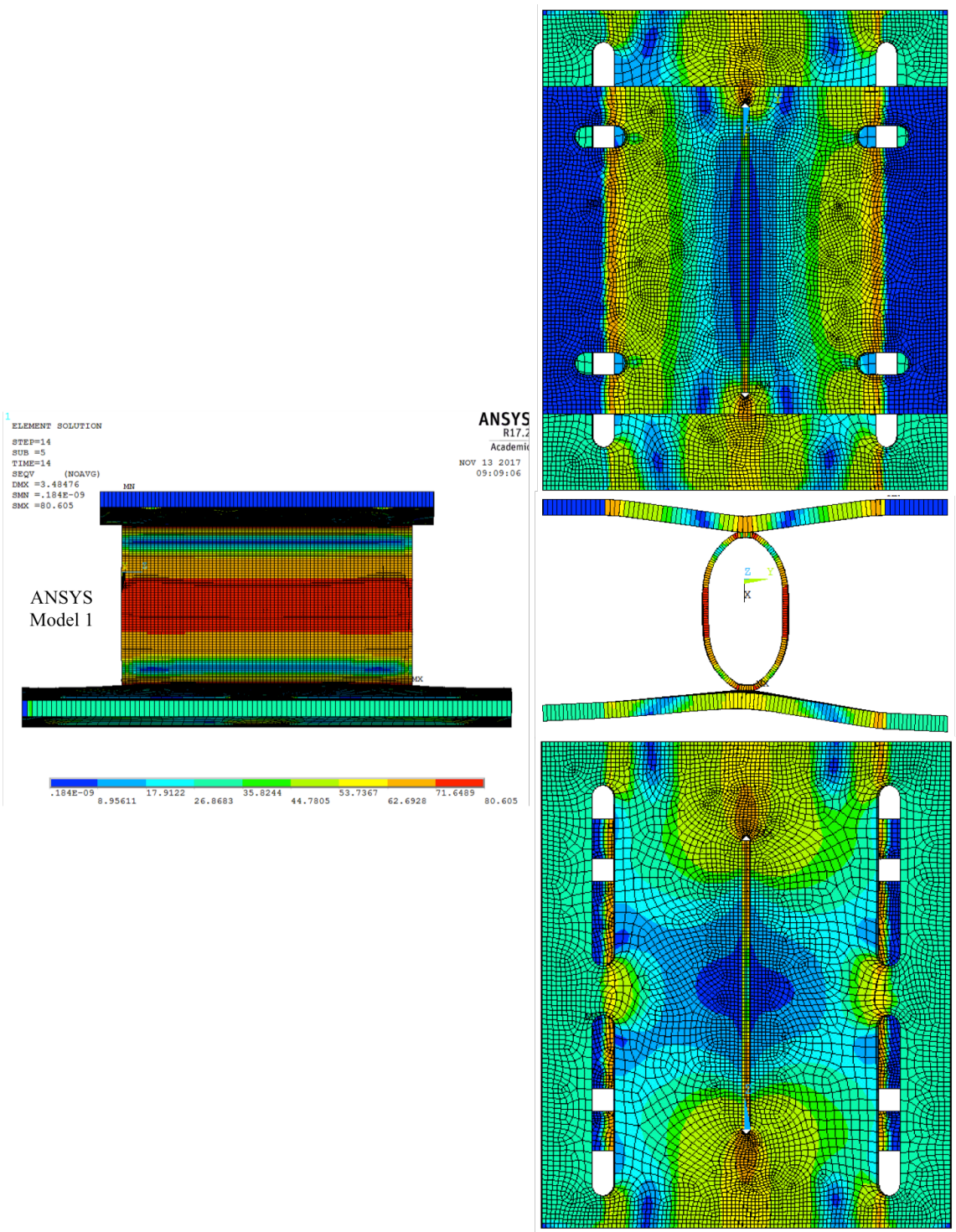

a)

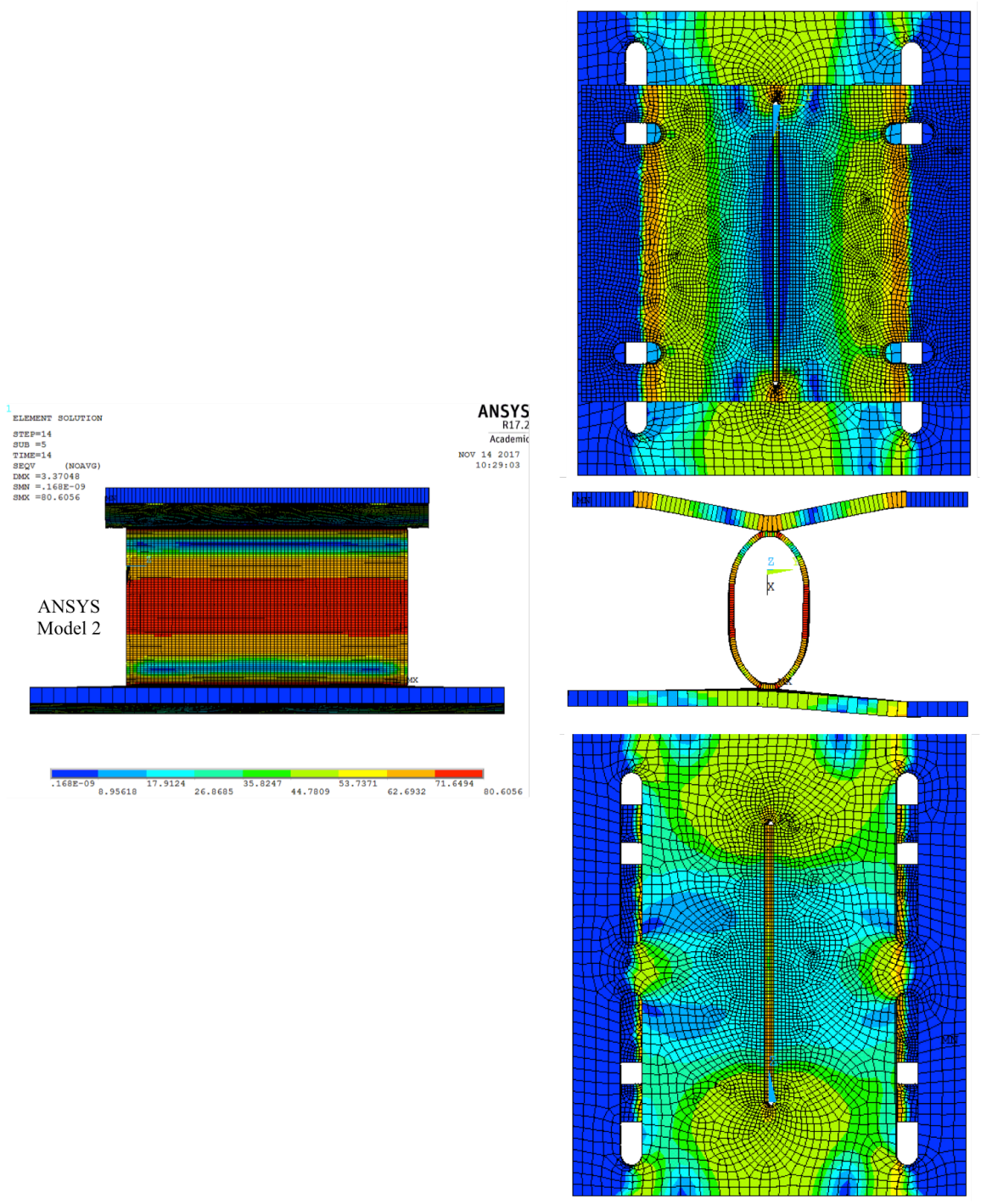
ELEMENT SOLUTION
STEP=14
SUB =5
TIME=14
SEQV (NOAVG)
DMX =3.37048
SMN =.168E-09
SMX =80.6056
ANSYS
R17.2
Academic
NOV 14 2017
10:29:03
ANSYS
Model 2
.168E-09
8.95618
17.9124
26.8685
35.8247
44.7809
53.7371
62.6932
71.6494
80.6056

b)

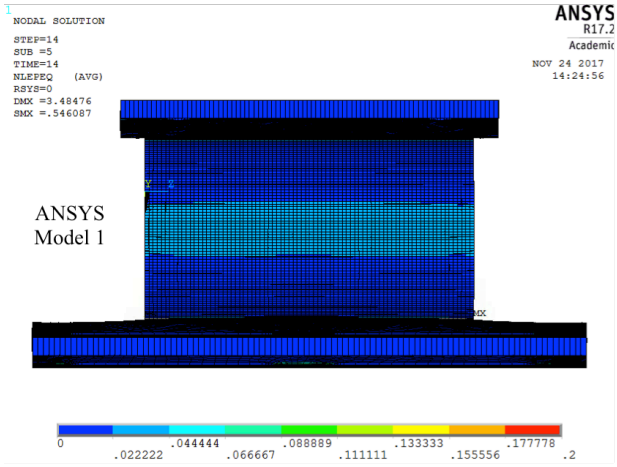
NODAL SOLUTION
STEP=14
SUB =5
TIME=14
NLEPEQ (AVG)
RSYS=0
DMX =3.48476
SMX =.546087
ANSYS
R17.2
Academic
NOV 24 2017
14:24:56
ANSYS
Model 1
0
.022222
.044444
.066667
.088889
.111111
.133333
.155556
.177778
.2

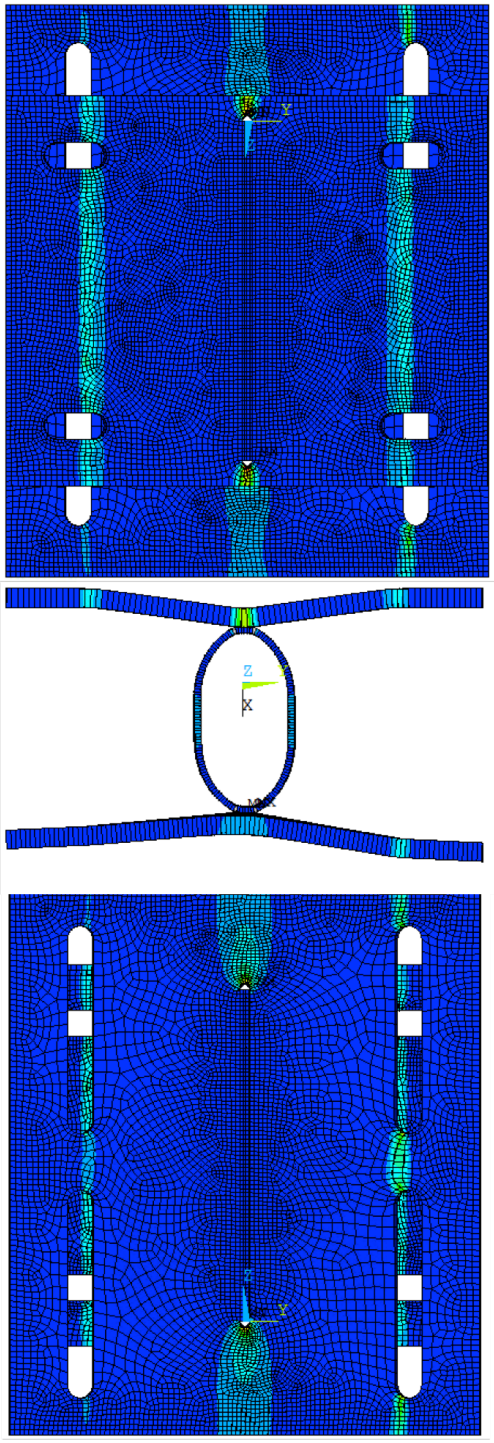

c)

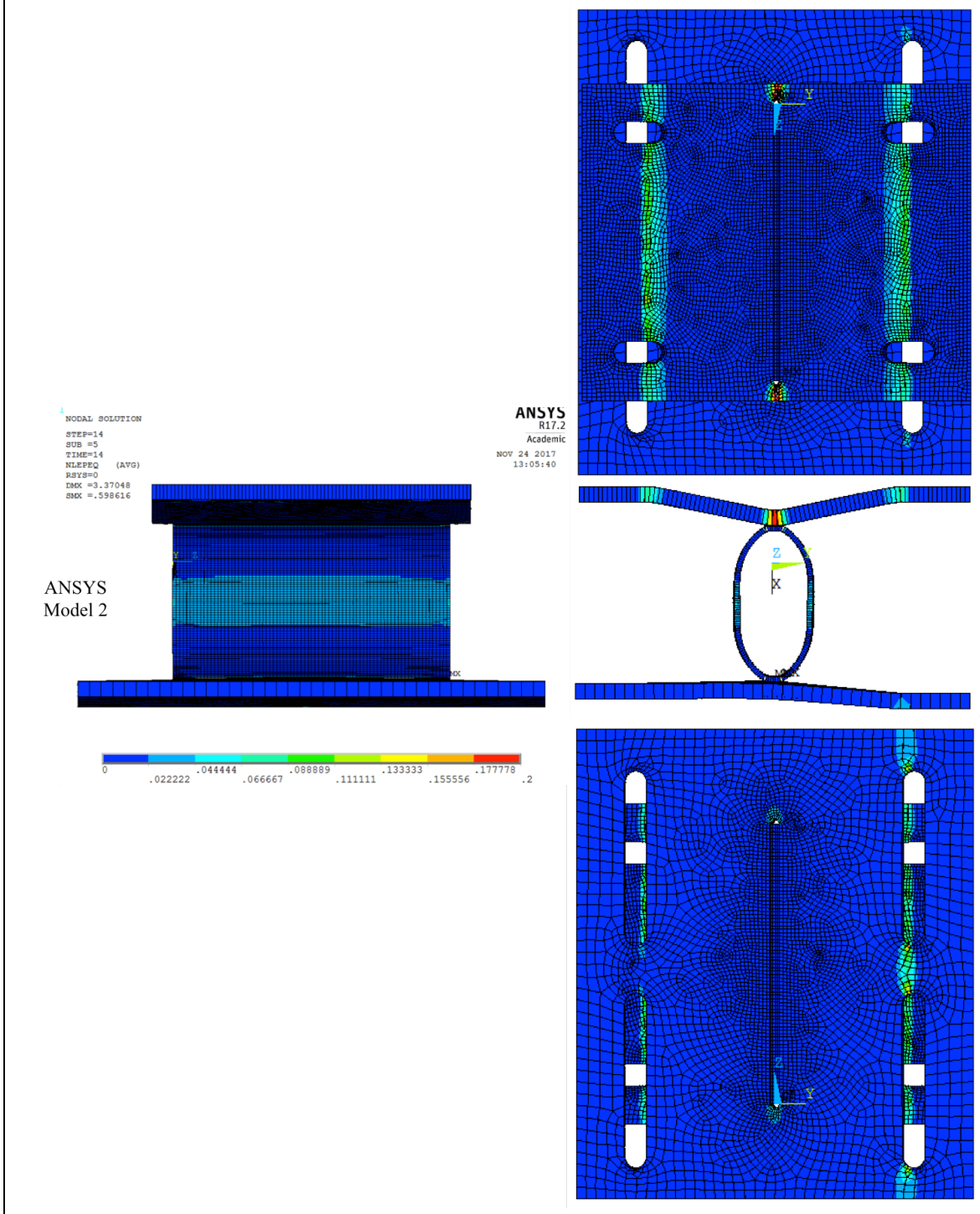
NODAL SOLUTION
STEP=14
SUB =5
TIME=14
NLEPEQ (AVG)
RSYS=0
DMX =3.37048
SMX =.598616
ANSYS
R17.2
Academic
NOV 24 2017
13:05:40
ANSYS
Model 2
0
.022222
.044444
.066667
.088889
.111111
.133333
.155556
.177778
.2

d)

Figure 4-9 MDC2 Convergence Study a) Deformation (x-direction) and rotation (about y-axis) applied in the FEA b) Vertical gravity load (z-direction) applied in the FEA c) Applied boundary conditions d) Approximate point locations on MDC2 cross section analyzed for convergence study e) Force-Deformation results f) Convergence results of P1 on HSS g) Convergence results of P2 on HSS

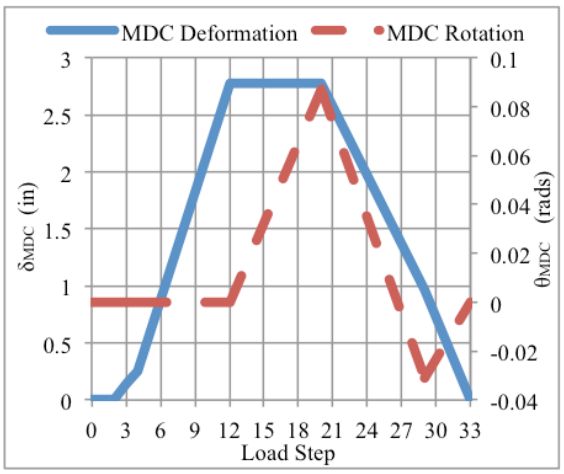

a)

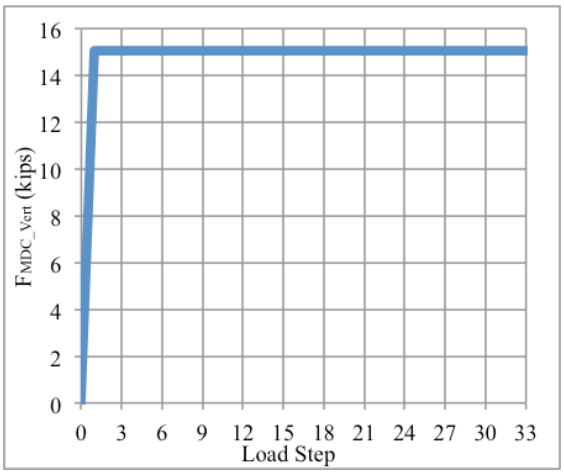

b)

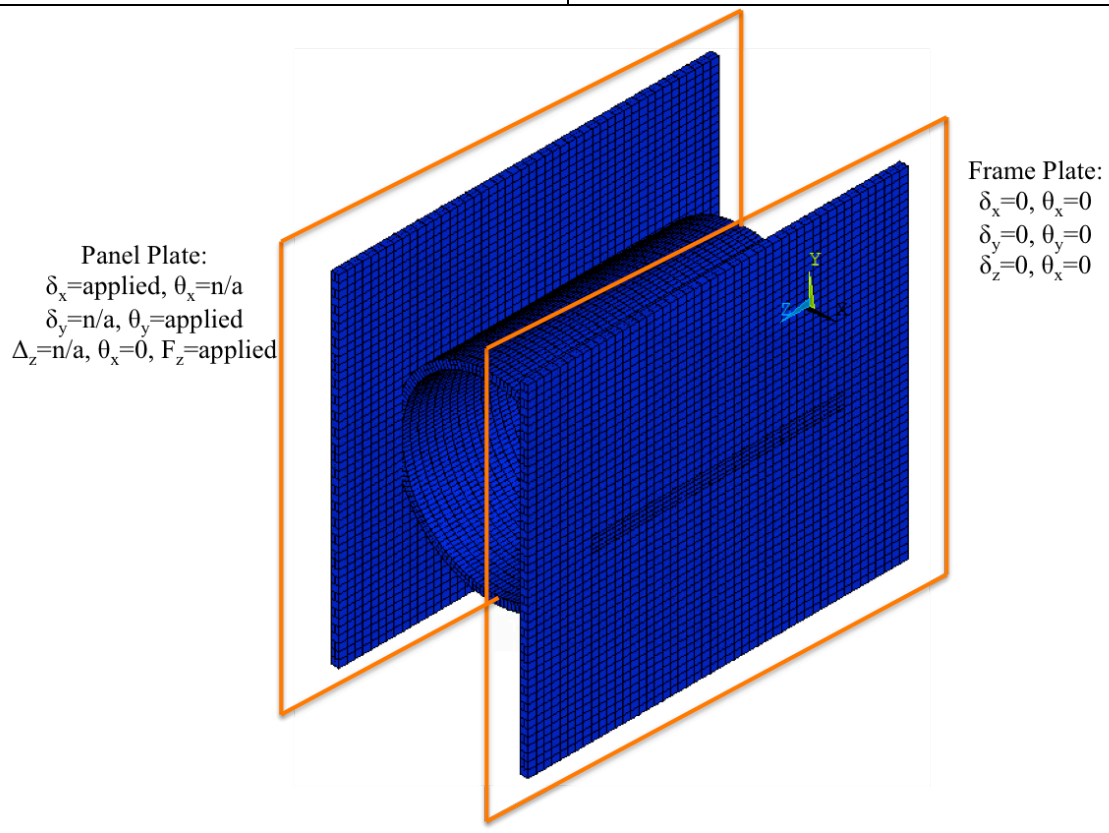

c)

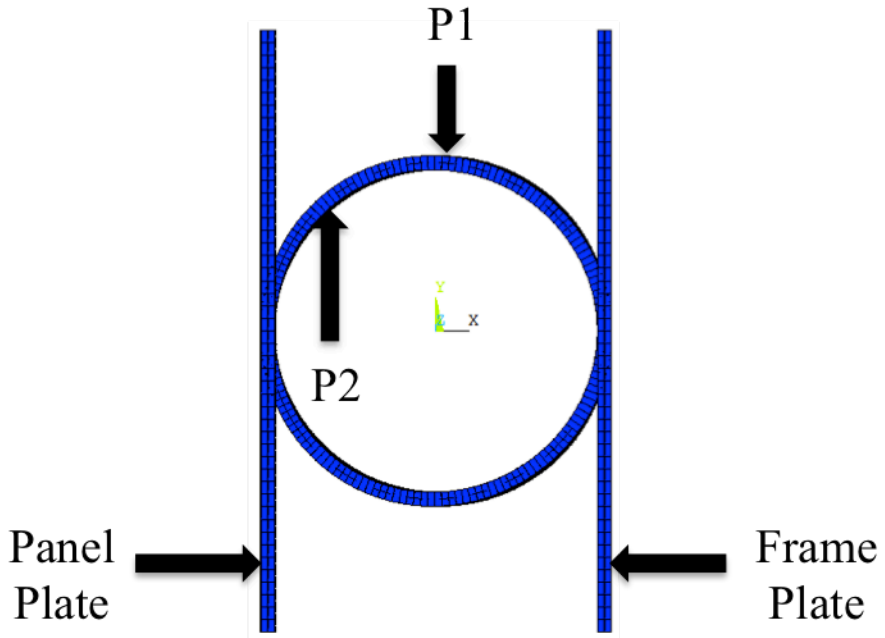
P1
P2
Panel
Plate
Frame
Plate

d)

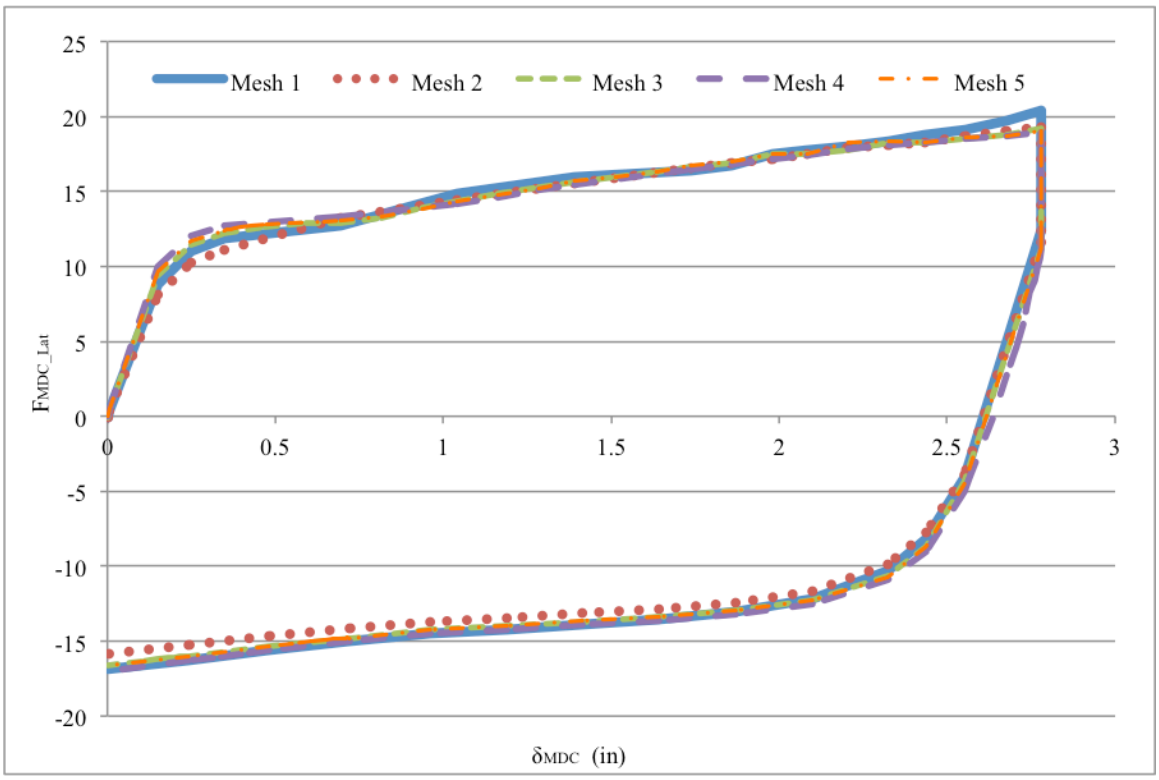
Mesh 1
Mesh 2
Mesh 3
Mesh 4
Mesh 5
25
20
15
10
5
0
-5
-10
-15
-20
0
0.5
1
1.5
2
2.5
3
FMDC_Lat
δMDC (in)

e)

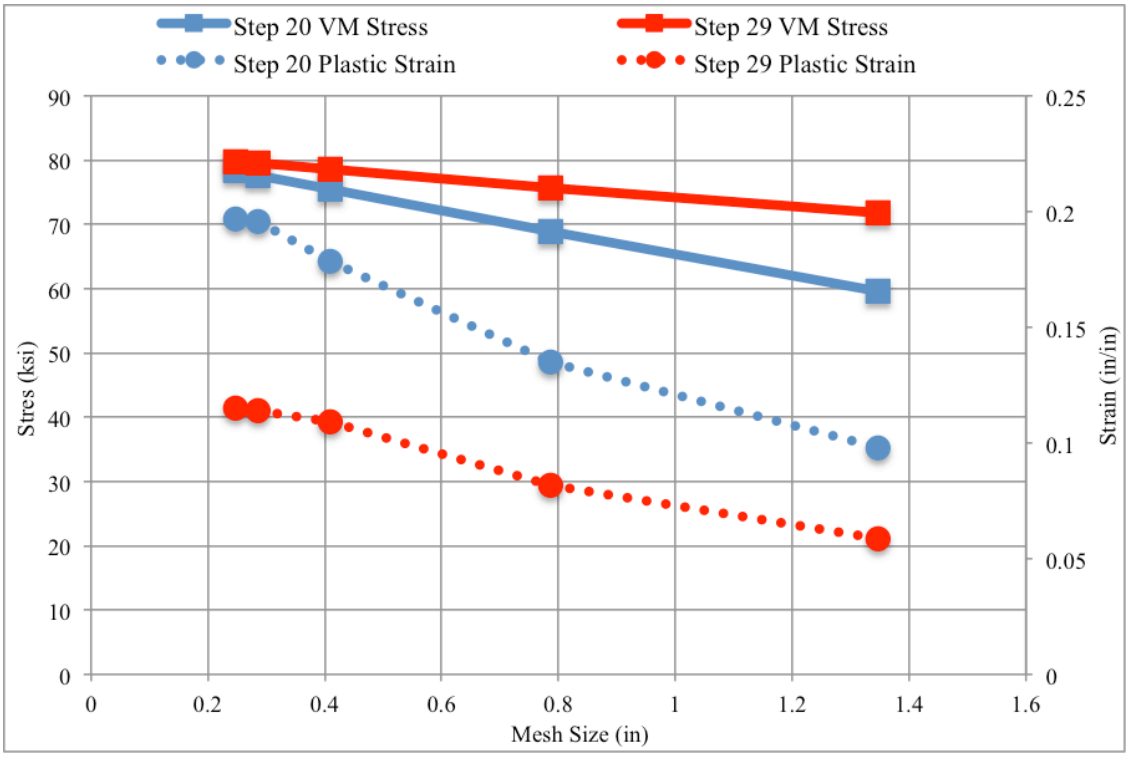
Step 20 VM Stress
Step 29 VM Stress
Step 20 Plastic Strain
Step 29 Plastic Strain
Stres (ksi)
Strain (in/in)
Mesh Size (in)
0
10
20
30
40
50
60
70
80
90
0
0.05
0.1
0.15
0.2
0.25
0
0.2
0.4
0.6
0.8
1
1.2
1.4
1.6

f)

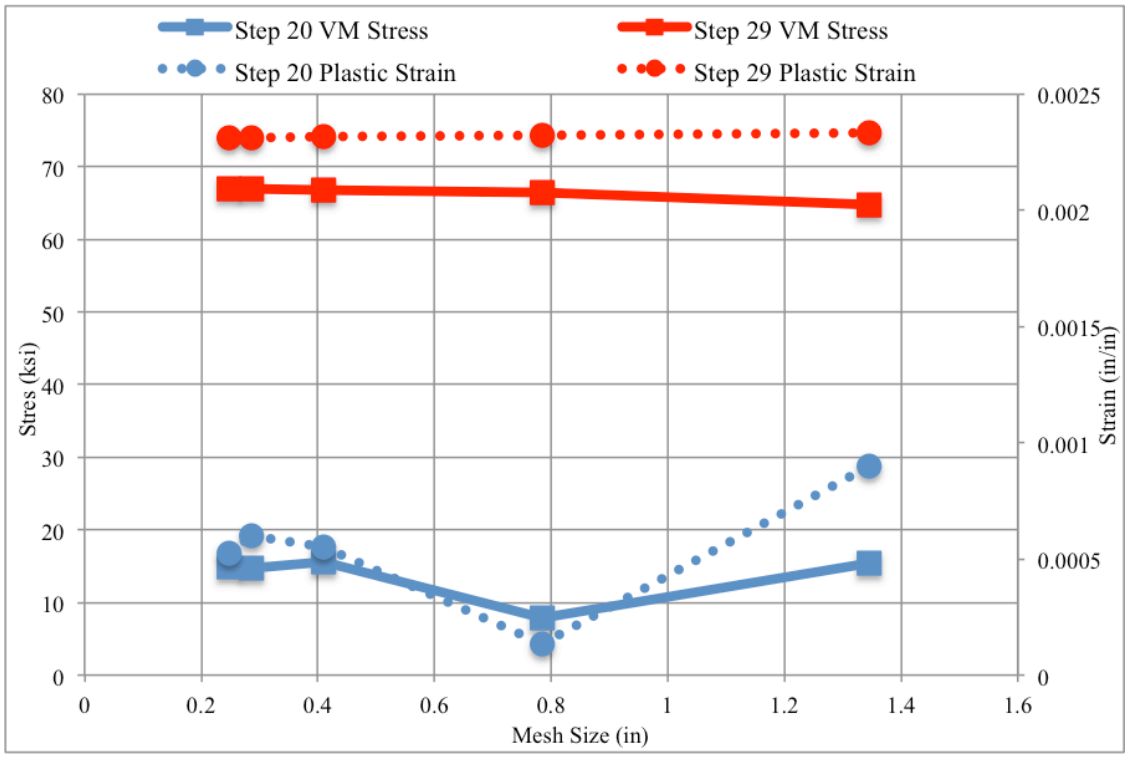
Step 20 VM Stress
Step 29 VM Stress
Step 20 Plastic Strain
Step 29 Plastic Strain
Stres (ksi)
Strain (in/in)
Mesh Size (in)
0
10
20
30
40
50
60
70
80
0
0.0005
0.001
0.0015
0.002
0.0025
0
0.2
0.4
0.6
0.8
1
1.2
1.4
1.6

g)

Figure 4-10 FEA Results of MDC2 a) Force-deformation curves of the FEA and MDC2 experiment b) Deformed shapes throughout the FEA c) Von-Mises stress (ksi) contours at the design deformation and rotation d) Equivalent plastic strain contours at the design deformation and rotation

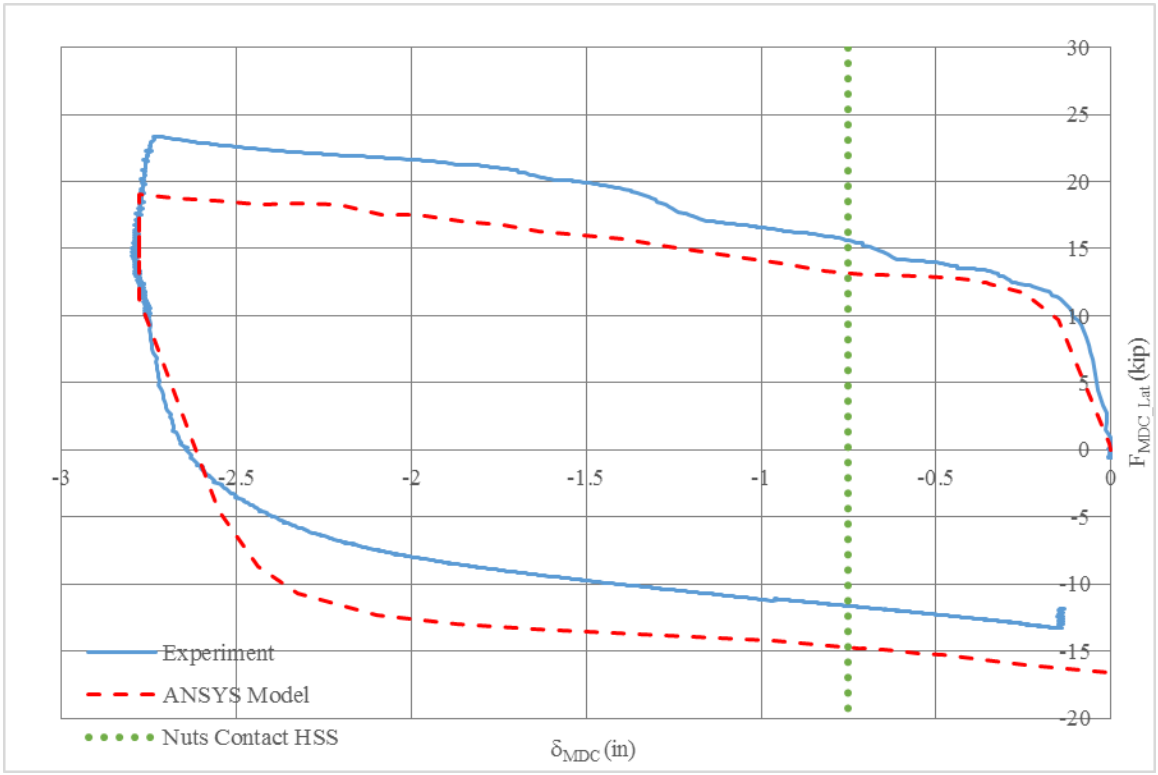

a)

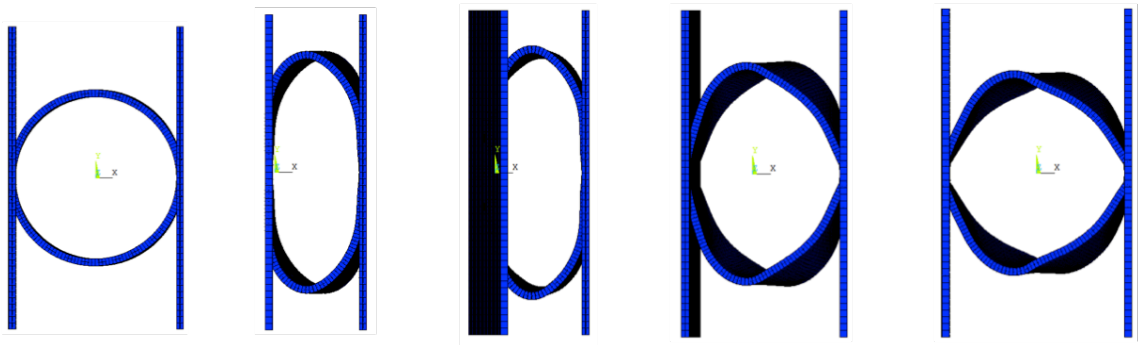

δ_{MDC} = 0”
Θ_{MDC} = 0 rads

δ_{MDC} = 2.78”
Θ_{MDC} = 0 rads

δ_{MDC} = 2.78”
Θ_{MDC} = 0.087 rads

δ_{MDC} = 0.96”
Θ_{MDC} = -0.031 rads

δ_{MDC} = 0”
Θ_{MDC} = 0 rads

b)

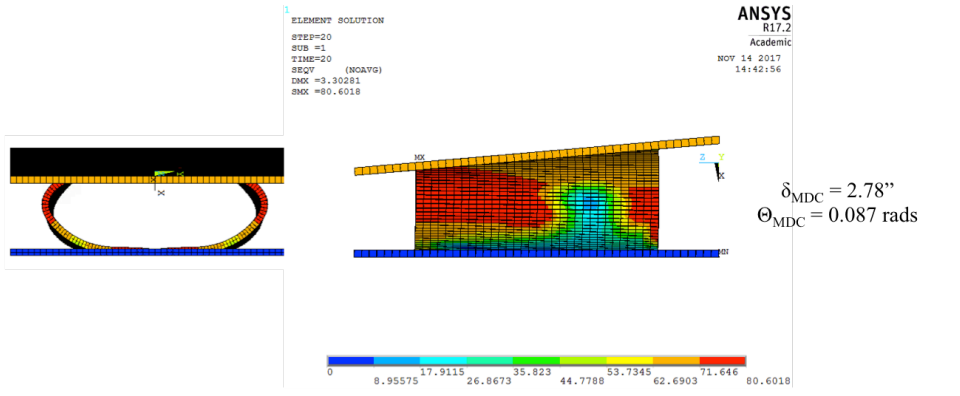

δ_{MDC} = 2.78”
Θ_{MDC} = 0.087 rads

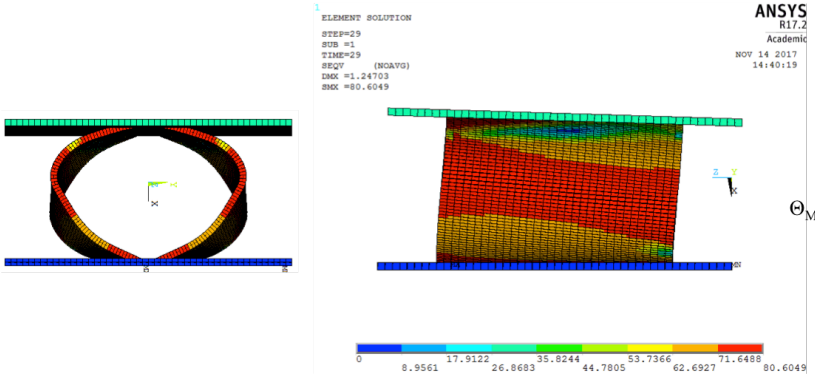

δ_{MDC} = 0.96”
Θ_{MDC} = -0.031 rads

c)

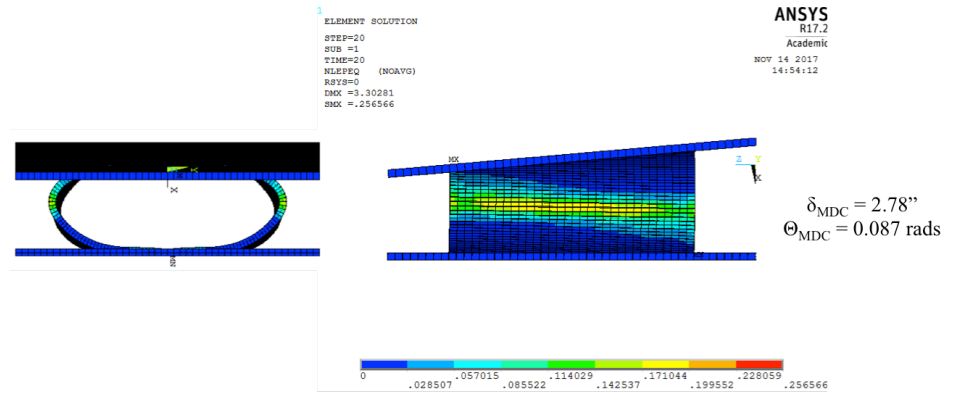

δ_{MDC} = 2.78”
Θ_{MDC} = 0.087 rads

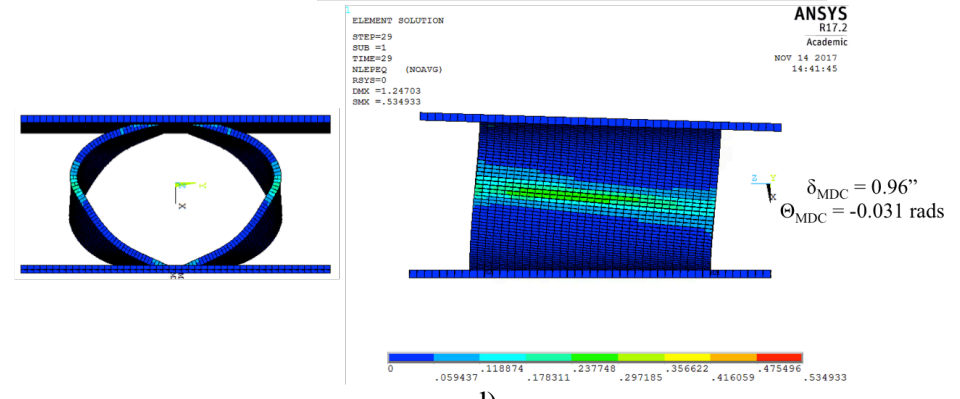

δ_{MDC} = 0.96”
Θ_{MDC} = -0.031 rads

d)

Figure 4-11 MDC3 Convergence Study a) Deformation (z-direction) applied in the FEA b) Approximate point locations on MDC3 cross section analyzed for convergence study c) Applied boundary conditions d)Force-Deformation results e) Convergence results of P1 on HSS f) Convergence results of P2 on HSS

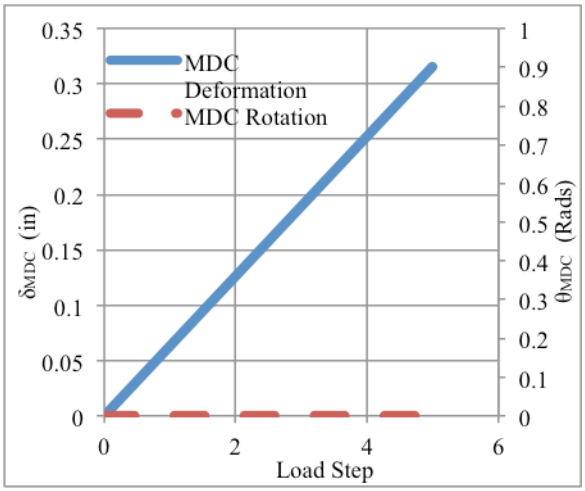

a)

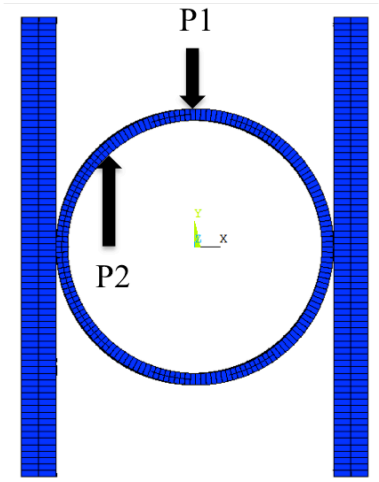

b)

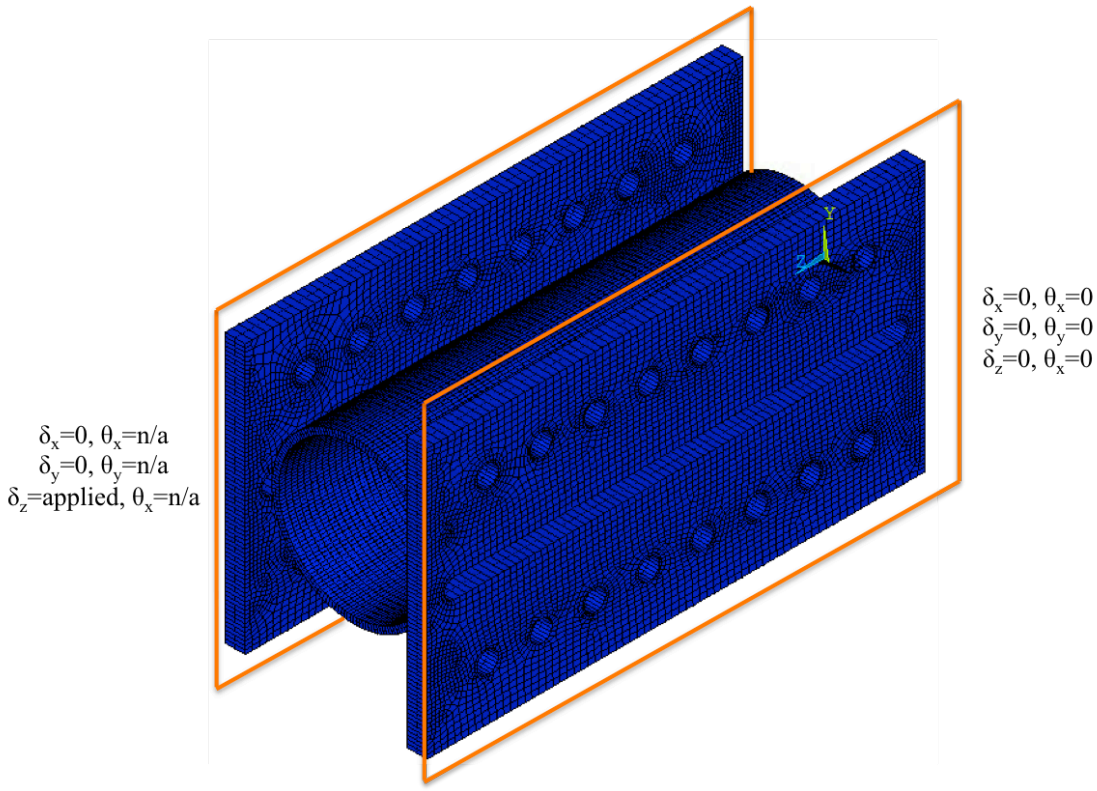

c)

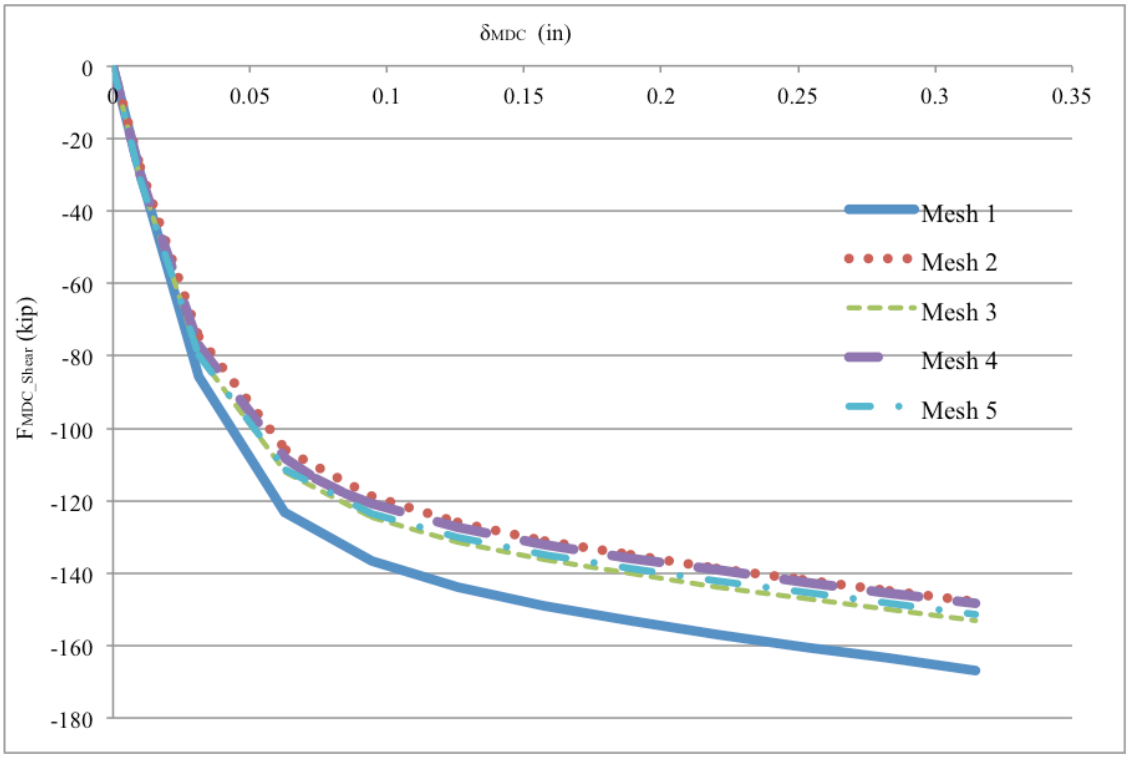
δMDC (in)
0
0.05
0.1
0.15
0.2
0.25
0.3
0.35
-20
-40
-60
-80
-100
-120
-140
-160
-180
FMDC_Shear (kip)
Mesh 1
Mesh 2
Mesh 3
Mesh 4
Mesh 5

d)

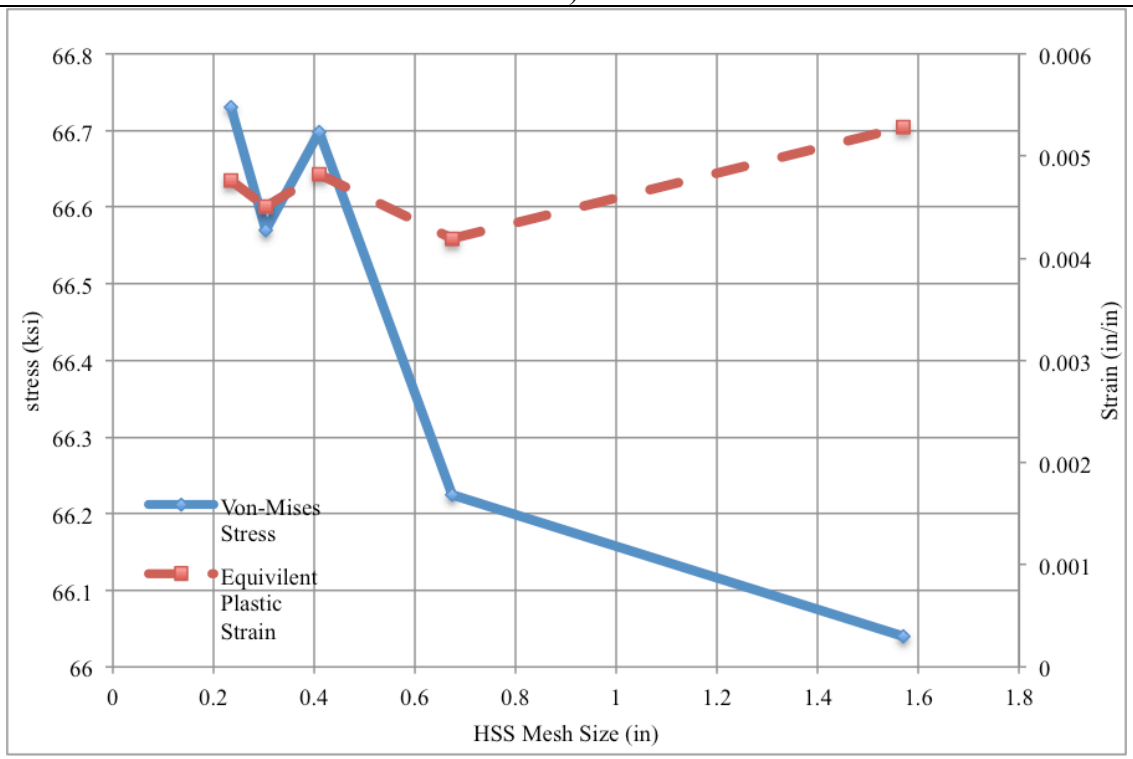
66.8
66.7
66.6
66.5
66.4
66.3
66.2
66.1
66
stress (ksi)
0.006
0.005
0.004
0.003
0.002
0.001
0
Strain (in/in)
0
0.2
0.4
0.6
0.8
1
1.2
1.4
1.6
1.8
HSS Mesh Size (in)
Von-Mises Stress
Equivilent Plastic Strain

e)

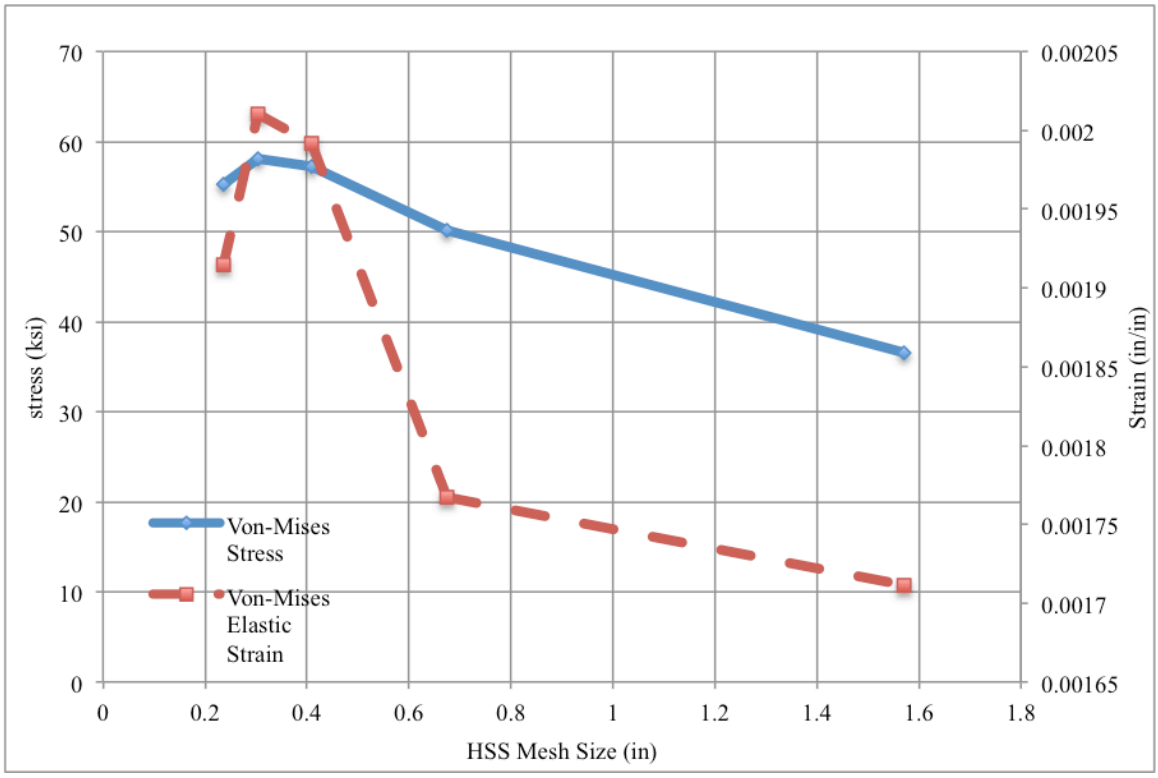
70
60
50
40
30
20
10
0
0.00205
0.002
0.00195
0.0019
0.00185
0.0018
0.00175
0.0017
0.00165
stress (ksi)
Strain (in/in)
0
0.2
0.4
0.6
0.8
1
1.2
1.4
1.6
1.8
HSS Mesh Size (in)
Von-Mises Stress
Von-Mises Elastic Strain

f)

Figure 4-12 FEA Results of MDC3 a) Force-deformation curves of the FEA and MDC3 experiment b) Deformed shapes throughout the FEA c) Von-Mises stress (ksi) contours at the design deformation d) Von-Mises elastic strain contours at the design deformation e) Equivalent plastic strain contours at the design deformation

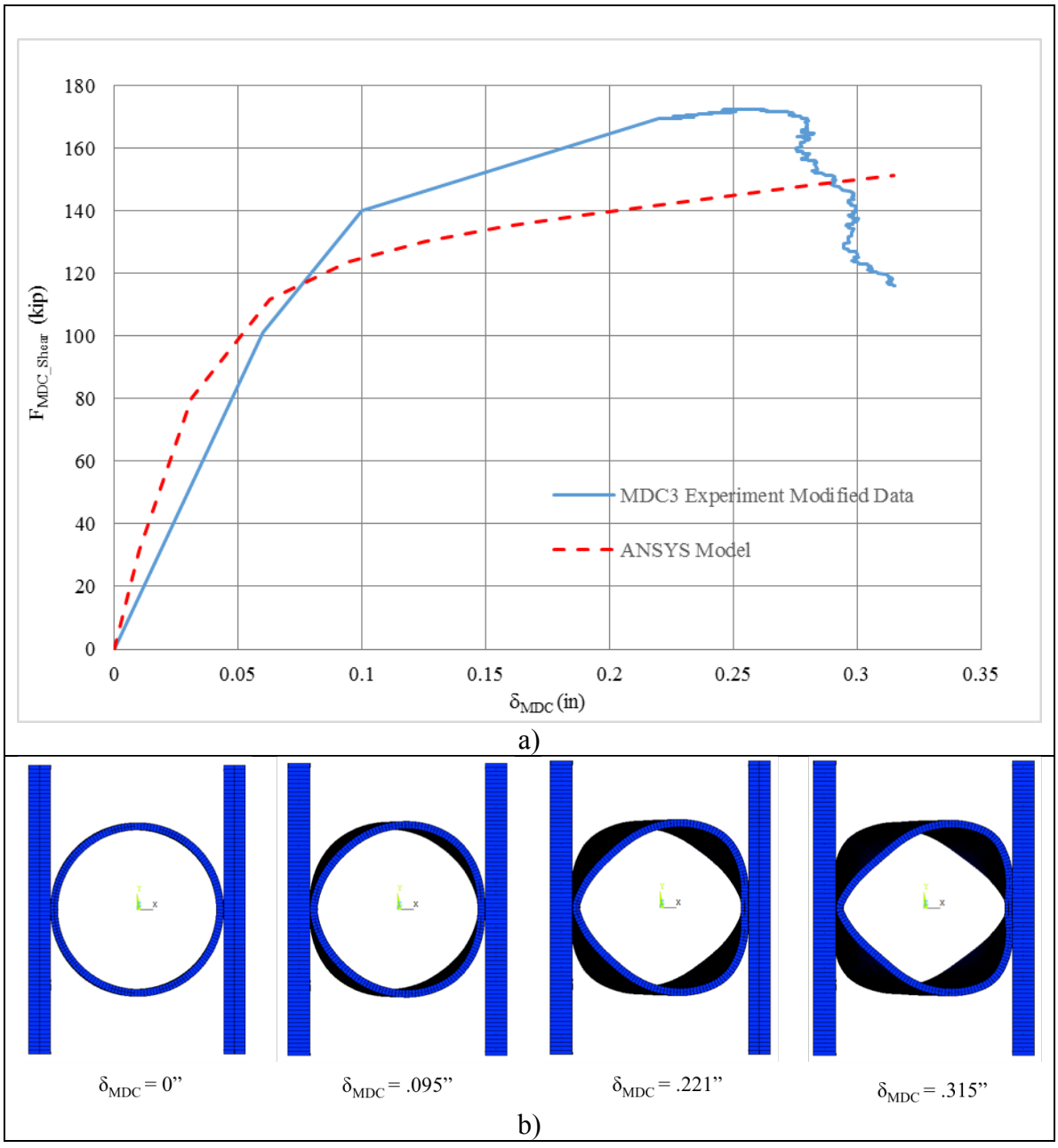

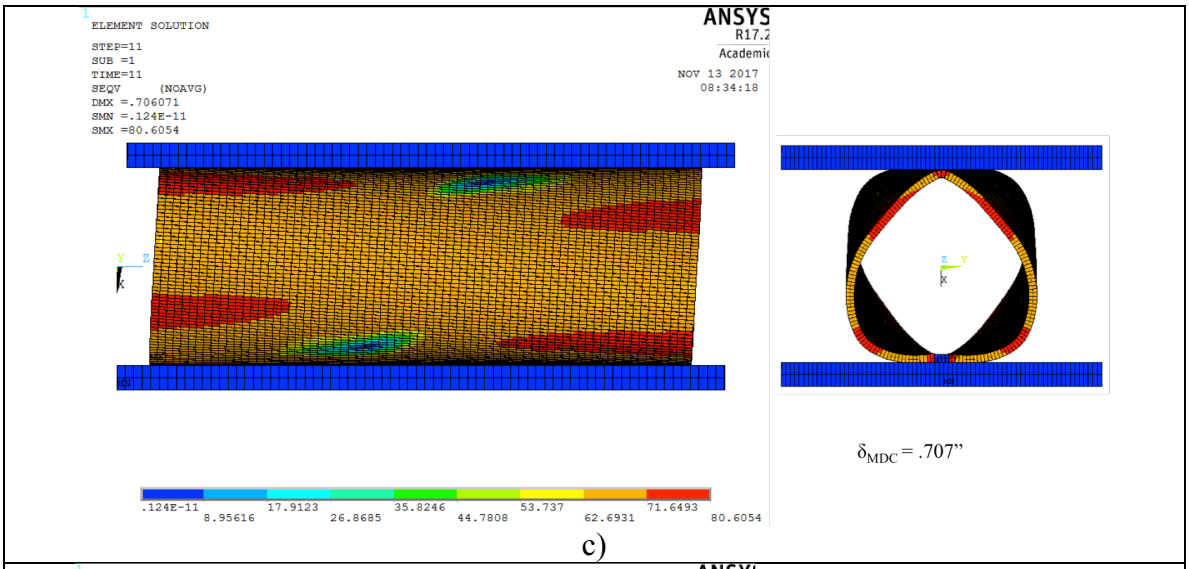

$\delta_{MDC} = .707"$

c)

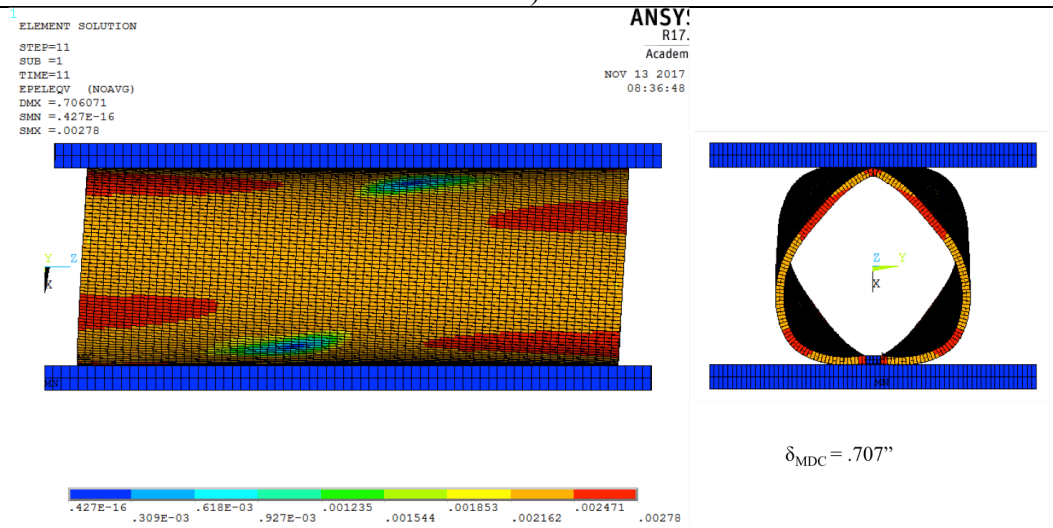

$\delta_{MDC} = .707"$

d)

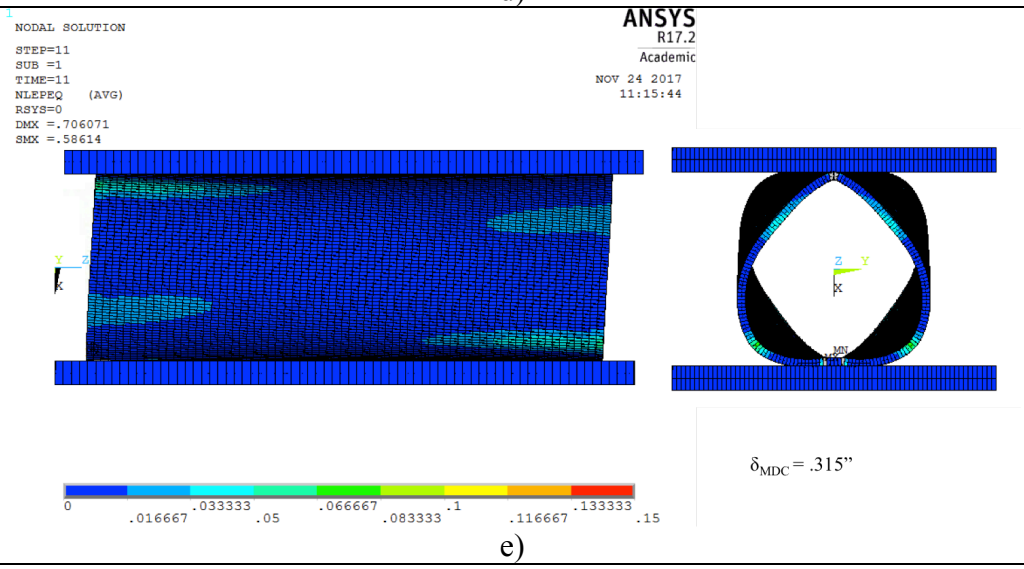

$\delta_{MDC} = .315"$

e)

5. Summary, Conclusions, and Recommendations for Further Research

This study evaluated three multi-hazard ductile connector (MDC) designs subjected to their respective critical hazardous loading conditions. Experimental tests were conducted on each MDC design to simulate the critical translations and rotations imposed on the MDC by the façade panel during the controlling hazardous loading. A finite element model of each MDC was developed and then validated to the experimental test results.

The critical MDC performance measures are compared to the theoretical design, experiments, and finite element analyses in Table 5-1. The critical loading scenario for MDC1 was seismic drift of the corner panel in the façade system, which is expected to create 3.1 inches of tensile translation and 0.025 radians of rotation. The MDC1 design maximum tensile force was 46 kips. Both the experimental results and finite element results achieved a maximum tensile force at the design translation and rotation within about a 10% difference from the design force. Yet, maximum tensile force varied by about 6.5% between the experimental and analytical results. MDC1 was designed to allow plastic deformations to develop in the HSS and each end plate in order to accommodate the deformations while limiting the peak force transfer. The HSS deformation was underestimated by the design and models, while both of the end plate deformations were overestimated. The MDC2 critical hazardous loading was based on carrying both the façade panel tributary gravity load and deformations resulting from blast loading on the façade panel. This critical loading scenario created -4 inches of compressive translation and +0.105 radians of rotation on the MDC, then reduced the compressive translation to -0.945 inches with a rotation of -0.037 radians. However, the

experiment did not impose the design-level deformations of the loading scenario due to limitations of the testing equipment and a desire to limit connection nut contact during testing. The experiment actually imposed a translation of -2.75 inches and +0.87 rads and then reduced it to -0.96 inches and +0.031 rad. The energy absorbed during the MDC experiment was 1.4% different than the design criteria, while the FEA energy absorbption varied from the design by about 15%. However, the maximum compressive force in the FEA was closer to the design compressive force than the experimental maximum compressive force. One source of variance between the MDC2 experimental finite element results is the nut contact with the HSS that occurred in the experiment. This contact was not modeled in the analysis and was not accounted for in the theoretical design. The MDC3 design criteria was based on the lateral seismic inertia force and lateral force of the corner façade panel contact. MDC3 needed to remain elastic up to an applied force of at least 135 kips. MDC3 achieved an elastic design load of 140 kips in the experiment and 120 kips in the finite element model. Overall, the MDC designs preformed as expected with differences between the theoretical design, experimental results, and finite element results likely acceptable for design.

The experimental test setup and validation of finite element modeling allows for further exploration of similar or potentially optimized MDC designs. Some recommendations for future research for multi-hazard design of building envelopes include:

- Considering a similar MDC configuration consisting of a circular HSS connected between two end plates, additional study of different HSS lengths, thickness, and diameters is needed to understand how these

geometric quantities impact the ability of the MDC to deform, rotate, and absorb energy. Furthermore, analysis could be performed to investigate the force-deformation behavior of the MDC in all degrees-of-freedom (independently) and the coupled behavior that could be used to define a general phenomenological model for the connectors.

- Further investigate the behavior and plastic mechanisms forming in the MDC1 end plates to better control the proportions of plastic deformations between the HSS and end plates.
- Evaluate MDC designs for different façade types including the deformation, rotations, and tributary loading levels they experience under similar hazardous loading conditions. New MDC designs may be necessary due to the inherent strength or plastic deformation limitations for different façade types.
- Experimental testing of a façade panel with all MDC types attached is needed to better understand the interaction between the panel and multiple connectors. Furthermore, development of an experimental test that allows for testing of multiple in-plane panels or orthogonal panels would allow for more complete understanding of the complex deformation kinematics and contact which must occur between panels and between the connectors to the framing. The Case Structural Engineering Laboratory has a facility and equipment that could potentially perform such testing.

	Maximum Tensile Force (kips)				Maximum HSS Translation (in)			
MDC 1	Design	Exp.	FEA Model 1	FEA Model 2	Design	Exp.	FEA Model 1	FEA Model 2
	45.9	50.7	47.5	50.9	1.6	1.95	1.44	1.55
	Maximum Panel Plate Translation (in)				Maximum Frame Plate Translation (in)			
	Design	Exp.	FEA Model 1	FEA Model 2	Design	Exp.	FEA Model 1	FEA Model 2
	0.75	0.58	0.86	1.17	0.75	0.58	0.80	0.38

MDC2	Energy Dissipation (kip-in)			Maximum Compressive Force (kips)		
	Design	Exp.	FEA	Design	Exp.	FEA
	42.4	43.0	35.7	19.1	23.3	19.0

MDC3	Elastic Strength (kips)			Ultimate Strength (kips)		
	Design	Exp.	FEA	Design	Exp.	FEA
	135	140	120	N/A	172.2	151.4

Table 5- 1 MDC performance objective comparison between design, experimental, and analytical methods

Appendix 1

Multi-Hazard Ductile Façade Connection Design

1. Background and Definitions

The use of multi-hazard ductile connectors (MDCs) for façade panel-to-structural frame connections in new low- to mid-rise steel buildings is being investigated in an effort to improve the lifetime performance of such structures. A preliminary design procedure has been developed which details MDCs for a given façade panel on a prototype building considering wind, seismic, blast, and impact hazards with varying performance objectives (current version: "MDCDesign_V4.5.xmcd"). The following directions/degrees-of-freedom are defined relative to the façade panel as-installed on a building (Fig. 1):

- Out-of-plane (OP): defined by a vector normal to the outer surface of the façade panel.
- Vertical (V): defined as the direction along the height of the panel/building.
- Lateral in-plane (LIP or IP): horizontal direction along the width of the panel/building; mutually perpendicular to the OP and V directions.

Three MDC types have been developed to resist demands in each of these directions (Fig. 2):

- MDC-1: provides a reaction force only in the OP direction. Includes slotted bolt holes to accommodate thermal expansion/contraction of the façade panel in the vertical and LIP directions, as well as seismic building drift in the LIP direction (floors connected to panel can move relative to one another without distorting the panel). One edge of the panel (top or bottom) will contain all of the MDC-1s, while the other edge has the MDC-2s and MDC-3. Three MDC-1s per panel are recommended to approximately mirror the OP support condition at the opposite panel edge.

- MDC-2: provides OP and V reaction forces. Includes slotted bolt holes for LIP panel thermal expansion/contraction. Two MDC-2s per panel are recommended to ease the panel installation process by allowing for simple kinematic adjustment of the panel at these gravity load-bearing connection points.
- MDC-3: provides OP and LIP reaction forces. Only one MDC-3 should be used per panel to allow for both LIP thermal expansion/contraction and LIP seismic building drift.

2. Façade System Loading and Performance Objectives

Façade systems enclose interior building spaces while providing protection, insulation, and aesthetic appeal from the exterior. Financial evaluation of typical low- to mid-rise steel buildings indicates that the façade system accounts for a significant portion of building material and construction costs. During seismic events, façade panel damage and detachment has been observed due to deformation incompatibility between the façade panels and attached floor slabs as the building stories undergo lateral drifts (Hutchinson *et al.*, 2014). Additionally, buildings subjected to extreme external lateral pressures, such as large explosive or strong wind/tornado/hurricane events, have a reduced chance of progressive collapse when the façade system remains intact (NIST, 2007). Therefore, it is in the interest of both public safety and reducing probable economic losses that the design and detailing of robust, practical façade systems is developed herein.

A building's façade system serves as the barrier separating the interior and exterior environments. Differences between these environments must be resolved by the façade system to maintain the integrity of the enclosure. Changes in temperature and

moisture content can create volumetric strains within the façade panels depending on material properties. Wind pressures incident upon a building's surface must be resisted by the façade panels, transferred to the structural frame, and, ultimately, resolved back to the ground via the foundation. A similar transfer of forces from the panels to the foundation must occur for any loads caused by the self-weight of the façade system; both lateral and vertical seismic inertia forces must be accounted for in addition to panel dead weight. Impulsive loads resulting from explosive blasts or impact debris due to blast or extreme wind events must also be considered to protect essential facilities from these rare but potentially high-damage hazards.

A list of credible hazards and desired performance objectives for a low- to mid-rise steel building frame with reinforced concrete façade panels and multi-hazard ductile connectors (MDCs) is provided in Table 1. The proposed MDC design approach achieves these performance objectives through capacity design principles and consideration of the interaction between building frame and façade panels. Characterization of the nature and magnitude of façade panel demands is the first step in the proposed MDC design methodology.

2.1 Minimum Façade System Design Requirements

ASCE 7-10 (2013) details minimum requirements for façade system design, including thermal/moisture effects and loads due to self-weight (dead load), seismic inertia, and wind. The system must provide an adequate load path for all out-of-plane (OP; direction normal to the exterior building surface), vertical (V; direction along the panel/building height), and lateral in-plane (LIP or IP; direction along the panel/building width, mutually perpendicular to the OP and V directions) loads. All minimum design loads must be

resisted elastically by the façade system. Wind and lateral seismic panel inertia are the minimum design OP demands. Lateral seismic panel inertia must also be considered in the LIP direction. Vertical demands include dead weight and vertical seismic panel inertia. The factored load combinations specified in ASCE 7 must be considered when determining controlling design demands for both the façade panel and connections to the structural frame in each degree-of-freedom.

2.1.1 Thermal/Moisture Effects and Minimum Panel Strength

The volumetric expansion and contraction due to changes in temperature and moisture content must be accounted for when designing reinforced concrete or brick and mortar cladding façade systems. These deformations are typically accommodated locally (within the façade system itself) using a combination of gaps between panels and degree-of-freedom releases in the façade panel-to-structural frame connections. The material coefficients of thermal and moisture expansion can be used to estimate the maximum (relative to nominal) panel dimensions, and joints can then be sized to allow for this expansion without contact occurring between panels. Joints also ease the installation process, and allow for some differential seismic displacement of the floors attached to a given façade panel without panels coming into contact. ASCE 7-10 Chapter 13.5.3 specifies a minimum panel joint size of ½", however a typical 13' by 30' reinforced concrete panel requires ¾" joints to allow for the expansion due to a design temperature fluctuation of +/- 50 degrees Fahrenheit. Without adequate joints, expanding panels can come into contact and rapidly develop large forces resulting in cracks and potential fracture of façade-to-frame connections.

The façade panel-to-structural frame connections must be able to accommodate both panel contraction and expansion due to thermal and moisture effects to avoid distortion and potential fracture as the panel deforms in-plane. This is typically achieved by including slotted bolt holes in the façade-to-frame connectors, and arranging these connections to allow for in-plane panel deformations while also providing reactions in each degree-of-freedom. The connection arrangement and slotted bolt hole details shown in Fig. 1 and Fig. 2, respectively, satisfy these criteria; all connectors provide OP reactions while the panel is free to deform in the LIP direction from the bottom-center connector (which provides a reaction in this direction), and in the vertical direction from the bottom edge of the panel, where two vertical reactions are present. This connection configuration also provides a "simply supported beam" condition considering the panel loaded in the OP direction (left side of Fig. 1).

For reinforced concrete panels, thermal and moisture effects require a minimum amount of reinforcement—with a reinforcement ratio of about 0.2%—to minimize cracking (ACI, 2011). This minimum reinforcement ratio can be used to determine the minimum flexural strength of the panel when subjected to (say, uniformly distributed) loading in the OP direction. For other cladding types, code requirements should be checked to ensure all minimum strength requirements are met. If no such requirements exist, typical as-built details of the chosen façade type should be used to calculate the minimum flexural capacity of the system for comparison with design wind and seismic OP load demands.

2.1.2 Panel Self-Weight, Seismic Inertia, and Wind Demands

The design-level wind pressure on a given façade panel can be calculated from the procedures in ASCE 7-10 Chapters 26 and 30. The design wind event for façade panels can be treated as a sustained, static load. A variety of factors—including building dimensions, location, and site exposure—are used to formulate a design pressure profile incident upon each building face. This pressure profile can then be integrated over the area of the panel of interest to determine a total OP design force. For simplicity, this design force can be treated as a uniformly distributed load over the surface area of each panel by dividing the total OP wind force by the panel's height and width. This approximation allows for simple calculation of the peak flexural demand (uniformly distributed load on a simply supported beam) to determine if the system requires additional reinforcement beyond its minimum flexural strength. For extreme wind events, such as tornadoes, the design wind pressure profile can be amplified by the square of the ratio of reference wind speeds—the sustained three-second gust at ten meters above-grade associated with an event of known annual probability of exceedance—to determine a "maximum considered" OP wind load.

The façade-to-frame connections must have adequate strength to support the panel's weight (dead load) in the vertical direction. The panel's mass also results in seismic inertial forces which act in the vertical, LIP, and OP directions. For panels not located at the corner of a building (so-called "interior" panels) the controlling vertical demand is the maximum of the panel dead load (with a load factor of 1.6), and the dead load (factor of 1.2) plus vertical seismic panel inertia ($2/3^{rds}$ of the design short-period spectral acceleration value multiplied by the panel weight). This vertical design force is shared equally between the (typically two) vertical load-bearing façade-to-frame

connectors. The only LIP load to consider for interior panels is the lateral seismic panel inertia, which can be calculated using the ASCE 7-10 procedure for determining seismic loads for nonstructural components (Chapter 13). This same force must also be considered in the OP direction. The OP seismic inertia force should be divided by the panel's surface area to obtain an equivalent uniformly distributed load which can be readily compared to the design OP wind demand (choose the controlling value considering seismic, wind, and minimum strength requirements). For "edge" panels located at the corner of a building, additional forces must be considered in both the vertical and LIP directions for the seismic load case to account for contact between panels during building drift.

2.2 Accommodation of Seismic Building Drift

In modern steel buildings, ductile design of the lateral force resisting system (LFRS) is used to economically resist large lateral forces during seismic events. Yield of the LFRS results in inelastic story drifts which must be accommodated by the façade system to avoid developing large forces due to in-plane distortion of the panels, which generally have large, axially-stiff in-plane cross sections. This is typically done through detailing of the façade-to-frame connections, similar to the approach taken for thermal/moisture effects.

Panels are anchored to the floor slabs above and below a given story, and differential motion of these slabs in the OP, V, and LIP directions relative to each façade panel must be accommodated by the connections. Vertical differential displacement between floors is typically much smaller than lateral drift and can essentially be ignored if proper accommodation of thermal/moisture expansion and contraction is included via

vertical slotted bolt holes and an appropriate connection configuration as previously discussed (Fig. 1 and Fig. 2). Story drift primarily in the LIP direction requires that the horizontal slotted bolt holes specified for thermal/moisture effects be expanded to allow for (plus/minus) the design maximum story drift (possibly considered as the code drift limit of 2.5% of the story height or $C_d\delta_e$ where C_d is the deflection amplification factor for the chosen LFRS and δ_e is the elastic story displacement under the elastic (reduced) design seismic inter-story shear). Building drift in the OP direction can be accommodated through bending of the connectors about the panel's LIP axis.

As a given story undergoes drift primarily in one direction, the panels located at the building's corners may experience deformation incompatibility due to differences in the anchorage of adjacent corner panels (Fig. 1). The "OP" panel—relative to the direction of story drift—is anchored to both the top and bottom floor considering drift in this direction, while the "IP" panel is only anchored to one of these floors (by its LIP connection). For the connection configuration shown in Fig. 1, contact between corner panels will occur if the OP panel rotates towards the IP panel, which is anchored laterally to the bottom floor. This contact can be avoided if a large, undesirable gap (equal to the design maximum story drift) is included between the panels. Alternatively, a standard gap can be used with connections that are detailed to act as a "fuse" along the load path to limit the force which develops as the corner panels come into contact, thereby accommodating seismic building drift through yielding of the connectors (Hutchinson *et al.*, 2014). The latter approach towards resolving the corner panel contact problem is taken in the proposed MDC design methodology, and the mechanics of this action will be developed in detail in a later section.

2.3 Impulsive Loading due to Blast and Impact Hazards

Impulsive loading on a building façade imparts an initial velocity to the panel mass based on the principle of momentum conservation; impulse is equal to initial momentum, which is the product of panel (effective) mass and initial velocity. This type of loading can result from a force (or pressure) acting over a duration of time which is much shorter (typically $1/5^{th}$ or less) than the fundamental period of vibration response of the structural system (Chopra, 2011). This is generally an appropriate characterization of an explosive blast when designing protective structures (DOD, 2008). Impulsive loading can also result from an elastic collision between a mass-containing body and structure, where momentum (or kinetic energy) is conserved. This can occur when debris due to a blast or high-wind event impacts the building's exterior. In either case, the integrity of the load path from façade panels, to connections, and through the main structural frame is critical for protecting the building's inhabitants, preventing infiltration of the blast or impact missile into the building (which can significantly increase economic losses), and minimizing the potential for progressive collapse due to damage of the primary structural system (NIST, 2007).

When an explosion occurs, a high-velocity overpressure wave propagates radially in all directions from the source of the blast. When this wave encounters a boundary plane, such as the side of a building, it reflects off of the surface, exerting a brief inward (positive) pressure. The duration of this pressure is typically about 0.01 seconds, which is much shorter than the fundamental period of vibration response of any typical façade system. The integral of positive reflected blast pressure over time yields the impulse value for protective design of the façade system. This value is a function of the charge

weight (W; typically presented in terms of equivalent pounds of TNT), straight-line distance between the charge and boundary surface, and the angle of incidence between the straight-line distance ray and boundary surface normal (DOD, 2008). A more general "standoff distance" term (denoted by the variable R), defined as the minimum along-ground distance between the blast source and building surface, is typically used along with W to characterize a blast event for structural design. These parameters are commonly combined into a single "scaled distance" value, Z, equal to R divided by the cubed root of W.

Design blast impulse values are provided in Table 2 for three ground-level blast scenarios (BS): BS1, with a standoff distance, R, of 30 feet and a charge weight, W, of 500 lbsTNT; BS2, with R = 100 feet and W = 300 lbsTNT; and BS3, with R = 200 feet and W = 100 lbsTNT. These values were obtained by integrating the positive pressure values over time calculated by the numerical procedure developed by Appelbaum (2013) for each blast scenario over a 30-foot wide by 13-foot high (typical bay width and story height dimensions; considered the nominal area of each façade panel) area on each story centered on a wide, tall building surface (to eliminate edge clearing effects). Note that all three blast scenarios have an impulse value of zero above a certain story elevation due to the increasing angle of incidence moving up the building height. These blast scenarios represent low- (BS3), intermediate- (BS2), and high- (BS1) intensity blast events which span the range of applicability of the methods used by Appelbaum's procedure in terms of scaled distance, Z.

Table 2 also includes design impact missile impulse values, which are adapted from the United States Nuclear Regulatory Commission (USNRC, 2007) for the

protection of nuclear facilities against tornado effects. The design missile for "global" (non-penetrative or local) failure is a car with mass and impact velocity determined by the mapped tornado wind regions shown in Fig. 3. This impact missile can strike at any elevation up to thirty feet above grade, and is treated as a uniformly distributed load for the impulsive/dynamic characterization of the system discussed in subsequent sections. Although the USNRC guidelines state that plastic deformation (energy dissipation) of the car can be considered during this collision, this can be conservatively ignored to obtain a larger design impact missile impulse value. The design impulse values in Table 2 are compared in Fig. 4.

For a given façade panel, the controlling impulsive loading scenario is a function of both the magnitude of the design impulse, as well as the performance objective for the façade system subjected to that event (Table 1). Large impulsive loading events are rare and the precise design scenario(s) will likely never occur; however, an economical, protective design can be achieved through consideration of a spectrum of loading scenarios and performance objectives. This is accomplished using capacity design principles to induce a desired progression of component damage with increasing demand along the load path where each behavioral transition is benchmarked by the controlling load type with the performance objective to remain within that particular damage state. This concept is illustrated in Fig. 5 for the OP loading conditions and performance objectives detailed thus far. The design resulting from this approach will ultimately be more robust when subjected to any load type than a design strictly considering the maximum magnitude event. The mechanics and design of each component will be

developed in subsequent sections to formulate a methodology capable of achieving all desired objectives and improving façade system performance.

3. Behavior and Mechanics of Components

The structural behavior and mechanics of each component along the façade-to-frame load path must be understood to develop a design methodology for multi-hazard ductile connectors (MDCs) capable of achieving all previously discussed performance objectives. The MDCs are critical as they link the façade panels to the primary structural frame and thus govern the interaction between these systems. An approach to MDC design which utilizes round hollow structural section (HSS) tubes as key force- and deformation-compliant elements along this load path has been investigated and is believed to effectively achieve all MDC design requirements (Lavarnway, 2013). This approach relies on highly plastic behavior and atypical section demands for an HSS tube application; the tubes are oriented such that OP demands on the façade panel exert a radial point force on the circular tube walls. Additionally, the tube wall section is subjected to eccentric longitudinal forces when supporting the panel in the LIP and vertical directions, which requires shear and flexural resistance from the tube wall section. These behaviors will be developed in the following subsections, beginning with the mechanics of façade panels and the ensuing demands imparted onto the MDCs.

3.1 Façade Panel

Common façade panel (or veneer) types include precast reinforced concrete, brick masonry, insulated metal panels, and exterior insulation and finish systems (EIFS). A façade system's mass—and, therefore, dead load, seismic inertial forces, and impulse-momentum—is generally concentrated in the veneer elements. Typical brick masonry

and EIFS applications include a backup wall consisting of cold-formed steel channel sections spaced at one- to two-foot intervals (on-center); these systems rely primarily on the flexural resistance of this backup wall to resist large OP loads. For reinforced concrete and insulated metal panel systems, both the mass and flexural resistance are integral to the veneer itself. Brick masonry systems are somewhat unique in that the veneer is considered as sacrificial (contains mass but has negligible flexural resistance) when subjected to blast loading (Salim *et al.*, 2005); these systems require regular anchorage (on, say, a 4-foot square grid) to the stud wall to provide (approximately) continuous support of the fragile veneer against OP loading. Note that this discussion refers generally to the façade "panel" as an integrated mass-and-resistance element (such as a precast reinforced concrete panel) for simplicity, however some façade systems have decoupled mass and resistance elements which conjointly form an effective "panel"; when considering such systems, the properties of the primary mass and resistance elements should be ascribed to the "panel" as described below.

3.1.1 Flexural Response to Uniformly Distributed OP Loading

A façade panel supported as shown in Fig. 1 can be idealized as a simply supported beam where the primary flexural element(s) provide the material and section properties required to characterize the system's response to OP loading. The required panel strength for the controlling minimum OP design load (wind, seismic inertia, and code-prescribed minimums or typical as-built details) can be calculated assuming these demands approximate a uniformly distributed load. The performance objective for these loads is for the panel to remain elastic, therefore the maximum moment due to a distributed load on a simply supported beam—equal to $wh^2/8$, where w is the load per unit length, and h

is the panel height—must not cause a maximum bending stress greater than the material's minimum nominal yield stress, σ_y, equal to the maximum moment divided by the elastic section modulus, S_x. The same calculation with the plastic section modulus, Z_x, replacing S_x can be used to determine a design panel strength for extreme wind loads.

The reaction forces at each edge of the panel "beam" are provided by the combined OP action of the MDCs along each edge. For a uniformly distributed load, the reaction force per edge, P, is equal to wh/2. A relationship between maximum panel moment under a uniformly distributed load and the edge reaction force is given by:

$$M=\frac{Ph}{4} \quad (1)$$

where M is the maximum panel moment, P is the edge reaction force, and h is the panel height. This relationship is critical for capacity design of the panel and MDCs to achieve the desired damage progression during extreme OP loading, where the MDCs yield prior to the panel thereby limiting the maximum moment in the panel and protecting the cladding from damage or failure. This MDC yield force per panel edge must be at least great enough to elastically resist the typical design OP demands (wind, seismic inertia, minimum panel strength requirements), and capacity protection of the panel can then be achieved through proportional strengthening of the panel's moment capacity relative to the strength of the MDCs. This "fuse" concept will be revisited in detail after the critical mechanics of the façade panel and MDCs have been fully developed.

3.1.2 Generalized Single Degree-of-Freedom Dynamic System

Design for impulsive OP loading relies on work-energy terms which can be derived from a generalized single degree-of-freedom dynamic representation of the façade system.

Here, the (maximum) panel deflection at panel mid-height is chosen as the generalized displacement, and convolution integrals are performed using the section properties and deflected shape function over the panel's height to determine the dynamically-equivalent SDoF mass and elastic stiffness. The shape function, $\psi(x)$, is assumed to be proportional to the first mode shape (with unit magnitude) for a simply supported beam with a constant cross section and is given by:

$$\psi(x)= \sin\left(\frac{\pi x}{h}\right) \tag{2}$$

where x is the dimension along the panel height, h. The equivalent SDoF elastic stiffness, k*, is given by:

$$k^*=EI_x \int_0^h \frac{d^2\psi(x)}{dx^2} dx \tag{3}$$

where E is the material's modulus of elasticity, and I_x is the cross section's moment of inertia. Note that Ix should be taken as the cracked section moment of inertia for reinforced concrete façade panels (can be estimated as, say, one half of the gross section moment of inertia). The generalized SDoF mass, m*, is required for calculation of the panel's initial velocity and kinetic energy when subjected to an impulsive load, and is given by:

$$m^*=m \int_0^h m\big(\psi(x)\big)^2 dx \tag{4}$$

where m is the panel mass per unit length (along the panel's height).

The generalized SDoF mass term given by Equation (4) is equal to one half the total panel mass assuming a constant cross section up the panel's height. This generalized "half mass" term is only valid if the panel supports—provided by the MDCs along each panel edge—remain elastic thereby providing the necessary boundary

conditions for first mode dynamic response (assumed shape function; Equation (2)) of the panels. For large impulsive loads, plastic response of the MDCs may be chosen as the performance objective (Table 1) to limit the edge force (and bending moment; Equation (1)) imparted onto the panel (Fig. 5). In these cases, the panel mass effectively translates in the OP direction as a rigid body with a unit shape function. Substituting a unit shape function into Equation (4) results in a generalized SDoF mass, m*, equal to the total mass of the panel. In summary, when considering impulsive OP loads where the MDCs are designed to act as plastic force-limiting elements (plastic MDC performance objective), the generalized SDoF mass should be taken as the full mass of the panel; otherwise (elastic MDC performance objective), the generalized mass should be taken as one half the total panel mass.

3.1.3 Kinetic, Elastic Potential, and Plastic Work Energies

The response of a façade system subjected to an impulsive load can be characterized using the generalized SDoF dynamic system developed in the previous section and an expression of energy conservation. The impulse divided by m* gives the initial velocity of the generalized SDoF system, v_i*. The initial kinetic energy of the (generalized) panel, KE_P, is equal to the product of one half m* and the initial velocity squared, which can be expressed as:

$$KE_P = \frac{I_D^2}{2m^*} \tag{5}$$

where ID is the design impulse value, and m* is the generalized SDoF system mass (Equation (4)). The inversely proportional relationship between initial kinetic energy and mass means that, from a design perspective, a more massive façade system (such as reinforced concrete panel or brick masonry systems) benefits from less kinetic energy

which must be conserved through elastic storage or plastic work for a given impulse magnitude.

Equation (5) represents the initial state of the system subjected to an impulsive load. The system will eventually come to rest, at which time the panel will be at its point of maximum deformation. The transition between these two states can be represented as:

$$KE_P=PE_P+W_P \tag{6}$$

where PE_P is the elastic potential energy stored in the deformed panel, and W_P is the plastic work performed during any permanent deformation of the panel. Equation (11) is an expression of energy conservation between the initial and deformed system states. The right-hand terms in this equation can be calculated from areas under the force-deformation (or moment-rotation) curve. Deriving these terms requires an understanding of the panel's force-deformation response from the elastic region to the point of failure.

The moment-rotation relationship of a flat, simply supported (along 2 edges) plate subjected to uniform impulsive loading can be approximated as linear-elastic perfectly-plastic with maximum moment taken as the average of the elastic ($S_xR_y\sigma_y$, where R_y is the expected material over-strength relative to the minimum nominal yield strength, σ_y) and plastic ($Z_xR_y\sigma_y$) section capacities (DOD, 2008). Substituting this maximum moment into Equation (1) and rearranging terms gives an expression for the panel edge reaction force, P, at (dynamic, elasto-plastic) flexural yield. This yield force can be divided by the equivalent OP stiffness at mid-height of the panel, k*, to obtain the maximum elastic panel deflection, δ_y, calculated as:

$$\delta_y=\frac{2}{hk^*}(S_x+Z_x)R_y\sigma_y \tag{7}$$

where k* is the generalized SDoF stiffness (Equation (3)), and all other terms have been previously defined. This stiffness and maximum deformation can be used to calculate the elastic potential energy of the deformed panel, PE_P, as:

$$PE_P = \frac{1}{2} k^* \delta_y^2 = \frac{1}{2} P \delta_y \tag{8}$$

where all terms have been previously defined. The right-most form of this equation is useful for the capacity design of MDCs as it puts the panel's elastic potential energy in terms of the OP reaction force per edge.

The yield deflection given by Equation (7) can be converted to a hinge rotation at yield, θ_y, considering small angle approximations and disregarding elastic deformations:

$$\theta_y = \frac{4\delta_y}{h} \tag{9}$$

where all terms have been previously defined. This conversion is useful when considering the panel's plastic work capacity; UFC 3-340-02 provides moment-rotation relationships with damage states correlated to plastic hinge rotations up to the point of failure (DOD, 2008). For a flat steel plate, twelve degrees of hinge rotation (six degrees at each end) corresponds to failure of the panel. Similar rotation limits for reinforced concrete slabs can be found in UFC 3-340-02, and are justified by examining the section mechanics of a typical six-inch thick reinforced concrete façade panel. These rotation limits, along with Equation (1), can be used to calculate the plastic work capacity of an (assumed) elasto-plastic façade panel:

$$W_P = \frac{Ph}{4}\left(\theta_{max} - \frac{1}{2}\theta_y\right) \tag{10}$$

where θ_{max} is the maximum plastic hinge rotation given by UFC 3-340-02 (or otherwise derived), and all other terms have been previously defined. This expression is put in

terms of the OP reaction force per panel edge, P, similar to Equation (8). The value which this panel edge reaction term takes is governed by the force-deformation relationship of the MDCs, which include round HSS tubes as a critical force-compliant element in the OP load path.

3.2 Round Hollow Structural Section (HSS) Tubes

The proposed MDC design approach includes round hollow structural section (HSS) tubes oriented such that OP panel demands apply a radial load to the circular tube walls (Fig. 1 and Fig. 2). For this type of load, the elastic stiffness, initial plastic mechanism strength, and post-yield hardening behaviors are of interest considering both crushing (radial deformation towards the section's center) and pulling (away from center) deformations. Additionally, MDCs which anchor the panels in the LIP and V directions rely on the tube wall section to elastically resist the combined shear and moment demands caused by these eccentric (relative to the tube's central longitudinal axis) forces.

3.2.1 Radial Force-Deformation Relationship

The elastic stiffness and initial plastic mechanism strength are identical in the radial crushing and pulling directions, however the post-yield behaviors differ due to the difference in boundary conditions resulting from the large deformation mechanics that develop: when crushed, the circular section is flattened along the (assumed rigid) plates on either side, while the pulling direction straightens the circular cross section without rigid boundary constraints until it acts essentially as a tension member. These behaviors are illustrated in Fig. 6.

3.2.1.1 Elastic Behavior

The initial plastic mechanism strength is the most critical mechanical property as it must be large enough to resist the panel edge reaction force for OP demands with an elastic MDC performance objective, and also determines the magnitude of post-yield forces in either loading direction. The initial plastic mechanism strength, P_0, can be calculated by the principle of virtual work considering the formation of four flexural plastic hinges:

$$P_0 = \frac{t_{HSS}^2 R_y \sigma_y l_{HSS}}{r_{HSS}} \tag{11}$$

where t_{HSS} is the HSS section wall thickness, l_{HSS} is the (longitudinal) length of the HSS section, r_{HSS} is the outer radius of the HSS section, and all other variables have been previously defined. The (linear) elastic stiffness, k_{HSS}, of a radially-deformed round HSS section (both crushing and pulling) is given by Roark's Formulas (Young & Budynas, 2002) as:

$$k_{HSS} = \left(\frac{\pi}{4} - \frac{2}{\pi}\right)^{-1} \left(\frac{E l_{HSS} t_{HSS}^3}{12 r_{HSS}^3}(1-\nu^2)\right) = \frac{(14779.3\text{ksi}) t_{HSS}^3 l_{HSS}}{r_{HSS}^3} \tag{12}$$

where E is the material modulus of elasticity (29000 ksi for steel), ν is the Poisson's ratio of the material (0.3 for steel), and all other terms have been previously defined. Equations (11) and (12) can be used to calculate the elastic potential energy of these radially-deforming HSS tubes, PE_{HSS}, given by:

$$PE_{HSS} = \frac{P_0^2}{2k_{HSS}} \tag{13}$$

where all terms have been previously defined.

3.2.1.2 Crushing Behavior

The post-yield HSS crushing behavior is critical for sizing the HSS for large design impulse scenarios, where a conservation of energy approach is used to determine the required MDC hysteretic work to ensure a desirable progression of damage in the connectors and façade panel. Both geometric effects and material stress-strain nonlinearity must be accounted for when formulating a force-deformation relationship for radial crushing of a thin-walled circular section. A suitably accurate model was formulated by Reid and Reddy (1978) which includes elliptically-deformed "plastica" hinge regions which spread along each side tube wall allowing for slope continuity (geometric effects), and a bilinear material stress-strain model (material nonlinearity). The resulting (normalized) force-deformation model is included in Fig. 6. This model has shown strong agreement with both experimental and analytical results (Reid & Reddy, 1978; Lavarnway, 2013), albeit without an elastic loading region.

For design purposes, the post-yield crushing model is approximated by a linear function which reaches twice the initial plastic mechanism strength ($2P_0$, where P_0 is given by Equation (11)) at a radial deformation equal to 2/3 the original tube diameter. This model simplifies the MDC blast design calculations while providing a nearly identical hysteretic work term to the conservation of energy expressions used to size the HSS tube for large blast scenarios. A deformation of 2/3 the original tube diameter is assumed to be the maximum crushing deformation for design because complete crushing of the tube is impossible due to the presence of bolts/nuts on the MDC plates. Additionally, the rapid strength increase observed beyond 2/3 the original tube diameter would require proportional strengthening of the façade and building frame and is thus

avoided. With these approximations, the plastic work capacity of a radially crushed HSS tube, W_{HSS}, is given by:

$$W_{HSS}=P_0\left(2r_{HSS}-\frac{3P_0}{2k_{HSS}}\right) \quad (14)$$

where all terms have been previously defined. Note that this work term represents the area under the idealized force-deformation curve shown in Fig. 6 (Equation (14) subtracts out elastic deformations, which are not pictured in Fig. 6).

3.2.1.3 Pulling Behavior

HSS pulling behavior is relevant for panels located at the corner of a building, where contact will occur during large seismic drifts. The assumed geometry of a radially pulled HSS includes rigid rotation of the HSS section about the plate-adjacent plastic hinges, and straightened "free" hinge regions spanning the points of tangency perpendicular to the plate surfaces (Fig. 6). The following relationship between pulling deformation, δ_{pull}, and the straightened length of the HSS section, l_p, can be derived:

$$\delta_{pull}=2r_{HSS}\left(\sin\left(\frac{\pi r_{HSS}-l_p}{2r_{HSS}}\right)-1\right)+l_p \quad (15)$$

where all terms have been previously defined. This changing geometry with increased pulling deformation reduces the effective radius, r_{eff}, between the plate-adjacent and "free" plastic hinges, which increases the plastic mechanism strength according to Equation (11) replacing r_{HSS} with r_{eff}. With the assumption that the total length around the deformed HSS section remains equal to its original circumference, the effective radius, r_{eff}, can be calculated as a function of the straightened length of HSS section by the following equation:

$$r_{eff}=r_{HSS}\left(1-\cos\left(\frac{\pi r_{HSS}-l_p}{2r_{HSS}}\right)\right) \quad (16)$$

where all terms have been previously defined. For a given pulling deformation, Equation (15) can be solved numerically for l_p, which can then be used to solve for r_{eff} using Equation (16). The effective radius, r_{eff}, replaces the r_{HSS} term in Equation (11), giving the following expression for the post-yield HSS pulling force, P_P:

$$P_P=\frac{1.5P_0r_{HSS}}{r_{eff}}\leq 2l_{HSS}t_{HSS}R_y\sigma_y \quad (17)$$

where 1.5 is a (conservative) factor to account for material stress-strain hardening, P_0 is the initial plastic mechanism strength (Equation (11)), r_{eff} is the effective radius (Equation (16)), and all other terms have been previously defined. The terms to the right of the inequality limit the pulling force to the expected yield force of the tube walls in pure tension.

The normalized HSS pulling force-deformation curve in Fig. 6 indicates a rapid stiffness increase as the section approaches the pure tension force limit. It is advantageous to limit the HSS pulling deformation to a maximum value preceding this rapid hardening to limit the force which develops when adjacent corner panels come into contact during seismic building drift. A suitable HSS deformation limit was found by disregarding the "straightening" of tube walls discussed in the previous paragraph and simply rotating the HSS section quadrants rigidly about four discrete plastic hinges. The maximum pulling deformation, δ_{limit}, which can be achieved by this method is given by:

$$\delta_{limit}=2r_{HSS}\left(\sqrt{2}-1\right) \quad (18)$$

where all terms have been previously defined. This value corresponds to rapid hardening behavior observed in the HSS pulling force-deformation model, as well as finite element

analysis (FEA) simulation results. For design purposes, any required outward OP MDC deformation greater than the value given by Equation (18) will be accommodated by yielding of the MDC plates at or below an HSS pulling force of about 3.5 times (Fig. 6) the initial plastic mechanism strength, P_0 (Equation (11)).

3.2.2 Tube Wall Section Shear and Flexural Demands

MDC types 2 and 3 anchor the panel in the vertical and LIP directions, respectively, in addition to their OP action. The tube's longitudinal axis must be oriented parallel to the non-OP anchorage direction (LIP for MDC-3, V for MDC-2s) to maximize the weld line and tube wall section stiffnesses considering these demands. All vertical and LIP demands have an elastic MDC performance objective (Table 1). To satisfy this criteria, the combined stresses acting on the tube wall sections must be evaluated to ensure premature failure of these MDCs does not occur under design-level loading. Yield of the tube wall section should be checked for the controlling combination of normal (OP) and shear (LIP for MDC-3, V for MDC-2s) stresses using a von Mises yield criterion (Fig. 7). Shear yield of the wall section should also be checked, particularly for short MDC-3 lengths on corner panels. As previously discussed, vertical and LIP loads are considered to act at mid-thickness of the veneer, which creates a moment demand (additional OP normal stress) for the tube wall section. Note that only OP loads with an elastic MDC performance objective should be considered when checking the combined stress on the section (i.e. if the controlling OP demand is a high-magnitude impulse where MDCs are expected to yield, do not combine this normal stress with others; instead, choose the largest OP force which requires elastic MDC response to combine).

4. Design of Components to Achieve Performance Objectives

The most critical MDC component is the length of round HSS tube which is proportioned between the three MDC types to elastically resist all LIP (MDC-3) and vertical (MDC-2s) demands while providing equal OP resistance (all MDC types) at the top and bottom panel edges to achieve all OP performance objectives (Table 1). The total length of HSS tube on each panel edge must be equal to ensure simultaneous yielding (crushing of HSS tubes) of the panel supports to capacity-protect the panel. The HSS tube in each MDC is attached to a steel plate on either side using a full-length steel bar welded to the outer surface of the tube, and then welded into the thickness of a through-slot in the plate. A group of bolts on each plate attaches the MDC to the façade panel on one side and structural frame on the other. Slotted bolt holes and strategic arrangement of the MDC types allow for accommodation of all thermal panel expansion/contraction and LIP building drifts without distorting the panel (Fig. 1 and Fig. 2). Each MDC component must be detailed to resist the expected—and, in the case of the MDC-2s and MDC-3, combined—forces along the load path to achieve all performance objectives in all degrees-of-freedom.

The flexural capacity of the façade panel is determined as a function of the MDCs' OP strength per panel edge to capacity-protect the panel during hazardous loading events. The OP strength of MDCs also determines how much force can be transferred from the façade system to the main structural framing. The collective strength capacity of all MDCs attached to each floor diaphragm whose OP action is parallel to the principal direction of a set of building LFRS frames can be thought of as a design lateral force demand for these frames in addition to the typical (wind, seismic) LFRS demands. The nature and magnitude of the various OP load types on the façade system limits the

probable proportion of the full MDC strength capacity which can realistically be considered as a design lateral force for the building LFRS. Capacity design of the LFRS for the maximum expected force transfer from the façade system represents another step towards bolstering building performance considering any type of hazardous loading scenario. This concept will be revisited after the MDC and façade panel design approaches are fully detailed in the following subsections.

4.1 Multi-Hazard Ductile Connectors (MDCs)

MDC design begins with determining the required length per façade panel edge of a chosen HSS section to meet all OP performance objectives. A seismically compact (per AISC 341) HSS section should be chosen at the start of the design and iterated upon if the resulting design is impractical. Note that, although the seismically compact section criteria in AISC 341 is for a round HSS tube compressed along its longitudinal axis (which is not the load case here), this or some other compactness criteria should still be included considering the highly ductile behavior expected of the HSS tubes. The total tube length per panel edge and distribution of this length amongst MDC types must be capable of achieving all performance objectives summarized in Table 3. Some iteration may be necessary to find an HSS section which requires a reasonable length per panel edge. If excessive tube length is required (say, greater than 100”), the required number of bolts and overall size of the connectors reduces the practicality of utilizing MDCs. However, if not enough tube length is required (say, less than 30” per edge), strength issues arise when proportioning the tube length per edge between the MDC-2s and MDC-3 due to moment demands caused by vertical and LIP load eccentricities, respectively.

Six-inch diameter HSS sections have been found to be effective for reinforced concrete panel MDC design

4.1.1 Sizing HSS Tube Length per Panel Edge for Out-of-Plane (OP) Demands

For non-impulsive demands with elastic MDC performance objectives, the controlling required HSS length (for a chosen section) per panel edge can be solved for using Equations (1) and (11):

$$l_{HSS} = \frac{whr_{HSS}}{2R_y\sigma_y t_{HSS}^2} = \frac{4Mr_{HSS}}{hR_y\sigma_y t_{HSS}^2} \tag{19}$$

where w is the uniformly distributed (force per unit panel height) load demand, M is the maximum panel moment resulting from w, and all other terms have been previously defined. This length should be compared to the maximum tube length obtained considering the impulsive loading scenarios and associated performance objectives, and the controlling (maximum) value should be chosen as the trial length per panel edge for the chosen HSS section moving into the V and LIP load considerations, which determine the distribution of total tube length to each MDC type. HSS section properties relate to design-critical OP behaviors by the proportional relationships given in Table 4. This table can be used to assist in the selection of a round HSS section depending on which OP design consideration (hazard plus performance objective; Table 1) controls the design tube length.

Design of the MDCs for the impulsive OP loading scenarios and performance objectives given in Table 3 relies on the conservation of energy expression given by Equation (6), with the addition of the HSS energy terms given by Equations (13) and (14) to the right-hand side, and substitution of the HSS crushing strength (Equation (11), Fig. 6). The l_{HSS} terms in the aforementioned equations can be thought of as the required tube

lengths per panel edge. Considering the generalized SDoF system upon which Equation (6) is based, the OP force-deformation action provided by the top and bottom sets of MDCs can be readily added into this system as OP translation at these connection points translates directly to translation at panel mid-height, which is the generalized displacement coordinate. To ensure capacity protection of the panel up to the maximum crushing deformation of the MDCs (Fig. 5), the panel edge reaction force term, P, in Equations (8) and (10) should be replaced by the maximum HSS tube crushing strength, $2P_0$ (two times Equation (11)). With these modifications to Equation (6), the impulsive loading design equation is given by:

$$KE_P=2PE_{HSS}+PE_P(2P_0)+2W_{HSS}+W_P(2P_0) \quad (20)$$

where KE_P is the initial elastic potential energy of the façade panel subjected to a known impulse (Equation (5)), PE_{HSS} is the elastic potential energy of the radially-crushed HSS tube length per panel edge (Equation (13)), $PE_P(2P_0)$ is the elastic potential energy of the façade panel (Equation (8)) with the maximum crushing strength, ($2P_0$, where P_0 is given by Equation (11)) of the HSS tube length per panel edge substituted for the panel edge reaction force, P, W_{HSS} is the plastic work capacity of the HSS tube lengths per panel edge (Equation (14)), and $W_P(2P_0)$ is the plastic work capacity of the façade panel with $2P_0$ replacing P in Equation (10). Note that the plastic work terms take values of zero whenever the performance objective for that component subjected to a given design impulse scenario is to remain elastic.

Substituting the known work-energy expressions into Equation (20) yields the following (equivalent) expression:

$$\frac{I_D^2}{2m^*}=\frac{P_0^2}{k_{HSS}}+P_0\delta_y+P_0\left(4r_{HSS}-\frac{3P_0}{k_{HSS}}\right)+\frac{P_0h}{2}\left(\theta_{max}-\frac{1}{2}\theta_y\right) \quad (21)$$

where all terms have been previously defined. This expression can be solved for P_0 for a given design impulse value. For a chosen HSS section, P_0 can then be solved for l_{HSS} per panel edge. This HSS length can be compared to the minimum length calculated from Equation (19), and the larger value (rounded up to, say, the nearest quarter inch) is chosen for MDC design using the chosen HSS section. The eccentric vertical and LIP demands can then be considered to proportion the total length per panel edge between MDC-2s and the MDC-3.

4.1.2 Accommodation of Corner Panel Contact during Seismic Building Drift

The previously discussed corner panel contact issue during seismic building drift can be accommodated through plastic yielding of the MDCs. This issue can be disregarded for "interior" façade panels, however it can largely control the choice of HSS cross section and distribution of tube lengths per MDC type for "edge" panels and should, therefore, be the next design consideration for edge panels once the OP performance objectives have been dealt with. With the connection configuration shown in Fig. 1 an initial distribution of, say, equal tube length per MDC can be made to estimate the relevant forces due to corner panel contact (in general, the MDC-3 will have a greater length than each MDC-2). This distribution of lengths and resulting contact forces can be iterated as needed until a reasonable design which satisfies all criteria is achieved.

The connector "fuse" approach is illustrated in Fig. 8 with a combined MDC mechanism (on the OP panel) which minimizes the internal work performed to accommodate the required deformation assuming rigid panel behavior. A straight line—along which the OP panel deformation varies linearly—can be drawn between the point

of panel contact and the perpendicular line about which the OP panel rotates (line of zero OP deformation). For each MDC, the perpendicular distance from the zero deformation line can be used to calculate the required OP deformation inwards (HSS crushing) or outwards (HSS pulling). The HSS crushing and pulling models are then prescribed these deformations, and the sum of their OP forces is the contact force, F_C, which develops between the panels during corner panel contact. Deformations input into the HSS pulling model should be limited by Equation (18), and any additional required OP deformation will be accommodated through outward yielding of the MDC plate(s); for typical MDC HSS sections and panel dimensions, the required OP MDC deformation only exceeds the value given by Equation (18) for the MDC (type 1) nearest to the panel contact location. The contact force must be resisted elastically by the MDC-3 on the IP panel, as well as through a vertical force-couple provided by the IP MDC-2s to resist the moment caused by the location of the contact force. Note that both of the adjacent panels which meet at a building corner must be designed to act as both the "OP" and "IP" panel to accommodate seismic panel contact due to building drift in either lateral direction.

The maximum vertical MDC-2 force due to seismic panel contact can be calculated by considering the panel as a beam (in the LIP-V plane) supported by the MDC-2s with an applied moment at one end equal to the contact force multiplied by the panel height (right side of Fig. 8). Resistance of this moment requires an upward contact force, F_{CV}, at the far-side MDC-2 given by:

$$F_{CV}=\frac{hF_C}{b} \tag{22}$$

where F_C is the lateral force due to corner panel contact during seismic building drift, b is the width of the façade panel, and all other terms have been previously defined. This

force is additive with the (factored) dead load and vertical seismic panel inertia, and should, therefore, be included when performing HSS tube wall section checks and connection detailing strength designs considering the seismic (plus factored dead load) load case. As with all V and LIP loads, the design contact forces given by Equations (21) and (22) are considered to act at mid-thickness of the veneer. This eccentricity must be included when considering the combined state(s) of stress which the MDC-2s and MDC-3 must elastically resist.

4.1.3 Eccentric Vertical (V) and Lateral in-Plane (LIP or IP) Demands

The controlling V and LIP load cases discussed in Sections 2.1.2 and 4.1.2 must include the eccentricity of these loads. Moment demands can be calculated by multiplying the controlling force values by a conservative design eccentricity. For simplicity, the façade panel (at mid-thickness) and structural frame (at the MDC plate-to-structural frame boundary) are assumed to have equal flexural stiffness; this implies that an inflection point (point of zero moment) in the deformed shape of the frame-MDC-panel system exists halfway between the "boundaries" (panel mid-thickness and MDC plate-to-frame boundary). The design eccentricity—illustrated in Fig. 9—is taken as the distance between this inflection point and the MDC plate-to-frame boundary. A conservative assumption that the MDC plates are one inch thick can be used, and the design eccentricity, e_{des}, can be calculated as:

$$e_{des} = \frac{t_F}{4} + r_{HSS} + t_P \tag{23}$$

where t_F is the thickness of the façade panel, t_P is the thickness of each MDC plate (preliminary assumption of one inch), and all other terms have been previously defined. The controlling vertical and LIP design forces should be multiplied by Equation (23) to

determine the design moments for MDC-2s and MDC-3, respectively. All combinations of the vertical/LIP, moment, and (elastic) OP demands must be considered when performing HSS tube wall limit state checks (Section 3.2.2), as well as detailing calculations for the MDC-to-plate welds and bolted connection designs.

4.1.4 Proportioning Total HSS Tube Length per Panel Edge for each MDC Type

With all design demands for the chosen HSS section and calculated tube length per panel edge, the distribution of tube lengths between MDC-2s and the MDC-3 can be determined. The connection configuration shown in Fig. 1 and discussed in Section 2 is assumed as this arrangement is compatible with all in-plane (thermal/moisture effects and seismic building drift) deformation requirements while also allowing for kinematic adjustment of the panel at the vertical load-bearing (MDC-2) connections during panel installation. The design tube length per edge should be divided evenly among the (three) MDC-1s along the top panel edge. Ideally, each MDC-1 should contain between one and two feet of tube because the plates attaching the tube to the structural frame will be at least long enough to accommodate the seismic drift bolt slots, and it is advantageous—particularly for edge panels, where plate yielding is used to accommodate panel contact due to seismic building drift—for the tube to span about the same length as these long slots. Four bolts are used to connect each MDC-1 plate (frame-side and panel-side): two above the HSS and two below. The length of the frame-side plate (in the direction of the tube's longitudinal axis) will be at least two long slots, plus two bolt-to-edge distances, plus one bolt centerline spacing distance. Assuming a story height of 13', an allowable drift of 2.5%, and bolt diameters of 1", the slot length is calculated to be +/- the building

drift (13'x0.025 = 4") plus the bolt diameter (1"), or about 9" total. Therefore, with the edge and centerline spacing, the total plate length will be about two feet.

The distribution of the total required HSS length per panel edge to the MDC-2s and MDC-3 can be determined once all controlling vertical, LIP, and moment demands are calculated. The length of tube in the MDC-2s and MDC-3 affects the HSS-to-plate weld and plate-to-panel/frame bolted connection details, which in turn affect the MDC plate dimensions. Some practical limits exist on the maximum height of MDC-2s (say, eighteen inches), as well as the MDC plate thickness which should be no greater than one inch (or whatever value was assumed for the design eccentricity) based on Equation (23). The recommended approach is to: (1) assume an HSS length for the MDC-2s; (2) determine the remaining HSS length per edge for the MDC-3; (3) check the MDC-2 and MDC-3 tube wall section limit states (Section 3.2.2 and Fig. 7); (4) calculate the required HSS-to-plate weld and bar sizes (which set a minimum MDC plate thickness); (5) determine MDC plate dimensions based on bending strength, bolt size/spacing, and connection limit states; (6) calculate the required number and size of bolts per MDC; and (7) iterate as needed until a reasonable design is achieved (change MDC-2 HSS length first, then, if necessary, choose a new HSS section). For interior panels, the length of tube per MDC-2 should be roughly between six inches and one foot. For edge panels, achieving the proper balance between HSS length proportioned to the MDC-2s and MDC-3 is more difficult due to the large seismic building drift panel contact force. For these panels, the HSS-2 tubes should be roughly eight to eighteen inches long, while the MDC-3 should have one to two feet of HSS tube.

4.1.5 Connection Detailing Considerations

The HSS-to-plate welds—illustrated in Fig. 9—consist of two legs spanning the full HSS tube length which connect the outer surface of the tube to a weld bar, and two full-length weld legs connecting the weld bar (on the back-side bar surface parallel to the HSS surface tangent) to the MDC plate through its thickness. The weld size can be specified by using the elastic vector analysis method (AISC, 2010b) to calculate the required weld strength per thickness for each source of stress (load and moment), and then combining these "stresses" using a vector sum of the normal and shear components for all load cases. Once the maximum weld "stress" is determined, the weld size can be specified per AISC 360 (2010b). Note that the bar-to-plate thickness welds will have a slightly reduced effective throat due to the oversize of the MDC plate slot (similar to a standard bolt hole; slot width 1/16-inch greater than weld bar width), therefore the thickness of each weld leg should be increased by 1/16-inch to ensure adequate strength considering the minimum plane area through the weld. The required weld thickness determines the minimum dimensions of the weld bar and MDC plate thickness; as shown in Fig. 9, the weld bar must have a width (tangent to HSS surface) equal to at least two weld thicknesses and a depth (into the plate thickness) of at least one weld thickness, while the MDC plate thickness is at least two weld thicknesses.

The weld bar width should be increased above the minimum if a larger cross sectional area (length—equal to the full length of the HSS tube—by width) is required to develop the full strength of the welds. For ease of construction, all MDC plates (types 1, 2, and 3) should have the same thickness, therefore the minimum MDC plate thickness for a given panel is the twice the maximum required weld thickness for all MDC types. The depth (into the MDC plate thickness) of the weld bars for each MDC should be the

largest nominal bar dimension increment for which the bar-to-MDC plate welds remain within the thickness of the MDC plate; this allows for easier access to the weld location during fabrication of the MDCs while maintaining a flat surface on the backside of each MDC plate. Note that a bevel along the inside edge of the MDC plate weld bar slot (Fig. 9) is necessary for the HSS tube to sit flush against the MDC plates, which is consistent with the boundary conditions in the round HSS crushing model (Fig. 6). This slot in the MDC plates should have a standard oversized width (1/16-inch greater than the weld bar width), and circular ends (Fig. 2) to allow for expansion of the weld filler material under stress and to eliminate stress concentrations in the plate due to geometric discontinuity. From the center of these circular slot-ends, the minimum bolt hole center-to-plate edge distance (AISC, 2010b) can be added to the length of the HSS tube per MDC to determine the minimum MDC plate dimension in the direction along the tube's longitudinal axis.

The MDC plate dimensions and bolted connection design are highly interdependent. Example illustrations of the bolts and slotted bolt holes for each MDC type and plate side are shown in Fig. 2 and Fig. 9. Four bolts are used for the MDC-1s to prevent the frame-side plates from becoming excessively long due to the long lateral slotted bolt holes. The length of these slotted holes is equal to +/- the maximum building story drift (2.5% of the story height for new construction) plus the bolt diameter. These long slots also serve as the lateral thermal expansion/contraction slots for the MDC-1s. Standard thermal expansion/contraction slots are included on the panel-side MDC-1 (vertical slots) and MDC-2 (lateral slots) plates. Thermal expansion slots have a length equal to the expected expansion/contraction of the panel (about +/- 3/8-inch for

reinforced concrete panels) plus the bolt diameter. Standard bolt holes are used for all MDC-3 bolts. All bolt hole centers—including at the extreme ends of slotted holes—should be at least one tube diameter away from the centerline of the HSS-to-plate connections to allow for access to the bolts/nuts during installation, and to prevent premature contact between the bolts/nuts and HSS tube wall during crushing as the tube flattens against the plates. For MDC-2s and the MDC-3, the number of bolts along the longitudinal axis of the HSS tube should be determined considering the minimum bolt hole center-to-center spacing (2-2/3 to 3 times the nominal bolt diameter) and available length of MDC plate in this direction. This close spacing limits undesirable bending of the plates about the axis perpendicular to the HSS tube's longitudinal axis. Following these guidelines, preliminary bolt diameters can be assumed—say, one inch for MDC-1s and ½-inch for MDC-2s and the MDC-3—and minimum bolt spacing requirements will determine the number of bolts and trial size of each MDC plate.

Once a trial MDC plate size has been determined, its plastic capacity can be calculated considering a uniform outward pulling force applied to the plate by the HSS tube. The plate can be analyzed as a beam with this pulling (point) force acting at its center and fixed boundary conditions provided by the bolt lines on either side of the HSS tube (bottom of Fig. 9a). The plastic mechanism of this "beam" requires hinges just inside the supports (bolt holes) and a hinge at the location of force application. For plates required to yield outwards to accommodate corner panel seismic contact (typically only MDC-1 frame-side plates), the rigid body kinematics of this plastic mechanism should be examined to ensure that the required outward deformation of the plate does not exceed the recommended limit of ten degrees (DOD, 2008) of hinge rotation for flexural plate

yield (bolts can be moved farther apart to reduce required rotation, if necessary). If the strength of the plates is less than the controlling outward MDC demand (with an elastic performance objective), the plate's height (along the HSS tube's longitudinal axis) and/or thickness can be increased. If a plate which is required to yield outward is calculated to be stronger than the HSS pulling force at its maximum deformation, the plate section can be reduced by drilling empty holes between the bolt holes and HSS tube centerline. Alternatively, another iteration of the MDC design can be attempted with a weaker HSS tube (larger radius and/or smaller thickness) to increase the required length of tube per panel edge, reduce MDC weld thickness and, consequently, minimum MDC plate thickness, thereby weakening the plate.

For plates on the panel side, the required prying stress from the bolt hole to the plate edge should also be calculated and limited (by extending the bolt-to-edge distance, if necessary) to less than the maximum compressive stress of the panel material. Regardless of which side the plate is on, the required prying force from each bolt line should be calculated to include in the bolt strength design procedure. For MDC-1s, this prying force plus the maximum OP force on the MDC should be used to size the four bolts on either side of the HSS tube. For MDC-2s and the MDC-3, these same forces should be considered along with shear interaction from the controlling vertical and LIP demands, respectively. If the required bolt diameters differ from those assumed to obtain a trial plate size, the process must be repeated to ensure all plate strength and bolt spacing and strength requirements are satisfied. Finally, the bolted connections and plate should be checked for bolt bearing/tear-out, block shear, net section fracture, and gross section

yield limit states to prevent premature failure along each MDC load path. A summary of MDC connection design considerations is provided in Table 5.

4.2 Capacity Design of Façade Panels

The required flexural strength of the façade panel is a function of the controlling support strength provided by MDCs. The target behavior of the system is for the panel to reach its maximum moment capacity when the HSS tubes reach their maximum crushing deformation corresponding to a force equal to twice their initial plastic mechanism strength, P_0 (Equation (11)). Assuming the demands on the panel approximate a uniformly distributed load, the design panel moment capacity, M_P, is given by:

$$M_P = \frac{P_0 h}{2} \tag{24}$$

where P_0 is the MDC strength per panel edge (Equation (11)) and all other terms have been previously defined. Proportioning the of the façade panel and MDCs strengths in this manner regardless of the controlling OP hazard and performance objective follows the capacity design philosophy of designing for a desired progression of damage along the load path. This approach provides a guarantee of some force-limited protection of the panel's integrity regardless of the loading type or magnitude.

4.3 Building Frame Interaction

Proportional strengthening of the façade system for high hazard events ultimately allows larger forces to propagate into the main building frame during such events. An early question raised in this research was whether this reinforcement would require proportional strengthening of the building's LFRS relative to traditional design lateral loads due to wind and seismic inertia. The resulting inter-story shear forces considering, say, all MDCs at their initial mechanism strength, P_0 (Equation (11)) is on the order of—

and in some cases exceeds—traditional LFRS design demands. However, the nature and likelihood of an event which would create such a load case is unknown and may be unrealistic. Preliminary analysis of buildings with MDCs subjected to blast scenarios suggests that, although several façade panels may develop their ultimate capacities, the spatial and temporal distribution of these forces acting on the main structural framing results in peak LFRS demands which are generally much smaller than what might be predicted considering a "façade strength development" LFRS design force equal to some fraction of the total potential force transfer from façade-to-frame. The analysis models used in this investigation included MDCs which frame directly into the main building floor mass (with rigid diaphragm constraints), and the inertia of this mass may be adequate to effectively "absorb" the brief, large forces the façade exerts on the main building frame (impulsive loading relative to the main building systems; see Equation (5) with large mass term). Additional work is required to determine if local elements at the MDC-to-frame interface might experience significant damage during these scenarios.

5. Integrated MDC Design Procedure

The detailed procedures from the previous sections will be summarized in this section with a step-by-step guideline to the proposed MDC design procedure. An example design of a reinforced concrete façade panel system with MDCs will be presented, as well as a discussion of the viability of the proposed approach for other common façade types.

5.1 Step-by-Step Design Guideline

1. A few known values and assumptions should be established going into the MDC design procedure, such as:

a. Gross building dimensions (BxDxH), location (story, interior or edge panel) and type (material weight/mass, flexural properties) of façade panel to be designed.
b. Establish performance objectives for panel subjected to various hazards (Table 1).
c. Assume a configuration for MDC types (Section 2, Fig. 1).

2. Assume a round HSS section (typically with diameter of four to six inches) and size the required length per panel edge to satisfy all OP demands (Section 4.1.1).
    a. Obtain design reference wind speed and seismic spectral acceleration values. Follow the procedures in ASCE 7-10 to calculate the design components and cladding load for the façade panel of interest. Also determine any minimum panel strengths which might provide a lower-bound limit on the MDC and panel strengths.
    b. Utilize design blast scenario impulse values (Table 2) and conservation of energy expression (Equation (20)) to determine controlling impulse scenario and required HSS tube length.
    c. Determine controlling HSS tube length per panel edge.
3. Capacity design the panel for the desired progression of damage during extreme OP loading (Section 4.2).
4. Calculate the controlling vertical and LIP load demands and their associated moments due to eccentricity.
    a. For corner panels, this includes the MDC demands from panel contact due to seismic building drift (Fig. 8).

b. Assume MDC plate thickness of one inch in Equation (23) for design eccentricity.

5. Proportion the required HSS length per edge between the different MDC types (Section 4.1.4).
    a. For MDC-1s, the length per edge should be divided evenly among the chosen number of MDC-1s (typically three).
    b. Follow guidelines (Section 4) and iterate as necessary to proportion HSS lengths for MDC-2s and MDC-3.
        i. Check tube wall limit states (Fig. 7).
6. Detail MDC welds, plates, and bolts (Section 4.1.5, Fig. 9).
    a. Determine required weld and bar sizes from controlling load combination.
    b. Set minimum MDC plate thickness equal to twice the maximum specified weld thickness among all MDCs.
    c. Assume trial bolt size and configuration and plate dimensions.
    d. Calculate plate bending strength and adjust dimensions (or iterate HSS section choice) as necessary to provide adequate strength.
    e. For plates on corner panels which are required to yield, check rigid body rotation kinematics to ensure plate hinge rotation is no greater than ten degrees. Modify plate section as necessary to ensure yielding.
    f. Calculate required number and size of bolts per MDC plate considering shear-axial force interaction and prying action due to plate bending.
    g. Check bolted connection limit states: bolt bearing/tear-out, block shear, net section fracture, and gross section yielding.

h. Adjust details and iterate as necessary until a satisfactory design is achieved.

7. Assess practicality of resulting design and iterate if necessary.

5.2 Example Design of Reinforced Concrete (RC) Façade Panel System with MDCs

Details of an example façade system with MDCs are provided in Table 6. This design was formulated for a representative office building in Los Angeles, CA, which is generally considered a high seismic, normal wind hazard region. The façade panels are six-inch thick normal weight reinforced concrete (5 ksi compressive strength, 60 ksi rebar yield stress) assumed to span the entire thirteen-foot high, thirty-foot wide story and bay dimensions. Full details of the calculations used to formulate this design are provided in the accompanying MathCAD document ("MDCDesign_V4.5.xmcd"). The façade panel strength factors shown in this table are relative to the strength of a panel with the code-prescribed minimum reinforcement ratio per ACI (2011); this minimum strength is calculated to be about 1150 kip-in for a 6-inch thick 30-foot wide panel with 5 ksi compressive strength concrete and reinforcing steel yield stress of 60 ksi. Note how the controlling performance objective changes moving up the building stories, as well as the differences in total and distribution of tube length between interior and edge panels.

The example MDC designs in Table 6 do not exactly match the cases which were examined using finite element analysis and experimental testing. This design methodology and the experimental testing protocols were developed in parallel, and recent refinements of the MDC design procedure could not be incorporated into the experimental test specimens. The original intention was to test all three MDC types designed for one specific panel on a prototype building, however the tested specimens are

more appropriately considered as individual components not necessarily installed on the same panel. Nevertheless, the tested specimens are representative of realistic designs in terms of tube section, tube length per MDC type, and bolt/weld detailing. FEA was performed using the experimental test specimens to directly compare and verify observed results, and the agreement between theoretical, analytical, and experimental values indicates a good understanding of the critical behaviors utilized in this design methodology.

5.3 Viability of MDC Design using HSS Tubes for Alternate Façade Panel Systems

The MDC design methodology detailed herein was largely developed considering precast reinforced concrete façade panels. This common façade type benefits from the inherent flexural strength considering even minimum reinforcement and cracked panel section moduli; the OP strength considering the minimum reinforcement ratio for temperature and shrinkage is often greater than the requirements for design wind and seismic forces. This panel type is also desirable for blast protection due to its high mass, which reduces the panel's initial kinetic energy and requires less plastic work/elastic energy storage to achieve a given performance objective (Equations (20) and (21)). Preliminary work has been done to determine the viability of the proposed MDC design approach for other common façade systems, including brick veneer with steel stud backing, exterior insulation and finish systems (EIFSs) with steel stud backing, and insulated metal panels (IMPs). Relative to the high-mass, high-strength reinforced concrete system, the brick veneer system is characterized as "intermediate" mass and strength. EIFSs have low mass and intermediate strength, while IMPs have low mass and strength.

The steel stud-backed systems (brick veneer and EIFS) rely primarily on cold-formed steel channels which comprise the backing wall during OP loading. The plastic work and elastic energy storage capacities of the proposed MDC design with reinforced concrete panels on the first story (most demanding/high-strength location) were used to back-calculate the required OP MDC plastic mechanism strength per edge (Equation (11)) and façade panel flexural strength (relative to typical as-built section strength) for the alternate façade panel types. Relative to the RC MDC design, the brick veneer design would require strengthening of the MDCs by a factor of about 1.5, while the steel stud wall requires 2.3 times its typical as-built strength. This can be accomplished by selecting thicker-walled sections for the MDC HSS tubes and cold-formed steel stud wall members. For EIFSs with steel stud backing, the MDCs must be strengthened by a factor of about 4.5 (relative to the RC design), while the panel/stud wall must be strengthened by a factor of about 3. This MDC strength can be achieved with a thicker-walled section and increased total tube length-per-edge, while the panel/stud wall strengthening is achievable with thicker stud wall member sections. These increases in strength are reasonable and will only decrease considering panels on upper stories, therefore the proposed MDC design approach is believed to be viable for typical steel stud wall-backed façade systems. The IMP façade type would require significant strengthening of the panel (by a factor of about 20) to enforce the capacity design principle (Equation (24)) employed in this design methodology and is, therefore, likely a poor choice for blast-protected structures.

6. Conclusions and Recommendations for Future Work

A design approach has been developed for multi-hazard ductile connectors (MDCs) to improve the performance of building façade systems subjected to extreme loading conditions. This approach utilizes large plastic deformation mechanics and capacity design principles to maintain the integrity of the building envelope considering blast, seismic, wind, and debris impact events. The proposed design procedure is believed to be viable for most common façade systems. Interaction forces between the reinforced façade system and building lateral force resisting system (LFRS) were examined, however insufficient evidence was found to warrant proportional strengthening of the LFRS beyond what is required for traditional lateral design forces (wind, seismic).

Additional work is needed to further refine the MDC design methodology to where these components can be practically implemented. A more thorough investigation of non-reinforced concrete façade panel façade systems is needed to fully understand what, if any, changes to the design approach or detailing practices are required to realistically incorporate these components into such systems. The corner panel contact problem should be examined using finite element analysis and (if possible) experimental testing to ensure the proposed accommodation mechanism can be achieved without local damage to the panel near the point of contact. The performance of individual panels (with MDCs), all panels on a given building side, and the entire building including interaction between the façade and LFRS are currently being investigated to quantify the improved performance afforded by the proposed design approach. While these ongoing research efforts may alter aspects of the design methodology detailed herein, the preceding discussion details the procedures which were followed to develop all experimental and analytical specimens.

e. For plates on corner panels which are required to yield, check rigid body rotation kinematics to ensure plate hinge rotation is no greater than ten degrees. Modify plate section as necessary to ensure yielding.

f. Calculate required number and size of bolts per MDC plate considering shear-axial force interaction and prying action due to plate bending.

g. Check bolted connection limit states: bolt bearing/tear-out, block shear, net section fracture, and gross section yielding.

h. Adjust details and iterate as necessary until a satisfactory design is achieved.

7. Assess practicality of resulting design and iterate if necessary.

5.2 Example Design of Reinforced Concrete (RC) Façade Panel System with MDCs

Details of an example façade system with MDCs are provided in

Table 1: Structural Hazards and System Performance Objectives

Hazard	Intensity	Return Period (years)	Building Component Performance		
			LFRS	MDCs	Façade Panels
Seismic	Low	75-350	Elastic or limited plasticity	Seismic drift accommodation	Elastic
	Design-basis	475	Plastic with acceptable max drift		
	Maximum-considered	2475	Plastic with acceptable max drift		
	Collapse-level	5000+	Highly plastic, potential failure		
Wind	Low	10-75	Elastic	Elastic	Elastic
	Design-basis	300-1700	Elastic	Elastic	
	Tornado	100,000-10,000,000	Elastic	Plastic	
Blast	Low	Maximum 125,000. Reduced significantly for essential structures	Elastic or limited plasticity	Elastic	Elastic
	Moderate		Elastic or limited plasticity	Plastic	Elastic
	High		Elastic or limited plasticity	Plastic	Plastic
Impact	Design-basis	???	Elastic	Plastic	Plastic
Notes:	Return periods given as ranges have exact values determined by building occupancy/usage.				
	Impact determined from tornado region with probability conditional on the occurrence of blast or tornado events.				

Table 2: Design Façade Impulse Values

Type:	Blast Scenario (BS)						Impact Missile (Tornado Region, TR)[a]					
Scenario:	BS1		BS2		BS3		TR1		TR2		TR3	
Parameter[b]:	R (ft)	W (lbsTNT)	R (ft)	W (lbsTNT)	R (ft)	W (lbsTNT)	M (lbs)	V (ft/s)	M (lbs)	V (ft/s)	M (lbs)	V (ft/s)
Value	30	500	100	300	200	100	4000	135	4000	112	2595	79
Story	Design Impulse (kip-s)											
9+	0		0		0		0		0		0	
8	0		0		0.110		0		0		0	
7	0		0		0.513		0		0		0	
6	0		0.842		0.764		0		0		0	
5	0		2.603		0.861		0		0		0	
4	2.528		3.323		0.884		0		0		0	
3	9.949		3.574		0.899		16.784		13.924		6.372	
2	14.563		3.768		0.908		16.784		13.924		6.372	
1	19.097		3.866		0.914		16.784		13.924		6.372	

Notes: a. Adapted from USNRC, 2007. Design impact missile (car) treated as non-deforming body. Applicable up to 30 ft. above grade.
b. R = Standoff distance, W = charge weight; M = missile mass, V = missile velocity.

Table 3: MDC Load Demands and Performance Objectives

Degree-of-Freedom		Loading	MDC Type(s)	Performance Objective
Out-of-Plane (OP) 1. Determine total required HSS tube length per panel edge.	Blast Scenario (BS)	BS1: R=30ft W=500lbsTNT	1, 2, 3	Plastic radial crushing (panel flexural yield)
		BS2: R=100ft W=300lbsTNT	1, 2, 3	Plastic radial crushing (elastic panel)
		BS3: R=200ft W=100lbsTNT	1, 2, 3	Elastic
	Wind	Tornado	1, 2, 3	Yield (capacity protect panel)
		Design-level	1, 2, 3	Elastic
	Seismic	Inertia (horizontal)	1, 2, 3	Elastic
		Edge panel contact (OP panel)	1, 2	Plastic radial pulling (low-strength "fuse")
	Impact Missile	Wind (high mass low velocity)	1, 2, 3	Yield (capacity protect panel)
		Blast (low mass high velocity)	1, 2, 3	Elastic
Vertical (V) 2. Allot total HSS tube length per panel edge to MDC-2s to elastically resist demands.	Self-Weight (Dead Load)	Downward vertical force	2	Elastic
		Moment due to eccentricity	2	Elastic (bending + OP normal stress)
	Seismic	Inertia (vertical)	2	Elastic
		Moment due to eccentricity	2	Elastic (bending + OP normal stress)
		Edge panel contact (IP panel)	2	Elastic
Lateral in-Plane (LIP or IP) 3. Ensure remaining tube length is adequate for IP dir.	Seismic	Inertia (horizontal)	3	Elastic
		Moment due to eccentricity	3	Elastic (bending + OP normal stress)
		Edge panel contact (IP panel)	3	Elastic

Table 4: Proportionality of HSS Tube Properties for OP Performance Objectives

MDC Performance Objective	OP Hazard(s)	HSS Property	Proportionality to HSS Tube Parameters		
			Radius, r	Thickness, t	Length, l
Elastic Response	Wind, Seismic Inertia	Plastic Mechanism Strength, P_0	$P_0 \alpha r^{-1}$	$P_0 \alpha t^2$	$P_0 \alpha l$
		Elastic Stiffness, k	$k \alpha r^{-3}$	$k \alpha t^3$	$k \alpha l$
		Yield Deformation, $\delta_y = P_0/k$	$\delta_y \alpha r^2$	$\delta_y \alpha t^{-1}$	N/A
	Blast (BS3)	Elastic Potential Energy, PE	PE α r	PE α t	PE α l
Plastic Response	Blast (BS1, 2)	Plastic Work Capacity, W	W α -r	W α t^2-t	W α l
	Seismic Contact (Edge Panels Only)	Post-Yield Crushing Hardening, αP_0 Post-Yield Pulling Hardening, αP_0	Hardening is more severe in pulling than crushing. Want to minimize pulling force.		

Table 5: Design Load Cases and Combinations for MDC Bolts and Welds

MDC Type	Design Load Case	Factored Loads per Direction		
		V	OP	LIP
MDC-1	Initial mechanism strength (P_0)	N/A	P_0 (outward)	N/A
	Maximum outward pulling force for seismic drift panel contact accommodation ($3.5P_0$; edge panels only)	N/A	$3.5P_0$ (outward)	N/A
MDC-2	Tributary dead load (D) at design eccentricity (e_{des})	1.6D	OP stress due to V loads applied at e_{des} (σ_{MV})	N/A
	D at e_{des} + P_0	1.2D	P_0 (outward) + σ_{MV}	N/A
	D + vertical seismic inertia (s_V) and vertical seismic panel contact force (c_V; edge panels only) at e_{des}	1.2D + s_V + c_V	Pulling force due to contact (c_{OP}; edge-most MDC-2 on edge panels only) + σ_{MV}	N/A
MDC-3	Initial mechanism strength (P_0)	N/A	P_0 (outward)	N/A
	Lateral seismic inertia (s_{LIP}) and lateral seismic panel contact force (c_{LIP}; edge panels only) at e_{des}	N/A	OP stress due to LIP loads applied at e_{des} (σ_{MLIP})	s_{LIP} + c_{LIP}

Table 6: Example Design of Reinforced Concrete Panel Façade System with MDCs

Location		Panel M_p			MDCs (all HSS6 sections)				
Story	Bay	Factor[a]	t_{HSS} (in)	Controlling Consideration	length per edge (in)	l_{HSS2} (in)	l_{HSS3} (in)	$P_{0,edge}$ (kips)	t_{plate} (in)
6	Interior	1.663	0.188	Elastic potential energy (BS3)	32.25	10	12.5	24.5	0.625
	Edge	1.385	0.125	Elastic strength (seismic inertia)	60.75	15	30.75	20.4	0.625
5	Interior	2.011	0.188	Elastic potential energy (BS3)	39	12	15	29.6	0.625
	Edge	2.011	0.188	Elastic potential energy (BS3)	39	12	15	29.6	0.875
4	Interior	2.089	0.188	Elastic potential energy (BS3)	40.5	12	16.5	30.7	0.625
	Edge	2.089	0.188	Elastic potential energy (BS3)	40.5	12	16.5	30.7	0.75
3	Interior	2.127	0.188	Elastic potential energy (BS3)	41.25	12	17.25	31.3	0.625
	Edge	2.127	0.188	Elastic potential energy (BS3)	41.25	12	17.25	31.3	0.875
2	Interior	3.729	0.312	Work capacity (BS1)	26.25	8	10.25	54.9	0.875
	Edge	3.675	0.188	Work capacity (BS1)	71.25	15.5	40.25	54.1	0.75
1	Interior	6.464	0.375	Work capacity (BS1)	31.5	10	11.5	95.1	0.75
	Edge	6.435	0.28	Work capacity (BS1)	56.25	15.5	25.25	94.7	1

Notes: a. Relative to flexural strength of reinforced concrete panel considering minimum temperature and shrinkage (T+S) reinforcement.

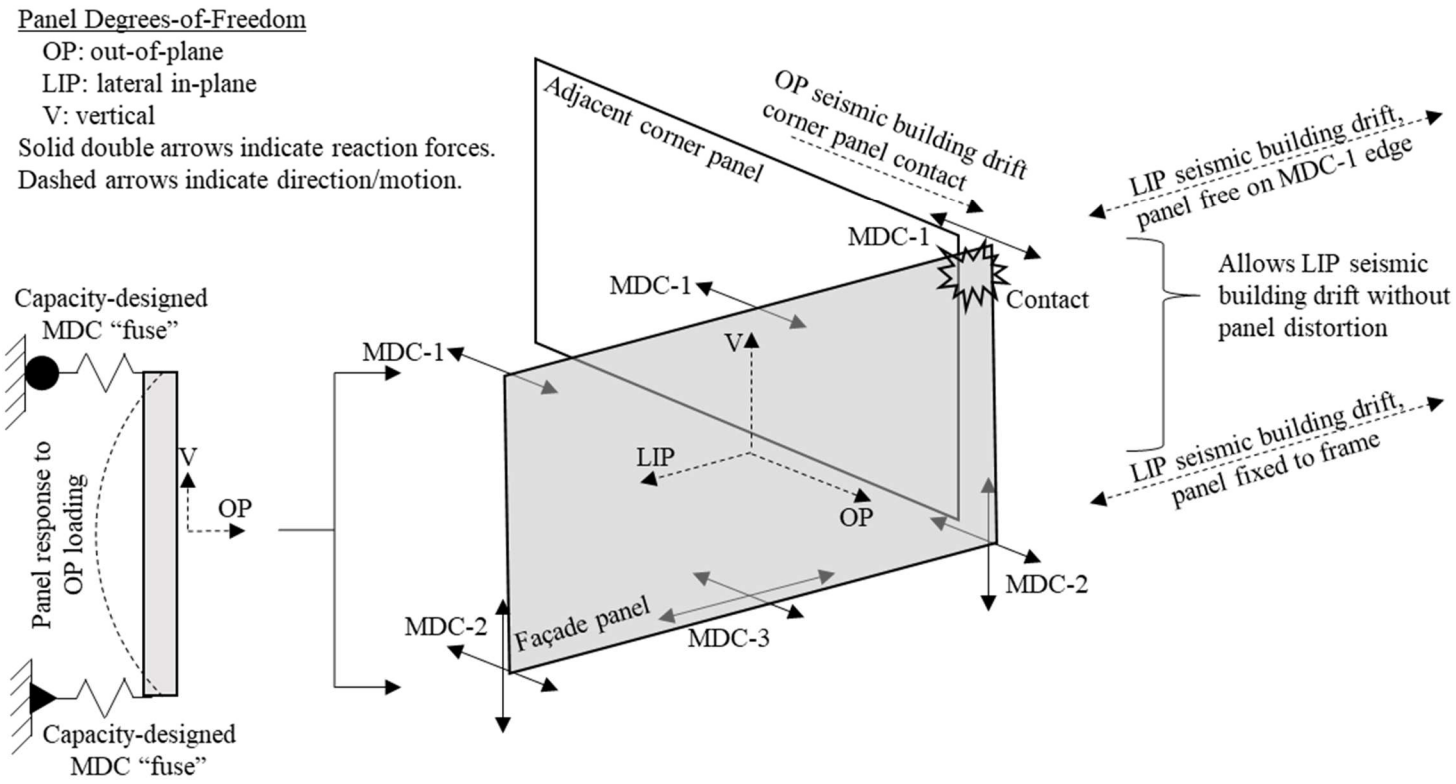

Fig. 1: Façade Panel with MDCs

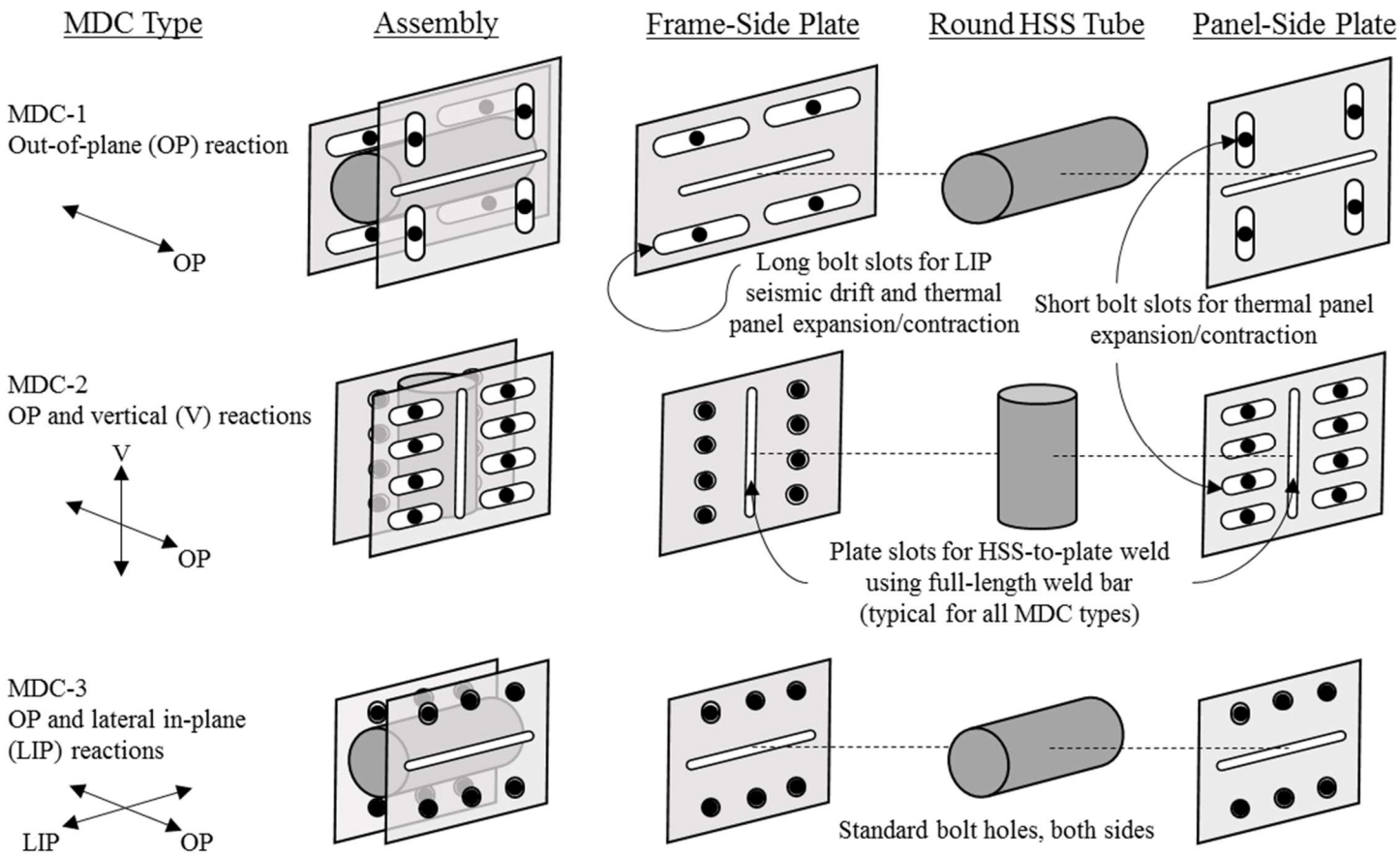

Fig. 2: MDC Illustrations

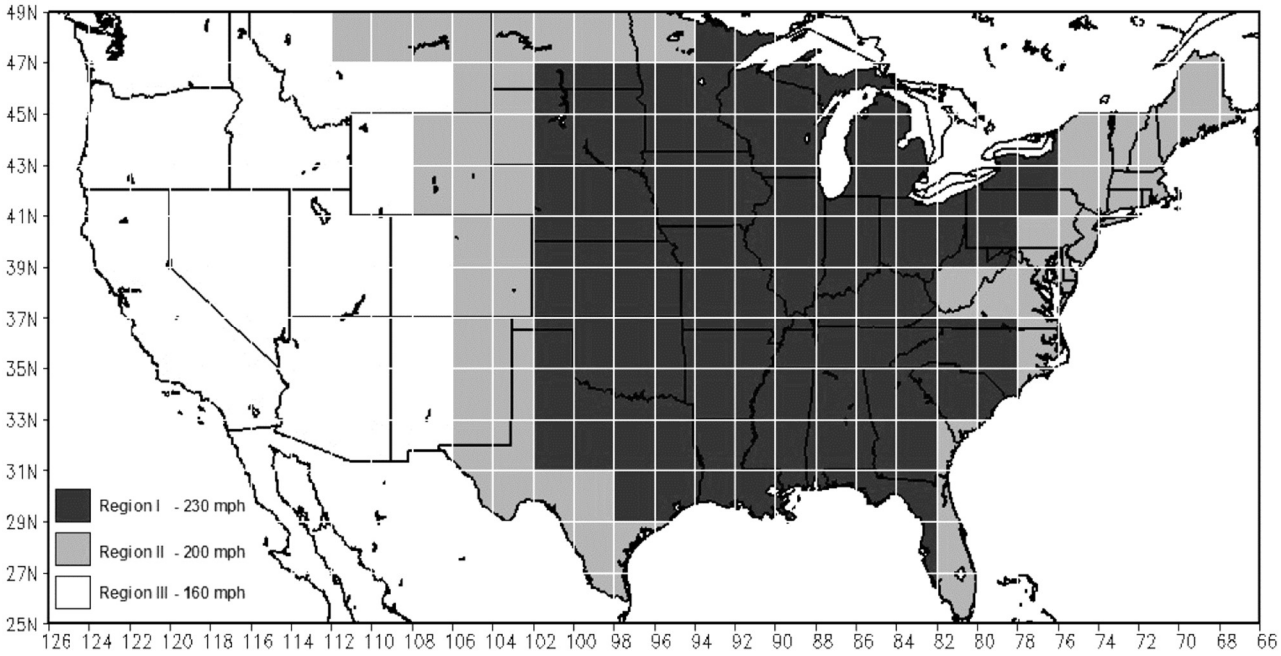

Fig. 3: Design Tornado Wind Regions (Adapted from USNRC, 2007)

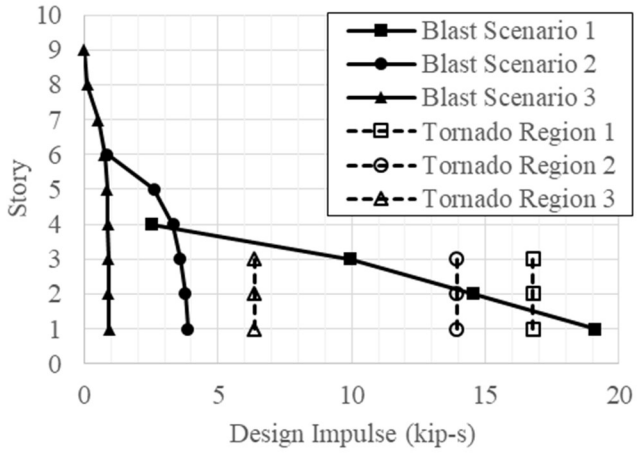

Fig. 4: Design Façade Impulse Values for 13’x30’ Façade Panel

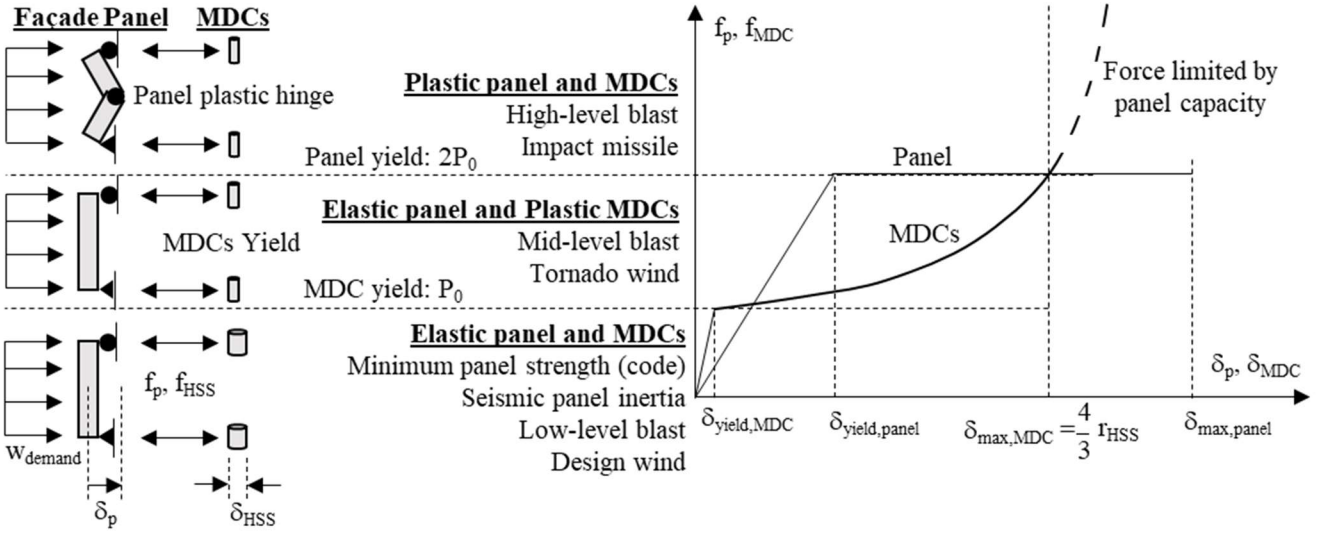

Fig. 5: MDC and Façade Panel Out-of-Plane Performance Objectives and Progression of Yielding

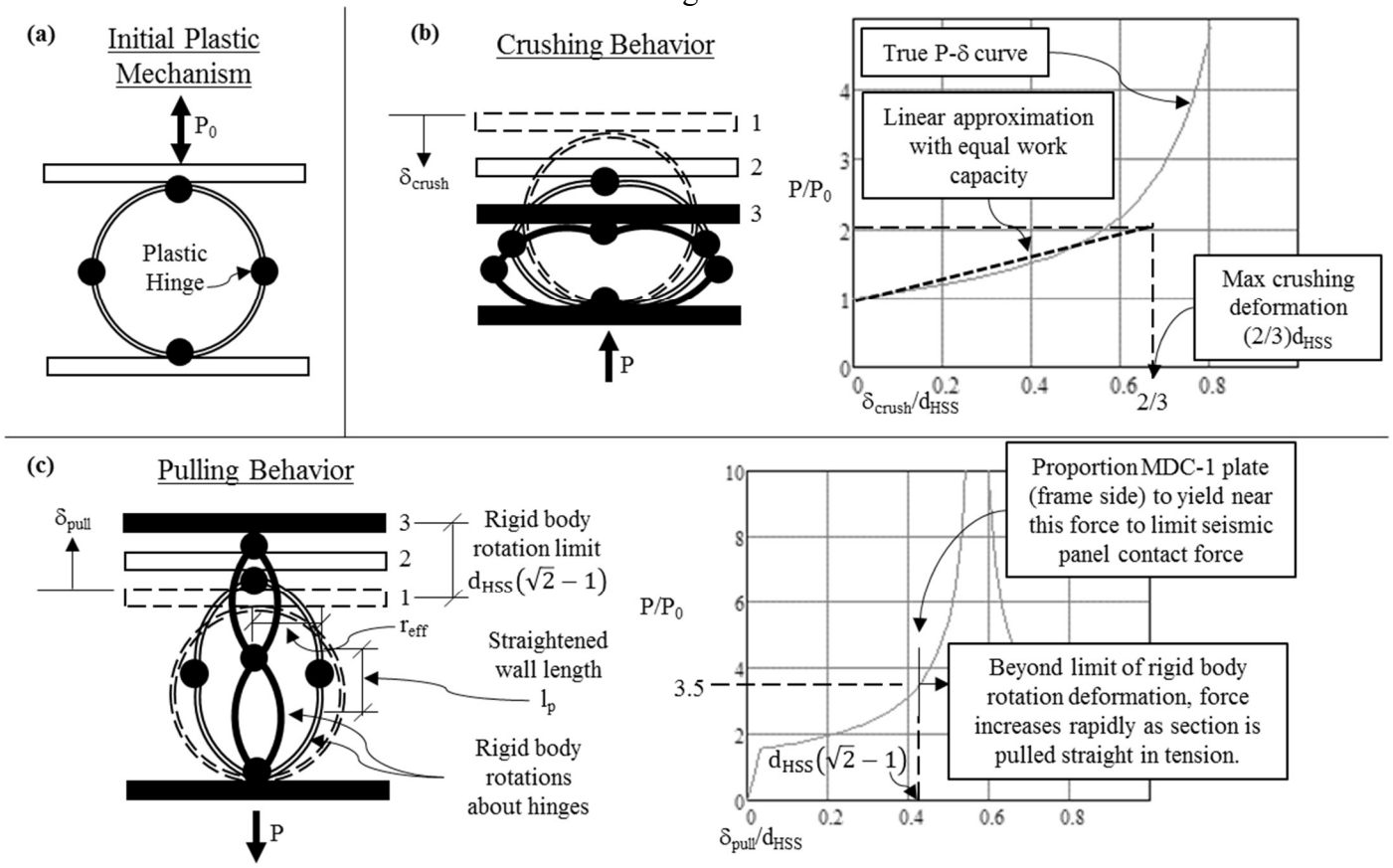

Fig. 6: Mechanics of Radially Deformed Round HSS (a) Initial Plastic Mechanism, (b) Crushing behavior, and (c) Pulling Behavior

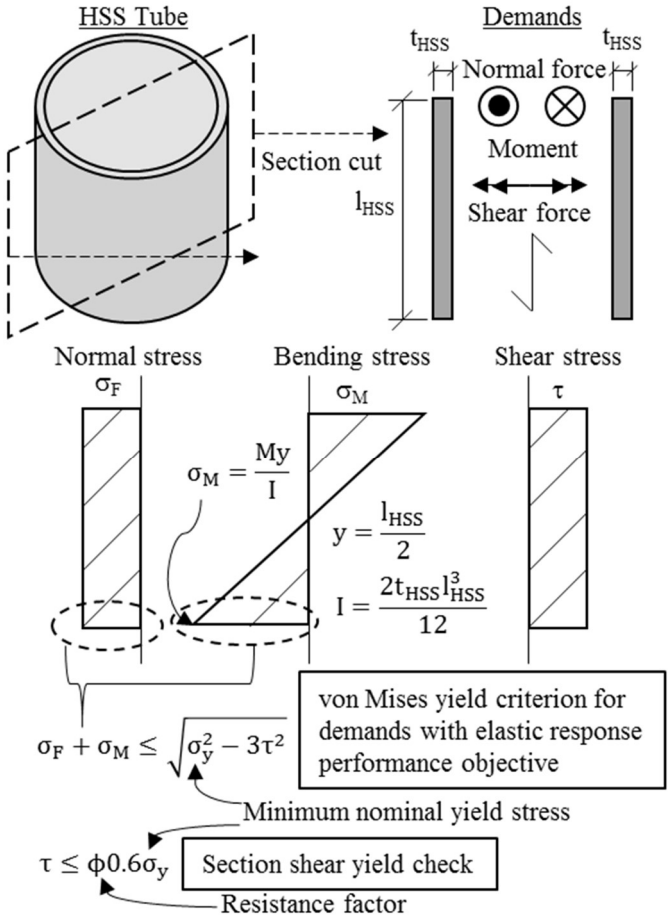

Fig. 7: HSS Tube Section Checks Considering Combined Stresses

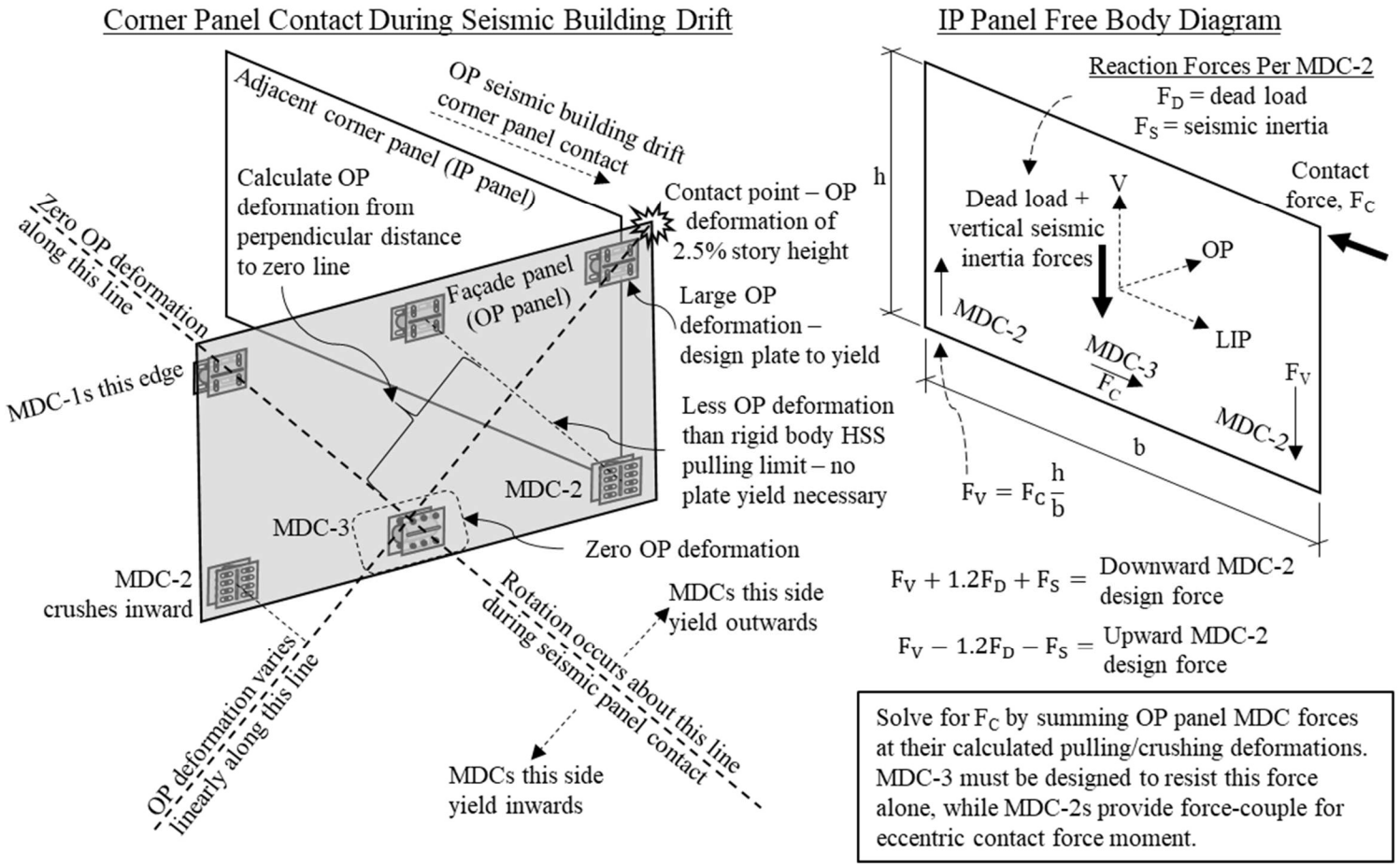

Fig. 8: Seismic Building Drift Corner Panel Contact Accommodation Mechanism

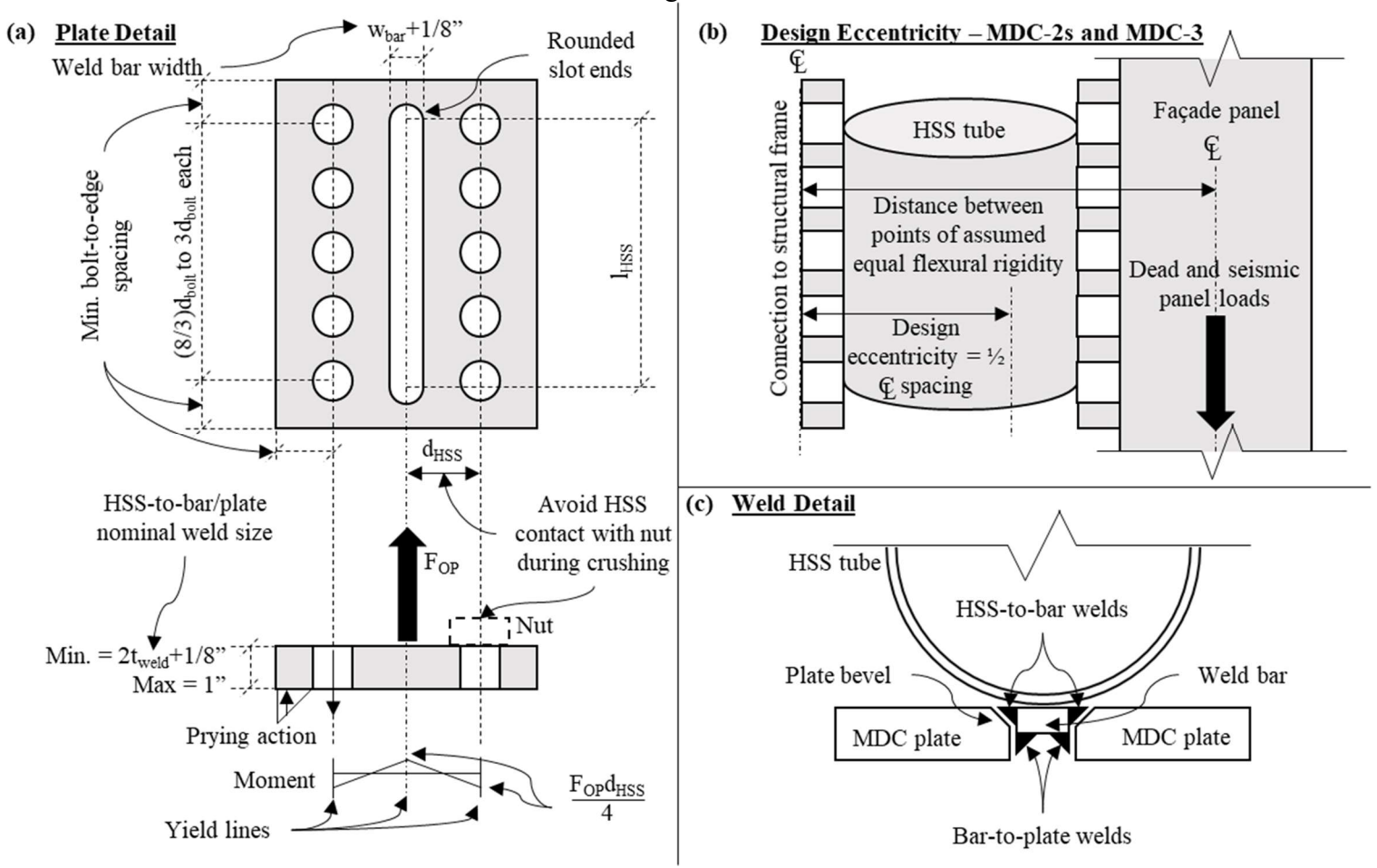

Fig. 9: MDC (a) Plate Detail, (b) Design Eccentricity, and (c) Weld Detail

References

ACI. (2011). *Building Code Requirements for Structural Concrete (ACI 318M-11) and Commentary*. Farmington Hills, MI: American Concrete Institute.

AISC. (2010a). *Seismic Provisions for Structural Steel Buildings*. Chicago, IL: American Institute of Steel Construction.

AISC. (2010b). *Specification for Structural Steel Buildings*. Chicago, IL: American Institute of Steel Construction.

Appelbaum, A. (2013). Structural Assessment of Multiple Story Steel Buildings Subjected to Blast Loads. Master's thesis: OhioLINK ETD.

ASCE (2013). *Minimum Design Loads for Buildings and Other Structures*. Reston, VA: American Society of Civil Engineers.

Chopra, A.K. (2011). *Dynamics of structures: Theory and applications to earthquake engineering*. 4th Edition. Upper Saddle River, N.J.: Pearson/Prentice Hall.

FEMA, ATC. (2012). Seismic Performance Assessment of Buildings. FEMA P-58-1. Applied Technology Council, Redwood City, CA.

Hutchinson, T., Pantoli, E., McMullin, K., Hildebrand, M., Underwood, G. (2014). "Seismic Drift Compatibility of Architectural Precast Concrete Panels and Connections: A Design Guide for Engineers." University of California, San Diego. Department of Structural Engineering, Report No. SSRP-14/16.

Lavarnway, D. (2013). Evaluating the use of Ductile Envelope Connectors for Improved Blast Protection of Structures. Master's thesis: OhioLINK ETD.

McKenna, F., & Fenves, G. L. (2004). OpenSees command language manual, version 1.5.2. *Pacific Earthquake Engineering Research Center*. (http://opensees.berkeley.edu).

National Institute of Standards and Technology (NIST). (2007). "Best Practices for Reducing the Potential for Progressive Collapse in Buildings". U.S. Department of Commerce. *Report NISTIR 7396*.

Reid, S.R., & Reddy, T.Y. (1978). Effect of strain hardening on the lateral compression of tubes between rigid plates. International Journal of Solids and Structures, 14(3), 213-225.

Salim, H., Muller, P., Dinan, R. (2005). Response of conventional steel stud wall systems under static and dynamic pressure. Journal of Performance of Constructed Facilities, 19(4), 267-276.

United States Department of Defense (DOD). (2008). "Unified Facilities Criteria, Structures to Resist the Effects of Accidental Explosion." *Report UFC 3-340-02*.

United States Nuclear Regulatory Commission (USNRC). (2007). Design-Basis Tornado and Tornado Missiles for Nuclear Power Plants. USNRC Regulatory Guide 1.76, Revision 1.

Young, W., & Budynas, R. (2002). *Roark's Formulas for Stress and Strain*. New York, NY: McGraw-Hill.

CASE SCHOOL OF ENGINEERING
CASE WESTERN RESERVE UNIVERSITY

PROJECT NO. _____

DATE 5 December 2017

PROJECT Multi-Hazard Design of Steel Buildings

BY Derek Slovenec

SUBJECT Multi-Hazard Ductile Connector (MDC) Design

Multi-Hazard Ductile Connector (MDC) Design Calculations

OBJECTIVE

The objective of this calculation is to develop a systematic design approach for façade panels and their connection to the structural frame which results in a system that achieves specified performance objectives when subjected to a variety of credible seismic, wind, blast, and impact hazards.

REFERENCES

1. Appelbaum, A. (2013). *Structural Assessment of Multiple Story Steel Buildings Subjected to Blast Loads*. Master's thesis: OhioLINK ETD.
2. ASCE. (2013). *Minimum Design Loads for Buildings and Other Structures*. Reston, VA: American Society of Civil Engineers.
3. Dusenberry, D.O. (2010). Handbook for Blast Resistant Design of Buildings. Hoboken, NJ: John Wiley & Son, Inc.
4. Lavarnway, D. (2013). *Evaluating the use of Ductile Envelope Connectors for Improved Blast Protection of Structures*. Master's thesis: OhioLINK ETD.
5. Reid, S.R., & Reddy, T.Y. (1978). Effect of strain hardening on the lateral compression of tubes between rigid plates. International Journal of Solids and Structures, 14(3), 213-225.
6. United States Nuclear Regulatory Commission (USNRC). (2007). Design-Basis Tornado and Tornado Missiles for Nuclear Power Plants. USNRC Regulatory Guide 1.76, Revision 1.
7. Young, W., & Budynas, R. (2002). *Roark's Formulas for Stress and Strain*. New York, NY: McGraw-Hill.

BACKGROUND AND ASSUMPTIONS

This research is focused on improving the lifetime hazard performance of new low- to mid-rise steel buildings. The use of blast resistant ductile connectors (BRDCs) to improve blast protection of structures was investigated by Lavarnway (2013), and the proposed use of round HSS tubes as an energy absorbing "fuse" element is adopted in this research. Design-basis wind and seismic hazards are taken from ASCE 7-10 (2013). Analytical tools for calculating the time history of a blast pressure wave on a building developed by Appelbaum (2013) are used in this research to calculate design blast impulse values assuming a story height of 13 feet and bay width of 30 feet. 6-inch thick reinforced concrete panels are currently assumed for the façade, although additional panel types will eventually be considered. Design blast and windborne projectiles are adopted from USNRC (2007).

METHODOLOGY

Design details for the façade panel and multi-hazard ductile connectors (MDCs) for the building story and location (interior or edge bay) of interest are generated from this step-by-step design process. A round HSS section is chosen by the user, and the required length of tube per panel edge is calculated considering the out-of-plane (OP) wind, seismic, blast, and impact hazard scenarios and performance objectives. This length per edge is divided among connectors of different types which provide the desired combination of reactions and releases to allow for thermal expansion of the panel and lateral in-plane (LIP or IP) seismic building drift accommodation. The current approach is to use three so-called MDC-1s on the top panel edge; these MDCs provide only OP reactions by including vertical short slotted bolt holes (for thermal expansion) in the HSS-to-panel connection, and long horizontal slotted bolt holes (for seismic drift and thermal expansion) in the HSS-to-frame connection. Additionally, the plates on either side of the MDC-1 HSS tubes are designed to yield to accommodate panel contact at building corners due to seismic building drift. On the bottom edge of the panel, the required total HSS tube length is divided into two MDC-2s, which provide vertical and OP reactions but include slotted holes for LIP thermal panel expansion, and a single MDC-3, which carries all LIP forces as well as an OP force in proportion to its HSS tube length.

Geometry	$H := 39ft$	$h := 13ft$	Total building height, story height
Building	$B := 180ft$		Total building width (design side)
	$P_V := 2$		Vertical position of design panel. Story #
	$h_M := h \cdot (P_V - 0.5) = 19.5 \cdot ft$		Mid-height of design story
	$P_L := "Edge"$		Lateral position of design panel. "Interior" or "Edge".
MDC HSS			
	$r_{HSS} := 3in$	$d_{HSS} := 2 \cdot r_{HSS}$	HSS radius and diameter
	$t_{HSS} := 0.25in$		HSS wall thickness (use nominal)
	$l_{V.max.HSS} := 18in$		Maximum vertical length of HSS tube
	$l_{V.min.HSS} := 12in$		Minimum vertical length of HSS tube
	$l_{L.min.HSS} := 6in$		Minimum lateral length of HSS tube (MDC3)
Hazards			
Wind	$V_D := 115mph$		Design wind gust speed (3s at 10m)
	$R_{TW} := 3$		Tornado wind region (see USNRC map). From most to least intense: 1, 2, 3.
Seismic	$S_S := 1.5$		Short period spectral acceleration
	$S_1 := 1$		1-second spectral acceleration
Connection configuration	$n_E := 3$		MDCs per facade panel edge
	$n_V := 2$		MDCs with vertical reaction
	$n_{IP} := 1$		MDCs with lateral in-plane reaction
	$n_{OP} := n_E + n_V + n_{IP} = 6$		MDCs with lateral out-of-plane reaction
Facade panel	$h_F := 13ft$		Height of facade panel
	$b_F := 30ft$		Width of facade panel
	$t_F := 6in$		Facade panel thickness (total)
	$c_c := 1in$		Facade panel cover concrete
	$\theta_F := 6deg$		Maximum allowable facade panel end rotation
	$\theta_{F.max} := 2 \cdot \theta_F = 12 \cdot deg$		Maximum panel plastic hinge rotation

Material properties

$E_s := 29000\text{ksi}$ $\nu_s := 0.30$ Steel modulus of elasticity

Steel

Steel Poisson's ratio

$G_s := \frac{E_s}{2\cdot(1+\nu_s)} = 1.115\times 10^4\cdot\text{ksi}$ Steel shear modulus

$\sigma_{yHSS} := 1.4\cdot 46\text{ksi} = 64.4\cdot\text{ksi}$ HSS material yield stress

$\sigma_{uHSS} := 1.3\cdot 62\text{ksi} = 80.6\,\text{ksi}$ HSS material ultimate stress

$\sigma_{yP} := 36\text{ksi}$ Plate material yield stress

$\sigma_{uP} := 58\text{ksi}$ Plate material ultimate stress

$\varepsilon_{yHSS} := \frac{\sigma_{yHSS}}{E_s} = 2.221\times 10^{-3}$ HSS material yield strain

$\varepsilon_{uHSS} := 0.04808$ HSS material ultimate strain (taken from ANSYS material model)

$E_{pHSS} := \frac{\sigma_{uHSS}-\sigma_{yHSS}}{\varepsilon_{uHSS}-\varepsilon_{yHSS}} = 353.254\,\text{ksi}$ HSS material plastic tangent modulus

Reinforced concrete

$f'_c := 5\text{ksi}$ $\sigma_{yRS} := 60\text{ksi}$ Panel concrete maximum compressive stress

Rebar yield stress

$E_c := 57000\cdot\sqrt{\frac{f'_c\cdot 1000}{\text{ksi}}}\cdot\frac{\text{ksi}}{1000} = 4.031\times 10^3\cdot\text{ksi}$ Panel concrete modulus of elasticity

$\gamma_c := 145\text{pcf}$ Concrete volumetric weight

$w_F := \gamma_c\cdot h_F\cdot b_F\cdot t_F = 28.275\,\text{kip}$ Weight of facade panel

Facade panel SDoF model

$\psi(x) := \sin\left(\frac{\pi\cdot x}{h_F}\right)$ Shape function

$I_{cr} := \frac{b_F\cdot t_F^3}{24} = 3.24\times 10^3\cdot\text{in}^4$ Panel cracked moment of inertia. Assume Icr = 1/2 Ig

$m_e := \frac{w_F}{g\cdot h_F}\cdot\int_0^{h_F}(\psi(x))^2\,dx = 0.037\cdot\frac{\text{kip}\cdot\text{s}^2}{\text{in}}$ Effective mass for elastic panel (half-sine)

$m_F := \frac{w_F}{g} = 0.073\cdot\frac{\text{kip}\cdot\text{s}^2}{\text{in}}$ Total facade panel mass

$k_s := E_c\cdot I_{cr}\cdot\int_0^{h_F}\left(\frac{d^2}{dx^2}\psi(x)\right)^2 dx = 167.533\cdot\frac{\text{kip}}{\text{in}}$ Generalized SDOF stiffness for panel in flexure

Round HSS tube force deformation model

$$P_0(l_{HSS}) := \frac{l_{HSS} \cdot t_{HSS}^2 \cdot \sigma_{yHSS}}{r_{HSS}}$$

Initial collapse mechanism strength for HSS tube

HSS tube crushing stiffness

$$k_{oHSS}(l_{HSS}) := \frac{E_s \cdot l_{HSS} \cdot t_{HSS}^3}{12 r_{HSS}^3} \cdot \left(1 - \nu_s^2\right) \cdot \left(\frac{\pi}{4} - \frac{2}{\pi}\right)^{-1}$$

From Roark's formulas

Maximum deformation and force of HSS

$$\delta_{HSS.max} := \frac{2}{3} \cdot d_{HSS}$$

$$P_{SH}(l_{HSS}) := 2\, P_0(l_{HSS})$$

From "MDCCrush.xmcd" at MDC deformation of 2/3 HSS diameter with material model assumed in this sheet, required force is double the initial collapse mechanism strength. Here, a bilinear force-deformation model is assumed for simplicity.

Yield deformation of HSS

$$\delta_{HSS.y}(l_{HSS}) := \frac{P_0(l_{HSS})}{k_{oHSS}(l_{HSS})}$$

Bilinear HSS crushing force-deformation model

$$P_C(l_{HSS}, \delta_{HSS}) := \begin{cases} k_{oHSS}(l_{HSS}) \cdot \delta_{HSS} & \text{if } \delta_{HSS} \le \delta_{HSS.y}(l_{HSS}) \\ P_0(l_{HSS}) + \delta_{HSS} \cdot \dfrac{P_{SH}(l_{HSS}) - P_0(l_{HSS})}{\delta_{HSS.max} - \delta_{HSS.y}(l_{HSS})} & \text{if } \delta_{HSS.y}(l_{HSS}) < \delta_{HSS} \le \delta_{HSS.max} \end{cases}$$

HSS tube pull/tension model

$$\delta_{pull.max} := \left(\sqrt{2} - 1\right) \cdot d_{HSS} = 2.485\ \text{in}$$

Deformation where force increases significantly due to axial tension of section

$$l_p := 1\,\text{in}$$

Initial value for plastic (straightened) length

A force-deformation model which approximates the HSS tube's behavior as it is pulled outwards radially is formulated here using simple geometry, observed FEA results, and theory similar to that which forms the basis for the HSS crushing model. This model is needed to calculate design-critical forces which develop during seismic panel contact.

Given

$$\delta_{pull} = 2 r_{HSS} \cdot \left(\sin\left(\frac{\pi \cdot r_{HSS} - l_p}{2 r_{HSS}}\right) - 1\right) + l_p$$

Relationship between total pulling deformation and straightened length of tube

$$L_p(\delta_{pull}) := \text{Find}(l_p)$$

$$R_{eff}(\delta_{pull}) := r_{HSS} \cdot \left(1 - \cos\left(\frac{\pi \cdot r_{HSS} - L_p(\delta_{pull})}{2 \cdot r_{HSS}}\right)\right)$$

Calculates the distance between plastic hinges perpendicular to the direction of pulling as a function of total pulling deformation

$$P_P(l_{HSS}, \delta) := \begin{cases} \min\left(\dfrac{1.5\, P_0(l_{HSS}) \cdot r_{HSS}}{R_{eff}(\delta)}, 2 \cdot l_{HSS} \cdot t_{HSS} \cdot \sigma_{yHSS}\right) & \text{if } \delta > \delta_{HSS.y}(l_{HSS}) \\ k_{oHSS}(l_{HSS}) \cdot \delta & \text{otherwise} \end{cases}$$

OP HSS force

$$P_{OP}(l_{HSS}, \Delta_{OP}) := \begin{cases} P_P(l_{HSS}, \Delta_{OP}) & \text{if } \Delta_{OP} > 0\,\text{in} \\ -P_C(l_{HSS}, |\Delta_{OP}|) & \text{if } \Delta_{OP} \le 0\,\text{in} \end{cases}$$

Normalized force-deformation models for pulling (top plot) and crushing (bottom plot) behaviors. Force is normalized by initial yield mechanism strength, while deformation is normalized by the diameter of the chosen HSS section. These plots are a function of the HSS diameter and wall thickness, i.e. these behaviors do not depend on tube length.

$\delta_{plot} := 0, 0.1in .. \delta_{HSS.max}$ $\delta_{pm} := -\delta_{HSS.max}, -\delta_{HSS.max} + 0.1in .. \delta_{HSS.max}$

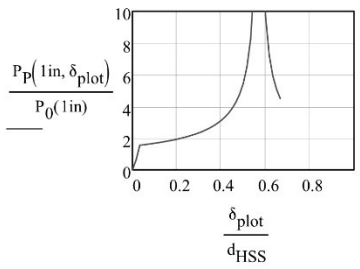

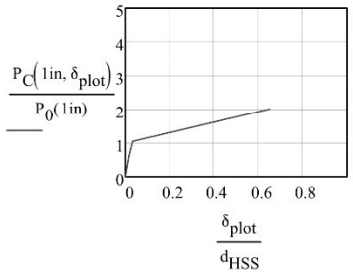

Combined pulling (positive) and crushing (negative) model plot

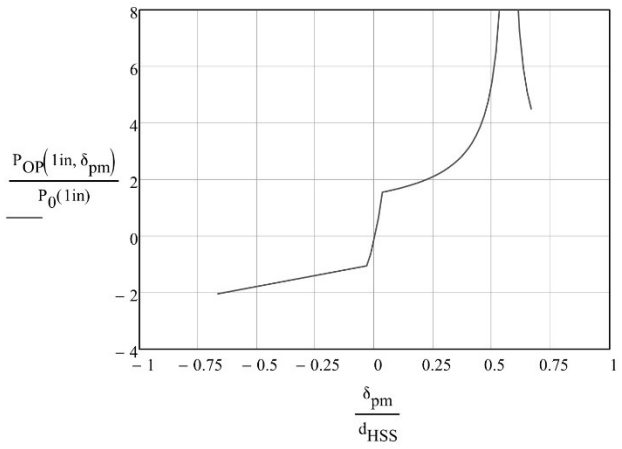

WIND

$G_f := 0.85$ Gust Factor

$K_{zt} := 1.0$ Topography Factor

$K_d := 0.85$ Directionality Factor

Velocity pressure exposure coefficient

$$K_{z.height} := \begin{pmatrix} 0 \\ 15 \\ 20 \\ 25 \\ 30 \\ 40 \\ 50 \\ 60 \\ 70 \\ 80 \\ 90 \\ 100 \\ 120 \\ 140 \\ 160 \\ 180 \\ 200 \end{pmatrix} ft \qquad K_{z.coeff} := \begin{pmatrix} 0.85 \\ 0.85 \\ 0.9 \\ 0.94 \\ 0.98 \\ 1.04 \\ 1.09 \\ 1.13 \\ 1.17 \\ 1.21 \\ 1.24 \\ 1.26 \\ 1.31 \\ 1.36 \\ 1.39 \\ 1.43 \\ 1.46 \end{pmatrix}$$

Height variable

$z := 0ft, 0.25ft .. H$

Velocity pressure exposure coefficient

$K_z(z) := \text{linterp}(K_{z.height}, K_{z.coeff}, z)$

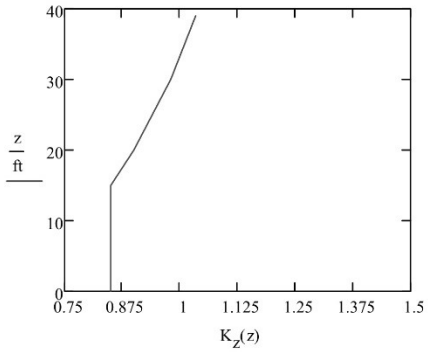

Velocity pressure

$$q_z(z) := 0.00256 \cdot K_z(z) \cdot K_{zt} \cdot K_d \cdot \left(\frac{V_D}{mph}\right)^2 \cdot psf$$

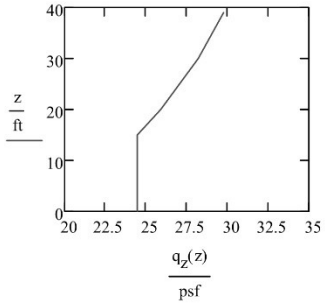

$q_h := q_z(H) = 2.066 \times 10^{-4}\,ksi$ — Velocity pressure at mean roof height

$GC_{pi} := 0.55$ — Product of internal pressure coefficient and gust response factor

Wind on building envelope facade panels

-Use Chap. 30 of ASCE 7-10 to calculate wind pressure on components and cladding
-peak pressure is critical load parameter since design objective is elastic panel response

Low-rise buildings (h<60ft)

$GC_{p.cc.LR} := -1.0$ — Fig. 30.4-1 (conservatively using H x 3')

$p_{cc.LR} := \left|q_h \cdot \left[GC_{p.cc.LR} - \left(GC_{pi}\right)\right]\right| = 46.122 \cdot psf$ — Pressure on panel

$F_{eLR} := \frac{p_{cc.LR} \cdot h_F \cdot b_F}{2} = 8.994 \cdot kip$ — Reaction force per panel edge (low-rise)

Mid-rise buildings (h>60ft)

Using 13'x30' = 390ft^2, 4 = -0.72, 5 = -1.1 — Fig. 30.6-1

$$GC_{p.cc.MR} := \begin{cases} -0.72 & \text{if } P_L = \text{"Interior"} \\ -1.1 & \text{if } P_L = \text{"Edge"} \end{cases} = -1.1$$

$p_{cc.MR} := \left|q_h \cdot GC_{p.cc.MR} - q_z\left(h_M\right) \cdot GC_{pi}\right| = 46.897 \cdot psf$ — Pressure on panel

$F_{eMR} := \frac{p_{cc.MR} \cdot h_F \cdot b_F}{2} = 9.145\,kip$ — Reaction force per panel edge (mid-rise)

$$F_{eW} := \begin{cases} F_{eLR} & \text{if } H < 60ft \\ F_{eMR} & \text{otherwise} \end{cases} = 8.994\,kip$$

Reaction force per panel edge for wind

Tornado wind

$$V_T := \begin{cases} 230\,\text{mph} & \text{if } R_{TW} = 1 \\ 200\,\text{mph} & \text{if } R_{TW} = 2 \\ 160\,\text{mph} & \text{if } R_{TW} = 3 \end{cases} = 160\,\text{mph}$$

Tornado wind (from USNRC)

$$P_{dTW} := \begin{cases} 1.2\,\text{psi} & \text{if } R_{TW} = 1 \\ 0.9\,\text{psi} & \text{if } R_{TW} = 2 \\ 0.6\,\text{psi} & \text{if } R_{TW} = 3 \end{cases} = 0.6\cdot\text{psi}$$

Tornado pressure drop (from USNRC)

$$F_{eTP} := \frac{h_F \cdot b_F \cdot P_{dTW}}{2} = 16.848\,\text{kip}$$

Reaction force per panel edge for tornado pressure drop.

$$I_M := \begin{cases} 4000\,\text{lb} & \text{if } R_{TW} = 1 \\ 4000\,\text{lb} & \text{if } R_{TW} = 2 \\ 2595\,\text{lb} & \text{if } R_{TW} = 3 \end{cases} = 2.595 \times 10^3\cdot\text{lb}$$

Impact missile mass, velocity, and impulse (from USNRC). Design impact missile is a (plastically deformable) car. Note that the energy absorbed by the car deforming is not included in the impact missile design calculations. Maximum height where impact missiles are considered is 30 ft.

$$I_V := \begin{cases} 135\,\frac{\text{ft}}{\text{s}} & \text{if } R_{TW} = 1 \\ 112\,\frac{\text{ft}}{\text{s}} & \text{if } R_{TW} = 2 \\ 79\,\frac{\text{ft}}{\text{s}} & \text{if } R_{TW} = 3 \end{cases} = 79\cdot\frac{\text{ft}}{\text{s}}$$

$$I_I := I_M \cdot I_V = 6.372\cdot\text{kip}\cdot\text{s}$$

$$F_{pT} := F_{eW}\left(\frac{V_T}{V_D}\right)^2 = 17.409\,\text{kip}$$

Reaction force per panel edge for tornado wind.

SEISMIC

$F_a := 1.0$ Site Coefficients

$F_v := 1.0$

$S_{DS} := 0.67 \cdot F_a \cdot S_S = 1.005$ Design short period spectral acceleration

$S_{D1} := 0.67 \cdot F_v \cdot S_1 = 0.67$ Design 1-second spectral acceleration

$I_F := 1.0$ Facade panel importance factor

$a_p := 1.25$

$R_p := 1$

Seismic inertia force for panel

$$F_S := \max\left[0.3 \cdot S_{DS} \cdot I_F \cdot w_F, \min\left[\frac{0.4 \cdot a_p \cdot S_{DS} \cdot w_F}{\left(\frac{R_p}{I_F}\right)} \cdot \left(1 + 2 \cdot \frac{h_M}{H}\right), 1.6 \cdot S_{DS} \cdot I_F \cdot w_F\right]\right] = 28.416\,\text{kip}$$

$F_{eS} := \frac{F_S}{2} = 14.208\,\text{kip}$ Seismic reaction force per panel edge

Temperature and shrinkage panel strength

$\beta_1 := 0.85 - 0.05 \cdot \frac{f'_c - 4\text{ksi}}{1\text{ksi}} = 0.8$ Coefficient for RC panel design

$$M_{TS} := 0.0018 \cdot b_F \cdot t_F \cdot \sigma_{yRS} \cdot \left(t_F - c_c - \frac{0.0018 \cdot t_F \cdot \sigma_{yRS}}{2 \cdot \beta_1 \cdot f'_c}\right) = 1.148 \times 10^3 \cdot \text{kip} \cdot \text{in}$$

$F_{eTS} := \left(\frac{P_0(1\text{in})}{P_{SH}(1\text{in})}\right) \cdot \frac{M_{TS} \cdot 4}{h_F} = 14.712\,\text{kip}$ Temperature and shrinkage panel strength reaction force at yield (capacity protect panel). Dividing by strain hardening factor is for blast protection - panel Mp at 2P0.

Controlling edge reaction force for elastic response design considerations

$F_{eF} := \max\left(F_{eTS}, F_{eW}, F_{eS}, F_{eTP}\right) = 16.848\,\text{kip}$

Minimum required elastic moment capacity

$$M_{cF} := \begin{cases} \max\left[\left(\frac{P_{SH}(1\text{in})}{P_0(1\text{in})}\right) \cdot \frac{F_{eF} \cdot h_F}{4}, M_{TS}\right] & \text{if } F_{cF} \neq F_{cTS} \\ M_{TS} & \text{otherwise} \end{cases} = 1.314 \times 10^3\,\text{in} \cdot \text{kip}$$

BLAST

Blast Scenarios

Standoff distances (ft)

$R_1 := 30\text{ft}$

$R_2 := 100\text{ft}$

$R_3 := 200\text{ft}$

Charge weights (lbs TNT)

$W_1 := 500\text{lbf}$

$W_2 := 300\text{lbf}$

$W_3 := 100\text{lbf}$

Impulse values

These values are obtained using a Matlab procedure assuming a panel height of 13ft and width of 30ft. For all scenarios, there is a height at which the blast pressure (and, therefore, impulse) is calculated as zero.

$$I_{i1} := \begin{pmatrix} 19.097 \\ 14.563 \\ 9.949 \\ 2.528 \\ 0 \\ 0 \\ 0 \\ 0 \\ 0 \end{pmatrix} \text{kip}\cdot\text{s} \qquad I_{i2} := \begin{pmatrix} 3.866 \\ 3.768 \\ 3.574 \\ 3.323 \\ 2.603 \\ 0.842 \\ 0 \\ 0 \\ 0 \end{pmatrix} \text{kip}\cdot\text{s} \qquad I_{i3} := \begin{pmatrix} 0.914 \\ 0.908 \\ 0.899 \\ 0.884 \\ 0.861 \\ 0.764 \\ 0.513 \\ 0.110 \\ 0 \end{pmatrix} \text{kip}\cdot\text{s}$$

Interior panels

$$I_{e1} := \begin{pmatrix} 18.574 \\ 14.429 \\ 9.949 \\ 2.528 \\ 0 \\ 0 \\ 0 \\ 0 \\ 0 \end{pmatrix} \text{kip}\cdot\text{s} \qquad I_{e2} := \begin{pmatrix} 3.584 \\ 3.497 \\ 3.324 \\ 3.118 \\ 2.455 \\ 0.809 \\ 0 \\ 0 \\ 0 \end{pmatrix} \text{kip}\cdot\text{s} \qquad I_{e3} := \begin{pmatrix} 0.868 \\ 0.863 \\ 0.854 \\ 0.840 \\ 0.817 \\ 0.725 \\ 0.492 \\ 0.107 \\ 0 \end{pmatrix} \text{kip}\cdot\text{s}$$

Edge panels

Design values taken from interior panel impulses because these always control over edge, are slightly easier to calculate, and are not significantly greater than the edge panel impulse values.

$I_{d1} := I_{i1P_V}$ Blast scenario 1

$I_{d2} := I_{i2P_V}$ Blast scenario 2

$I_{d3} := I_{i3P_V}$ Blast scenario 3

Performance objectives	Facade Panel	MDCs
Blast Scenario 1:	Yield and reach maximum end rotation	Yield and reach maximum deformation
Blast Scenario 2:	Remain elastic	Yield
Blast Scenario 3:	Remain elastic	Remain elastic

Conservation of energy
PE = potential (elastic)
KE = kinetic
W = Work (hysteretic)
F = facade panel
M = MDCs

	With MDCs	Without MDCs
BS1:	$KE_F - (W_F + W_M) = 0$	$KE_F - W_F = 0$
BS2:	$KE_F - W_M = PE_F$	$KE_F = PE_F$
BS3:	$KE_F = PE_F + PE_M$	$KE_F = PE_F$

Kinetic energy of panel

$$v_F(I, m) := \frac{I}{m}$$ Velocity = impulse/mass

$$KE_e(I) := \frac{1}{2} \cdot m_e \cdot \left(v_F\left(I, m_e\right)\right)^2$$ Kinetic energy for elastic panel motion

$$KE_p(I) := \frac{1}{2} m_F \cdot \left(v_F\left(I, m_F\right)\right)^2$$ Kinetic energy for rigid body panel motion

Panel edge reaction force

$$F_{ee.F}\left(l_{HSS}\right) := P_0\left(l_{HSS}\right) \cdot n_E$$ For elastic panel and MDCs

$$F_{p.F}\left(l_{HSS}\right) := P_{SH}\left(l_{HSS}\right) \cdot n_E$$ For plastic MDCs

Panel maximum deflection at flexural yield

$$\delta_{ee.F}\left(l_{HSS}\right) := \frac{5 \cdot F_{ee.F}\left(l_{HSS}\right) \cdot h_F^{\,3}}{192 E_c \cdot I_{cr}}$$ Elastic panel and MDCs

$$\delta_{p.F}\left(l_{HSS}\right) := \frac{5 \cdot F_{p.F}\left(l_{HSS}\right) \cdot h_F^{\,3}}{192 E_c \cdot I_{cr}}$$ Plastic MDCs

Facade panel flexural capacity

$$M_{ee.F}\left(l_{HSS}\right) := \frac{F_{ee.F}\left(l_{HSS}\right) \cdot h_F}{4}$$ Elastic panel and MDCs

$$M_{p.F}\left(l_{HSS}\right) := \frac{F_{p.F}\left(l_{HSS}\right) \cdot h_F}{4}$$ Plastic MDCs

Facade panel hinge rotation at onset of flexural yield

$$\theta_{ee.F}\left(l_{HSS}\right) := \frac{4 \cdot \delta_{ee.F}\left(l_{HSS}\right)}{h_F}$$ Elastic panel and MDCs

$$\theta_{p.F}\left(l_{HSS}\right) := \frac{4 \cdot \delta_{p.F}\left(l_{HSS}\right)}{h_F}$$ Plastic MDCs

MDC work

$$W_{MDC}\left(l_{HSS}\right) := \frac{n_{OP}}{2} \cdot \left(P_{SH}\left(l_{HSS}\right) + P_0\left(l_{HSS}\right)\right)\left(\delta_{HSS.max} - \delta_{HSS.y}\left(l_{HSS}\right)\right)$$

MDC elastic potential energy

$$PE_{MDC}\left(l_{HSS}\right) := \frac{n_{OP} \cdot \delta_{HSS.y}\left(l_{HSS}\right) \cdot P_0\left(l_{HSS}\right)}{2}$$

Panel work

$$W_F\left(l_{HSS}\right) := M_{p.F}\left(l_{HSS}\right) \cdot \left(\theta_{F.max} - \frac{1}{2} \cdot \theta_{p.F}\left(l_{HSS}\right)\right)$$

Panel elastic potential energy

$$PE_{ee.F}\left(l_{HSS}\right) := \frac{1}{2} \cdot k_s \cdot \delta_{ee.F}\left(l_{HSS}\right)^2$$

$$PE_{ep.F}\left(l_{HSS}\right) := \frac{1}{2} \cdot k_s \cdot \delta_{p.F}\left(l_{HSS}\right)^2$$

Functions to solve for each blast scenario. -For a given impulse, set these equations equal to zero and find the roots, which are the HSS tube length per MDC required to satisfy the stated performance objectives

$$BS_1(l_{HSS}) := KE_p(I_{d1}) - \left(W_{MDC}(l_{HSS}) + W_F(l_{HSS})\right)$$

$$BS_2(l_{HSS}) := KE_p(I_{d2}) - \left(W_{MDC}(l_{HSS}) + PE_{ep.F}(l_{HSS})\right)$$

$$BS_3(l_{HSS}) := KE_e(I_{d3}) - \left(PE_{ec.F}(l_{HSS}) + PE_{MDC}(l_{HSS})\right)$$

"Plastic" facade panel kinetic energy used whenever MDCs will crush because this uses full panel mass, whereas "elastic" KE uses effective SDOF panel mass

$$l_{e.HSS} := \frac{F_{eF} \cdot r_{HSS}}{n_E \cdot \sigma_{yHSS} \cdot t_{HSS}^2} = 4.186\ \text{in}$$

HSS tube length from T+S, wind, and seismic design considerations

$$L_{HSS} := l_{e.HSS}$$

Given $BS_1(L_{HSS}) = 0$

HSS tube lengths which satisfy blast scenario performance objectives. Choose tube length which maximizes required panel strength

$$l_{BS1.HSS} := \text{Find}(L_{HSS}) = 13.296\ \text{in} \qquad M_{BS1.F} := M_{p.F}(l_{BS1.HSS}) = 4.174 \times 10^3\ \text{in·kip}$$

Given $BS_2(L_{HSS}) = 0$

$$l_{BS2.HSS} := \text{Find}(L_{HSS}) = 2.06\ \text{in} \qquad M_{BS2.F} := M_{p.F}(l_{BS2.HSS}) = 646.85\ \text{in·kip}$$

Given $BS_3(L_{HSS}) = 0$

$$l_{BS3.HSS} := \text{Find}(L_{HSS}) = 8.639\ \text{in} \qquad M_{BS3.F} := M_{cc.F}(l_{BS3.HSS}) = 1.356 \times 10^3\ \text{in·kip}$$

Required HSS length for impact missile. Same performance objective as BS1.

$$T_I(l_{HSS}) := KE_p(I_I) - \left(W_{MDC}(l_{HSS}) + W_F(l_{HSS})\right)$$

Given $T_I(L_{HSS}) = 0$

$$l_{TI.HSS} := \begin{cases} 0\text{in} & \text{if } h \cdot P_V - h_F \geq 30\text{ft} \\ \text{Find}(L_{HSS}) & \text{otherwise} \end{cases} = 2.485\ \text{in}$$

$$M_{TI} := M_{p.F}(l_{TI.HSS}) = 780.122\ \text{in·kip}$$

Required HSS length for tornado wind (maximum HSS crushing deformation).

$$l_{TW.HSS} := \frac{F_{pT} \cdot r_{HSS}}{n_E \cdot \sigma_{yHSS} \cdot t_{HSS}^2} \cdot \left(\frac{P_0(1\text{in})}{P_{SH}(1\text{in})}\right) = 2.163\ \text{in}$$

Controlling plastic HSS design length and hazard

$$M_{TW} := \frac{n_E P_{SH}(l_{TW.HSS}) \cdot h_F}{4} = 678.97\ \text{in·kip}$$

$$l_{p.HSS} := \max(l_{BS1.HSS}, l_{BS2.HSS}, l_{TW.HSS}, l_{TI.HSS}) = 13.296\ \text{in}$$

Controlling HSS length

$$l_{c.HSS} := \max(l_{e.HSS}, l_{p.HSS}, l_{BS3.HSS}) = 13.296\ \text{in}$$

Controlling average tube length per MDC

$$l_{des.HSS} := \text{Ceil}(l_{c.HSS}, 0.25\text{in}) = 13.5\ \text{in}$$

Panel capacity for yield to occur at max HSS crushing def.

$$M_{des.F} := \frac{n_E P_{SH}(l_{des.HSS}) \cdot h_F}{4} = 4.238 \times 10^3\ \text{in·kip}$$

Contolling elastic design consideration

$$C_{elastic} := \begin{cases} \text{"Strength: T+S"} & \text{if } F_{eF} = F_{eTS} \\ \text{"Strength: design wind"} & \text{if } F_{eF} = F_{eW} \\ \text{"Strength: tornado pressure drop"} & \text{if } F_{eF} = F_{eTP} \\ \text{"Strength: seismic"} & \text{if } F_{eF} = F_{eS} \\ \text{"Potential energy: BS3"} & \text{if } l_{c.HSS} = l_{BS3.HSS} \end{cases} = \text{"Strength: tornado pressure drop"}$$

Contolling plastic design consideration

$$C_{plastic} := \begin{cases} \text{"Work capacity: BS1"} & \text{if } l_{p.HSS} = l_{BS1.HSS} \\ \text{"Work capacity: BS2"} & \text{if } l_{p.HSS} = l_{BS2.HSS} \\ \text{"Strength: tornado wind"} & \text{if } l_{p.HSS} = l_{TW.HSS} \\ \text{"Work capacity: impact missile"} & \text{if } l_{p.HSS} = l_{TI.HSS} \end{cases} = \text{"Work capacity: BS1"}$$

Contolling HSS performance objective

$$C_{HSS} := \begin{cases} \text{"Plastic performance"} & \text{if } l_{c.HSS} = l_{p.HSS} \\ \text{"Elastic performance"} & \text{if } l_{c.HSS} = l_{e.HSS} \vee l_{c.HSS} = l_{BS3.HSS} \end{cases} = \text{"Plastic performance"}$$

Lateral tube length on bottom edge - single tube, MDC3

$$l_{HSS.3} := \begin{cases} \max\left(n_E \cdot l_{des.HSS} - n_V \cdot l_{V.min.HSS}, l_{L.min.HSS}\right) & \text{if } l_{des.HSS} > l_{V.min.HSS} \\ l_{L.min.HSS} & \text{otherwise} \end{cases} = 16$$

Vertical tube length on bottom edge per MDC2

$$l_{HSS.2} := l_{V.min.HSS} = 12\,\text{in}$$

Lateral tube length on top edge per MDC1

$$l_{HSS.1} := \frac{n_V \cdot l_{HSS.2} + l_{HSS.3}}{n_E} = 13.5\,\text{in}$$

Tube length per edge

$$l_{HSS.E} := n_V \cdot l_{HSS.2} + l_{HSS.3} = 40.5\,\text{in}$$

Length, initial plastic mechanism, and panel strengths for each performance objective

$l_{BS1.HSS} = 13.296\,\text{in}$ $P_0\left(l_{BS1.HSS}\right) = 17.839\,\text{kip}$ $M_{BS1.F} = 4.174 \times 10^3\,\text{in·kip}$

$l_{BS2.HSS} = 2.06\,\text{in}$ $P_0\left(l_{BS2.HSS}\right) = 2.764\,\text{kip}$ $M_{BS2.F} = 646.85\,\text{in·kip}$

$l_{BS3.HSS} = 8.639\,\text{in}$ $P_0\left(l_{BS3.HSS}\right) = 11.59\,\text{kip}$ $M_{BS3.F} = 1.356 \times 10^3\,\text{in·kip}$

$l_{TW.HSS} = 2.163\,\text{in}$ $P_0\left(l_{TW.HSS}\right) = 2.902\,\text{kip}$ $M_{TW} = 678.97\,\text{in·kip}$

$l_{TI.HSS} = 2.485\,\text{in}$ $P_0\left(l_{TI.HSS}\right) = 3.334\,\text{kip}$ $M_{TI} = 780.122\,\text{in·kip}$

Comparing minimum (temperature and shrinkage) panel strengths to those for each performance objective.

$M_{TS} = 1.148 \times 10^3\,\text{in·kip}$ $M_{eF} = 1.314 \times 10^3\,\text{in·kip}$ $\frac{M_{TW}}{M_{TS}} = 0.592$

$\frac{M_{eF}}{M_{TS}} = 1.145$ $\frac{M_{BS3.F}}{M_{TS}} = 1.182$ $\frac{M_{BS2.F}}{M_{TS}} = 0.564$ $\frac{M_{BS1.F}}{M_{TS}} = 3.638$ $\frac{M_{TI}}{M_{TS}} = 0.68$

Edge panel seismic contact geometry
Determine required OP deformation of all MDCs during contact based on known mechanism and each MDC's distance from the point of contact.

$o_v := \min\left(\frac{l_{des.HSS}}{2} + 1\,ft, 2\,ft\right)$ $o_l := 3\,ft$ Assumptions for lateral and vertical offsets from panel corners to the location of the MDC HSS center

$m_1 := \frac{2 \cdot o_v - h_F}{\frac{b_F}{2} - o_l} = -0.823$ Slope of line with zero OP deformation

$m_2 := \frac{-1}{m_1} = 1.215$ Slope of line perpendicular to zero deformation line (displacement line)

$b_1 := o_v - m_1 \cdot \frac{b_F}{2} = 166.875\,in$ y-intercept of line of zero deformation

$b_2 := h_F - m_2 \cdot b_F = -281.468\,in$ y-intercept of displacement line

$x_i := \frac{b_2 - b_1}{m_1 - m_2} = 219.98\,in$ x-coordinate of line intersection

$y_i := m_1 \cdot x_i + b_1 = -14.15\,in$ y-coordinate of line intersection

$d_0 := \sqrt{(b_F - x_i)^2 + (h_F - y_i)^2} = 220.356\,in$ Distance from contact point to zero deformation

$\Delta_S := 0.025 \cdot h_F = 3.9\,in$ Maximum seismic inter-story displacement

Top MDC closest to edge

$b_3 := (h_F - o_v) - m_1 \cdot (b_F - o_l) = 403.875\,in$ y-intercept of line perpendicular to displacement line going through MDC location

$x_3 := \frac{b_2 - b_3}{m_1 - m_2} = 336.265\,in$

$y_3 := m_1 \cdot x_3 + b_3 = 127.157\,in$ Coordinates of this MDC line's intercept with the displacement line

$d_3 := \sqrt{(b_F - x_3)^2 + (h_F - y_3)^2} = 37.353\,in$ Distance from intersection to contact point

$\Delta_{OP.TE} := \frac{\Delta_S \cdot (d_0 - d_3)}{d_0} = 3.239\,in$ OP deformation of top MDC closest to edge

Top middle MDC

$b_4 := (h_F - o_v) - m_1 \cdot \left(\frac{b_F}{2}\right) = 285.375\,in$ y-intercept of line perpendicular to displacement line going through MDC location

$x_4 := \frac{b_2 - b_4}{m_1 - m_2} = 278.123\,in$

$y_4 := m_1 \cdot x_4 + b_4 = 56.503\,in$ Coordinates of this MDC line's intercept with the displacement line

$d_4 := \sqrt{(b_F - x_4)^2 + (h_F - y_4)^2} = 128.855\,in$ Distance from intersection to contact point

$\Delta_{OP.TM} := \frac{\Delta_S \cdot (d_0 - d_4)}{d_0} = 1.619\,in$ OP deformation of top middle MDC

Bottom MDC closest to edge

$b_5 := (o_v) - m_1 \cdot (b_F - o_l) = 285.375\ in$ — y-intercept of line perpendicular to displacement line going through MDC location

$x_5 := \frac{b_2 - b_5}{m_1 - m_2} = 278.123\ in$

$y_5 := m_1 \cdot x_5 + b_5 = 56.503\ in$ — Coordinates of this MDC line's intercept with the displacement line

$d_5 := \sqrt{(b_F - x_5)^2 + (h_F - y_5)^2} = 128.855\ in$ — Distance from intersection to contact point

$\Delta_{OP.BE} := \frac{\Delta_S \cdot (d_0 - d_5)}{d_0} = 1.619\ in$ — OP deformation of top MDC closest to edge

Bottom interior-side MDC

$b_6 := (o_v) - m_1 \cdot (o_l) = 48.375\ in$ — y-intercept of line perpendicular to displacement line going through MDC location

$x_6 := \frac{b_2 - b_6}{m_1 - m_2} = 161.838\ in$

$y_6 := m_1 \cdot x_6 + b_6 = -84.804\ in$ — Coordinates of this MDC line's intercept with the displacement line

$d_6 := \sqrt{(b_F - x_6)^2 + (h_F - y_6)^2} = 311.857\ in$ — Distance from intersection to contact point

$\Delta_{OP.BI} := \frac{\Delta_S \cdot (d_0 - d_6)}{d_0} = -1.619\ in$ — OP deformation of bottom far-side MDC

Limit HSS pulling deformation based on rigid body rotation geometry of HSS section. If the required deformation in the connection (Δ) exceeds the HSS limit (δ), plate yielding will need to be incorporated into the design of that MDC.

$\delta_{p.HSS.lim} := 2 \cdot \sqrt{2} \cdot r_{HSS} - d_{HSS} = 2.485\ in$

$\delta_{OP.TE} := \begin{cases} \delta_{p.HSS.lim} & \text{if } \Delta_{OP.TE} > \delta_{p.HSS.lim} \\ \Delta_{OP.TE} & \text{otherwise} \end{cases} = 2.485\ in$

$\delta_{OP.TM} := \begin{cases} \delta_{p.HSS.lim} & \text{if } \Delta_{OP.TM} > \delta_{p.HSS.lim} \\ \Delta_{OP.TM} & \text{otherwise} \end{cases} = 1.619\ in$

$\delta_{OP.BE} := \begin{cases} \delta_{p.HSS.lim} & \text{if } \Delta_{OP.BE} > \delta_{p.HSS.lim} \\ \Delta_{OP.BE} & \text{otherwise} \end{cases} = 1.619\ in$

Total contact force

$F_C := P_{OP}(l_{HSS.1}, \delta_{OP.TE}) + P_{OP}(l_{HSS.1}, \delta_{OP.TM}) + P_{OP}(l_{HSS.2}, \delta_{OP.BE}) + P_{OP}(l_{HSS.2}, \Delta_{OP.BI}) = 111.652\ kip$

$F_{c.V} := \frac{h_F \cdot F_C}{b_F} = 48.383\ kip$ — Total vertical force due to contact

$F_{c.v} := F_{c.V} = 48.383\ kip$ — Maximum downward vertical force one MDC will take due to contact

$F_{C.L} := \frac{F_C}{n_{IP}} = 111.652\ kip$ — Lateral in-plane force per MDC due to contact

Calculate load combinations for each MDC

$F_{d.V} := \frac{w_F}{n_V} = 14.137\,kip$ Panel dead load (V)

$F_{s.V} := \frac{\frac{2}{3} \cdot S_{DS} \cdot w_F}{n_V} = 9.472\,kip$ Vertical seismic inertia force (V)

$F_{C.v} := \begin{cases} F_{c.V} & \text{if } F_{c.V} - F_{d.V} - F_{s.V} > F_{c.v} + F_{d.V} + F_{s.V} \\ F_{c.v} & \text{otherwise} \end{cases} = 48.383\,kip$

$F_{s.L} := \frac{F_S}{n_{IP}} = 28.416\,kip$ $F_{s.OP} := \frac{F_S}{n_{OP}} = 4.736\,kip$ Lateral seismic inertia force (LIP, OP)

$F_{W.OP} := \frac{\max(F_{eW}, F_{pT})}{n_E} = 5.803\,kip$ Wind load (OP)

Vertical design loading under seismic hazard

$F_{S.V} := \begin{cases} 1.2F_{d.V} + F_{s.V} & \text{if } P_L = \text{"Interior"} \\ 1.2F_{d.V} + F_{s.V} + F_{C.v} & \text{if } P_L = \text{"Edge"} \end{cases} = 74.82\,kip$

Vertical design loading for dead weight alone

$F_{D.V} := 1.6 \cdot F_{d.V} = 22.62\,kip$

Lateral in-plane design force (seismic hazard)

$F_{IP} := \begin{cases} F_{s.L} & \text{if } P_L = \text{"Interior"} \\ F_{s.L} + F_{C.L} & \text{if } P_L = \text{"Edge"} \end{cases} = 140.069\,kip$

Inwards out-of-plane design force (blast)

$F_{B.OP.i}(l_{HSS}) := P_C(l_{HSS}, \delta_{HSS.max})$

Outwards out-of-plane design force (blast)

$F_{B.OP.o}(l_{HSS}, \delta_{OP}) := \begin{cases} P_0(l_{HSS}) & \text{if } P_L = \text{"Interior"} \\ P_P(l_{HSS}, \delta_{OP}) & \text{if } P_L = \text{"Edge"} \end{cases}$

Seismic OP design force

$F_{S.OP} := F_{s.OP} = 4.736\,kip$

Design eccentricity of loads

$e_{des} := \frac{1}{2} \cdot \left(\frac{t_F}{2} + d_{HSS} + 2in \right) - 1in = 4.5\,in$

Assumes 1in MDC plates and inflection point at halfway distance between facade panel centroid and connection point to frame. This is the distance between the inflection point and the frame-side HSS-to-plate welds.

Design moments due to eccentricity of loads

$M_{S.V} := F_{S.V} \cdot e_{des} = 336.689\,in \cdot kip$

$M_{D.V} := F_{D.V} \cdot e_{des} = 101.79\,in \cdot kip$

$M_{IP} := F_{IP} \cdot e_{des} = 630.309\,in \cdot kip$

HSS tube section checks - seismic compactness, stress due to longitudinal loads and bending caused by eccentricty of loading, tube wall rupture strength

$$S_{compact} := \begin{cases} \text{"Compact"} & \text{if } \frac{2 \cdot r_{HSS}}{t_{HSS}} \le \frac{E_s}{\sigma_{yHSS}} \\ \text{"Not Compact"} & \text{otherwise} \end{cases} = \text{"Compact"}$$

$\phi_y := 0.9$ Yield limit state resistance factor

$\phi_r := 0.75$ Rupture limit state resistance factor

Cross section moment of inertia and maximum distance from neutral axis

$$I_{HSS.2} := \frac{2 \cdot t_{HSS} \cdot (l_{HSS.2})^3}{12} = 72\,in^4 \qquad y_{HSS.2} := \frac{l_{HSS.2}}{2} = 6\,in$$

$$I_{HSS.3} := \frac{2 \cdot t_{HSS} \cdot (l_{HSS.3})^3}{12} = 187.172\,in^4 \qquad y_{HSS.3} := \frac{l_{HSS.3}}{2} = 8.25\,in$$

Normal stress due to bending

Normal stress due to OP forces

$$\sigma_{HSS.2} := \frac{\max(M_{D.V}, M_{S.V}) \cdot y_{HSS.2}}{I_{HSS.2}} = 28.057\,ksi \qquad \sigma_{HSS.3} := \frac{M_{IP} \cdot y_{HSS.3}}{I_{HSS.3}} = 27.782\,ksi$$

$$\sigma_{HSS.OP2} := \begin{cases} \frac{\max(F_{S.OP}, F_{W.OP}, F_{B.OP.i}(l_{HSS.2}), F_{B.OP.o}(l_{HSS.2}, \delta_{OP.BE}))}{2 \cdot t_{HSS} \cdot l_{HSS.2}} & \text{if } P_L = \text{"Edge"} \\ \frac{\max(F_{S.OP}, F_{W.OP}, F_{B.OP.i}(l_{HSS.2}), P_0(l_{HSS.2}))}{2 \cdot t_{HSS} \cdot l_{HSS.2}} & \text{otherwise} \end{cases} = 5.88\,ksi$$

$$\sigma_{HSS.OP3} := \begin{cases} \frac{\max(F_{S.OP}, F_{W.OP}, F_{B.OP.i}(l_{HSS.3}), P_0(l_{HSS.2}))}{2 \cdot t_{HSS} \cdot l_{HSS.3}} & \text{if } P_L = \text{"Edge"} \\ \frac{\max(F_{S.OP}, F_{W.OP}, F_{B.OP.i}(l_{HSS.3}), P_0(l_{HSS.2}))}{2 \cdot t_{HSS} \cdot l_{HSS.3}} & \text{otherwise} \end{cases} = 5.476\,ksi$$

Shear stress due to longitudinal loading

$$\tau_{HSS.2} := \frac{\max(F_{D.V}, F_{S.V})}{2 \cdot t_{HSS} \cdot l_{HSS.2}} = 12.47\,ksi \qquad \tau_{HSS.3} := \frac{F_{IP}}{2 \cdot t_{HSS} \cdot l_{HSS.3}} = 16.978\,ksi$$

Check shear yield strength

$$V_{HSS.2} := \frac{1.4 \tau_{HSS.2}}{0.6 \cdot \phi_y \cdot \sigma_{yHSS}} = 0.502 \qquad V_{HSS.3} := \frac{1.4 \tau_{HSS.3}}{0.6 \cdot \phi_y \cdot \sigma_{yHSS}} = 0.683$$

$$C_{HSS.V.2} := \begin{cases} \text{"Yield"} & \text{if } V_{HSS.2} \ge 1 \\ \text{"OK"} & \text{otherwise} \end{cases} = \text{"OK"} \qquad C_{HSS.V.3} := \begin{cases} \text{"Yield"} & \text{if } V_{HSS.3} \ge 1 \\ \text{"OK"} & \text{otherwise} \end{cases} = \text{"OK"}$$

Check section yield with reduced capacity due to shear stress

$$Y_{HSS.2} := \frac{\sigma_{HSS.2} + \sigma_{HSS.OP2}}{\sqrt{\left(\frac{\sigma_{yHSS}}{1.4}\right)^2 - 3 \cdot \tau_{HSS.2}^{\,2}}} = 0.836 \qquad Y_{HSS.3} := \frac{\sigma_{HSS.3} + \sigma_{HSS.OP3}}{\sqrt{\left(\frac{\sigma_{yHSS}}{1.4}\right)^2 - 3 \cdot \tau_{HSS.3}^{\,2}}} = 0.94$$

$$C_{HSS.Y.2} := \begin{cases} \text{"Yield"} & \text{if } Y_{HSS.2} \ge 1 \\ \text{"OK"} & \text{otherwise} \end{cases} = \text{"OK"} \qquad C_{HSS.Y.3} := \begin{cases} \text{"Yield"} & \text{if } Y_{HSS.3} \ge 1 \\ \text{"OK"} & \text{otherwise} \end{cases} = \text{"OK"}$$

Weld Design
2 weld legs on either side of small bar which is welded into plate gap

$l_{weld.1} := l_{HSS.1} = 13.5\ in$

$l_{weld.2} := l_{HSS.2} = 12\ in$

$l_{weld.3} := l_{HSS.3} = 16.5\ in$

Weld lengths for MDCs taken as the total HSS length. Two plates joined by the HSS weld bar connect the MDC to the panel and frame on either side

Design weld force per length.
-Factor of 1.5 included where weld is loaded normal to its longitudinal axis (AISC 360 Eq. J2-5).

$r_{B.OP.i} := \frac{F_{B.OP.i}(l_{HSS.1})}{2 \cdot 1.5 \cdot (l_{HSS.1})} = 0.913\ kpi$ Inward out-of-plane loading (blast)

$r_{B.OP.o1} := \frac{F_{B.OP.o}(l_{HSS.1}, \delta_{OP.TE})}{2 \cdot 1.5 \cdot (l_{HSS.1})} = 1.471\ kpi$ Outward out-of-plane loading (blast)

$r_{B.OP.o2} := \frac{F_{B.OP.o}(l_{HSS.2}, \delta_{OP.BE})}{2 \cdot 1.5 \cdot (l_{HSS.2})} = 0.98\ kpi$

Weld stresses for each hazard are calculated separately since the design stress is calculated from the controlling load combination, which is unknown at this stage.

$r_{S.OP} := \frac{F_{S.OP}}{2 \cdot 1.5 \cdot (2 \cdot l_{HSS.E})} = 0.019\ kpi$ Seismic out-of-plane loading

$r_{W.OP} := \frac{F_{W.OP}}{2 \cdot 1.5 \cdot (2 \cdot l_{HSS.E})} = 0.024\ kpi$ Wind out-of-plane loading

$r_{D.2} := \frac{F_{D.V}}{2 \cdot l_{weld.2}} = 0.943\ kpi$ Vertical dead load

$r_{S.2} := \frac{F_{S.V}}{2 \cdot l_{weld.2}} = 3.117\ kpi$ Vertical seismic inertia plus dead load

$r_3 := \frac{F_{IP}}{2 \cdot l_{weld.3}} = 4.245\ kpi$ Lateral in-plane loading carried entirely by MDC3

Weld bending properties

$I_{w.2} := \frac{2(l_{weld.2})^3}{12} = 288 \cdot in^3$ Moment of inertia per thickness for vertical welds

$I_{w.3} := \frac{2(l_{weld.3})^3}{12} = 748.688 \cdot in^3$ Moment of inertia per thickness for lateral welds, MDC3

$y_{w.2} := \frac{l_{weld.2}}{2} = 6\ in$ Maximum distance from neutral axis for vertical welds

$y_{w.3} := \frac{l_{weld.3}}{2} = 8.25\ in$ Maximum distance from neutral axis for lateral welds, MDC3

Maximum weld bending stress

$$r_{D.M2} := \frac{M_{D.V} \cdot y_{w.2}}{I_{w.2}} = 2.121\ \text{kpi}$$ Vertical welds

$$r_{S.M2} := \frac{M_{S.V} \cdot y_{w.2}}{I_{w.2}} = 7.014\ \text{kpi}$$

$$r_{M3} := \frac{M_{IP} \cdot y_{w.3}}{I_{w.3}} = 6.946\ \text{kpi}$$ Lateral welds, MDC3

Combined stress due to load combinations

$$r_{DB.weld.2} := \sqrt{\left(\max\left(r_{B.OP.i}, r_{B.OP.o2}\right) + r_{D.M2}\right)^2 + r_{D.2}^2} = 3.241\ \text{kpi}$$ Dead+Blast

Vertical welds for MDC2

$$r_{DS.weld.2} := \sqrt{\left(r_{S.OP} + r_{S.M2}\right)^2 + r_{S.2}^2} = 7.694\ \text{kpi}$$ Dead+Seismic

$$r_{DW.weld.2} := \sqrt{\left(r_{W.OP} + r_{D.M2}\right)^2 + r_{D.2}^2} = 2.342\ \text{kpi}$$ Dead+Wind

Lateral welds for MDC3

$$r_{BW.weld.3} := \max\left(r_{B.OP.i}, r_{W.OP}\right) = 0.913\ \text{kpi}$$ Blast or wind

$$r_{S.weld.3} := \sqrt{\left(r_{S.OP} + r_{M3}\right)^2 + r_3^2} = 8.156\ \text{kpi}$$ Seismic

Determine controlling combined stress to use for design

$$r_{weld.2} := \max\left(r_{DB.weld.2}, r_{DS.weld.2}, r_{DW.weld.2}\right) = 7.694\ \text{kpi}$$

$$r_{weld.3} := \max\left(r_{BW.weld.3}, r_{S.weld.3}\right) = 8.156\ \text{kpi}$$

$$r_{weld.1} := \max\left(r_{B.OP.i}, r_{B.OP.o1}, r_{W.OP}, r_{S.OP}\right) = 1.471\ \text{kpi}$$

Design weld size specifications

$$\phi_w := 0.75$$ Weld strength reduction factor

$$F_{EXX} := 70\text{ksi}$$ Electrode material strength

$$w_{min} := \frac{3}{16}\text{in}$$ Minimum specified weld size

$$w_{spec}(r) := \max\left(w_{min}, \text{Ceil}\left(\frac{\sqrt{2} \cdot r}{0.6 F_{EXX} \cdot \phi_w}, \frac{1\text{in}}{16}\right)\right)$$ Function for determining specified weld size for a given stress

MDC1 welds

$$w_{weld.1} := w_{spec}\left(r_{weld.1}\right) = 3 \cdot \frac{\text{in}}{16}$$

MDC2 welds

$$w_{weld.2} := w_{spec}\left(r_{weld.2}\right) = 6 \cdot \frac{\text{in}}{16}$$

MDC3 welds

$$w_{weld.3} := w_{spec}\left(r_{weld.3}\right) = 6 \cdot \frac{\text{in}}{16}$$

Design forces for weld bars.

$$F_{MDC.1} := 0.6 \cdot F_{EXX} \cdot \sqrt{2} \cdot w_{weld.1} \cdot l_{HSS.1} = 150.349\ \text{kip}$$ MDC1 lateral HSS tubes

$$F_{MDC.2} := 0.6 \cdot F_{EXX} \cdot \sqrt{2} \cdot w_{weld.2} \cdot l_{HSS.2} = 267.286\ \text{kip}$$ MDC2 vertical HSS tubes

$$F_{MDC.3} := 0.6 \cdot F_{EXX} \cdot \sqrt{2} \cdot w_{weld.3} \cdot l_{HSS.3} = 367.519\ \text{kip}$$ MDC3 lateral HSS tubes

Design of weld bar

For bars, thickness is typically specified in 1/8" increments, while width is specified in 1/4" increments. Here, "thickness" is taken as the dimension going into the MDC plates because more control over the exact length in this direction is needed.

NOTE: above note is valid for variable names (w/t), but the specified increments have been swapped to minimize gap between plate hole and weld bar in the width dimension's direction.

$$w_{bar.str.1} := Ceil\left(\frac{F_{MDC.1}}{\sigma_{yP}\cdot l_{HSS.1}}, \frac{1\,in}{8}\right) = 0.375\,in$$

$$w_{bar.str.2} := Ceil\left(\frac{F_{MDC.2}}{\sigma_{yP}\cdot l_{weld.2}}, \frac{1\,in}{8}\right) = 0.625\,in$$

$$w_{bar.str.3} := Ceil\left(\frac{F_{MDC.3}}{\sigma_{yP}\cdot l_{weld.3}}, \frac{1\,in}{8}\right) = 0.625\,in$$

$$w_{bar.min.1} := Ceil\left(2\cdot w_{weld.1} - \frac{1}{8}in, \frac{1\,in}{8}\right) = 0.25\,in$$

$$w_{bar.min.2} := Ceil\left(2\cdot w_{weld.2} - \frac{1}{8}in, \frac{1\,in}{8}\right) = 0.625\,in$$

$$w_{bar.min.3} := Ceil\left(2\cdot w_{weld.3} - \frac{1}{8}in, \frac{1\,in}{8}\right) = 0.625\,in$$

Bar widths based on strength and geometry requirements

$$w_{bar.1} := \max\left(w_{bar.str.1}, w_{bar.min.1}\right) = 0.375\,in$$

$$w_{bar.2} := \max\left(w_{bar.str.2}, w_{bar.min.2}\right) = 0.625\,in$$

$$w_{bar.3} := \max\left(w_{bar.str.3}, w_{bar.min.3}\right) = 0.625\,in$$

Gaps in plates are 1/8" wider than bars

$$w_{gap.1} := w_{bar.1} + 0.125\,in = 0.5\,in$$

$$w_{gap.2} := w_{bar.2} + 0.125\,in = 0.75\,in$$

$$w_{gap.3} := w_{bar.3} + 0.125\,in = 0.75\,in$$

MDC plate minimum thicknesses based on geometry of welds - take maximum of these as minimum plate thickness for all MDCs for ease of construction

$$t_{p.min.1} := 2\cdot w_{weld.1} + \frac{1\,in}{4} = 0.625\,in$$

$$t_{p.min.2} := 2\cdot w_{weld.2} + \frac{1\,in}{4} = 1\,in$$

$$t_{p.min.3} := 2\cdot w_{weld.3} + \frac{1\,in}{4} = 1\,in$$

Length of weld bars into MDC plates (1/4" increments) with space for through-thickness weld plus a minimum 1/16" edge spacing between weld and plate corner

$$t_{p.w} := \max\left(t_{p.min.1}, t_{p.min.2}, t_{p.min.3}\right) = 1\,in$$

$$t_{bar.1} := Floor\left(t_{p.w} - 0.0625in - w_{weld.1} + 0.00001\,in, 0.25in\right) = 0.75\,in$$

$$t_{bar.2} := Floor\left(t_{p.w} - 0.0625in - w_{weld.2} + 0.00001\,in, 0.25in\right) = 0.5\,in$$

$$t_{bar.3} := Floor\left(t_{p.w} - 0.0625in - w_{weld.3} + 0.00001\,in, 0.25in\right) = 0.5\,in$$

Plate Design

Design plates for outward OP yielding

$\theta_{pc} := 10\,deg$ $\theta_{pb} := \frac{\theta_{pc}}{2} = 5\cdot deg$ Rotation of plastic hinges which accommodate OP deformation

Distance between plate and bolt hole centerlines. Controlled by allowable plate rotation and required OP deformation for edge panels, otherwise limited by access to bolts.

$$l_{b.TE} := Ceil\left[\begin{cases} max\left[\left(\frac{\Delta_{OP.TE} - \delta_{OP.TE}}{\tan(\theta_{pb})}\right), r_{HSS}\right] & \text{if } P_L = \text{"Edge"} \\ r_{HSS} & \text{if } P_L = \text{"Interior"} \end{cases}, 0.25\,in\right] = 8.75\,in$$

$$l_{b.BE} := Ceil\left[\begin{cases} max\left[\left(\frac{\Delta_{OP.BE} - \delta_{OP.BE}}{\tan(\theta_{pb})}\right), r_{HSS}\right] & \text{if } P_L = \text{"Edge"} \\ r_{HSS} & \text{if } P_L = \text{"Interior"} \end{cases}, 0.25\,in\right] = 3\,in$$

Outwards pulling force per MDC

$$T_{P.1} := \begin{cases} P_P(l_{HSS.1}, \delta_{OP.TE}) & \text{if } P_L = \text{"Edge"} \\ max(F_{B.OP.o}(l_{HSS.1}, \delta_{OP.TE}), F_{W.OP}, F_{S.OP}) & \text{otherwise} \end{cases} = 59.564\,kip$$

$$T_{P.2} := \begin{cases} P_P(l_{HSS.2}, \delta_{OP.BE}) & \text{if } P_L = \text{"Edge"} \\ max(F_{B.OP.o}(l_{HSS.2}, \delta_{OP.BE}), F_{W.OP}, F_{S.OP}) & \text{otherwise} \end{cases} = 35.281\,kip$$

$T_{P.3} := max(P_0(l_{HSS.3}), F_{W.OP}, F_{S.OP}) = 22.138\,kip$

Moment caused by pulling force at a distance from bolt centerlines

$$M_{C.1} := \frac{T_{P.1}\cdot l_{b.TE}}{4} = 130.297\,in\cdot kip$$

$$M_{C.2} := \frac{T_{P.2}\cdot l_{b.BE}}{4} = 26.461\,in\cdot kip$$

$$M_{C.3} := \frac{T_{P.3}\cdot l_{b.BE}}{4} = 16.603\,in\cdot kip$$

Plate thickness based on this loading - for edge panels, want minimum plate thickness, for interior panels, want yield stress < My/I.

$$t_{C.1} := \begin{cases} t_{p.w} & \text{if } P_L = \text{"Edge"} \wedge \Delta_{OP.TE} > \delta_{OP.TE} \\ max\left(Ceil\left(\sqrt{\frac{6\cdot M_{C.1}}{l_{HSS.1}\cdot \sigma_{yP}}}, 0.125\,in\right), t_{p.w}\right) & \text{otherwise} \end{cases} = 1\,in$$

$$t_{C.2} := \begin{cases} t_{p.w} & \text{if } P_L = \text{"Edge"} \wedge \Delta_{OP.BE} > \delta_{OP.BE} \\ max\left(Ceil\left(\sqrt{\frac{6\cdot M_{C.2}}{l_{HSS.2}\cdot \sigma_{yP}}}, 0.125\,in\right), t_{p.w}\right) & \text{otherwise} \end{cases} = 1\,in$$

$$t_{C.3} := \begin{cases} t_{p.w} & \text{if } P_L = \text{"Edge"} \\ max\left(Ceil\left(\sqrt{\frac{6\cdot M_{C.3}}{l_{HSS.3}\cdot \sigma_{yP}}}, 0.125\,in\right), t_{p.w}\right) & \text{otherwise} \end{cases} = 1\,in$$

Set all plate thicknesses to the maximum value (for ease of construction)

$t_{p.des} := max(t_{C.1}, t_{C.2}, t_{C.3}) = 1\,in$

Actual plate moment capacity considering bending in the plane of the HSS cross section - full plastic strength for edge panels requiring additional OP deformation, elastic for all other panels.

$$M_{p.1} := \begin{cases} \frac{l_{HSS.1} \cdot t_{p.des}^2}{4} \cdot \sigma_{yP} & \text{if } P_L = \text{"Edge"} \wedge \Delta_{OP.TE} > \delta_{OP.TE} \\ \frac{l_{HSS.1} \cdot t_{p.des}^2}{6} \cdot \sigma_{yP} & \text{otherwise} \end{cases} = 121.5 \text{ in} \cdot \text{kip}$$

$$M_{p.2} := \begin{cases} \frac{l_{HSS.2} \cdot t_{p.des}^2}{4} \cdot \sigma_{yP} & \text{if } P_L = \text{"Edge"} \wedge \Delta_{OP.BE} > \delta_{OP.BE} \\ \frac{l_{HSS.2} \cdot t_{p.des}^2}{6} \cdot \sigma_{yP} & \text{otherwise} \end{cases} = 72 \text{ in} \cdot \text{kip}$$

$$M_{p.3} := \frac{l_{HSS.3} \cdot t_{p.des}^2}{6} \cdot \sigma_{yP} = 99 \text{ in} \cdot \text{kip}$$

Design minimum edge distance from bolt hole center based on prying action of plate on concrete panel

$$l_{e.p.1} := \text{Ceil}\left(\sqrt{\frac{2M_{p.1}}{l_{HSS.1} \cdot f'_c}}, 0.125\text{in}\right) = 2 \text{ in}$$

$$l_{e.p.2} := \text{Ceil}\left(\sqrt{\frac{2M_{p.2}}{l_{HSS.2} \cdot f'_c}}, 0.125\text{in}\right) = 1.625 \text{ in}$$

$$l_{e.p.3} := \text{Ceil}\left(\sqrt{\frac{2M_{p.3}}{l_{HSS.3} \cdot f'_c}}, 0.125\text{in}\right) = 1.625 \text{ in}$$

Prying force per line of bolts
-Reduced due to the reduction in plate moment capacity due to presence of bolt holes. Factor of ~0.75 for MDC2 and MDC3, ~0.5 for MDC1

$$P_{pry.1} := 0.5 \frac{2M_{p.1}}{l_{e.p.1}} = 60.75 \text{ kip}$$

$$P_{pry.2} := 0.75 \frac{2M_{p.2}}{l_{e.p.2}} = 66.462 \text{ kip}$$

$$P_{pry.3} := 0.75 \frac{2M_{p.3}}{l_{e.p.3}} = 91.385 \text{ kip}$$

Total length of plate along the HSS tube's longitudinal axis

$$h_{p.1} := l_{HSS.1} + 2\text{in} = 15.5 \text{ in}$$

$$h_{p.2} := l_{HSS.2} + 2\text{in} = 14 \text{ in}$$

$$h_{p.3} := l_{HSS.3} + 2\text{in} = 18.5 \text{ in}$$

OP force per MDC due to design bending moment, (2/3*L*P=M from moment diagram assuming N.A. at mid-height of plate)

$$P_{M.2} := \frac{3}{2l_{HSS.2}} \cdot \max\left(M_{D.V}, M_{S.V}\right) = 42.086\ \text{kip}$$

$$P_{M.3} := \frac{3}{2l_{HSS.3}} \cdot M_{IP} = 57.301\ \text{kip}$$

Total OP force per MDC plate including OP loading, prying force, and design moment (where applicable).

$$P_{p.1} := 2P_{pry.1} + T_{P.1} = 181.064\ \text{kip}$$

$$P_{p.2} := P_{M.2} + 2P_{pry.2} + T_{P.2} = 210.29\ \text{kip}$$

$$P_{p.3} := P_{M.3} + 2P_{pry.3} + T_{P.3} = 262.208\ \text{kip}$$

Limit length between bolts along longitudinal axis of HSS tubes to keep plate elastic when bending in the plane of this axis and the plate's thickness.
-This dimension should be at least 1" to allow for CL spacing of 2+2/3 bolt diameters for smallest structural bolts (d=3/8"). Increase minimum plate thickness (above) if necessary.

$$L_{bc}\left(l_{HSS}, f_{OP}\right) := \sqrt{\frac{2 \cdot 1\,\text{in} \cdot \sigma_{yP} \cdot t_{p.des}^{2} \cdot l_{HSS}}{f_{OP}}}$$

Considers 1" width of plate "beam" between bolts in line. "Beam" assumed to be fixed-fixed at bolt centerlines.

$$L_{b.1} := L_{bc}\left(l_{HSS.1}, P_{p.1}\right) = 2.317\ \text{in}$$

$$L_{b.2} := L_{bc}\left(l_{HSS.2}, P_{p.2}\right) = 2.027\ \text{in}$$

$$L_{b.3} := L_{bc}\left(l_{HSS.3}, P_{p.3}\right) = 2.129\ \text{in}$$

Total number of bolts required per plate. Minimum of 4 (one at each corner)

$$n_{bs.1} := \max\left[2\left(\text{Ceil}\left(\frac{h_{p.1}}{L_{b.1}}, 1\right) - 1\right), 4\right] = 12$$

$$n_{bs.2} := \max\left[2\left(\text{Ceil}\left(\frac{h_{p.2}}{L_{b.2}}, 1\right) - 1\right), 4\right] = 12$$

$$n_{bs.3} := \max\left[2\left(\text{Ceil}\left(\frac{h_{p.3}}{L_{b.3}}, 1\right) - 1\right), 4\right] = 16$$

$$n_{bs.1} := 4$$

Set number of bolts on MDC1 equal to minimum - long slotted holes make more bolts impractical. Larger bolts will be specified for strength and the prying bolt-to-edge distance will be applied in both directions to account for plate yielding in both directions.

Bolt Design

$\phi_b := 0.75$ Bolt strength reduction factor

A325 bolts, threads not excluded

$F_{nt} := 90\text{ksi}$ Tensile stress capacity

$F_{nv} := 54\text{ksi}$ Shear stress capacity

MDC1 plate bolt diameter

$$d_{b.1} := \max\left(\text{Ceil}\left(\sqrt{\frac{4 \cdot P_{p.1}}{\phi_b \cdot \pi \cdot F_{nt} \cdot n_{bs.1}}}, \frac{1}{8}\text{in}\right), \frac{3}{8}\text{in}\right) = 1\text{ in}$$

$$d_{b.2.min} := \sqrt{\frac{\left(4 \max\left(F_{D.V}, F_{S.V}\right)\right)}{1.3 \cdot \pi \cdot \phi_b \cdot n_{bs.2} \cdot F_{nv}}} = 0.388\text{ in}$$

$f_{b.v} := F_{nv}$ $\quad d_{b.v} := d_{b.2.min}$

Design bolt stress considering shear-axial interaction (AJSC 360 Eq. J3-3a).

Given

$$f_{b.v} = \min\left(1.3F_{nt} - \frac{F_{nt}}{\phi_b \cdot F_{nv}} \cdot \frac{4 \max\left(F_{D.V}, F_{S.V}\right)}{\pi \cdot d_{b.v}^{2} \cdot n_{bs.2}}, F_{nt}\right) = 0$$

$d_{b.v} > d_{b.2.min} = 0$

$$d_{b.v} = \max\left(\text{Ceil}\left(\sqrt{\frac{4 \cdot P_{p.2}}{\phi_b \cdot \pi \cdot f_{b.v} \cdot n_{bs.2}}}, \frac{1}{8}\text{in}\right), \frac{3}{8}\text{in}\right)$$

MDC2 plate bolt diameter

$d_{b.2} := \text{Find}\left(d_{b.v}\right) = 0.75\text{ in}$

$$f_{b.2} := \min\left(1.3F_{nt} - \frac{F_{nt}}{\phi_b \cdot F_{nv}} \cdot \frac{4 \max\left(F_{D.V}, F_{S.V}\right)}{\pi \cdot d_{b.2}^{2} \cdot n_{bs.2}}, F_{nt}\right) = 85.638\text{ ksi}$$

$$d_{b.3.min} := \sqrt{\frac{\left(4F_{IP}\right)}{1.3 \cdot \pi \cdot \phi_b \cdot n_{bs.3} \cdot F_{nv}}} = 0.46\text{ in}$$

$f_{b.L} := F_{nv}$ $\quad d_{b.L} := d_{b.3.min}$

Given

$$f_{b.L} = \min\left(1.3F_{nt} - \frac{F_{nt}}{\phi_b \cdot F_{nv}} \cdot \frac{4F_{IP}}{\pi \cdot d_{b.L}^{2} \cdot n_{bs.3}}, F_{nt}\right) = 0$$

$d_{b.L} > d_{b.3.min}$

$$d_{b.L} = \max\left(\text{Ceil}\left(\sqrt{\frac{4 \cdot P_{p.3}}{\phi_b \cdot \pi \cdot f_{b.L} \cdot n_{bs.3}}}, \frac{1}{8}\text{in}\right), \frac{3}{8}\text{in}\right)$$

MDC3 plate bolt diameter

$$d_{b.3} := \text{Find}\left(d_{b.L}\right) = 0.75\,\text{in}$$

$$f_{b.3} := \min\left(1.3F_{nt} - \frac{F_{nt}}{\phi_b \cdot F_{nv}} \cdot \frac{4F_{IP}}{\pi \cdot d_{b.3}^{\,2} \cdot n_{bs.3}}, F_{nt}\right) = 72.965\,\text{ksi}$$

Minimum bolt hole centerline spacing

$$l_{e.min}\left(d_b\right) := \begin{cases} 0.5\text{in} & \text{if } 0.374\text{in} \le d_b \le 0.376\text{in} \\ 0.75\text{in} & \text{if } 0.499\text{in} \le d_b \le 0.501\text{in} \\ 0.875\text{in} & \text{if } 0.624\text{in} \le d_b \le 0.626\text{in} \\ 1\text{in} & \text{if } 0.74\text{in} \le d_b \le 0.76\text{in} \\ 1.125\text{in} & \text{if } 0.874\text{in} \le d_b \le 0.876\text{in} \\ 1.25\text{in} & \text{if } 0.999\text{in} \le d_b \le 1.001\text{in} \\ 1.5\text{in} & \text{if } 1.124\text{in} \le d_b \le 1.126\text{in} \\ 1.625\text{in} & \text{if } 1.24\text{in} \le d_b \le 1.26\text{in} \\ 1.25 \cdot d_b & \text{otherwise} \end{cases}$$

Minimum bolt hole centerline to plate edge distance based on AISC specification.

$$l_{c.b.1} := l_{c.min}\left(d_{b.1}\right) = 1.25\,\text{in}$$

$$l_{e.b.2} := l_{e.min}\left(d_{b.2}\right) = 1\,\text{in}$$

$$l_{e.b.3} := l_{e.min}\left(d_{b.3}\right) = 1\,\text{in}$$

Spacing of bolts in a row

$$l_{s.b.1} := \frac{8}{3} \cdot d_{b.1} = 2.667\,\text{in}$$

$$l_{s.b.2} := \frac{8}{3} \cdot d_{b.2} = 2\,\text{in}$$

$$l_{s.b.3} := \frac{8}{3} \cdot d_{b.3} = 2\,\text{in}$$

Determine final (gross) plate dimensions and perform base plate checks

$$h_{P.1} := \text{Ceil}\left(\max\left(h_{p.1}, 2 \cdot l_{e.p.1} + l_{s.b.1}\right), 0.25\text{in}\right) = 15.5\ \text{in}$$

Plate heights (dimension along longitudinal axis of HSS tube)

$$h_{P.2} := \text{Ceil}\left[\max\left[h_{p.2}, 2 \cdot l_{e.b.2} + \left(\frac{n_{bs.2}}{2} - 1\right) \cdot l_{s.b.2}\right], 0.25\text{in}\right] = 14\ \text{in}$$

$$h_{P.3} := \text{Ceil}\left[\max\left[h_{p.3}, 2 \cdot l_{e.b.3} + \left(\frac{n_{bs.3}}{2} - 1\right) \cdot l_{s.b.3}\right], 0.25\text{in}\right] = 18.75\ \text{in}$$

Plate widths (perpendicular to HSS tube's longitudinal axis).

$$b_{P.1} := \text{Ceil}\left[2 \cdot \left(\max\left(l_{e.p.1}, l_{e.b.1}\right) + l_{b.TE}\right) - 0.001\text{in}, 0.25\text{in}\right] = 21.5\ \text{in}$$

$$b_{P.2} := \text{Ceil}\left[2 \cdot \left(\max\left(l_{e.p.2}, l_{e.b.2}\right) + l_{b.BE}\right), 0.25\text{in}\right] = 9.25\ \text{in}$$

$$b_{P.3} := \text{Ceil}\left[2 \cdot \left(\max\left(l_{c.p.3}, l_{c.b.3}\right) + r_{HSS}\right), 0.25\text{in}\right] = 9.25\ \text{in}$$

Base plate design checks

$$b_{f.1} := r_{HSS} = 3\ \text{in}$$

Pseudo-flange width taken as HSS radius

$$b_{f.2} := r_{HSS} = 3\ \text{in}$$

$$b_{f.3} := r_{HSS} = 3\ \text{in}$$

Determine critical cantilever dimensions

$$m_{p.1} := \frac{h_{P.1} - 0.95 \cdot l_{HSS.1}}{2} = 1.338\ \text{in} \qquad n_{p.1} := \frac{b_{P.1} - 0.8 \cdot b_{f.1}}{2} = 9.55\ \text{in}$$

$$m_{p.2} := \frac{h_{P.2} - 0.95 \cdot l_{HSS.2}}{2} = 1.3\ \text{in} \qquad n_{p.2} := \frac{b_{P.2} - 0.8 \cdot b_{f.2}}{2} = 3.425\ \text{in}$$

$$m_{p.3} := \frac{h_{P.3} - 0.95 \cdot l_{HSS.3}}{2} = 1.537\ \text{in} \qquad n_{p.3} := \frac{b_{P.3} - 0.8 \cdot b_{f.3}}{2} = 3.425\ \text{in}$$

$$n_{pp.1} := \frac{\sqrt{l_{HSS.1} \cdot b_{f.1}}}{4} = 1.591\ \text{in}$$

$$n_{pp.2} := \frac{\sqrt{l_{HSS.2} \cdot b_{f.2}}}{4} = 1.5\ \text{in}$$

$$n_{pp.3} := \frac{\sqrt{l_{HSS.3} \cdot b_{f.3}}}{4} = 1.759\ \text{in}$$

$$l_{c.1} := \max\left(m_{p.1}, n_{p.1}, n_{pp.1}\right) = 9.55\ \text{in}$$

$$l_{c.2} := \max\left(m_{p.2}, n_{p.2}, n_{pp.2}\right) = 3.425\ \text{in}$$

$$l_{c.3} := \max\left(m_{p.3}, n_{p.3}, n_{pp.3}\right) = 3.425\ \text{in}$$

Minimum plate thicknesses based on base plate design

$$t_{bp.1} := l_{c.1} \cdot \sqrt{\frac{F_{MDC.1}}{0.9 \cdot \sigma_{yP} \cdot b_{P.1} \cdot h_{P.1}}} = 1.127 \text{ in}$$

$$t_{bp.2} := l_{c.2} \cdot \sqrt{\frac{F_{MDC.2}}{0.9 \cdot \sigma_{yP} \cdot b_{P.2} \cdot h_{P.2}}} = 0.864 \text{ in}$$

$$t_{bp.3} := l_{c.3} \cdot \sqrt{\frac{F_{MDC.3}}{0.9 \cdot \sigma_{yP} \cdot b_{P.3} \cdot h_{P.3}}} = 0.876 \text{ in}$$

Check to see if these thicknesses are greater than the design thickness

$$C_{bp.t.1} := \begin{cases} \text{"OK"} & \text{if } t_{p.des} \geq t_{bp.1} \\ \text{"Plate yield expected"} & \text{otherwise} \end{cases} = \text{"Plate yield expected"}$$

$$C_{bp.t.2} := \begin{cases} \text{"OK"} & \text{if } t_{p.des} \geq t_{bp.2} \\ \text{"Plate yield expected"} & \text{otherwise} \end{cases} = \text{"OK"}$$

$$C_{bp.t.3} := \begin{cases} \text{"OK"} & \text{if } t_{p.des} \geq t_{bp.3} \\ \text{"Plate yield expected"} & \text{otherwise} \end{cases} = \text{"OK"}$$

Check various limit states for final detailed design

$$t_{p.1in.f} := \sqrt{\frac{3 \cdot P_{M.2} \cdot l_{HSS.2}}{4in \cdot \sigma_{yP}}} = 3.244\ in$$?!? One inch plate strip subjected to flexure under service load

Gross section yielding

$$t_{p.agy.2} := \frac{\max\left(F_{D.V}, F_{S.V}\right)}{b_{P.2} \cdot \sigma_{yP}} = 0.225\ in \qquad t_{p.agy.3} := \frac{F_{IP}}{b_{P.3} \cdot \sigma_{yP}} = 0.421\ in$$

Net section fracture

$$t_{p.anf.2} := \frac{\max\left(F_{D.V}, F_{S.V}\right)}{\left(b_{P.2} - 2 \cdot d_{b.2}\right) \cdot \sigma_{uP}} = 0.166\ in \qquad t_{p.anf.3} := \frac{F_{IP}}{\left(b_{P.3} - 2 \cdot d_{b.3}\right) \cdot \sigma_{uP}} = 0.312\ in$$

Bolt bearing/tear-out

$$t_{p.bto.2} := \frac{\max\left(F_{D.V}, F_{S.V}\right)}{2 \cdot l_{e.b.2} \cdot 2.4 \cdot \sigma_{uP} + 1.2\left(n_{bs.2} - 2\right) \cdot \left(l_{s.b.2} - d_{b.2}\right) \cdot \sigma_{uP}} = 0.065\ in$$

$$t_{p.bto.3} := \frac{F_{IP}}{2 \cdot l_{e.b.3} \cdot 2.4 \cdot \sigma_{uP} + 1.2\left(n_{bs.3} - 2\right) \cdot \left(l_{s.b.3} - d_{b.3}\right) \cdot \sigma_{uP}} = 0.094\ in$$

Block shear

$$l_{gv.2} := 2 \cdot \left[l_{e.b.2} + \left(\frac{n_{bs.2}}{2} - 1\right) \cdot l_{s.b.2}\right] = 22\ in$$

$$l_{nv.2} := l_{gv.2} - \left(n_{bs.2} - 1\right) \cdot d_{b.2} = 13.75\ in$$

$$l_{gt.2} := 2 \max\left(l_{e.b.2}, l_{e.p.2}\right) = 3.25\ in$$

$$t_{p.bv.2} := \frac{\max\left(F_{D.V}, F_{S.V}\right)}{l_{gt.2} \cdot \sigma_{uP} + 0.6 \max\left(l_{gv.2} \cdot \sigma_{yP}, l_{nv.2} \cdot \sigma_{uP}\right)} = 0.112\ in$$

$$l_{gv.3} := 2 \cdot \left[l_{e.b.3} + \left(\frac{n_{bs.3}}{2} - 1\right) \cdot l_{s.b.3}\right] = 30\ in$$

$$l_{nv.3} := l_{gv.3} - \left(n_{bs.3} - 1\right) \cdot d_{b.3} = 18.75\ in$$

$$l_{gt.3} := 2 \max\left(l_{e.b.3}, l_{e.p.3}\right) = 3.25\ in$$

$$t_{p.bv.3} := \frac{F_{IP}}{l_{gt.3} \cdot \sigma_{uP} + 0.6 \max\left(l_{gv.3} \cdot \sigma_{yP}, l_{nv.3} \cdot \sigma_{uP}\right)} = 0.167\ in$$

$$C_{p.agy} := \begin{cases} \text{"OK"} & \text{if } \max\left(t_{p.agy.2}, t_{p.agy.3}\right) < t_{p.des} \\ \text{"Increase plate thickness"} & \text{otherwise} \end{cases} = \text{"OK"}$$

$$C_{p.anf} := \begin{cases} \text{"OK"} & \text{if } \max\left(t_{p.anf.2}, t_{p.anf.3}\right) < t_{p.des} \\ \text{"Increase plate thickness"} & \text{otherwise} \end{cases} = \text{"OK"}$$

$$C_{p.bto} := \begin{cases} \text{"OK"} & \text{if } \max\left(t_{p.bto.2}, t_{p.bto.3}\right) < t_{p.des} \\ \text{"Increase plate thickness"} & \text{otherwise} \end{cases} = \text{"OK"}$$

$$C_{p.bv} := \begin{cases} \text{"OK"} & \text{if } \max\left(t_{p.bv.2}, t_{p.bv.3}\right) < t_{p.des} \\ \text{"Increase plate thickness"} & \text{otherwise} \end{cases} = \text{"OK"}$$

SUMMARY

	$P_V = 2$	Building story
	$P_L =$ "Edge"	Location of panel - building "interior" or "edge"
Hazard magnitudes	$S_{DS} = 1.005$ $S_{D1} = 0.67$	Seismic short (S.DS) and 1-second period (S.D1) design spectral acceleration values
	$V_D = 115\ \text{mph}$ $V_T = 160\ \text{mph}$	Design (V.D) and tornado (V.T) reference wind velocities
Facade panel	$M_{des.F} = 4.238 \times 10^3\ \text{in}\cdot\text{kip}$	Required facade panel moment capacity
	$\frac{M_{des.F}}{M_{TS}} = 3.694$	Factor of increase for panel moment capacity relative to T+S
HSS tube	$d_{HSS} = 6\ \text{in}$	HSS tube diameter
	$t_{HSS} = 0.25\ \text{in}$	HSS tube wall thickness
	$C_{elastic} =$ "Strength: tornado pressure drop"	Controlling elastic performance objective
	$C_{plastic} =$ "Work capacity: BS1"	Controlling plastic performance objective
	$C_{HSS} =$ "Plastic performance"	Controlling overall HSS performance objective
	$l_{des.HSS} \cdot n_E = 40.5\ \text{in}$	HSS total tube length per panel edge required for OP design objectives
	$P_0(l_{des.HSS}) = 18.112\ \text{kip}$	MDC initial collapse mechanism strength
	$P_{SH}(l_{des.HSS}) = 36.225\ \text{kip}$	MDC strength at large crushing deformation
	$l_{HSS.E} = 40.5\ \text{in}$	HSS total tube length per panel edge
	$n_V \cdot l_{HSS.2} = 24\ \text{in}$	Total HSS tube length with vertical reaction (MDC-2s)
	$l_{HSS.2} = 12\ \text{in}$	HSS tube length per MDC-2 (vertical reaction)
	$l_{HSS.3} = 16.5\ \text{in}$	MDC3 HSS tube length (single tube)
Shear rupture and section yield checks for tubes subjected to multiple loads with eccentricity	$C_{HSS.V.2} =$ "OK"	MDC2s - if either rupture or yield limit state are expected, increase variable l.V.min.HSS on first page of this document
	$C_{HSS.Y.2} =$ "OK"	
	$C_{HSS.V.3} =$ "OK"	MDC3 lateral reaction tube - if either rupture or yield limit state are expected, increase variable l.V.min.HSS on first page of this document
	$C_{HSS.Y.3} =$ "OK"	
Check for seismic compactness of chosen HSS section	$S_{compact} =$ "Compact"	

HSS plates	$t_{p.des} = 1\ in$		Plate thickness for all MDCs
	$h_{P.1} = 15.5\ in$	$n_E = 3$	Plate height for MDC1s (assuming 3 on top edge only)
	$b_{P.1} = 21.5\ in$		Plate width for MDC1s
	$h_{P.2} = 14\ in$		Plate height for MDC2s (assuming 3 per edge)
	$b_{P.2} = 9.25\ in$	$n_V = 2$	Plate width for MDC2s
	$h_{P.3} = 18.75\ in$		MDC3 (lateral IP tube)
	$b_{P.3} = 9.25\ in$		
HSS plate limit state checks.	$C_{p.agy} = \text{"OK"}$		Gross section yield
	$C_{p.anf} = \text{"OK"}$		Net section fracture
	$C_{p.bto} = \text{"OK"}$		Bolt bearing/tear-out
	$C_{p.bv} = \text{"OK"}$		Block shear
HSS plate thickness check from AISC manual base plate design calculations.	$C_{bp.t.1} = \text{"Plate yield expected"}$		MDC1s
	$C_{bp.t.2} = \text{"OK"}$		MDC2s
	$C_{bp.t.3} = \text{"OK"}$		MDC3
Welds -Lengths shown are per tube and per weld leg. See summary page 1 for MDC info (number of tubes, orientation, etc.)	$w_{weld.1} = 3 \cdot \frac{in}{16}$	$l_{weld.1} = 13.5\ in$	MDC1 welds
	$w_{weld.2} = 6 \cdot \frac{in}{16}$	$l_{weld.2} = 12\ in$	MDC2 welds
	$w_{weld.3} = 6 \cdot \frac{in}{16}$	$l_{weld.3} = 16.5\ in$	MDC3 welds
Weld bar dimensions -Width is the dimension tangent to the HSS tube wall, thickness is the dimension into the thickness of the plate	$w_{bar.1} = 0.375\ in$	$t_{bar.1} = 0.75\ in$	MDC1 bars
	$w_{bar.2} = 0.625\ in$	$t_{bar.2} = 0.5\ in$	MDC2 bars
	$w_{bar.3} = 0.625\ in$	$t_{bar.3} = 0.5\ in$	MDC3 bars
	$n_{bs.1} = 4$	$d_{b.1} = 1\ in$	MDC1s
Bolts -Number of bolts per MDC split evenly between plate on either side of the HSS tube.	$n_{bs.2} = 12$	$d_{b.2} = 0.75\ in$	MDC2s
	$n_{bs.3} = 16$	$d_{b.3} = 0.75\ in$	MDC3

Minimum distance from bolt centerlines to plate edge in the direction perpendicular to the HSS tube's longitudinal axis. Based on prying strength of concrete. Should not be taken as less than l.e.b.min below.

$l_{b.TE} = 8.75\ in$ MDC1s

$l_{b.BE} = 3\ in$ MDC2s and MDC3

$l_{e.p.1} = 2\ in$ MDC1s

$l_{c.p.2} = 1.625\ in$ MDC2s

$l_{e.p.3} = 1.625\ in$ MDC3

Minimum distance from bolt centerlines to plate edges in any direction based on AISC specification and bolt sizes.

$l_{e.b.1} = 1.25\ in$ MDC1s

$l_{e.b.2} = 1\ in$ MDC2s

$l_{c.b.3} = 1\ in$ MDC3

Minimum centerline-to-centerline spacing of bolts based on AISC specification and bolt sizes.

$l_{s.b.1} = 2.667\ in$ MDC1s

$l_{s.b.2} = 2\ in$ MDC2s

$l_{s.b.3} = 2\ in$ MDC3

Values for testing
-Limits: OP = ~60k, LIP/V = 22k

$P_P(l_{HSS.1}, \delta_{OP.TE}) = 59.564\ kip$ OP pulling force for MDC1

$P_P(l_{HSS.2}, \delta_{OP.BE}) = 35.281\ kip$ OP pulling force for MDC2

$P_{SH}(l_{HSS.1}) = 36.225\ kip$ OP crushing force for MDC1

$P_{SH}(l_{HSS.2}) = 32.2\ kip$ OP crushing force for MDC2

$\max(F_{D.V}, F_{S.V}) = 74.82\ kip$ Vertical design force per MDC2

$F_{D.V} = 22.62\ kip$ Dead load per MDC2

$F_{IP} = 140.069\ kip$ LIP design force (MDC3)

Appendix 2

Multi-Hazard Ductile Façade Connection Fabrication Drawings

NOTES: HSS A500 GRADE C 46 KSI STEEL.
ALL PLATES AND BARS A36 STEEL.
ALL WELDS E70 ELECTRODE.

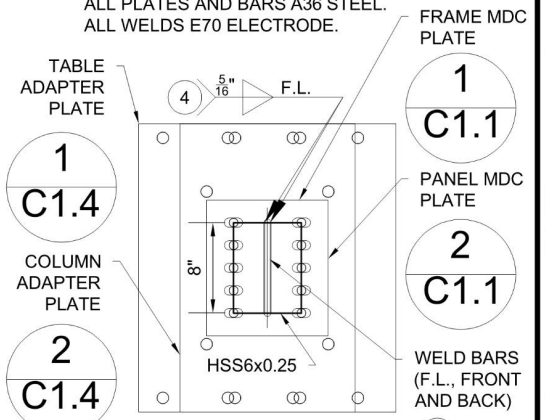

1 FRONT VIEW

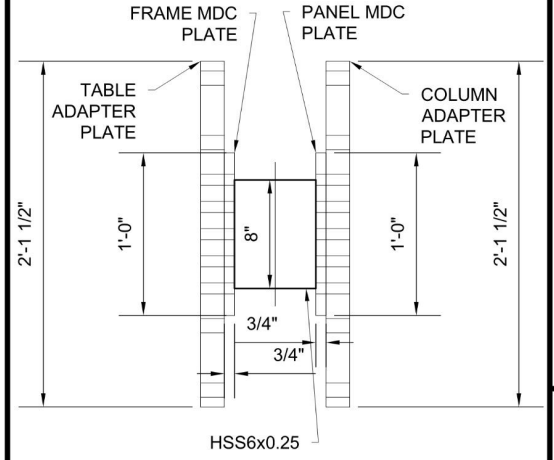

2 SIDE VIEW

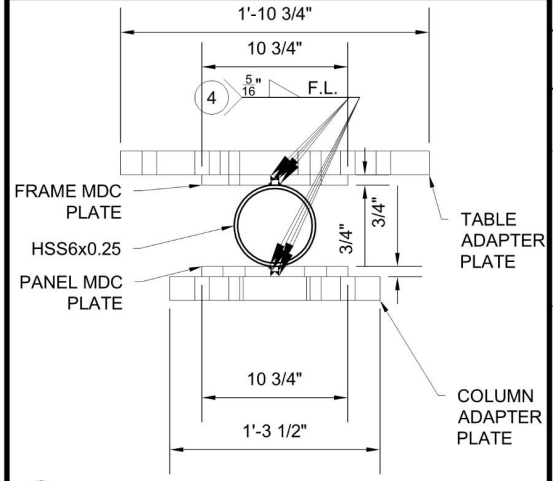

3 TOP VIEW

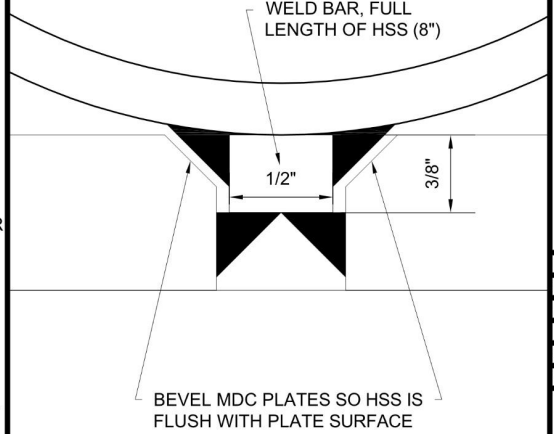

4 WELD DETAIL

ALL WELDS 5/16", FULL LENGTH (8")

CASE WESTERN RESERVE UNIVERSITY
CIVIL ENGINEERING DEPT.

MULTI-HAZARD DUCTILE CONNECTOR
EXPERIMENTAL DESIGNS

DRAWN BY:	DES
CHECKED BY:	
APPROVED BY:	
DATE:	05/16/2017
SHEET:	1 of 9
SCALE:	N/A

SHEET TITLE:

C1.0

MDC-2 ASSEMBLY

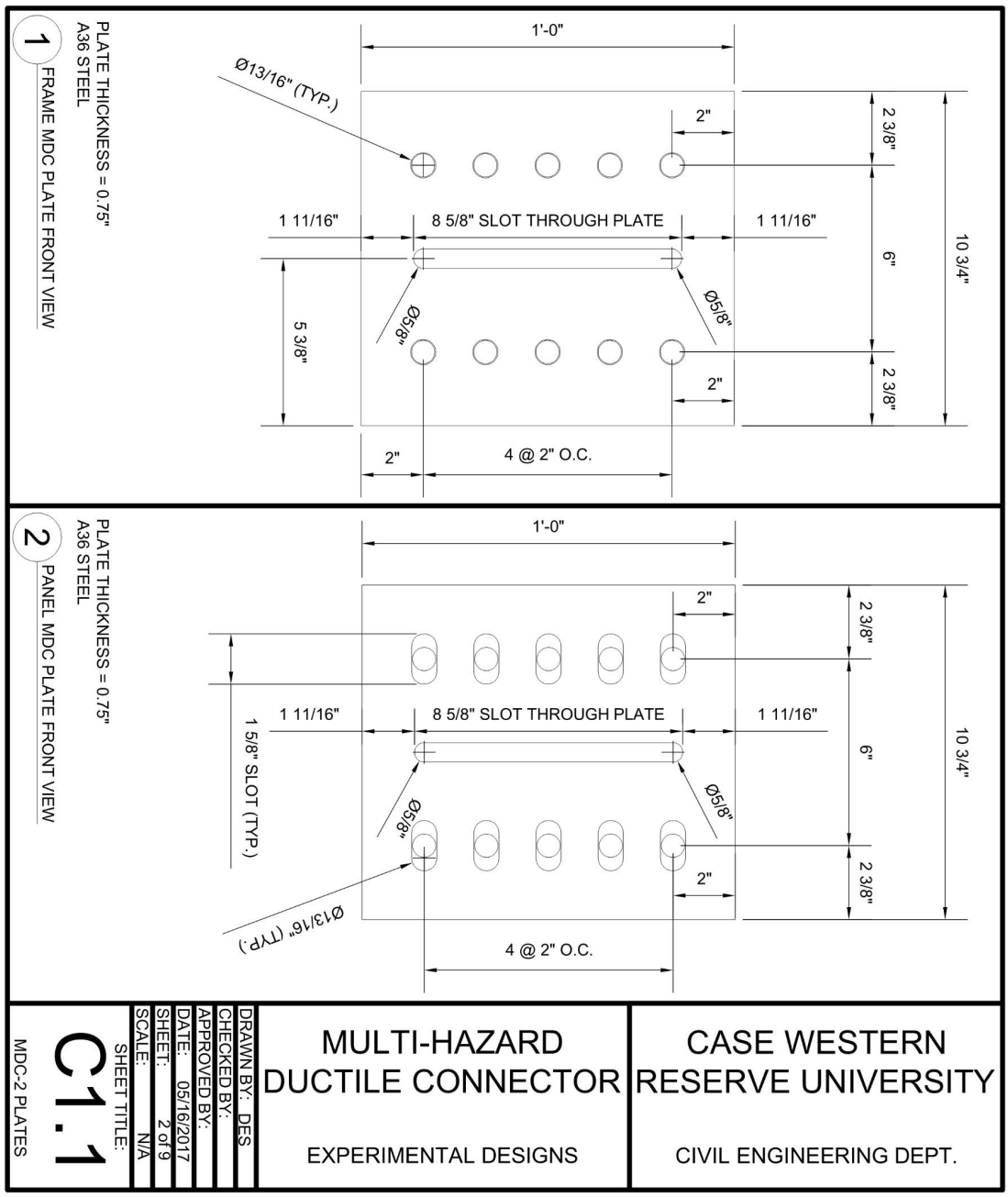
1
PLATE THICKNESS = 0.75"
A36 STEEL
FRAME MDC PLATE FRONT VIEW
1'-0"
Ø13/16" (TYP.)
2"
2 3/8"
6"
10 3/4"
1 11/16"
8 5/8" SLOT THROUGH PLATE
1 11/16"
5 3/8"
Ø5/8"
Ø5/8"
2"
2 3/8"
2"
4 @ 2" O.C.
2
PLATE THICKNESS = 0.75"
A36 STEEL
PANEL MDC PLATE FRONT VIEW
1'-0"
2"
2 3/8"
1 5/8" SLOT (TYP.)
1 11/16"
8 5/8" SLOT THROUGH PLATE
1 11/16"
6"
10 3/4"
Ø5/8"
Ø5/8"
2"
2 3/8"
Ø13/16" (TYP.)
4 @ 2" O.C.
MULTI-HAZARD
DUCTILE CONNECTOR
EXPERIMENTAL DESIGNS
CASE WESTERN
RESERVE UNIVERSITY
CIVIL ENGINEERING DEPT.
DRAWN BY: DES
CHECKED BY:
APPROVED BY:
DATE: 05/16/2017
SHEET: 2 of 9
SCALE: N/A
SHEET TITLE:
C1.1
MDC-2 PLATES

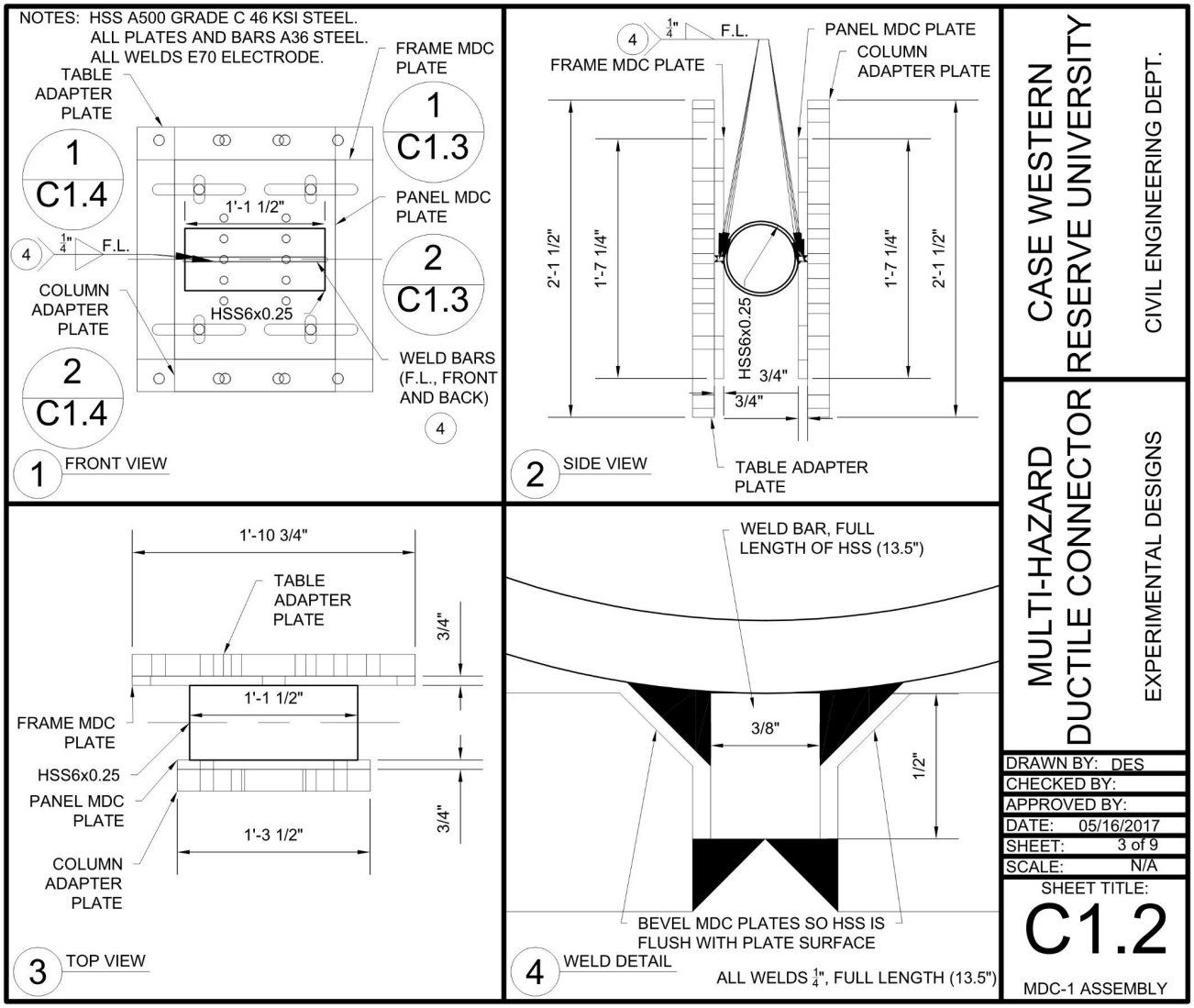

CASE WESTERN RESERVE UNIVERSITY
CIVIL ENGINEERING DEPT.

MULTI-HAZARD DUCTILE CONNECTOR
EXPERIMENTAL DESIGNS

DRAWN BY:	DES
CHECKED BY:	
APPROVED BY:	
DATE:	05/16/2017
SHEET:	3 of 9
SCALE:	N/A

SHEET TITLE:
C1.2
MDC-1 ASSEMBLY

1 PLATE THICKNESS = 0.75"
A36 STEEL
FRAME MDC PLATE FRONT VIEW

2 PLATE THICKNESS = 0.75"
A36 STEEL
PANEL MDC PLATE FRONT VIEW

MULTI-HAZARD DUCTILE CONNECTOR

EXPERIMENTAL DESIGNS

CASE WESTERN RESERVE UNIVERSITY

CIVIL ENGINEERING DEPT.

DRAWN BY: DES
CHECKED BY:
APPROVED BY:
DATE: 05/16/2017
SHEET: 4 of 9
SCALE: N/A
SHEET TITLE:

C1.3

MDC-1 PLATES

1
TABLE ADAPTER PLATE FRONT VIEW
PLATE THICKNESS = 1.75"
A36 STEEL
2'-1 1/2"
6"
1'-1 1/2"
6"
2 1/8"
5 3/4"
5 3/4"
5 3/4"
3 3/8"
6"
8 3/8"
6"
1 1/4"
1 1/4"
6"
1'-10 3/4"
Ø1 1/16"
Ø1 1/16"
Ø13/16" (TYP.)
Ø1 1/16" (TYP.)
Ø1 1/16"
Ø1 1/16"
8 3/4"
4 @ 2" O.C.
8 3/4"
2
COLUMN ADAPTER PLATE FRONT VIEW
PLATE THICKNESS = 1.75"
A36 STEEL
2'-1 1/2"
6"
1'-1 1/2"
6"
Ø1 1/16"
4 3/4"
2 3/8"
Ø1 1/16"
4 7/8"
1 1/4"
1 1/4"
Ø13/16" (TYP.)
6"
10 3/4"
5 3/4"
1'-3 1/2"
Ø1 1/16" (TYP.)
Ø1 1/16"
Ø1 1/16"
4 7/8"
8 3/4"
4 @ 2" O.C.
8 3/4"
DRAWN BY: DES
CHECKED BY:
APPROVED BY:
DATE: 05/16/2017
SHEET: 5 of 9
SCALE: N/A
SHEET TITLE:
C1.4
ADAPTER PLATES
MULTI-HAZARD DUCTILE CONNECTOR
EXPERIMENTAL DESIGNS
CASE WESTERN RESERVE UNIVERSITY
CIVIL ENGINEERING DEPT.

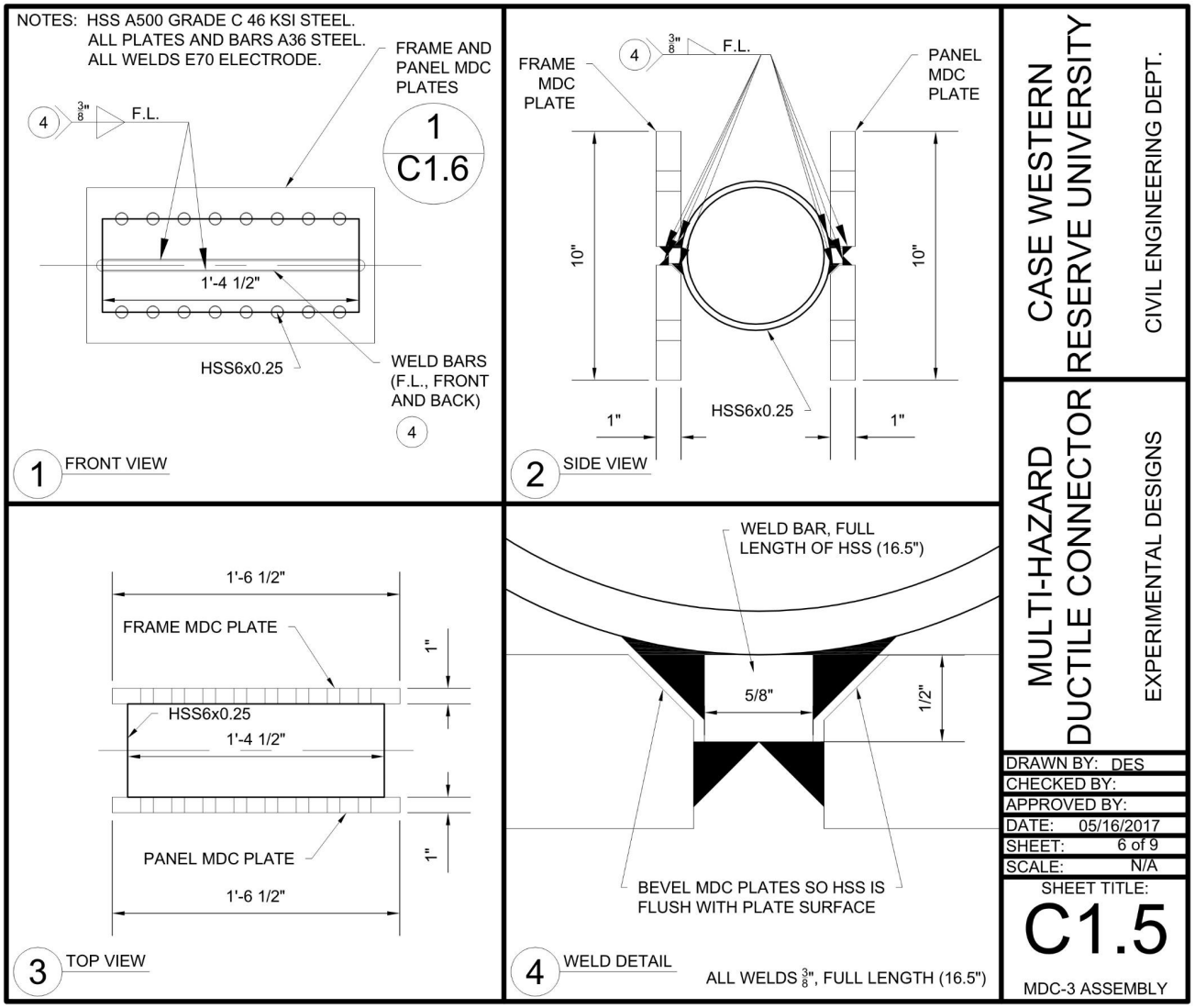
NOTES: HSS A500 GRADE C 46 KSI STEEL.
ALL PLATES AND BARS A36 STEEL.
ALL WELDS E70 ELECTRODE.
FRAME AND PANEL MDC PLATES
4
3/8"
F.L.
1
C1.6
1'-4 1/2"
HSS6x0.25
WELD BARS (F.L., FRONT AND BACK)
4
1 FRONT VIEW
FRAME MDC PLATE
PANEL MDC PLATE
10"
10"
1"
HSS6x0.25
1"
2 SIDE VIEW
1'-6 1/2"
FRAME MDC PLATE
1"
HSS6x0.25
1'-4 1/2"
PANEL MDC PLATE
1"
1'-6 1/2"
3 TOP VIEW
WELD BAR, FULL LENGTH OF HSS (16.5")
5/8"
1/2"
BEVEL MDC PLATES SO HSS IS FLUSH WITH PLATE SURFACE
4 WELD DETAIL
ALL WELDS 3/8", FULL LENGTH (16.5")
CASE WESTERN RESERVE UNIVERSITY
CIVIL ENGINEERING DEPT.
MULTI-HAZARD DUCTILE CONNECTOR
EXPERIMENTAL DESIGNS
DRAWN BY: DES
CHECKED BY:
APPROVED BY:
DATE: 05/16/2017
SHEET: 6 of 9
SCALE: N/A
SHEET TITLE:
C1.5
MDC-3 ASSEMBLY

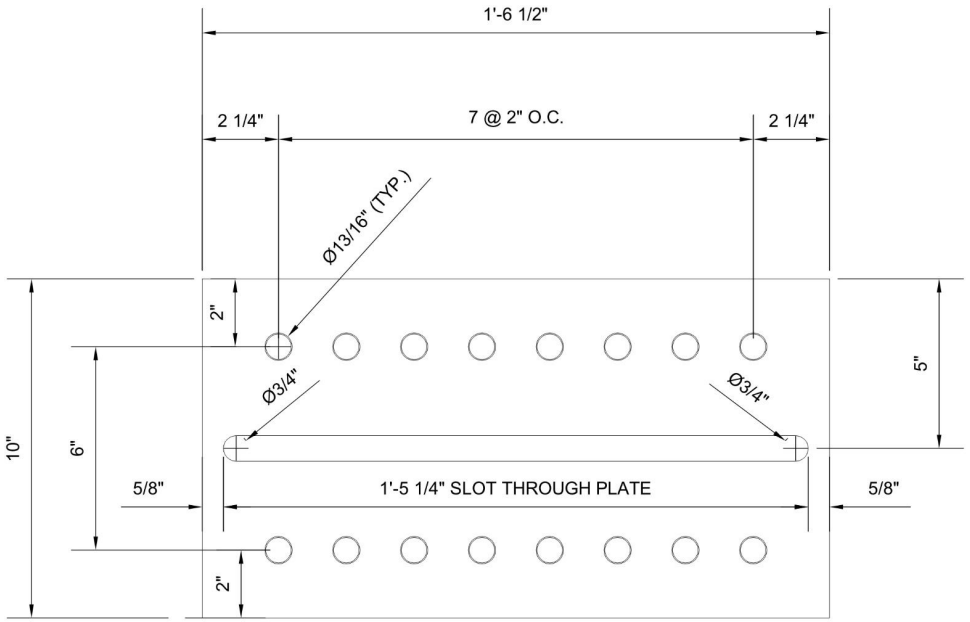

1 FRAME AND PANEL MDC PLATE FRONT VIEW

PLATE THICKNESS = 1"
A36 STEEL
PANEL AND FRAME MDC PLATES ARE IDENTICAL.

CASE WESTERN RESERVE UNIVERSITY
CIVIL ENGINEERING DEPT.

MULTI-HAZARD DUCTILE CONNECTOR
EXPERIMENTAL DESIGNS

DRAWN BY:	DES
CHECKED BY:	
APPROVED BY:	
DATE:	05/16/2017
SHEET:	7 of 9
SCALE:	N/A

SHEET TITLE:

C1.6

MDC-3 PLATES

NOTES: ALL W-SECTIONS A992 STEEL.
ALL WELDS E70 ELECTRODE.
HORIZONTAL AND VERTICAL LOAD ARM PAIRS ARE IDENTICAL (180° ROTATION)

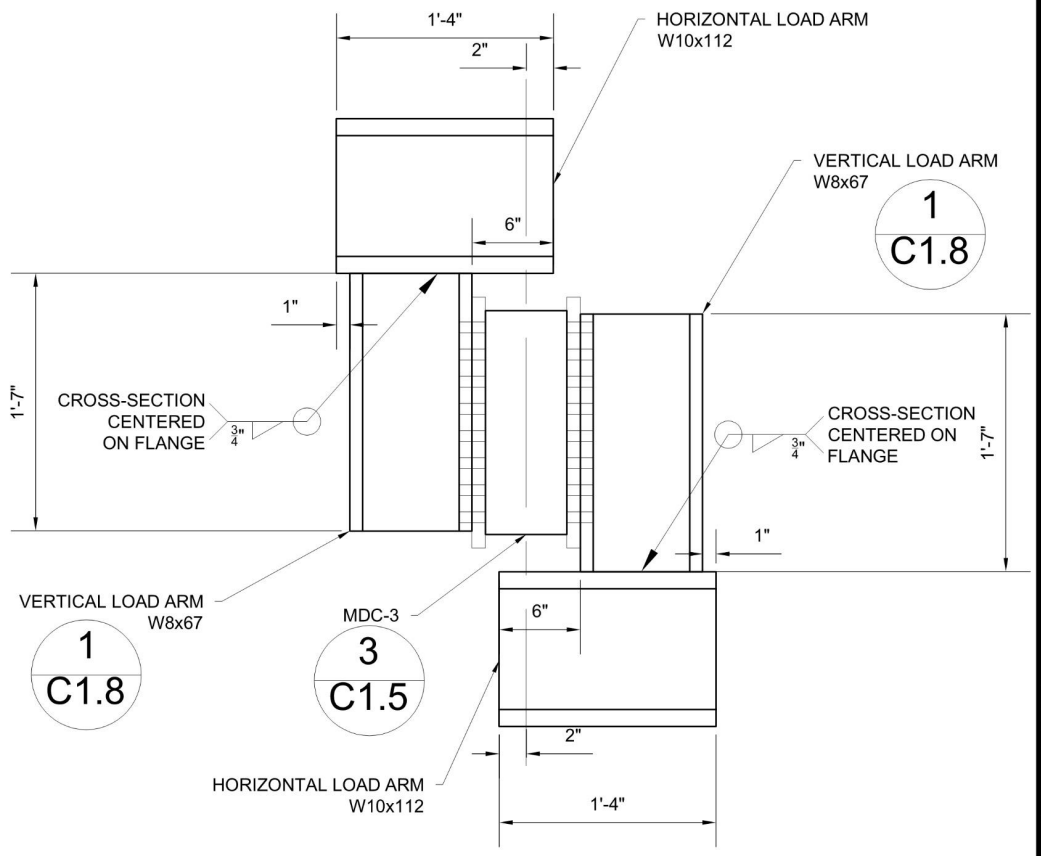

1 FRONT VIEW

TOTAL HEIGHT OF ASSEMBLY = 44.875"
TOTAL WIDTH = 28"

CASE WESTERN RESERVE UNIVERSITY
CIVIL ENGINEERING DEPT.

MULTI-HAZARD DUCTILE CONNECTOR
EXPERIMENTAL DESIGNS

DRAWN BY:	DES
CHECKED BY:	
APPROVED BY:	
DATE:	05/16/2017
SHEET:	8 of 9
SCALE:	N/A

SHEET TITLE:
C1.7
MDC-3 TEST SETUP

NOTES: ALL W-SECTIONS A992 STEEL.
ALL WELDS E70 ELECTRODE.
1'-7"
BOLT HOLES THIS FLANGE ONLY
3/4"
VERTICAL LOAD ARM TO HORIZONTAL LOAD ARM
2
W8x67
1 FRONT VIEW
1'-7"
1"
7 @ 2" O.C.
4"
6" CENTERED
Ø13/16" TYP.
1"
7 @ 2" O.C.
4"
3/4"
VERTICAL LOAD ARM TO HORIZONTAL LOAD ARM
W8x67
2 SIDE VIEW
CASE WESTERN RESERVE UNIVERSITY
CIVIL ENGINEERING DEPT.
MULTI-HAZARD DUCTILE CONNECTOR
EXPERIMENTAL DESIGNS
DRAWN BY: DES
CHECKED BY:
APPROVED BY:
DATE: 05/16/2017
SHEET: 9 of 9
SCALE: N/A
SHEET TITLE:
C1.8
VERTICAL LOAD ARM

Appendix 3

MDC1/2 Experimental Setup Design Calculation

Determination of Maximum Actuator and Table Forces Based on MDC Specimen Loading Scenarios

Revision: 2

Project: MDC

Date: 3/2/2017

Performed By: Laura Rendos

Checked By: Dr. Michael Pollino

Maximum Loading for Facade Panel Connections

Yield Strengths Are From Slovenec Design (Appendix 1)

Considering Out-of-Plane (OOP), Lateral In-Plane (LIP), and Vertical In-Plane (VIP) for a 3 Story Building.

Each Facade Panel Is Assumed to Have 6 Connections to the LFRS

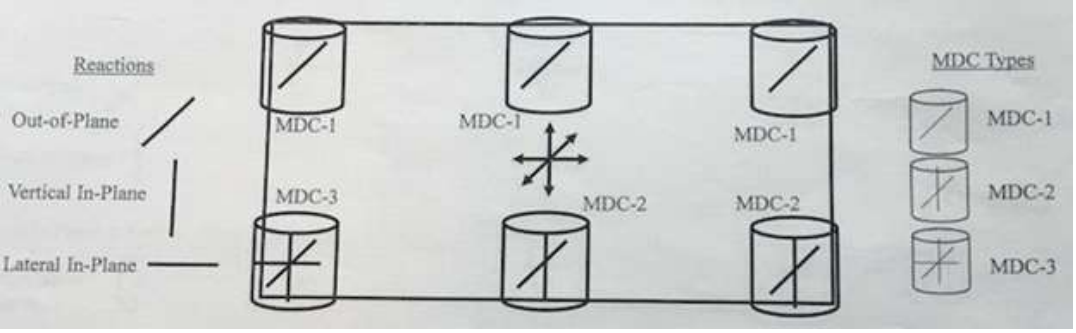

6 Connections Experience OOP Loading, 3 Connections Experience VIP, 1 Connection Experiences LIP

Peak Loading, Deformation, and Rotation Per Connection

OOP Max Loading:

Lateral Seismic Inertia (Outward/Tension):	$P_{EO} := -7.1kip$	(15th Story)
Blast Scenario 1 (Inward/Compression):	$P_B := 107.02kip$	(1st Story)
Max Inward Deformation:	$\Delta_{oop\_in} := 4in$	
Rotation Associated with Inward Deformation:	$\theta_{oop\_in} := .105rad$	
Max Outward Deformation:	$\Delta_{oop\_out} := -3.9in$	
Rotation Associated with Outward Deformation:	$\theta_{oop\_out} := -.025rad$	

LIP Max Loading:

Lateral Seismic Inertia :	$P_{EL} := 42.62kip$	(15th Story)
Contact Force:	$P_{cL} := 60.39kip$	(3rd Story)
Max Lateral Deformation:	$\Delta_{lip} := 3.9in$	
Rotation Associated with Max Deformation:	$\theta_{lip} := .025rad$	

VIP Max Loading:

Panel Dead Weight	$P_D := 15.08kip$	(All Stories)
Vertical Seismic Intertia:	$P_{EV} := 6.35kip$	(All Stories)
Contact Force:	$P_{cv} := 20.13kip$	(3rd Story)
Max Vertical Deformation:	$\Delta_{vip} := .75in$	
Rotation Associated with Max Deformation:	$\theta_{vip} := 0rad$	

Experimental Setup for Loading Scenarios

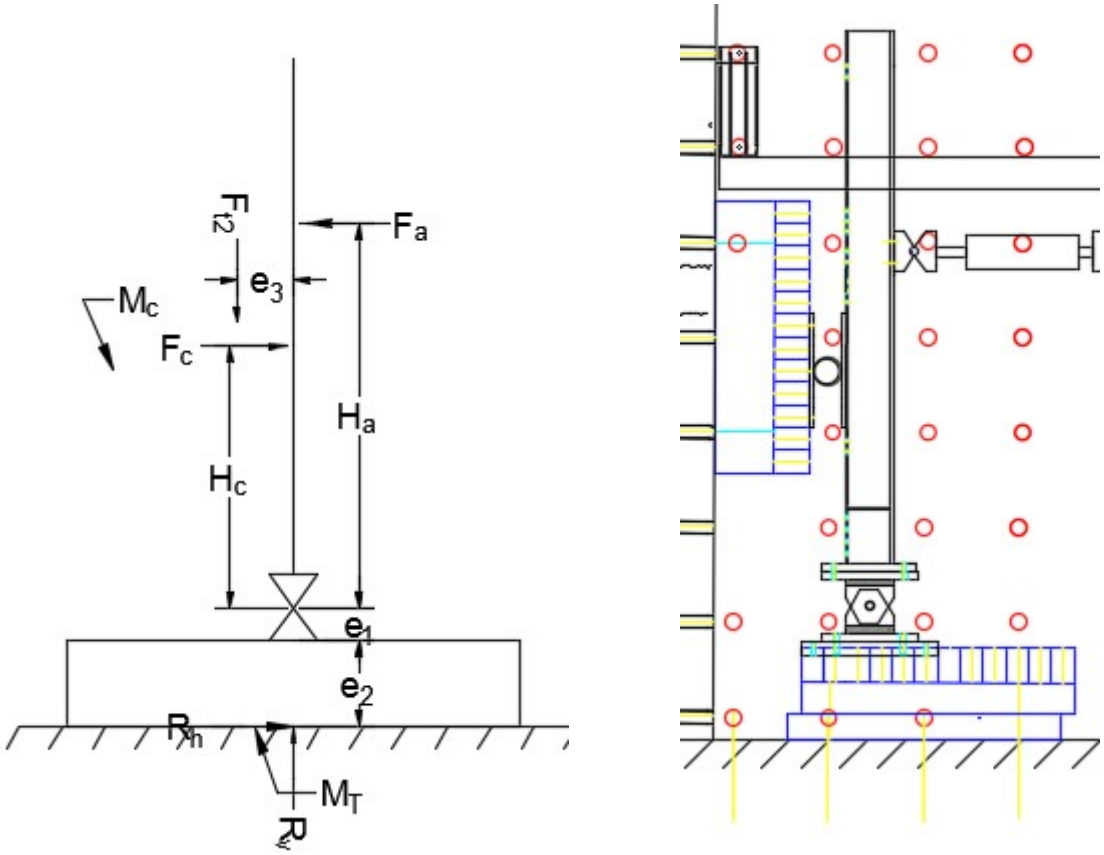

A loading diagram that includes load from the floor shake table, wall shake table, actuator, and MDC. This reperesents compression on the connection. Tension on the connection will result in forces acting in the opposite directions

F_c= Force in MDC

F_a= Force in actuator

F_{t1}= Force in floor shake table

F_{t2}= Force in wall shake table

R_h= Horizontal reaction at floor table base

R_v= Vertical reaction at floor table base

M_T= Moment at floor table base

$H_a := 9.07ft$ = Height of center of actuator to RB pin

$H_c := 7.75ft$ = Height of center of connection to RB pin

$e_1 := 10in$ = Eccentricity from top of table to RB pin

$e_2 := 2ft$ = Height of floor shake table

$e_3 := 9.5in$ = Total width of MDC

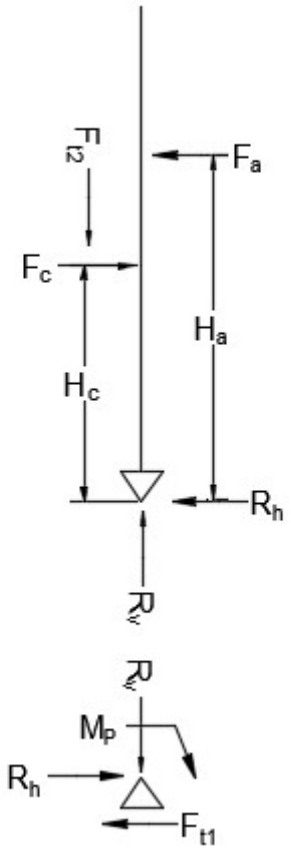

Rocker Bearing Column

Rocker Bearing Base

The free body diagrams for the rocker bearing base and the rocker bearing column. The two components are conected with a pin.

Mp = Moment about the pin

Deformations and Rotations for Loading Scenarios 1 & 2

(OOP and VIP Loading)

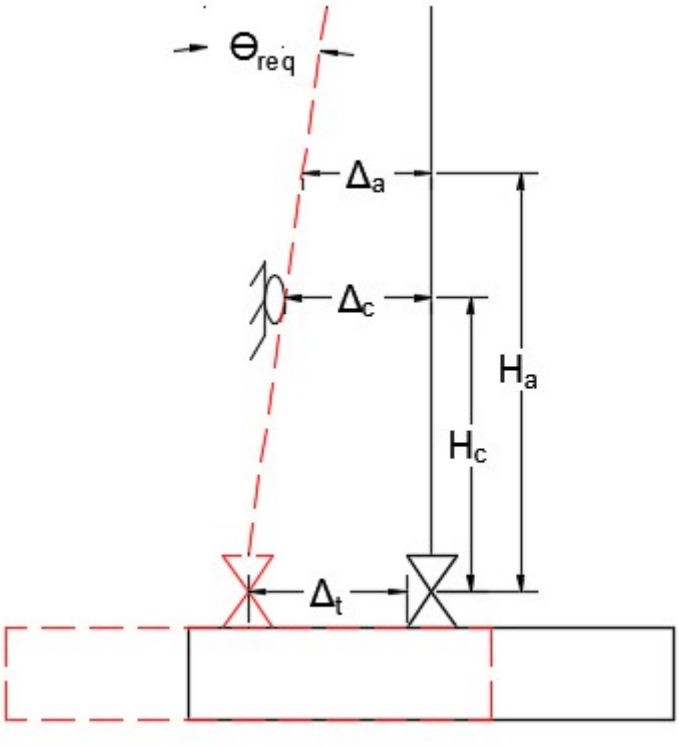

A diagram showing the MDC, rocker bearing column, and rocker bearing and floor shake table. The required MDC rotation and the deformations resulting from the rotation are included. The diagram reperesents positive defomrations in the calculations.

θ_{req} = Required rotation on connection with respect to vertical axis

Δ_a = Required stroke of actuator

Δ_c = Deformation of MDC

Δ_t = Required stroke of floor shake table

Loading Scenario 1: MDC 2 Experiences OOP Blast Loading

Required MDC Deformation (OOP): $\Delta_{c\_1} := \Delta_{oop\_in} = 4 \cdot in$

Required MDC Rotation: $\theta_{req\_1} := \theta_{oop\_in} = 0.105$

OOP Loading (Blast): $F_{c\_1} := P_B = 107.02 \cdot kip$

VIP Loading (Panel Dead): $F_{t2\_1} := P_D = 15.08 \cdot kip$

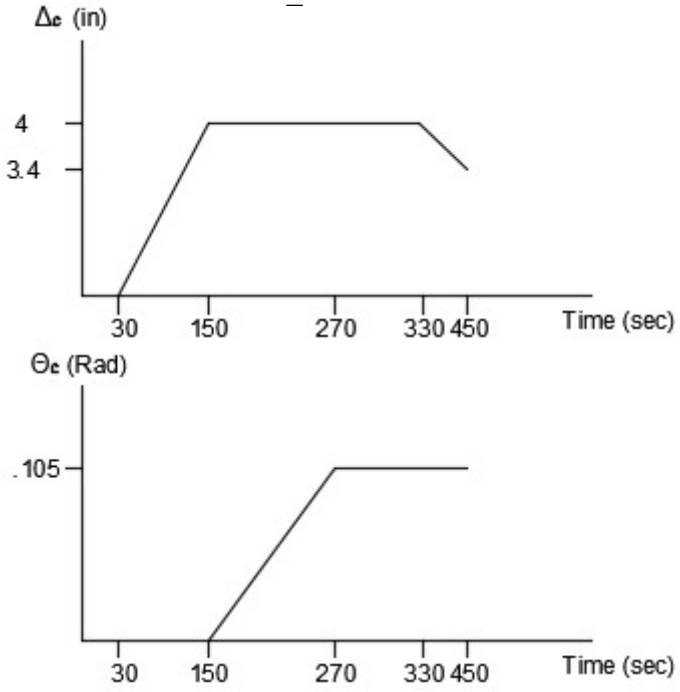

MDC OOP Deformation and Rotation

The panel dead load will be applied to the MDC vertically before any other loads are applied. The MDC rotation does not begin until the required MDC deformation has been reached.The required deformation is achieved by moving the table and actuator simulateously at the same rate. The required MDC deformation is constant while the rotation occurs. The rotation is then applied by moving on the table and actuator simultaneously at different rates and different directions. Once the required rotation and deformation are achieved, the MDC deformation will reduce due to the change in pressure direction of the blast.

Sum of Moments About Bottom of RB Column: $F_{a\_1} := \frac{\left(F_{c\_1} \cdot H_c - F_{t2\_1} \cdot e_3\right)}{H_a} = 90.129 \cdot kip$

Sum of Horizontal Forces on RB Column: $R_{h\_1} := F_{c\_1} - F_{a\_1} = 16.891 \cdot kip$

Sum of Vertical Forces On RB Column: $R_{v\_1} := F_{t2\_1} = 15.08 \cdot kip$

Sum of Horizontal Forces on Rocker Bearing Base: $F_{t1\_1} := R_{h\_1} = 16.891 \cdot kip$

Sum of Moments About Bottom of Rocker Bearing Base: $M_{p\_1} := R_{h\_1} \cdot e_1 = 14.076 \cdot kip \cdot ft$

Final Actuator and Floor Table Stroke:

Given

$$\Delta_{t1\_1} + \frac{\left(\Delta_{a\_1} - \Delta_{t1\_1}\right) \cdot H_c}{H_a} = \Delta_{c\_1}$$

$$\frac{\Delta_{a\_1} - \Delta_{t1\_1}}{H_a} = \theta_{req\_1}$$

$$\text{Find}\left(\Delta_{a\_1}, \Delta_{t1\_1}\right) \rightarrow \begin{pmatrix} 0.1016 \cdot m + 0.13859999999999999 \cdot ft \\ 0.1016 \cdot m - 0.81375 \cdot ft \end{pmatrix}$$

$\Delta_{a\_1} := 0.1016 \cdot m + 0.13859999999999999 \cdot ft = 5.663 \cdot in$

$\Delta_{t1\_1} := 0.1016 \cdot m - 0.81375 \cdot ft = -5.765 \cdot in$

The floor shake table and actuator will move a stroke length of 4in simultaneously. Once this stroke length is reached, the floor table will move back to a stroke length of -5.765in and the actuator will move forward to a stroke length of 5.663in over the same period of time. This will cause the MDC rotation to occur while maintaining the maximum MDC deformation.

Equipment Force & Deformation Summary for Scenario 1 (OOP Blast on MDC 2)

Maximum Actuator Force: $F_{a\_1} = 90.129 \cdot kip$

Maximum Actuator Stroke: $\Delta_{a\_1} = 5.663 \cdot in$

Maximum Floor Table Force: $F_{t1\_1} = 16.891 \cdot kip$

Maximum Floor Table Stroke: $\Delta_{t1\_1} = -5.765 \cdot in$

Maximum Wall Table Force: $F_{t2\_1} = 15.08 \cdot kip$

Maximum Wall Table Stroke: $\Delta_{t2\_1} := 0in$

Loading Scenario 2: MDC 1 Experiences OOP Seismic Loading

Required MDC Deformation: $\Delta_{c\_2} := \Delta_{oop\_out} = -3.9 \cdot in$

Required MDC Rotation: $\theta_{req\_2} := \theta_{oop\_out} = -0.025$

OOP Loading (Seismic): $F_{c\_2} := P_{EO} = -7.1 \cdot kip$

VIP Loading (Does Not Carry VIP): $F_{t2\_2} := 0kip$

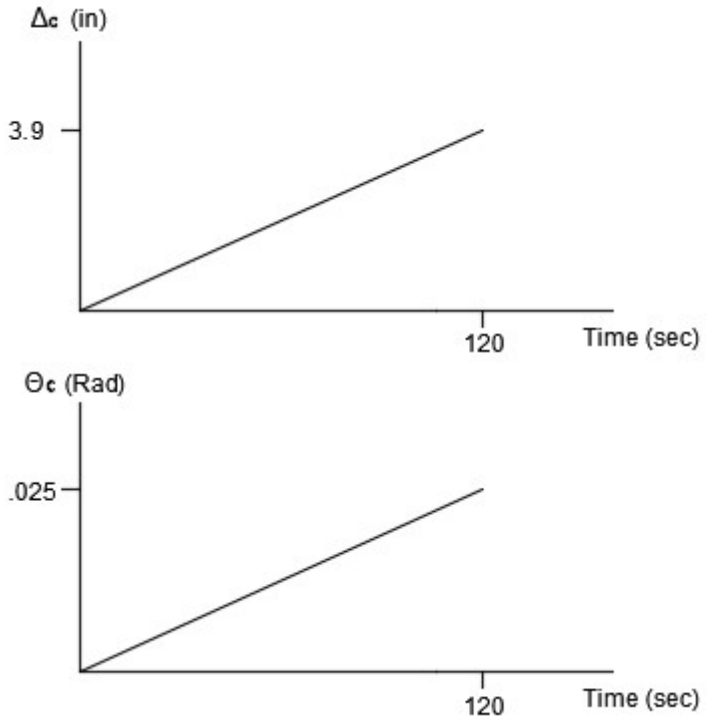

The MDC rotation and connection deformation occur simultaneously. The floor table and actuator will be both be moved at constant rates over a period of time to achieve the required MDC deformation and rotation.

Sum of Moments About Bottom of RB Column: $F_{a\_2} := \left(\frac{H_c}{H_a}\right) \cdot F_{c\_2} = -6.067 \cdot kip$

Sum of Horizontal Forces on RB Column: $R_{h\_2} := F_{c\_2} - F_{a\_2} = -1.033 \cdot kip$

Sum of Vertical Forces On RB Column: $R_{v\_2} := F_{t2\_2} = 0 \cdot kip$

Sum of Horizontal Forces on Rocker Bearing Base: $F_{t1\_2} := R_{h\_2} = -1.033 \cdot kip$

Sum of Moments About Bottom of Rocker Bearing Base: $M_{p\_2} := R_{h\_2} \cdot e_2 = -2.067 \cdot kip \cdot ft$

Final Actuator and Floor Table Stroke:

Given

$$\Delta_{t1\_2} + \frac{\left(\Delta_{a\_2} - \Delta_{t1\_2}\right) \cdot H_c}{H_a} = \Delta_{c\_2}$$

$$\frac{\Delta_{a\_2} - \Delta_{t1\_2}}{H_a} = \theta_{req\_2}$$

$$\text{Find}\left(\Delta_{a\_2}, \Delta_{t1\_2}\right) \rightarrow \begin{pmatrix} -0.09906 \cdot m - 0.032999999999999999999 \cdot ft \\ 0.19375 \cdot ft - 0.09906 \cdot m \end{pmatrix}$$

$\Delta_{a\_2} := -0.09906 \cdot m - 0.032999999999999999999 \cdot ft = -4.296 \cdot in$

$\Delta_{t1\_2} := 0.19375 \cdot ft - 0.09906 \cdot m = -1.575 \cdot in$

The floor shake table will move to a stroke length of -4.3in and the actuator will move to a stroke length of -1.575in simultaneously. This will cause the maximum MDC deformation and rotation to occur simultaneously.

Equipment Force & Deformation Summary for Scenario 2 (OOP Seismic on MDC 1)

Maximum Actuator Force: $F_{a\_2} = -6.067 \cdot kip$

Maximum Actuator Stroke: $\Delta_{a\_2} = -4.296 \cdot in$

Maximum Floor Table Force: $F_{t1\_2} = -1.033 \cdot kip$

Maximum Floor Table Stroke: $\Delta_{t1\_2} = -1.575 \cdot in$

Maximum Wall Table Force: $F_{t2\_2} = 0 \cdot kip$

Maximum Wall Table Stroke: $\Delta_{t2\_2} := 0in$

Summary of Maximum Equipment Forces

Maximum Actuator Force:	$F_{a\_max} = 90.129 \cdot kip$
Maximum Actuator Force Loaing Condition:	$Loading_{max\_act} =$ "Blast OOP, Scenario 1"
Maxiumum Actuator Stroke:	$\Delta_{a\_max} = 5.663 \cdot in$
Maximum Actuator Stroke Loading Condition:	$Stroke_{max\_act} =$ "Blast OOP, Scenario 1"
Floor Table Max Actuator Force:	$F_{t1\_max} = 16.891 \cdot kip$
Maximum Floor Table Loading Condition:	$Loading_{max\_t1} =$ "Blast OOP, Scenario 1"
Maximum Floor Table Stroke:	$\Delta_{t1\_max} = 5.765 \cdot in$
Maximum Floor Table Stroke Loading Condition:	$Stroke_{max\_t1} =$ "Blast OOP, Scenario 1"
Wall Table Max Actuator Force:	$F_{t2\_max} = 15.08 \cdot kip$
Maximum Wall Table Loading Condition:	$Loading_{max\_t2} =$ "Blast OOP, Scenario 1"
Maximum Wall Table Stroke:	$\Delta_{t2\_max} = 0 \cdot in$
Maximum Wall Table Stroke Loading Condition:	$Stroke_{max\_t2} =$ "Seismic OOP, Scenario 2"

Calculations for Equipment Used in Experimental Test Setup

Revision: 4

Project: MDC

Date: 5/17/2017

Performed By: Laura Rendos

Checked By: Dr. Michael Pollino

All calculations were performed in accordance with AISC 360-10: Specifications for Structural Steel Buildings (AISC 2010b) using steel section properties from the Steel Construction Manual Thirteenth Edition (AISC 2011).

Envelope Loads on Rocker Bearing (RB) Column

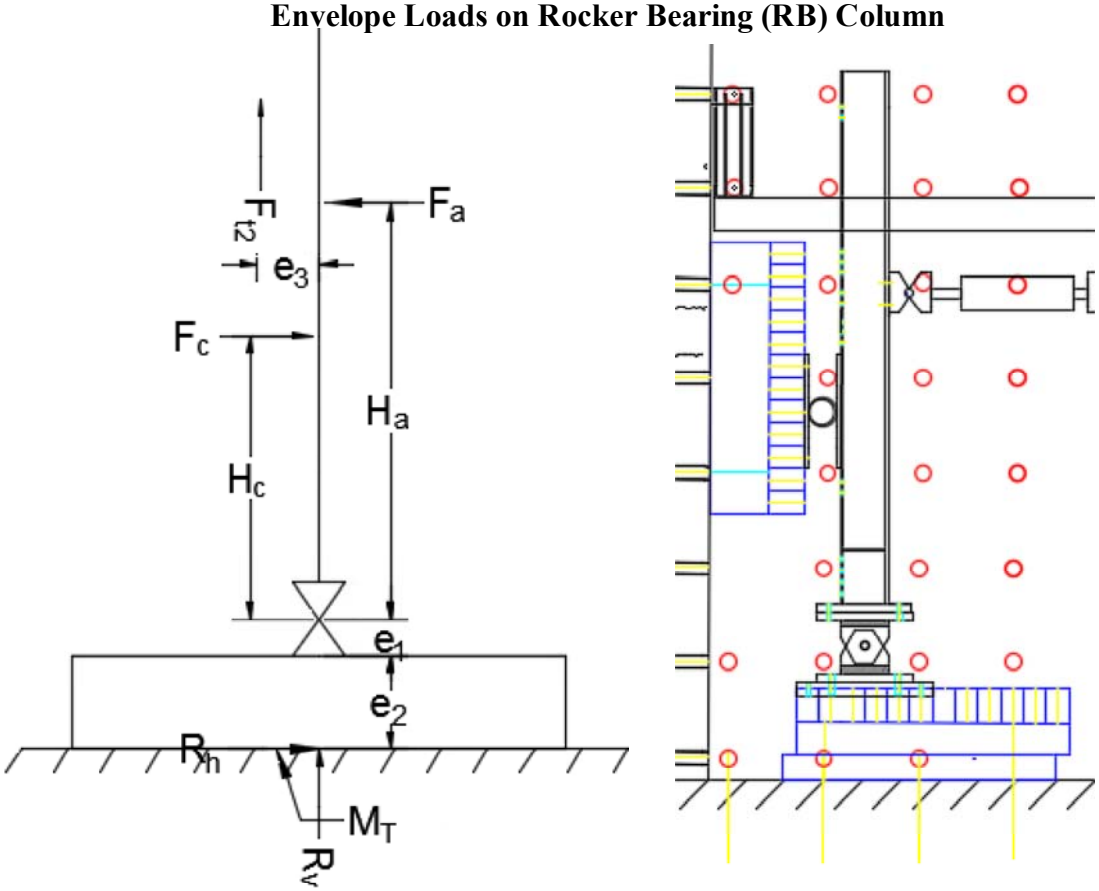

F_c= Force in connection

$F_a := 110kip$ = Maximum force in actuator

$F_{t1} := 22kip$ = Maximum force in floor shake table

$F_{t2} := 22kip$ = Maximum force in wall shake table

R_h= Horizontal reaction at bottom of RB column

R_v= Vertical reaction at bottom of RB column

$H_a := 9.1ft$ = Height of center of actuator to RB pin

$H_c := 7.6ft$ = Height of center of connection to RB pin

$e_1 := 10in$ = Eccentricity from top of table to RB pin

$e_2 := 2ft$ = Height of shake table

$e_3 := 15.5in$ = Width of connection and plates

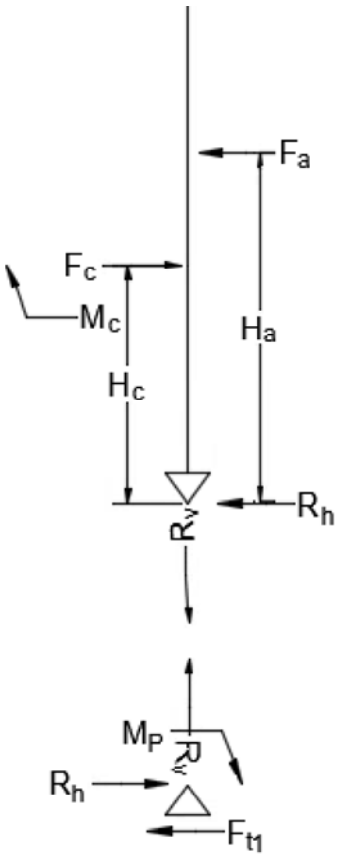

Rocker Bearing (RB) Column

Rocker Bearing Base

Moment at Connection from Table 2: $M_c := F_{t2} \cdot e_3 = 28.417 \cdot kip \cdot ft$

Sum Moments About Bottom of RB Column: $0 = F_{t2}e_3 - F_cH_c + F_aH_a$

$$F_c := \frac{F_a \cdot H_a + M_c}{H_c} = 135.45 \cdot kip$$

Sum Vertical Forces on RB Column: $R_v := F_{t2} = 22 \cdot kip$

Sum Horozontal Forces on RB Colum $R_h := F_c - F_a = 25.45 \cdot kip$

R_h is over the force capacity of the table actuators.

Horizontal Force on RB Base $R_h := 22kip$

Sum Horozontal Forces on RB Colum $F_c := F_a + R_h = 132 \cdot kip$

Vertical Force on RB Column: $$F_{t2} := \frac{F_c \cdot H_c - F_a \cdot H_a}{e_3} = 1.703 \cdot kip$$

Both tables and the actuators are within their force capacity.

RB Column Shear

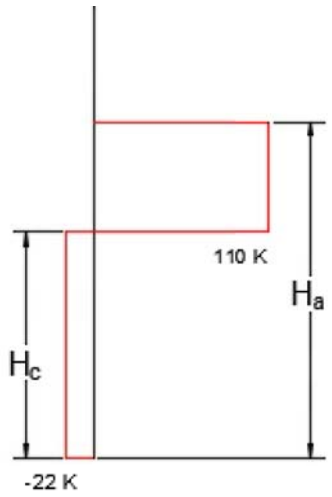

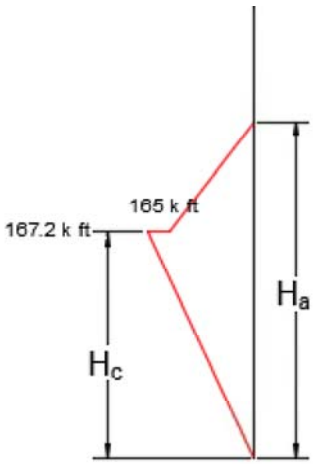

RB Column Bending

$M_{max} := 167.2kip \cdot ft$

Although all both tables and the actuators cannot all be at their capacities at the same time, assume so for the experimental component design.

Adjusted Vertical Force (For Design of Experiment Components):

$R_v := 22kip$

$F_{t2} := R_v = 22 \cdot kip$

Compactness Check

Rocker Bearing Column is a W12x58 section and is 11.4' tall.

Yield Stress (Preffered for W Shape): $F_y := 50ksi$

Steel Modulus of Elasticity: $E := 29000ksi$

Compactness Criteria: $\lambda_p := .38 \cdot \sqrt{\frac{E}{F_y}} = 9.152$

Flanges: $\lambda_f := 7.82$ Flanges are compact

Web: $\lambda_w := 27.0$ Web is not compact

The flanges do not need to be checked seperately because they are compact.

Yielding Check:

Section Modulus: $S_x := 78in^3$

Moment Capacity: $\phi M_n := .9 \cdot F_y \cdot S_x = 292.5 \cdot kip \cdot ft$

Demand to Capacity Ratio: $DC := \frac{M_{max}}{\phi M_n} = 0.572$

Because the demand to capacity ratio is less than 1, the RB column will not experience yielding under the maximum actuator loading.

Lateral Torsional Buckling Check

Braced RB Column Length: $L_b := 10ft$

Minor Radius of Gyration: $r_y := 2.51in$

Limiting Length: $L_p := 1.76 \cdot r_y \cdot \sqrt{\frac{E}{F_y}} = 8.866 \cdot ft$

$L_p < L_b$; Further checks required

RB Column Moment Capacity (Based on 11.4' Unbraced Length): $\phi M_n := 309kip \cdot ft$

Demand to Capacity Ratio: $DC := \frac{M_{max}}{\phi M_n} = 0.541$

Because the demand to capacity ratio is less than 1, the RB column will not experience lateral torsional buckling under the maximum actuator loading.

Flange Prying Check (at specimen to rocker bearing column connection):

Force Normal to Flange: $F_n := F_c = 132 \cdot kip$

Flange Thickness on W 12x58 Rocker Bearing Column: $t_f := .64in$

Yield Strength of Flange: $F_y := 50ksi$

Flange Local Bending Strength: $\phi R_n := 2 \cdot .9 \cdot 6.25 \cdot F_v \cdot t_f^{\,2} = 230.4 \cdot kip$

Demand to Capacity Ratio: $DC := \frac{F_n}{\phi R_n} = 0.573$

The DC ratio is less than 1, therefore the rocker bearing column will not exerience flange prying at its connection with the testing specimen.

Flange Prying Check (at actuator to rocker bearing column connection):

Force Normal to Flange: $F_n := F_a = 110 \cdot kip$

Flange thickness and yield strength the same as above. The flange local bending strength is also the same as above.

Demand to Capacity Ratio: $DC := \frac{F_n}{\phi R_n} = 0.477$

The DC ratio is less than 1, therefore the rocker bearing column will not exerience flange prying at its connection with the actuator.

Attaching Actuator to Reaction Frame (RF) Column

The RF column is a W24x103 and is 12ft in height. The actuator plate will be bolted to the W24 section with a minimum of 4 bolts. Assume that the actuators will be acting at full capacity in tension.

Force in Actuator: $F_a = 110 \cdot kip$

Bolt Sizing:

Minimum Tensile Strength Per Bolt: $r_{n\_min} := \frac{F_a}{4} = 27.5 \cdot kip$

Tensile Strength of 3/4" Bolt (A325 Strength): $\phi r_n := 29.8kip$

Demand to Capacity Ratio: $DC := \frac{F_a}{4 \cdot \phi r_n} = 0.923$

Assuming that the actuators reach their maximum capacity, 4 3/4" diameter bolts of A325 strength are adequate to attach to actuator plate to the RF column.

Flange Prying Check (at actuator plate to RF column connection):

Force Normal to Flange: $F_n := F_a = 110 \cdot kip$

Flange Thickness on W24x103 RF Column: $t_f := .98in$

Yield Strength of Flange: $F_y := 50ksi$

Flange Local Bending Strength: $\phi R_n := 2 \cdot .9 \cdot 6.25 \cdot F_y \cdot t_f^2 = 540.225 \cdot kip$

Demand to Capacity Ratio: $DC := \frac{F_n}{\phi R_n} = 0.204$

The DC ratio is less than 1, therefore the RF column will not exerience flange prying at its connection with the actuator plate. The same force will be normal to the flange on the other side of the RF column where the diagonal brace connects to the RF column. The connection of the diagonal brace to the RF column will not experience flange prying either

Capacity of Reaction Frame (RF) Column

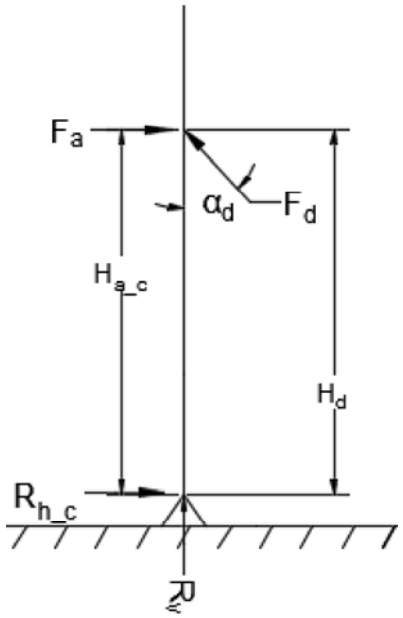

Free Body Diagram at the Center of the RF Column were the Diagonal Brace and Actuator Forces Intersect

F_d= Force in diagonal brace

F_a= Force in actuator

R_{h_c}= Horizontal reaction at RF column base

R_v = Vertical reaction at RF column base

$H_{a\_c} := 10.75ft$ = Height of actuator from RFcolumn base

$H_d := 10.75ft$ = Height of diagonal brace from pin

$\alpha_d := 43deg$ = Angle of diagonal brace from vertical axis

Sum Moment Around RF Column Base: $M_{base} = 0 = F_a(H_{a\_c}) - \sin(\alpha_d)F_d(H_d)$

$$F_d := \frac{F_a \cdot H_{a\_c}}{\sin(\alpha_d) \cdot H_d} = 161.291 \cdot kip$$

Sum of Horizontal Forces: $R_{h\_c} := -F_a + \sin(\alpha_d) \cdot F_d = 1.309 \times 10^{-14} \cdot kip$

Because the diagonal brace force intersects the actuator force, the diagonal brace takes all the force and the W24 RF column does not experience shear or bending over its length.

Reaction Frame Column Diagonal Brace

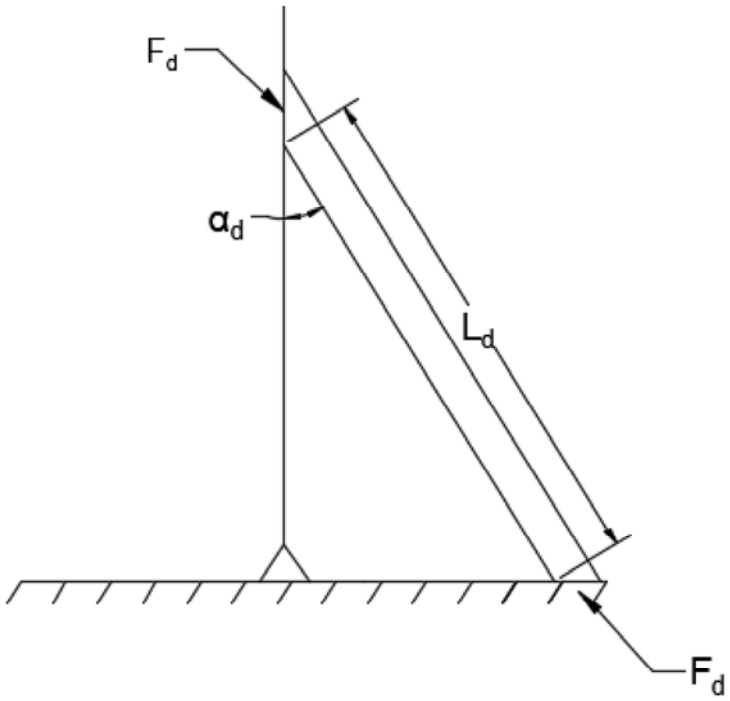

F_d = force in diagonal brace

$L_d := 12.33ft$ = Shortest length of diagonal brace

$F_y := 46ksi$

$E := 29000ksi$

Assuming a HSS 6x6x3/8 that is a pin-pin column

Flexural Bucking Check

Effective Length Factor: $k := 1.0$

Minor Radius of Gyration: $r_v := 2.28in$

KL/r Ratio: $ratio := \frac{k \cdot L_d}{r_v} = 64.895$

Gross Section Area: $A_g := 7.58in^2$

Ratio: $ratio := 4.71 \cdot \sqrt{\frac{E}{F_y}} = 118.261$ Greater than KL/r ratio

Elastic Buckling Stress: $F_e := \frac{\pi^2 E}{\left(\frac{k \cdot L_d}{r_y}\right)^2} = 67.964 \cdot ksi$

Critical Buckling Load: $F_{cr} := .658^{\left(\frac{F_y}{F_e}\right)} \cdot F_y = 34.652 \cdot ksi$

Nominal Compressive Strength: $\phi P_n := .9 F_{cr} \cdot A_g = 236.396 \cdot kip$

Demand to Capacity Ratio: $DC := \frac{F_d}{\phi P_n} = 0.682$

The DC ratio is less than 1, the diagonal brace will not experience flexural buckling

Flange Prying Check (at connection of diagonal brace to RF column):

See above calculation for flange prying at the actuator plate connection to RF column.

Weld Capacity Check (at both plate to diagonal brace connections)

Length of Weld (Around 4 Faces of 6" Length of the HSS Diagonal): $L_{weld} := 24in$

Strength of Filler: $F_{nw} := .6 \cdot 70ksi$

Appoximate Weld Depth: $D_{weld} := .3125in$

Area of Weld: $A_{we} := .707 \cdot D_{weld} \cdot L_{weld} = 5.302 \cdot in^2$

Strength of Weld: $\phi R_n := .75 \cdot F_{nw} \cdot A_{we} = 167.029 \cdot kip$

Force Acting on Weld: $F_d = 161.291 \cdot kip$

Demand to Capacity Ratio: $DC := \frac{F_d}{\phi R_n} = 0.966$

A weld thickness of 5/16" is required to bring the demand to capacity ratio of the welds below 1.

Flange Prying Check (at connection of diagonal brace to foundation beam):

The unstiffened foundation beam is a W14x145. This section was checked without stiffeners to be conservative

Force Normal to Flange: $F_n := F_d \cdot \cos\left(\alpha_d\right) = 117.961 \cdot kip$

Flange thickness of Foundation Beam: $t_f := 1.09in$

Flange Local Bending Strength: $\phi R_n := 2 \cdot .9 \cdot 6.25 \cdot F_y \cdot t_f^{\,2} = 614.842 \cdot kip$

Demand to Capacity Ratio: $DC := \frac{F_n}{\phi R_n} = 0.192$

The DC ratio is less than one, therefore the foundation beam will not experience flange pyring at its connection with the diagonal brace.

Rocker Bearing Base Plate Design Using Max Actuator Capacity

Reference:\\labhomes\LabHome$\ler56\Desktop\2-55kip setup\columncalcs_Rev3.xmcd

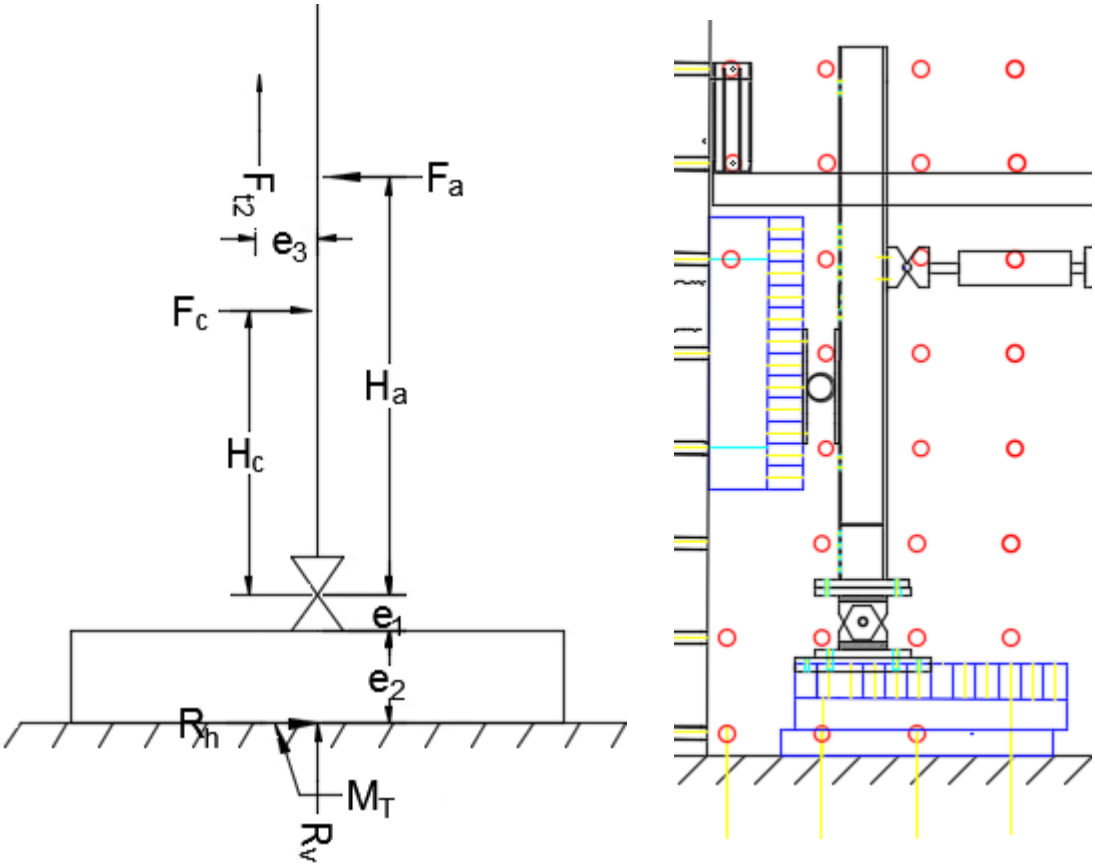

F_c= Force in MDC

$F_a = 110 \cdot kip$ = Force in actuators

$F_{t1} = 22 \cdot kip$ = Force in floor shake table

$F_{t2} = 22 \cdot kip$ = Force in wall shake table

R_h= Horizontal reaction at bottom of RB column

R_v= Vertical reaction at bottom of RB column

$H_a = 9.1 \cdot ft$ = Height of center of actuator to RB pin

$H_c = 7.6 \cdot ft$ = Height of center of connection to RB pin

$e_1 = 10 \cdot in$ = Eccentricity from top of table to RB pin

$e_2 = 24 \cdot in$ = Height of floor shake table

$e_3 = 15.5 \cdot in$ = Total Width of MDC

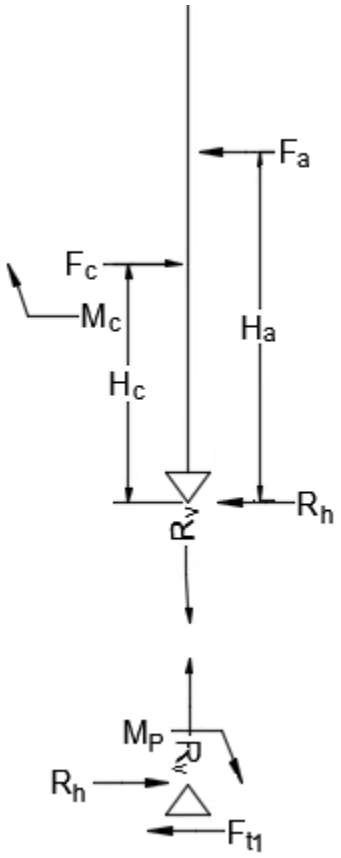

Rocker Bearing
(RB) Column

Rocker Bearing Base

$F_c = 132 \cdot kip$ =Force in MDC

$R_h = 22 \cdot kip$ = Horizontal reaction at bottom of RB column

$R_v = 22 \cdot kip$ = Vertical reaction at bottom of RB column

$F_a = 110 \cdot kip$ = Force in actuators

Base Plate Under Rocker Bearing

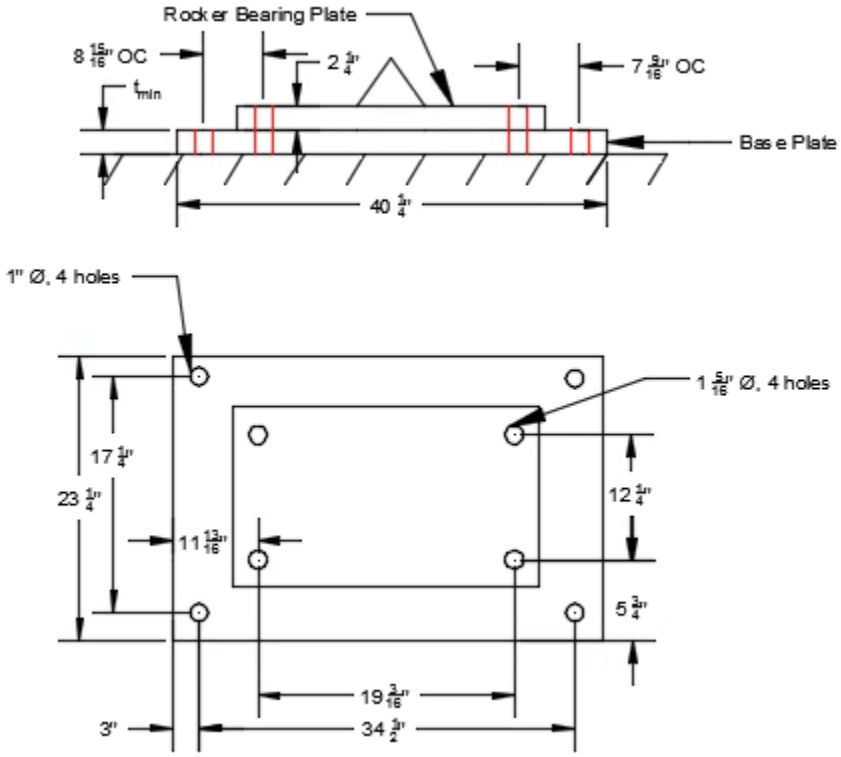

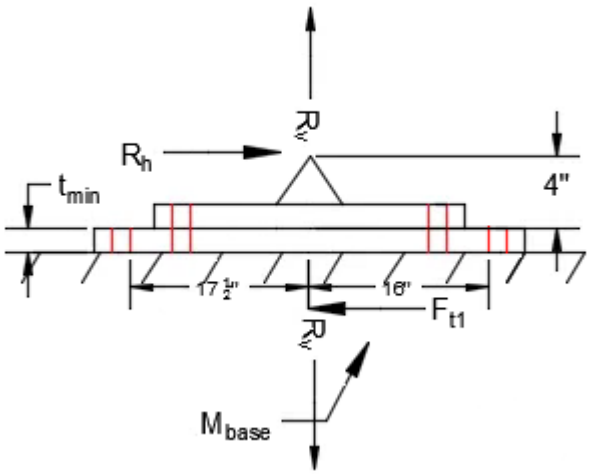

Initially assume that t_{min} is 1"

Total Vertical Force Acting on Base Plate: $F_{total} := R_v + \frac{R_h \cdot (4in + 1in)}{34.5in} = 25.188 \cdot kip$

Force Acting on Left Base Plate Bolt Line: $F_{left} := \frac{F_{total} \cdot (16 \cdot in + .5in)}{34.5in} = 12.047 \cdot kip$

Force Acting on Right Base Plate Bolt Line: $F_{right} := F_{total} - F_{left} = 13.142 \cdot kip$

Plate Yielding Check

Maximum Plate Width Between 1"ϕ and 1 5/16"ϕ Holes: $b_{prime} := 8.9375in$

Tributary Length of Plate (Excluding Bolt Holes): $p := 23.25in - 2(1.3125in) = 20.625 \cdot in$

Yield Strength (Preferred For Plates: $F_y := 36ksi$

Min Required Strength for a Bolt Line: $T := \max\left(F_{left}, F_{right}\right) = 13.142 \cdot kip$

Minimum Plate Thickness (No Prying): $t_{min\_yield} := \sqrt{\frac{4 \cdot T \cdot b_{prime}}{.9 \cdot p \cdot F_y}} = 0.838 \cdot in$

Plate Hole Shearing Check

The diameter is 1 5/16" on top plate, so calculations assume 1 1/4" bolts.

Required Nut Thickness: $t_{nut} := 1.21875in$

Yield Strenght of Nut: $F_{y\_nut} := 132ksi$

Minimum Plate Thickness to Avoid Hole Shearing: $t_{min\_hole} := \left(\frac{F_{y\_nut}}{F_y}\right) \cdot t_{nut} = 4.469 \cdot in$

However, the top plate bolts are very overdesigned for this application. Adjust the plate thickness based on the ratio of bolt capacity to needed capacity

Required Tensile Capacity of a Bolt (2 bolts in each Line): $F_{bolt} := \frac{T}{2} = 6.571 \cdot kip$

Available Tensile Capacity in 1 1/4" Bolt: $\phi R_n := 82.8kip$

Modified Minimum Plate Thickness to Avoid Hole Shearing: $t_{min\_hole} := \left(\frac{F_{bolt}}{\phi R_n}\right) \cdot t_{min\_hole} = 0.355 \cdot in$

Minimum Base Plate Thickness: $t_{min} := \max\left(t_{min\_yield}, t_{min\_hole}\right) = 0.838 \cdot in$

Use a 1" thick plate as assumed for the rocker bearing base plate.

Demand to Capacity Ratio: $DC := \frac{\left(t_{min}\right)^2}{(1in)^2} = 0.703$

The demand to capacity ratio is less than 1, therefor a 1" thick plate is adequate for the rocker bearing base plate.

Plates of Reaction Frame Diagonal Brace

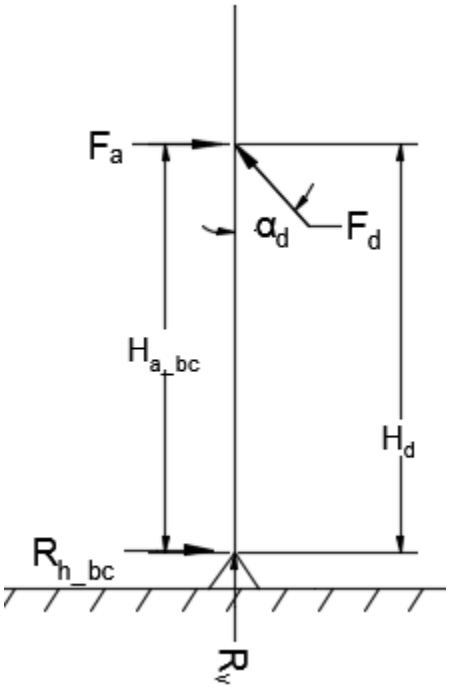

$F_d = 161.291 \cdot kip$ = Force in diagonal brace

$\alpha_d = 43 \cdot deg$ = Angle of diagonal brace

$F_{d\_h} := F_d \cdot \sin\left(\alpha_d\right) = 110 \cdot kip$ = Horizontal force in diagonal brace

$F_{d\_v} := F_d \cdot \cos\left(\alpha_d\right) = 117.961 \cdot kip$ = Vertical force in diagonal brace

Foundation Beam to Diagonal Brace Plate Calculations

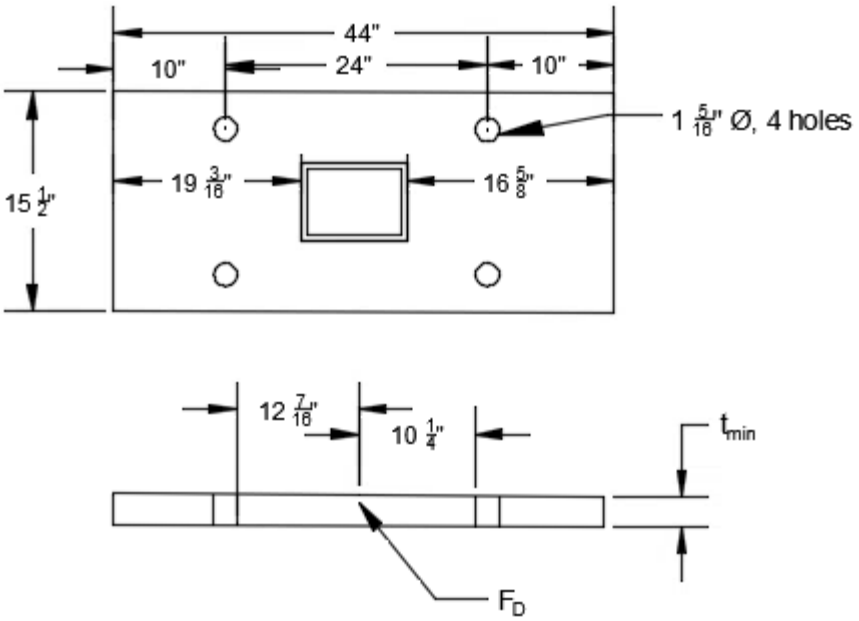

The above dimensions assume that a 1 3/4" thick plate is used at t_{min}.
The diagonal is an HSS6x6x3/8.

Force Acting on Left Plate Bolt Line:

$$F_{left} := \frac{F_{d\_v} \cdot (10.25in + .5 \cdot 1.3125in)}{24in} = 53.604 \cdot kip$$

Force Acting on Right Plate Bolt Line:

$$F_{right} := F_{d\_v} - F_{left} = 64.356 \cdot kip$$

Plate Yielding Check

Maximum Distance Between HSS and Hole Line: $b_{prime} := 19.1875in - 10in = 9.188 \cdot in$

Tributary Length of Plate (Excluding Bolt Holes): $p := 15.5in - 2(1.3125in) = 12.875 \cdot in$

Yield Strength (Preferred For Plates): $F_y := 36ksi$

Required Strength for Bolt Line: $T := \max(F_{left}, F_{right}) = 64.356 \cdot kip$

Minimum Plate Thickness (Prying Included): $t_{min\_yield} := \sqrt{\frac{2 \cdot T \cdot b_{prime}}{.9 \cdot p \cdot F_y}} = 1.684 \cdot in$

Demand to Capacity Ratio: $DC := \frac{(t_{min\_yield})^2}{(1.75in)^2} = 0.926$

The demand to capacity ratio is less than 1, therefor a 1 3/4" thick plate is adequate for the diagonal brace plate on the foundation beam.

Required Number of Bolts Based on Combined Shear and Tension
(Diagonal foundation beam plate to foundation beam)
Assume 4 1 1/4" diameter bolts will be used

Force on Bolt Line Due to Prying: $F_{pry} := \frac{\frac{p \cdot (1.75in)^2 \cdot F_y}{4}}{\left(\frac{2}{3}\right)10in} = 53.23 \cdot kip$

Max Tensile Force Per Bolt: $F_{ten} := .5 \cdot (T + F_{pry}) = 58.793 \cdot kip$

Minimum Required Tensile Stress Per Bolt: $f_t := \frac{F_{ten}}{\left[\pi\left(\frac{1.25in}{2}\right)^2\right]} = 47.909 \cdot ksi$

Factored Nominal Tensile Stress Per Bolt: $\phi F_{nt} := 67.5ksi$

Factored Nominal Shear Stress Per Bolt: $\phi F_{nv} := 40.5ksi$

$(f_t / \phi F_{nt}) + (f_v / \phi F_{nv}) = 1.3$

Required Shear Stress Per Bolt:

$$f_v := \left[1.3 - \left(\frac{f_t}{\phi F_{nt}}\right)\right]\phi F_{nv} = 23.905\cdot ksi$$

Available Shear Strength of Per Bolt:

$$\phi r_n := f_v \cdot \left[\pi\left(\frac{1.25in}{2}\right)^2\right] = 29.335\cdot kip$$

Shear Force Acting Per Bolt:

$$F_{shear} := \frac{F_{d\_h}}{4} = 27.5\cdot kip$$

Demand to Capacity Ratio:

$$DC := \frac{F_{shear}}{\phi r_n} = 0.937$$

4 bolts of 1 1/4" diameter are adequate to resist the combined tension and shear force at the diagonal brace plate to foundation beam connection.

Reaction Frame Column to Diagonal Brace Plate Calculatons

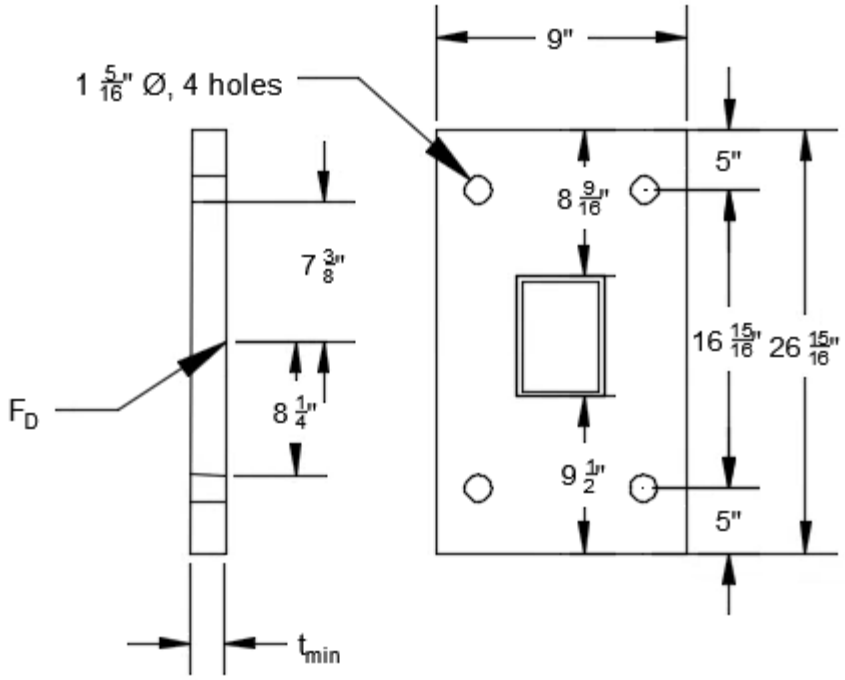

The above dimensions assume that a 1 3/4" thick plate is used at t_{min}.

Force Acting on Top Plate Bolt Line:

$$F_{top} := \frac{F_{d\_h}\cdot(8.25in + .5\cdot 1.3125in)}{16.9375in} = 57.841\cdot kip$$

Force Acting on Bottom Plate Bolt Line:

$$F_{bot} := F_{d\_h} - F_{top} = 52.159\cdot kip$$

Plate Yielding Check

Maximum Distance Between HSS and Bolt Line: $b_{prime} := 9.5in - 5in = 4.5 \cdot in$

Tributary Length of Plate (Excluding Bolt Holes): $p := 9in - 2(1.3125in) = 6.375 \cdot in$

Yield Strength (Preferred For Plates: $F_y := 36ksi$

Required Strength for 4 Plate Bolts: $T := \max(F_{bot}, F_{top}) = 57.841 \cdot kip$

Minimum Plate Thickness (Prying Included): $t_{min\_yield} := \sqrt{\frac{2T \cdot b_{prime}}{.9 \cdot p \cdot F_y}} = 1.588 \cdot in$

Demand to Capacity Ratio: $DC := \frac{(t_{min\_yield})^2}{(1.75in)^2} = 0.823$

The demand to capacity ratio is less than 1, therefor a 1 3/4" thick plate is adequate for the diagonal brace plate on the RF column.

Required Bolts Based on Combined Shear and Tension
(Diagonal column plate to actuactor column)
Assume 4 1 1/4" diameter bolts will be used

Force on Bolt Line Due to Prying: $F_{pry} := \frac{\frac{p \cdot (1.75in)^2 \cdot F_y}{4}}{\left(\frac{2}{3}\right)5in} = 52.713 \cdot kip$

Max Tensile Force Per Bolt: $F_{ten} := .5 \cdot (T + F_{prv}) = 55.277 \cdot kip$

Minimum Required Tensile Stress Per Bolt: $f_t := \frac{F_{ten}}{\left[\pi\left(\frac{1.25in}{2}\right)^2\right]} = 45.044 \cdot ksi$

Factored Nominal Tensile Stress Per Bolt: $\phi F_{nt} := 67.5ksi$

Factored Nominal Shear Stress Per Bolt: $\phi F_{nv} := 40.5ksi$

$(f_t / \phi F_{nt}) + (f_v / \phi F_{nv}) = 1.3$

Required Shear Stress $f_v := \left[1.3 - \left(\frac{f_t}{\phi F_{nt}}\right)\right]\phi F_{nv} = 25.624 \cdot ksi$

Per Bolt:
Available Shear Strength Per Bolt: $\phi r_n := f_v \cdot \left[\pi\left(\frac{1.25in}{2}\right)^2\right] = 31.445 \cdot kip$

Shear Force Acting Per Bolt: $F_{shear} := \frac{F_{d\_v}}{4} = 29.49 \cdot kip$

Demand to Capacity Ratio: $DC := \frac{F_{shear}}{\phi r_n} = 0.938$

4 bolts of 1 1/4" diameter are adequate to resist the combined tension and shear force at the diagonal brace plate to RF column connection.

2- 55kip Actuator Plate (Without Current Stiffening)

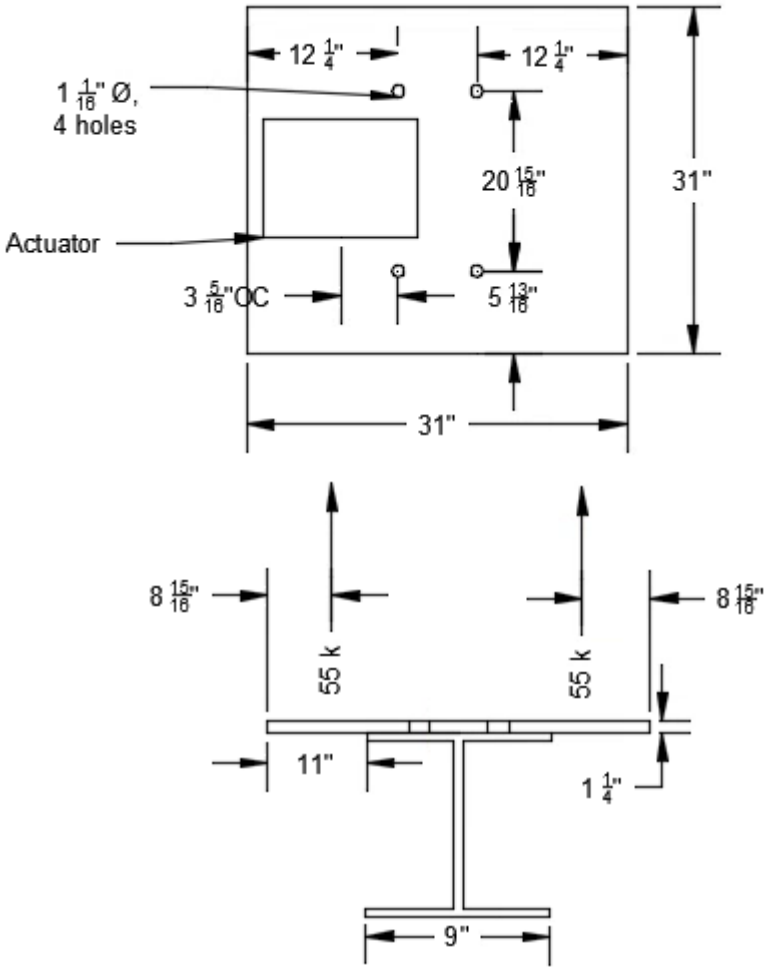

The above drawings do not show the current stiffening on the plate. The calculations below will provide conservative results for the required plate thickness.

Plate Yielding Check

Maximum Distance from F_D to Inner Bolt Hole: $b_{prime} := 3.3125in$

Tributary Length of Plate (Excluding Bolt Holes): $p := 31in - 2(1.0625in) = 28.875 \cdot in$

Yield Strength (Preferred For Plates: $F_y := 36ksi$

Required Strength Per Bolt Line: $T := 55kip = 55 \cdot kip$

Minimum Plate Thickness (No Prying): $t_{min\_yield} := \sqrt{\frac{4 \cdot T \cdot b_{prime}}{.9 \cdot p \cdot F_y}} = 0.883 \cdot in$

Demand to Capacity Ratio: $DC := \frac{\left(t_{min\_yield}\right)^2}{(1.25in)^2} = 0.499$

The demand to capacity ratio is less than 1, therefore a 1 1/4" thick plate is adequate for the actuator plate.

Lateral Support Bracing Calculations

Reference:\\labhomes\LabHome$\ler56\Desktop\2-55kip setup\plate calcs_rev1.xmcd

Approximated Lateral Loads on the Columns

$A_{rbc} := R_v = 22 \cdot kip$ = rocker bearing column axial force

$A_{ac} := F_d \cdot \cos(\alpha_d) = 117.961 \cdot kip$ = reaction frame column axial force

$P_{rbc} := .05 \cdot A_{rbc} = 1.1 \cdot kip$ = 5% of the rocker bearing column axial force

$P_{ac} := .05 \cdot A_{ac} = 5.898 \cdot kip$ = 5% of the reaction frame column axial force

Capacity of Rocker Bearing Column (Minor Axis)

The rocker bearing column is a W12x58 section and is 11.4' tall. It was previously calculated that the flanges are compact while the web is noncompact.

Unbraced Length of Rocker Bearing Column: $L_b := 11.1ft$

Moment on Rocker Bearing Column Due to Lateral Loading: $M_{max} := P_{rbc} \cdot L_b = 12.21 \cdot kip \cdot ft$

Yielding Check:

Section Modulus: $S_y := 21.4in^3$

Yield Strength (Preferred for W Shape Sections): $F_y := 50ksi$

Moment Capacity: $\phi M_n := .9 \cdot F_y \cdot S_y = 80.25 \cdot kip \cdot ft$

Demand to Capacity Ratio: $DC := \frac{M_{max}}{\phi M_n} = 0.152$

The demand to capacity ratio is less than 1. Therefore, the rocker bearing column will not experience yielding under the approximated lateral loading.

Flange Local Buckling:

Flange local buckling is not applicable because the flanges of the rocker bearing column are compact.

Capacity of Reaction Frame Column (Minor Axis)

The reaction frame column is a W24x103 section and is 12' tall.

Unbraced Length of Reaction Frame Column: $L_b := 7.2ft$

Moment on Reaction Frame Column Due to Lateral Loading: $M_{max} := P_{ac} \cdot L_b = 42.466 \cdot kip \cdot ft$

Yielding Check:

Section Modulus: $S_y := 26.5in^3$

Yield Strength (Preferred for W Shape Sections): $F_y := 50ksi$

Moment Capacity: $\phi M_n := .9 \cdot F_y \cdot S_y = 99.375 \cdot kip \cdot ft$

Demand to Capacity Ratio: $DC := \frac{M_{max}}{\phi M_n} = 0.427$

The demand to capacity ratio is less than 1. Therefore, the reaction frame column will not experience yielding under the approximated lateral loading.

Flange Local Buckling:

Steel Modulus of Elasticity: $E = 2.9 \times 10^4 \cdot ksi$

Compactness Criteria: $\lambda_p := .38 \cdot \sqrt{\frac{E}{F_y}} = 9.152$

Flanges: $\lambda_f := 4.59$ Flanges are compact.

Flange local buckling is not applicable because the flanges of the reaction frame column are compact.

Lateral Bracing for Rocker Bearing Column

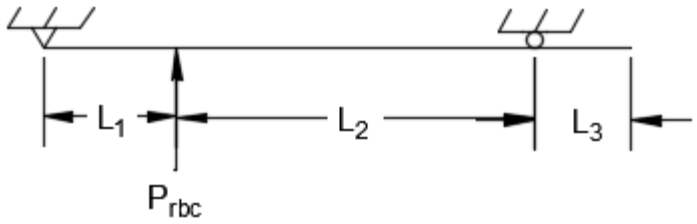

$L_1 := 2.72ft$ = distance from center of pin to center of rocker bearing column

$L_2 := 5.33ft$ = distance from center of rocker bearing column to center of wall anchor

$L_3 := 1.9ft$ = distance from center of wall anchor to center of reaction frame column

$L_{total} := L_1 + L_2 + L_3 = 9.95 \cdot ft$ = total beam distance

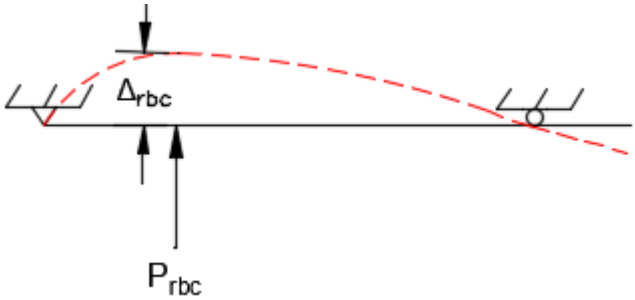

Δ_{rbc} = deformation of bracing at the rocker bearing column

The lateral bracing will be provided by 2 sections that are conservatively equivilent to an HSS 6x4x1/8.

Stiffness Check:

Major Moment of Interia of HSS 6x4x1/8: $I_x := 11.4in^4$

Deformation of Lateral Bracing at RBC: $\Delta_{rbc} := \frac{P_{rbc} \cdot L_1^2 \cdot L_2^2}{3 \cdot E \cdot I_x \cdot (L_1 + L_2)} = 0.05 \cdot in$

Stiffness of Setup: $\beta := \frac{P_{rbc}}{\Delta_{rbc}} = 21.983 \cdot \frac{kip}{in}$

Unbraced Length of Rocker Bearing Column: $L_{b\_rbc} := 11.1ft$

Required Bracing Stiffness: $\beta_{req} := \left(\frac{1}{.75}\right) \cdot \left(\frac{A_{rbc}}{L_{b\_rbc}}\right) = 0.22 \cdot \frac{kip}{in}$

DC Ratio: $DC := \frac{\beta_{req}}{\beta} = 0.01$

The DC ratio is less than 1, therefore the lateral bracing stiffness is suitable for laterally bracing the RB column

Strength Check:

Sum of Moments Around Pin: $0 = -P_{rbc}(L_1) + R_{roll}(L_1 + L_2)$

Pin Reaction (Closest to Rocker Bearing Column): $R_{roll} := \frac{P_{rbc} \cdot L_1}{L_1 + L_2} = 0.372 \cdot kip$

Sum of Forces: $0 = R_{pin} + R_{roll} - P_{rbc}$

Roller Reaction (Closest to RF Column): $R_{pin} := P_{rbc} - R_{roll} = 0.728 \cdot kip$

Shear Diagram of Bracing HSS

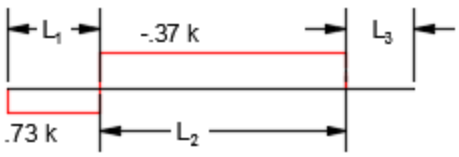

Moment Diagram of Bracing HSS

Maximum Moment on Lateral Bracing: $M_{max} := R_{pin} \cdot L_1 = 1.981 \cdot kip \cdot ft$

Yielding Check:

Major Elastic Section Modulus (HSS 6x4x1/8): $S_x := 3.81in^3$

Yield Strength (Preferred Grade): $F_y := 46ksi$

Section Moment Capacity: $\phi M_n := .9 \cdot F_y \cdot S_x = 13.145 \cdot kip \cdot ft$

Demand to Capacity Ratio: $DC := \frac{M_{max}}{\phi M_n} = 0.151$

The DC ratio is less than 1, therefore the lateral bracing HSS will not experience plastic yielding.

Web Local Buckling Check:

The webs are compact based on a flange width of 6". Web local buckling is not applicable to this lateral bracing.

Flange Local Buckling Check:

The flanges are compact based on a web height of 4". Flange local buckling is not applicable to this lateral bracing.

Shear on Threaded Rods Connecting HSS Lateral Bracing to Wall Anchors:

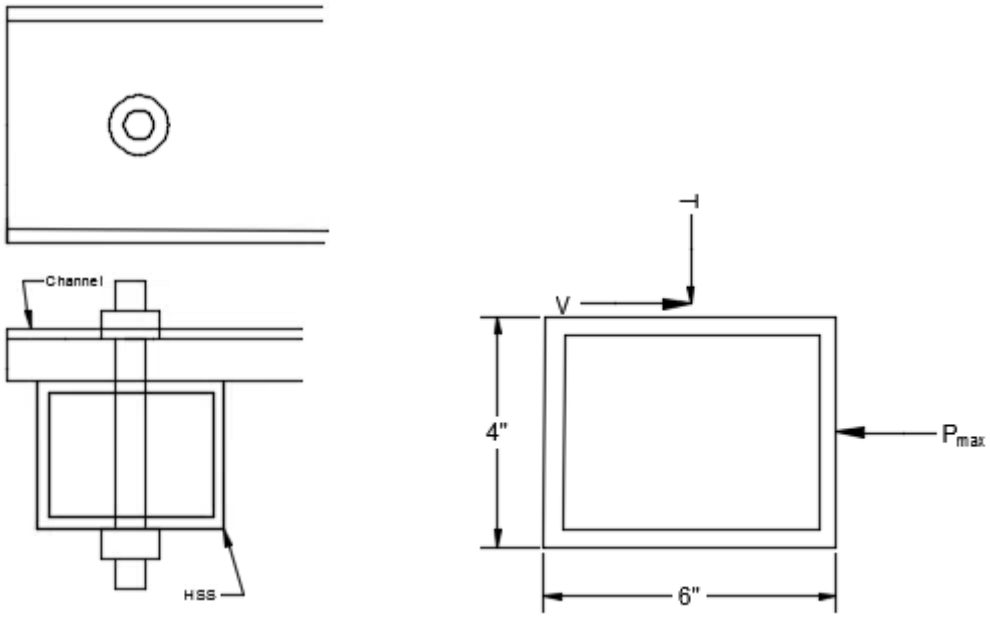

1 threaded rod will connect the HSS 6x4x1/4 to the channel of the wall anchor. One of the threaded rods will be centered on the channel and the other will be 1" off-center.

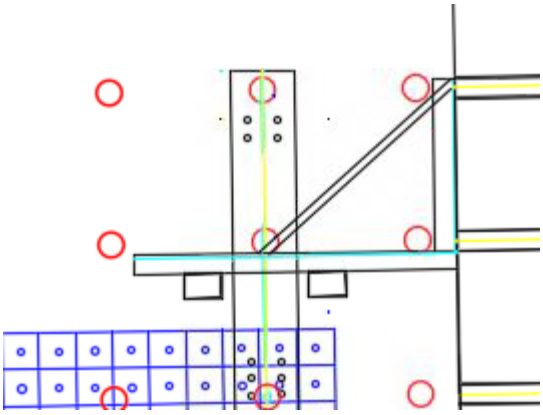

Required Threaded Rod Size Based on Combined Shear and Tension
(Rods Connecting Lateral Bracing to Wall Anchor)
Assume one 1" diameter threaded rod will be used to connect each side of the lateral bracing to the wall anchors. The rod which will be in double shear due to going through 2 walls of the HSS lateral bracing.

Maximum Shear at Anchor Locations: $P_{max} := \max\left(R_{pin}, R_{roll}\right) = 0.728 \cdot kip$

Max Tensile Force Per Rod (Sum Moments About Top Right Corner of HSS): $F_{ten} := \left(\frac{2in}{3in}\right) \cdot P_{max} = 0.486 \cdot kip$

Minimum Required Tensile Stress Per Rod:

$$f_t := \frac{F_{ten}}{\left[\pi\left(\frac{1in}{2}\right)^2\right]} = 0.618 \cdot ksi$$

Factored Nominal Tensile Stress Per Rod:

$$\phi F_{nt} := 67.5ksi$$

Factored Nominal Shear Stress Per Rod:

$$\phi F_{nv} := 40.5ksi$$

$$(f_t / \phi F_{nt}) + (f_v / \phi F_{nv}) = 1.3$$

Required Shear Stress Per Rod:

$$f_v := \left[1.3 - \left(\frac{f_t}{\phi F_{nt}}\right)\right]\phi F_{nv} = 52.279 \cdot ksi$$

Available Shear Strength of Per Rod:

$$\phi r_n := f_v \cdot \left[\pi\left(\frac{1in}{2}\right)^2\right] = 41.06 \cdot kip$$

Demand to Capacity Ratio:

$$DC := \frac{P_{max}}{\phi r_n} = 0.018$$

One threaded rod of 1" diameter can adequately resist the forces being transfered from the lateral bracing to the wall anchors.

Lateral Support (RB Column)

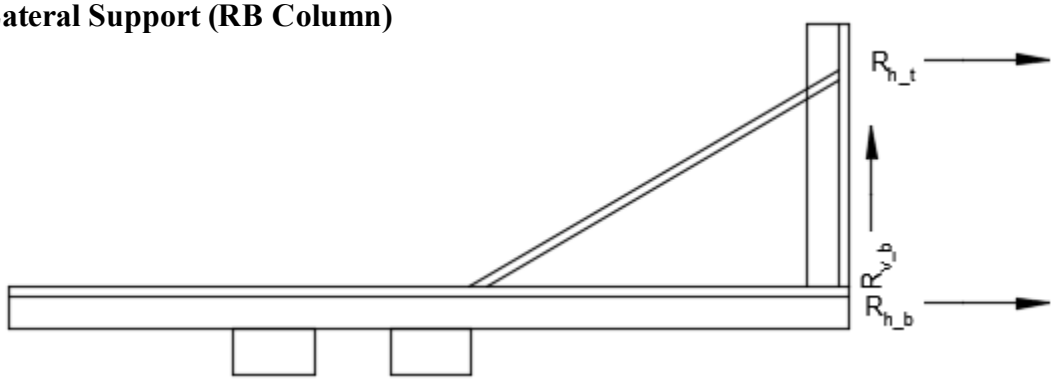

Using MC8x21.4 sections for the vertical wall anchor component, MC10x28.5 for the horizontal wall anchor component, and HSS 1 1/4"x 1 1/4"x 3/16" for the diagonal. The wall anchor sections are approximations because the sections were available in the structures lab. The wall anchors are attached to the strong wall with a top and bottom threaded rod.

Loading Scenario 1 (Left HSS Loaded):

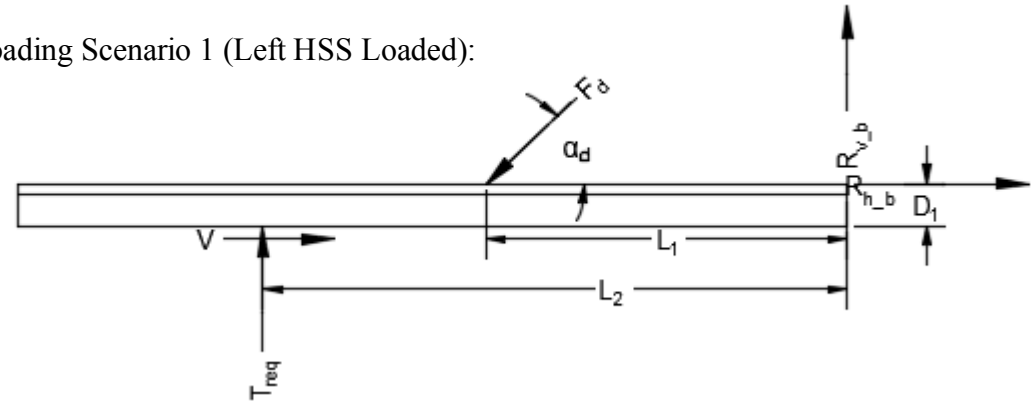

$D_1 := 3.875in$ = Height of Channel

$L_1 := 30in$ = Length to Center of Diagonal

$L_2 := 50.375in$ = Length to Center of Left HSS

$\alpha_d := 42deg$ = Angle of Diagonal

$V := \max\left(R_{pin}, R_{roll}\right) = 0.728 \cdot kip$

$T_{req} := \left(\frac{2in}{3in}\right) \cdot \max\left(R_{pin}, R_{roll}\right) = 0.486 \cdot kip$

Sum of Moments About Top Right Corner:

$0 = -F_{d\_1}\sin(\alpha_d)L_1 + T_{req}L_2 - VD_1$

$F_{d\_1} := \frac{T_{req} \cdot L_2 - V \cdot D_1}{\sin\left(\alpha_d\right) \cdot L_1} = 1.078 \cdot kip$

Sum of Horizontal Forces:

$R_{h\_1} := F_{d\_1} \cdot \cos\left(\alpha_d\right) - V = 0.073 \cdot kip$

Sum of Vertical Forces:

$R_{v\_1} := F_{d\_1} \cdot \sin\left(\alpha_d\right) - T_{req} = 0.236 \cdot kip$

Channel Shear Diagram

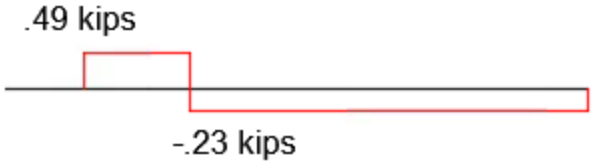

Maximum Moment:

$M_{max\_1} := T_{req} \cdot \left(L_2 - L_1\right) = 0.824 \cdot kip \cdot ft$

Loading Scenario 2 (Right HSS Loaded):

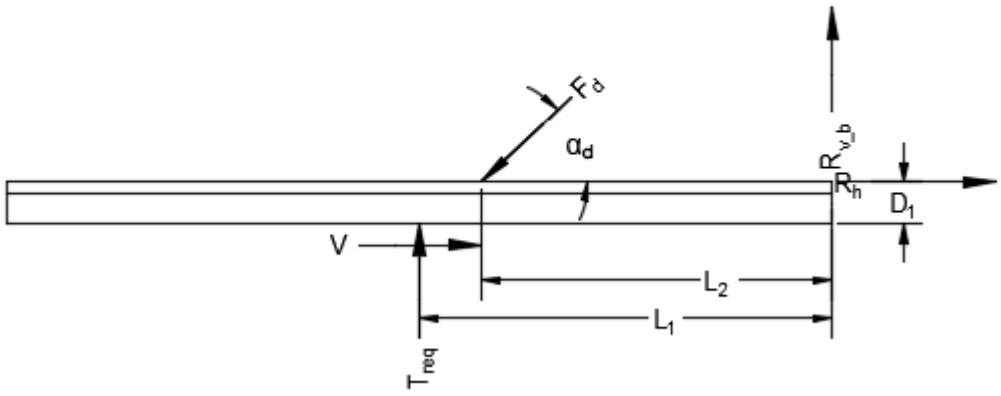

$D_1 := 3.875in$ = Height of Channel

$L_1 := 33.75in$ = Length to Center of Right HSS

$L_2 := 30in$ = Length to Center of Diagonal

Sum of Moments About Top Right Corner: $0 = -F_{d\_2}\sin(\alpha_d)L_2 + T_{req}L_1 - VD_1$

$$F_{d\_2} := \frac{T_{req}\cdot L_1 - V\cdot D_1}{\sin\left(\alpha_d\right)\cdot L_2} = 0.676\cdot kip$$

Sum of Horizontal Forces: $R_{h\_2} := F_{d\_2}\cdot\cos\left(\alpha_d\right) - V = -0.226\cdot kip$

Sum of Vertical Forces: $R_{v\_2} := F_{d\_1}\cdot\sin\left(\alpha_d\right) - T_{req} = 0.236\cdot kip$

Channel Shear Diagram

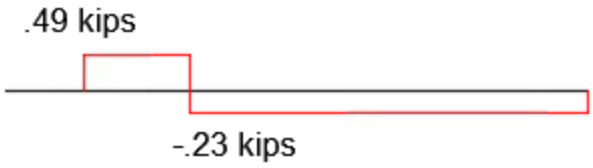

Maximum Moment: $M_{max\_2} := T_{req}\cdot\left(L_1 - L_2\right) = 0.152\cdot kip\cdot ft$

Max Moment for Wall Anchors: $M_{max} := \max\left(M_{max\_1}, M_{max\_2}\right) = 0.824\cdot kip\cdot ft$

Yielding Check

Yield Strength: $F_y := 36ksi$

Elastic Modulus of MC 10
(Horizontal Wall Anchor Component): $S_y := 3.99in^3$

Nominal Flexural Strength: $\phi M_n := .9 \cdot F_y \cdot S_y = 10.773 \cdot kip \cdot ft$

Demand to Capacity Ratio: $DC := \frac{M_{max}}{\phi M_n} = 0.077$

The DC ratio is less than 1, therefore the wall anchor will not experience plastic deformation.

Flange Local Buckling Check

Flanges are compact on the MC 10x28.8 with a yield strength of 50 ksi (yield strength of channel section being used in the wall anchors is unknown). Assume that the flanges are compact and flange local buckling is not applicable.

Weld of Channel Sections (Where 2 Channels Form 90 deg Angle)

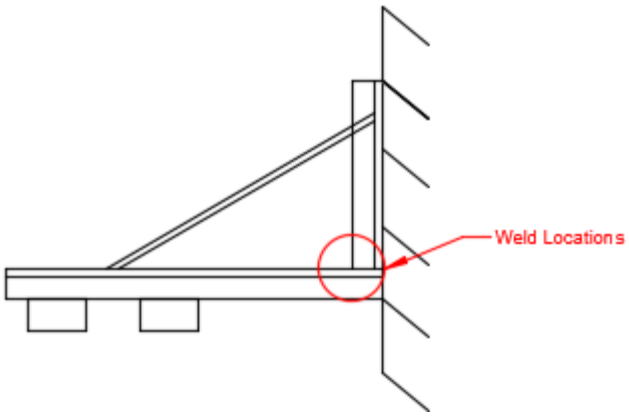

Maximum Force on Weld (Resultant of the horizontal and vertical reaction forces of each loading scenario):

$$F_{max} := \max\left[\sqrt{\left(R_{h\_1}\right)^2 + \left(R_{v\_1}\right)^2}, \sqrt{\left(R_{h\_2}\right)^2 + \left(R_{v\_2}\right)^2}\right] = 0.327 \cdot kip$$

Approximate Length of Weld
(Around 3 Inner Channel Faces of
Vertical Channel): $L_{weld} := 8in$

Strength of Filler: $F_{nw} := .6 \cdot 70ksi$

Appoximate Weld Depth: $D_{weld} := .25in$

Area of Weld: $A_{we} := .707 \cdot D_{weld} \cdot L_{weld} = 1.414 \cdot in^2$

Strength of Weld: $\phi R_n := .75 \cdot F_{nw} \cdot A_{we} = 44.541 \cdot kip$

Force Acting on Weld: $F_{max} = 0.327 \cdot kip$

Demand to Capacity Ratio: $DC := \frac{F_{max}}{\phi R_n} = 7.333 \times 10^{-3}$

A weld thickness of 1/4" is adequate for the connection of the channel components of the wall anchor.

Lateral Bracing Diagonal Sections

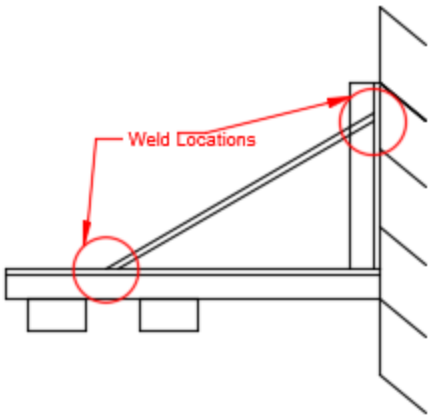

Assuming 2 Diagonal Sections Per Wall Anchor, Each 1 1/4"x 1 1/4" x 3/16"

Maximum Diagonal Section Force: $F_{d\_max} := .5 \cdot \max\left(F_{d\_1}, F_{d\_2}\right) = 0.539 \cdot kip$

Weld at End of Diagonals:

Approximate Length of Weld (Around 4 Faces of a Diagonal): $L_{weld} := 4 \cdot 1.25in = 5 \cdot in$

Strength of Filler: $F_{nw} := .6 \cdot 70ksi$

Appoximate Weld Depth: $D_{weld} := .25in$

Area of Weld: $A_{we} := .707 \cdot D_{weld} \cdot L_{weld} = 0.884 \cdot in^2$

Strength of Weld: $\phi R_n := .75 \cdot F_{nw} \cdot A_{we} = 27.838 \cdot kip$

Force Acting on Weld: $F_{d\ max} = 0.539 \cdot kip$

Demand to Capacity Ratio: $DC := \frac{F_{d\_max}}{\phi R_n} = 0.019$

A weld thickness of 1/4" is adequate for the connection of the diagonal compnents to the channel components of the wall anchor.

Diagonal Capacity

Diagonal is an HSS 1 1/4x 1 1/4 x 3/16

Maximum Force in the Diagonal: $F_{d\_max} = 0.539 \cdot kip$

Effective Length Factor: $k := 1$

Length of Longest Side of Diagonal: $L := 41in$

Effective Length of Diagonal: $L_{eff} := k \cdot L = 3.417 \cdot ft$

Allowable Concentric Load: $P_{allow} := 12kip - \left(4ft - L_{eff}\right) \cdot \left(\frac{4kip}{ft}\right) = 9.667 \cdot kip$

Demand to Capacity Ratio: $DC := \frac{F_{d\_max}}{P_{allow}} = 0.056$

The DC ratio is less than 1, therefore the diagonal sections of the wall anchors can support the load on the lateral bracing.

Lateral Bracing Support (RF Column)

$A_{ac} = 117.961 \cdot kip$ = RF Column Axial Load

$P_{ac} = 5.898 \cdot kip$ = 5% of RF Column Axial Load

Loading Scenarios for the bracing:

Loading 1: RF column/column plate is in center of wall plate during the blast loading scenario experimental setup

Loading 2: RF column/column plate is off-center of wall plate during seismic loading scenario experimental setup

Assume that actuators are at 110 kip capacity during either loading scenario.

Threaded Rod Capacity (Between Column Plate and Wall Plate):

2 threaded rods transfer forces between the column plate and the wall plate. The rods will each receive half of the RF column lateral load due to being centered with respect to the RF column and the lateral bracing column plate

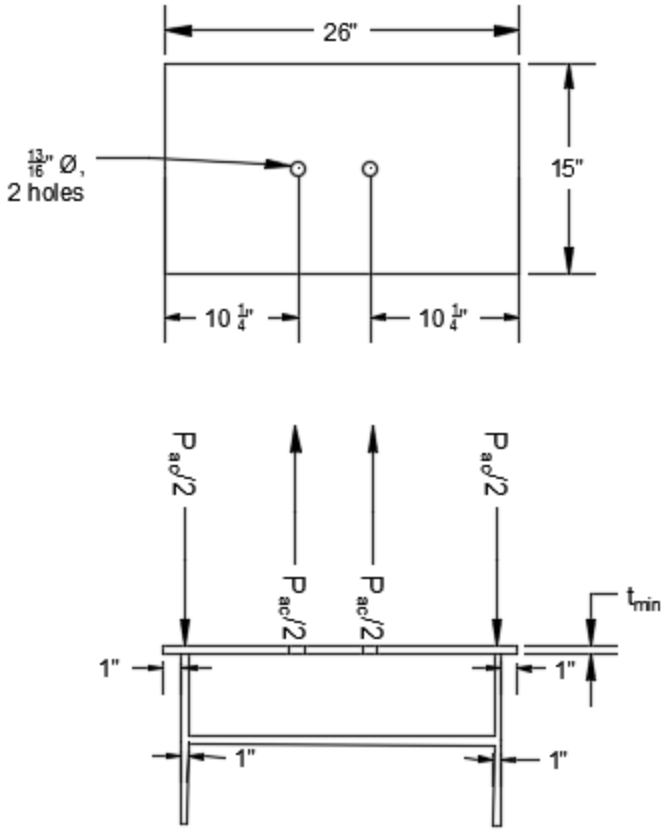

Tension in Threaded Rods: $T_{rod} := \frac{P_{ac}}{2} = 2.949 \cdot kip$

Tensile Strength of Threaded Rod (Using Equivilent Bolt Strength): $\phi r_n := 29.8kip$

Demand to Capacity Ratio: $DC := \frac{T_{rod}}{\phi r_n} = 0.099$

Two threaded rods of 3/4" diameter are adequate to connect the column plate and the wall plate in the actuator column lateral bracing.

RF Column Plate During Loading Scenario 1 or Loading Scenario 2

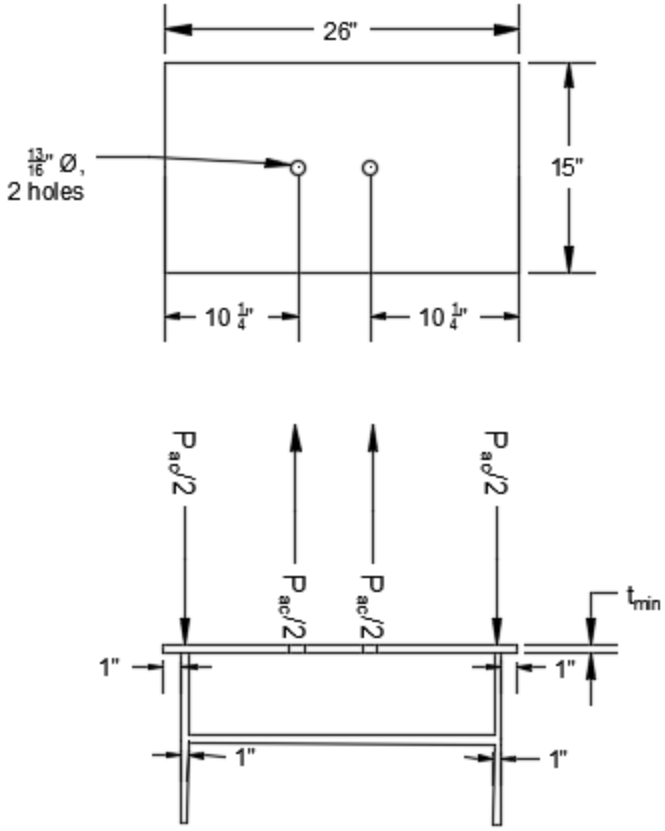

Plate Yielding Check

Maximum Distance Between HSS and Rod Line: $b_{prime} := 10.25in - 1in - .5 \cdot 1in = 8.75 \cdot in$

Tributary Length of Plate (Excluding Rod Holes): $p := 15in - .8125in = 14.188 \cdot in$

Yield Strength (Preferred For Plates: $F_y := 36ksi$

Required Strength Per Threaded Rod: $T := T_{rod} = 2.949 \cdot kip$

Minimum Plate Thickness (No Prying): $t_{min\_yield} := \sqrt{\frac{4T \cdot b_{prime}}{.9 \cdot p \cdot F_y}} = 0.474 \cdot in$

Demand to Capacity Ratio: $DC := \frac{\left(t_{min\_yield}\right)^2}{(.75in)^2} = 0.399$

The demand to capacity ratio is less than 1, therefor a 3/4" thick plate with the above dimensions has adequate strength for the column plate of the RF column lateral bracing.

Plate to RF Column Welds

Assuming 15" welds along each flange.

Approximate Length of Weld: $L_{weld} := 30in$

Strength of Filler: $F_{nw} := .6 \cdot 70ksi$

Appoximate Weld Depth: $D_{weld} := .25in$

Area of Weld: $A_{we} := .707 \cdot D_{weld} \cdot L_{weld} = 5.303 \cdot in^2$

Strength of Weld: $\phi R_n := .75 \cdot F_{nw} \cdot A_{we} = 167.029 \cdot kip$

Force Acting on Weld: $P_{ac} = 5.898 \cdot kip$

Demand to Capacity Ratio: $DC := \frac{P_{ac}}{\phi R_n} = 0.035$

A weld thickness of 1/4" is adequate for the connection of the actuator column lateral bracing plate to the RF column.

RF Column Wall Plate During Loading Scenario 1

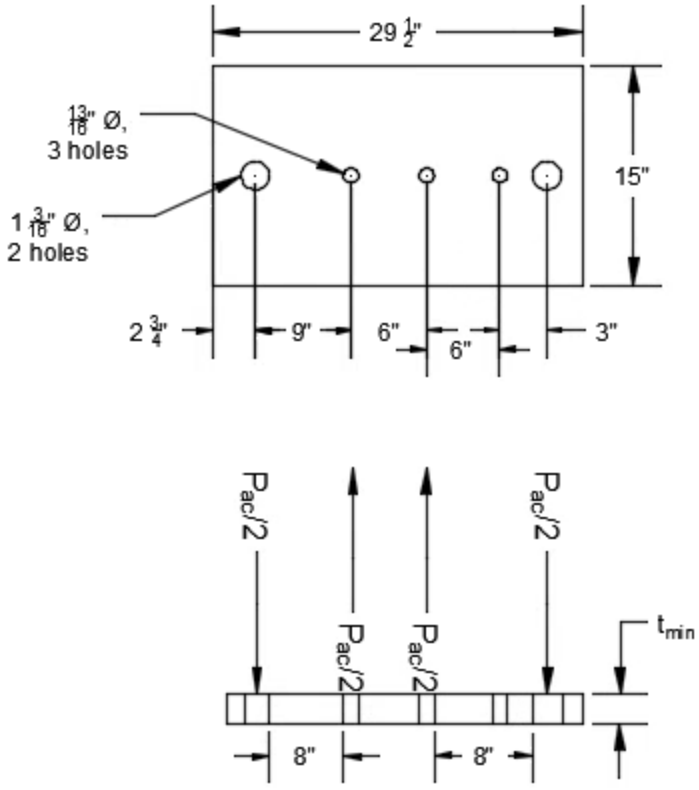

Plate Yielding Check

Maximum Distance Between HSS and Rod Line: $b_{prime} := 8in + .5(.8125in) + .5(1.1875in) = 9 \cdot in$

Tributary Length of Plate (Excluding Rod Holes): $p := 15in - 1.1875in = 13.813 \cdot in$

Yield Strength (Preferred For Plates: $F_y := 36ksi$

Required Strength Per Threaded Rod: $T := T_{rod} = 2.949 \cdot kip$

Minimum Plate Thickness (No Prying): $t_{min\_1} := \sqrt{\frac{4T \cdot b_{prime}}{.9 \cdot p \cdot F_y}} = 0.487 \cdot in$

RF Column Wall Plate During Loading Scenario 2

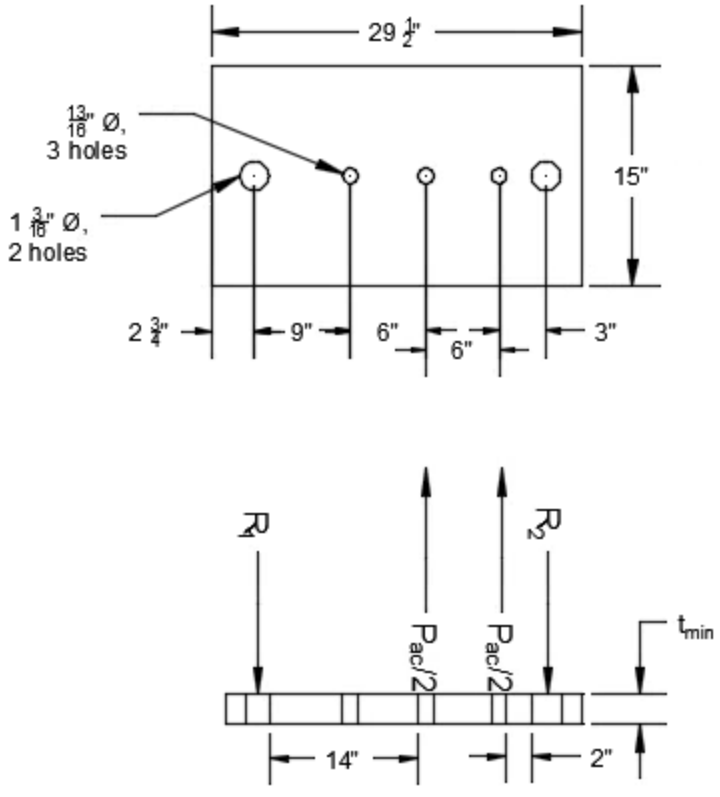

Plate Yielding Check

Maximum Distance Between HSS and Rod Line: $b_{prime} := 14in + .5(.8125in) + .5(1.1875in) = 15 \cdot in$

Tributary Length of Plate (Excluding Rod Holes): $p := 15in - 1.1875in = 13.813 \cdot in$

Yield Strength (Preferred For Plates): $F_y := 36ksi$

Required Strength Per Threaded Rod: $T := T_{rod} = 2.949 \cdot kip$

Minimum Plate Thickness: $t_{min\_2} := \sqrt{\frac{4T \cdot b_{prime}}{.9 \cdot p \cdot F_y}} = 0.629 \cdot in$

Minimum Required Wall Plate Thickness: $t_{min} := \max\left(t_{min\_1}, t_{min\_2}\right) = 0.629 \cdot in$

Thickness controlled by loading scenario 2. Use a 1/2" thick plate for the wall plate on the actuator column lateral bracing.

Demand to Capacity Ratio: $DC := \frac{\left(t_{min}\right)^2}{(.75in)^2} = 0.703$

The demand to capacity ratio is less than 1, therefore a 3/4" thick plate with the above dimensions has adequate strength for the wall plate of the RF column lateral bracing.

RF Column Lateral Bracing Plate System Stiffness Check

Loading Scenario 1:

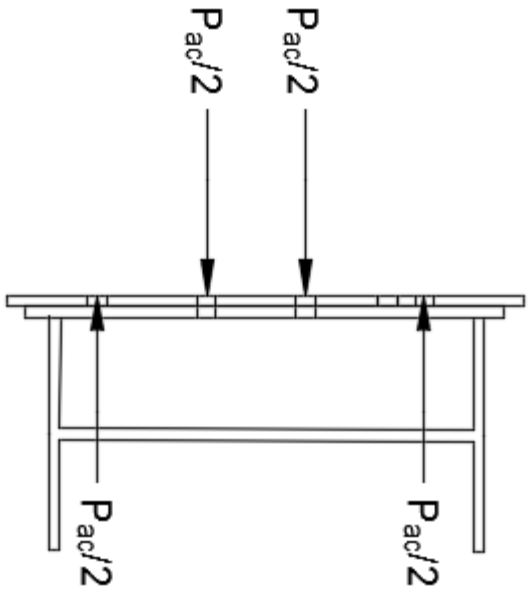

Assume the stiffness of the threaded rod and diwydag bars are negligable. Only the column plate and wall plate are providing stiffness for the RF column.See previous plate calculations for dimensions of both the RF column and wall plate.

Plate Length Between Diwydag Bars (Reaction Points): $L := 29.5in - 2(2.75in) = 24 \cdot in$

Plate Thickness (Both Plates): $t := .75in$

Major Moment of Interia of Plates: $I := \frac{2L \cdot t^3}{12} = 1.687 \cdot in^4$

Length From Threaded Rod to Diwydag Bars: $a := 9in$

Steel Modulus of Elasticity: $E = 2.9 \times 10^4 \cdot ksi$

Load on Threaded Rods: $T_{rod} = 2.949 \cdot kip$

Max Deflection of Plate: $\Delta_{acp} := \left(\frac{T_{rod} \cdot a}{24 \cdot E \cdot I}\right)\left(3L^2 - 4a^2\right) = 0.032 \cdot in$

Plate Stiffness: $\beta_{acp\_1} := \frac{T_{rod}}{\Delta_{acp}} = 92.949 \cdot \frac{kip}{in}$

Loading Scenario 2:

Assume the stiffness of the threaded rod and diwydag bars are negligable. Only the RF column plate and wall plate are providing stiffness for the RF column. See previous plate calculations for dimensions of both the RF column and wall plate.

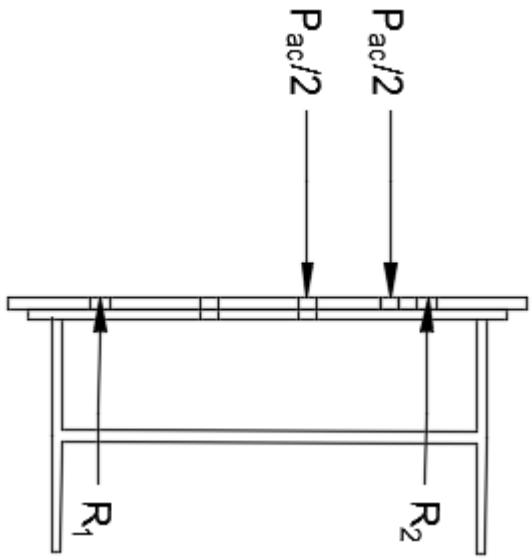

Approximate the forces through 2 threaded rods as one force centered between the rods.

Plate Length Between Diwydag Bars (Reaction Points): $L = 24 \cdot in$

Plate Thickness (Both Plates): $t = 0.75 \cdot in$

Major Moment of Interia of Plates: $I = 1.687 \cdot in^4$

Modulus of Elasticity: $E = 2.9 \times 10^4 \cdot ksi$

Load Through Both Rods: $P := P_{ac} = 5.898 \cdot kip$

Distance From Right Diwydag Bar to Load: $a := 9in + 6in + .5 \cdot 6in = 18 \cdot in$

Distance From Load to Left Diwydag Bar: $b := 3in + .5 \cdot 6in = 6 \cdot in$

Max Deflection: $$\Delta_{acp} := \frac{P \cdot a \cdot b \cdot (a + 2b) \cdot \sqrt{3 \cdot a \cdot (a + 2 \cdot b)}}{27 \cdot E \cdot I \cdot L} = 0.024 \cdot in$$

Plate Stiffness: $$\beta_{acp\_2} := \frac{P}{\Delta_{acp}} = 243.172 \cdot \frac{kip}{in}$$

Minimum Plate Stiffness: $$\beta_{min} := \min\left(\beta_{acp\_1}, \beta_{acp\_2}\right) = 92.949 \cdot \frac{kip}{in}$$

Unbraced Length of RF Column: $L_{b\_ac} := 6.25ft$

Required Bracing Stiffness (Treat as 1 Intermediate Nodal Brace): $$\beta_{req} := \left(\frac{1}{.75}\right) \cdot \left(\frac{2A_{ac}}{L_{b\_ac}}\right) = 4.194 \cdot \frac{kip}{in}$$

Demand to Capacity Ratio: $$DC := \frac{\beta_{req}}{\beta_{min}} = 0.045$$

The demand to capacity ratio is less than 1, therefore the stiffness of the lateral bracing plate system is adequate to brace the RF column.

55 kip Actuator Spacer Checks

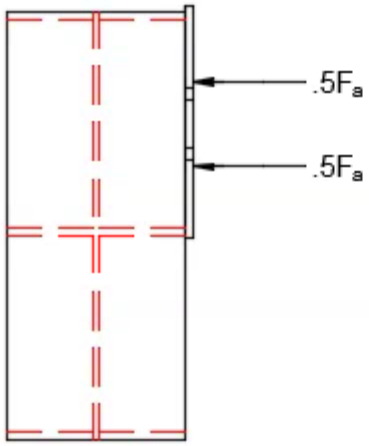

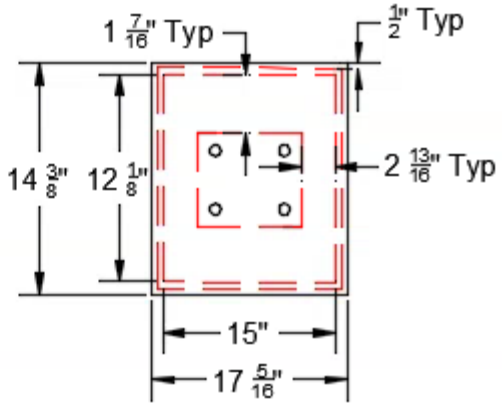

Plate Bending Check

Maximum Force from Actuator: $F_{a\_max} := 55kip$

Maximum Force Per Rod: $F_{max} := \frac{F_{a\_max}}{4} = 13.75 \cdot kip$

Force Acting on Each Bolt Line: $F_{line} := 2 \cdot F_{max} = 27.5 \cdot kip$

Maximum Distance Between Actuator Edge and Spacer Stiffener: $b_{prime} := 2.8125in$

Tributary Length of Plate: $p := 12.125in$

Yield Strength (A36 Preferred Grade For Plates): $F_y := 36ksi$

Minimum Plate Thickness: $t_{min} := \sqrt{\frac{4 \cdot F_{line} \cdot b_{prime}}{.9p \cdot F_y}} = 0.887 \cdot in$

Demand to Capacity Ratio: $DC := \frac{(.5in)^2}{(t_{min})^2} = 0.317$

A plate thickness of 1/2 inches is not adequate if the yield strength of the plate is 36ksi (A36 Steel).

Adjusted Yield Strength (A529 Gr 55): $F_y := 55ksi$

Minimum Plate Thickness: $t_{min} := \sqrt{\frac{4 \cdot F_{line} \cdot b_{prime}}{.9p \cdot F_y}} = 0.718 \cdot in$

Demand to Capacity Ratio: $DC := \frac{(.5in)^2}{(t_{min})^2} = 0.485$

A plate thickness of 1/2 inches is still not adequate if the yield strength of the plate is 55ksi (A529 Steel).

Adjusting Calculation for 2 Way Plate Action

Minimum Yield Strength: $F_y := 36ksi$

Area of Plate: $A_{plate} := 12.125in \cdot 15in = 181.875 \cdot in^2$

Load Per Length of Bearing Perimeter of Plate: $w := \frac{55kip}{2(12in) + 2(15in)} = 1.019 \cdot \frac{kip}{in}$

Side Ratio: $ratio := \frac{15}{12.125} = 1.237$

Max moment on 12" Side: $M_{max\_1} := 0.1017 \cdot w \cdot (12in)^2 = 14.916 \cdot kip \cdot in$

Chose the most conservative coefficient (assumes all edges are pinned and side ratio is 2)

Max Moment on 15" Side: $M_{max\_2} := .0531 \cdot w \cdot (15in)^2 = 12.169 \cdot kip \cdot in$

Chose the most conservative coefficient (assumes all edges are fixed and side ratio is 1)

Max Plate Moment: $M_{max} := \max(M_{max\_1}, M_{max\_2}) = 14.916 \cdot kip \cdot in$

Minimum Plate Thickness: $t_{min} := \sqrt{\frac{4 \cdot M_{max}}{.9p \cdot F_y}} = 0.39 \cdot in$

Demand to Capacity Ratio: $DC := \frac{(.5in)^2}{(t_{min})^2} = 1.646$

An A36 plate with a thickness of 0.5in can be used when 2-way action is accounted for in the plate loading.

Plate Shearing Check

Maximum Shear Force: $V_{max} := F_{line} = 27.5 \cdot kip$

Adjusted Yield Strength (A529 Gr 50): $F_y = 36 \cdot ksi$

Compactness Coefficient: $C_v := 1$

Depth of Plate: $d := 15in$

Minimum Plate Thickness: $t_{min} := \frac{V_{max}}{.9 \cdot .6 \cdot F_y \cdot d \cdot C_v} = 0.094 \cdot in$

Demand to Capacity Ratio: $DC := \frac{t_{min}}{.5in} = 0.189$

A plate thickness of 1/2in is adequate for the shear acting on the plate. The plate thickness is controlled by bending.

Threaded Rod Check

Steel Modulus of Elasticity: $E := 29000ksi \quad = \sigma/\varepsilon$

Maximum Force Per Rod: $F_{max} = 13.75 \cdot kip$

Diameter of Rod: $D_{rod} := .75in$

Area of Rod: $A_{rod} := \pi \cdot \left(\frac{D_{rod}}{2} \right)^2 = 0.442 \cdot in^2$

Stress on Rod: $\sigma := \frac{F_{max}}{A_{rod}} = 31.124 \cdot ksi$

Strain on Rod: $\varepsilon := \frac{\sigma}{E} = 1.073 \times 10^{-3} = \Delta L/L$

Length of Rod in MDC1 Test: $L_1 := 13in$

Change in Length of Rod During MDC1 Test: $\Delta L_1 := \varepsilon \cdot L_1 = 0.014 \cdot in$

Comparision of the Change in Rod Length to Imposed MDC1 Deformation: $ratio := \frac{\Delta L_1}{3.24in} = 4.306 \times 10^{-3}$

Length of Rod in MDC2 Test: $L_2 := 20in$

Change in Length of Rod During MDC1 Test: $\Delta L_2 := \varepsilon \cdot L_2 = 0.021 \cdot in$

Comparision of the Change in Rod Length to Imposed MDC1 Deformation: $ratio := \frac{\Delta L_2}{4in} = 5.366 \times 10^{-3}$

The deformation of the actuator/spacer/RB column threaded rods are insignificant when compared to the total deformation of the MDC. Therefore, the rods do not need to be torqued and hex head bolts do not need to be used.

Foundation Beam to Concete Floor Diwydag Bars

Coefficient of Static Friction (Steel on Concrete): $\mu := .45$

Horizontal Force: $F_h := 55kip$

Required Normal Force: $N := \frac{F_h}{\mu} = 122.222 \cdot kip$

Weight of Foundation Beam: $F_w := 3500lbf$

Required Total Tension Force on Foundation Beam Bars: $F_{req} := N - F_w = 118.722 \cdot kip$

Number of Bars: $num := 14$

Diameter of Bars: $d := 1.12in$

Minimum Tension Per Bar: $F_{min} := \frac{F_{req}}{num} = 8.48 \cdot kip$

Safety Factor on Bar Tension: $SF := 4.5$

Bar Tension With Safety Factor: $F_{bar} := SF \cdot F_{min} = 38.161 \cdot kip$

Area of Enerpac RCH-606 Pump: $A_{pump} := 12.73in^2$

Pressure of Pump to Provide Required Bar Tension: $P := \frac{F_{bar}}{A_{pump}} = 2.998 \times 10^3 \cdot psi$

Using a safety factor of 4.5 against sliding friction, the diwydag bars are required to be post tensioned to about 3000 psi on the Enerpac RCH-606 pump.

Using One 55kip Actuator:

$F_a := 55kip$ = Max Force of Actuator

$H_{a\_c} := 10.75ft$ = Height of actuator from RF column base

$H_d := 10.75ft$ = Height of diagonal from pin

$\alpha_d := 43deg$ = Angle of diagonal from vertical axis

Sum Moment Around RF Column Base: $M_{base} = 0 = F_a(H_{a\_c}) - \sin(\alpha_d)F_d(H_d)$

Max Force in Diagonal Brace: $F_d := \frac{F_a \cdot H_{a\_c}}{\sin(\alpha_d) \cdot H_d} = 80.645 \cdot kip$

Max Vertical Force in Diagonal Brac $F_{d\_vert} := F_d \cdot \cos(\alpha_d) = 58.98 \cdot kip$

Very Conservative Scenario: Diagonal distributes vertical force to only the 4 foundation bolts around the diaognal base plate.

Total Tension on Four Foundation Beam Bolts Around Diagonal: $T_{total} := F_{bar} + \frac{F_{d\_vert}}{4} = 52.906 \cdot kip$

Minimum Yield Load of Bars: $F_y := 59.3kip$

D/C Ratio When Actuator Provides 55kip of Tension: $SF := \frac{F_y}{T_{total}} = 1.121$

The diwydag bars will not fail in tension due to the applied post tension and the maximur test tension that will be loaded onto the bolts. These calculations assume the worst case scenario that the vertical force in the diagonal is distributed to only four foundation beam bars that are closest to it.

Diagonal Brace Base Plate to Foundation Beam Bolts

Max Vertical Force in Diagonal Brace $F_{d\_vert} = 58.98 \cdot kip$

Number of Bolts in Diagonal Brace Base Plate: $num := 4$

Tension per Bolt: $F_{bolt} := \frac{F_{d\_vert}}{num} = 14.745 \cdot kip$

Bolt Condition Factor (For Lubricated Bolts): $k := .18$

Diameter of Bolts: $d := 1.25in$

Required Torque Per Bolt: $T := k \cdot F_{bolt} \cdot d = 276.47 \cdot lbf \cdot ft$

Applied Torque Per Bolt: $T_{app} := 600lbf \cdot ft$ (Max Torque of Torque Wrench)

Applied Force Per Bolt: $F_{app} := \frac{T_{app}}{k \cdot d} = 32 \cdot kip$

Safety Factor: $SF := \frac{F_{app}}{F_{bolt}} = 2.17$

More torque was applied to the bolts than necessary to pretension the bolts to the maximum tension force they will experience.

Recommended AISC Minimum Bolt Pretension (For 1 1/4" A325 Diameter Bolts): $T_{rec} := 71kip$

The amount that the bolt was pretensioned is less than the minimum AISC recommended tension.

Total Tension (Per Bolt): $T_{total} := F_{app} + \frac{F_{d\_vert}}{4} = 46.745 \cdot kip$

Available Tensile Strength of 1" Diameter A325 Bolts (Per Bolt): $\phi r_n := 82.8kip$

Safety Factor When Actuator Provides 55kip of Tension (Per Bolt): $SF := \frac{\phi r_n}{T_{total}} = 1.771$

The bolts will not fail in tension due to the tension applied trough torque and the maximum tension that will be loaded onto the bolts.

Diagonal Brace Top Plate to RF Column Bolts

Max Horizontal Force in Diagonal Brace: $F_h = 55 \cdot kip$

Number of Bolts in Diagonal Brace Plate $num := 2$
(2 of 4 Bolts Can be Pretensioned):

Tension per Bolt: $F_{bolt} := \frac{F_h}{num} = 27.5 \cdot kip$

Bolt Condition Factor $k := .18$
(For Lubricated Bolts):

Diameter of Bolts: $d := 1.25in$

Required Torque Per Bolt: $T := k \cdot F_{bolt} \cdot d = 515.625 \cdot lbf \cdot ft$

Applied Torque Per Bolt: $T_{app} := 600lbf \cdot ft$ (Max Torque of Torque Wrench)

Applied Force Per Bolt: $F_{app} := \frac{T_{app}}{k \cdot d} = 32 \cdot kip$

Safety Factor: $SF := \frac{F_{app}}{F_{bolt}} = 1.164$

More torque was applied to the bolts than necessary to pretension the bolts to the maximum tension force they will experience.

Recommended AISC
Minimum Bolt Pretension $T_{rec} := 71kip$
(For 1 1/4" A325 Diameter Bolts):

The amount that the bolt was pretensioned is less than the minimum AISC recommended tension.

Total Tension (Per Bolt): $T_{total} := F_{app} + \frac{F_{d\_vert}}{4} = 46.745 \cdot kip$

Available Tensile Strength of
1" Diameter A325 Bolts (Per Bolt): $\phi r_n := 82.8kip$

Safety Factor When Actuator
Provides 55kip of Tension (Per Bolt): $SF := \frac{\phi r_n}{T_{total}} = 1.771$

The bolts will not fail in tension due to the tension applied trough torque and the maximum tension that will be loaded onto the bolts.

Floor Shake Table

Coefficient of Static Friction (Steel on Concrete): $\mu := .45$

Horizontal Force: $F_h := 22kip$

Required Normal Force: $N := \frac{F_h}{\mu} = 48.889 \cdot kip$

Weight of Floor Shake Table: $F_w := 5000lbf$

Required Total Tension Force on Shake Table Bolts: $F_{req} := N - F_w = 43.889 \cdot kip$

Number of Bolts: $num := 4$

Tension per Bolt: $F_{bolt} := \frac{F_{req}}{num} = 10.972 \cdot kip$

Bolt Condition Factor: $k := .2$

Diameter of Bolts: $d := 1in$

Required Torque Per Bolt: $T := k \cdot F_{bolt} \cdot d = 182.87 \cdot lbf \cdot ft$

Applied Torque Per Bolt: $T_{app} := 600lbf \cdot ft$ (Max Torque of Torque Wrench)

Applied Force Per Bolt: $F_{app} := \frac{T_{app}}{k \cdot d} = 36 \cdot kip$

Safety Factor: $SF := \frac{F_{app}}{F_{bolt}} = 3.281$

More torque was applied to the bolts than necessary to keep the floor shake table from sliding on the concrete floor.

Recommended AISC Minimum Bolt Pretension (For 1" Diameter Bolts): $T_{rec} := 51kip$

The amount that the bolt was pretensioned is less than the minimum recommended AISC tension.

Wall Shake Table

Coefficient of Static Friction: $\mu := .45$

Weight of Wall Shake Table: $F_w := 5000lbf$

Maximum Vertical Force: $F_v := 22kip + F_w = 27 \cdot kip$

Required Normal Force: $N := \frac{F_v}{\mu} = 60 \cdot kip$

Required Total Tension Force on Table Diwydag Bars: $F_{req} := N = 60 \cdot kip$

Number of Bars: $num := 4$

Diameter of Bars: $d := .75in$

Minimum Tension Per Bar: $F_{min} := \frac{F_{req}}{num} = 15 \cdot kip$

Safety Factor on Bar Tension: $SF := 1.7$

Bar Tension With Safety Factor: $F_{bar} := SF \cdot F_{min} = 25.5 \cdot kip$

Area of Enerpac RCH-606 Pump: $A_{pump} := 8.64in^2$

Pressure of Pump to Provide Required Bar Tension: $P := \frac{F_{bar}}{A_{pump}} = 2.951 \times 10^3 \cdot psi$

Using a safety factor of 1.7 against sliding friction, the diwydag bars are required to be post tensioned to about 3000 psi on the Simplex RC 306T pump.

Appendix 4

Lavarnway (2013) Tension Test Data

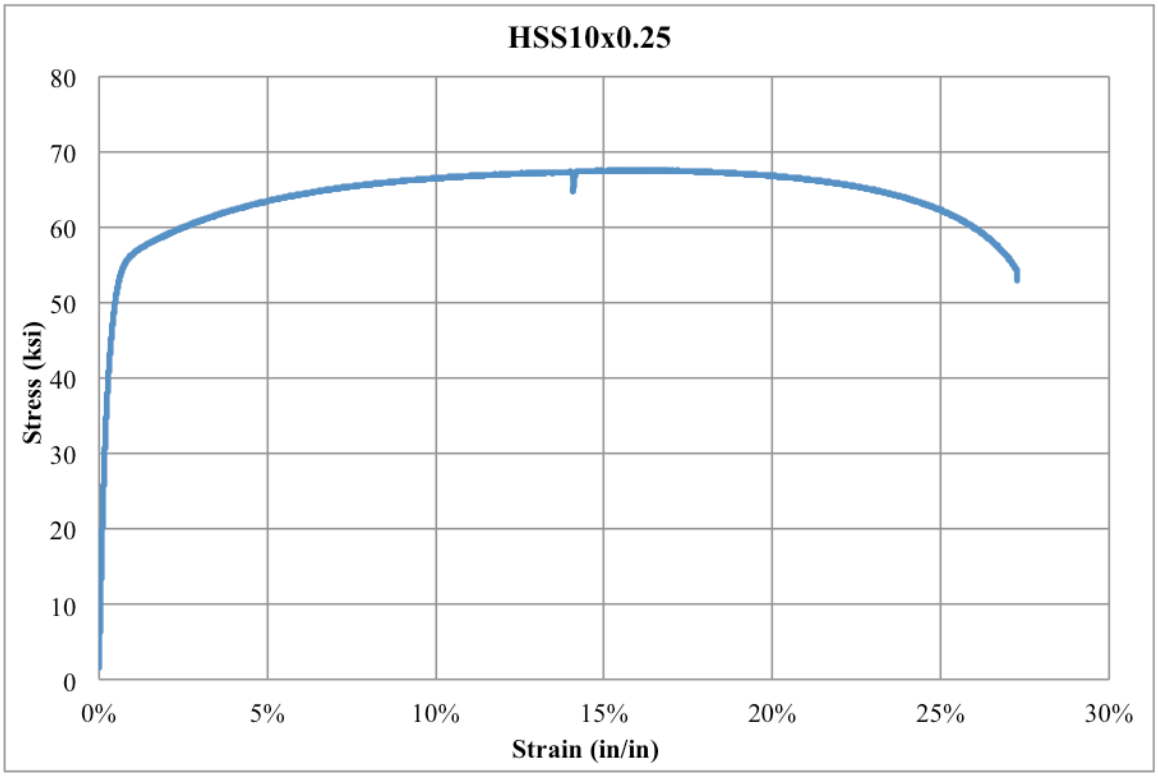
HSS10x0.25
Stress (ksi)
80
70
60
50
40
30
20
10
0
0%
5%
10%
15%
20%
25%
30%
Strain (in/in)

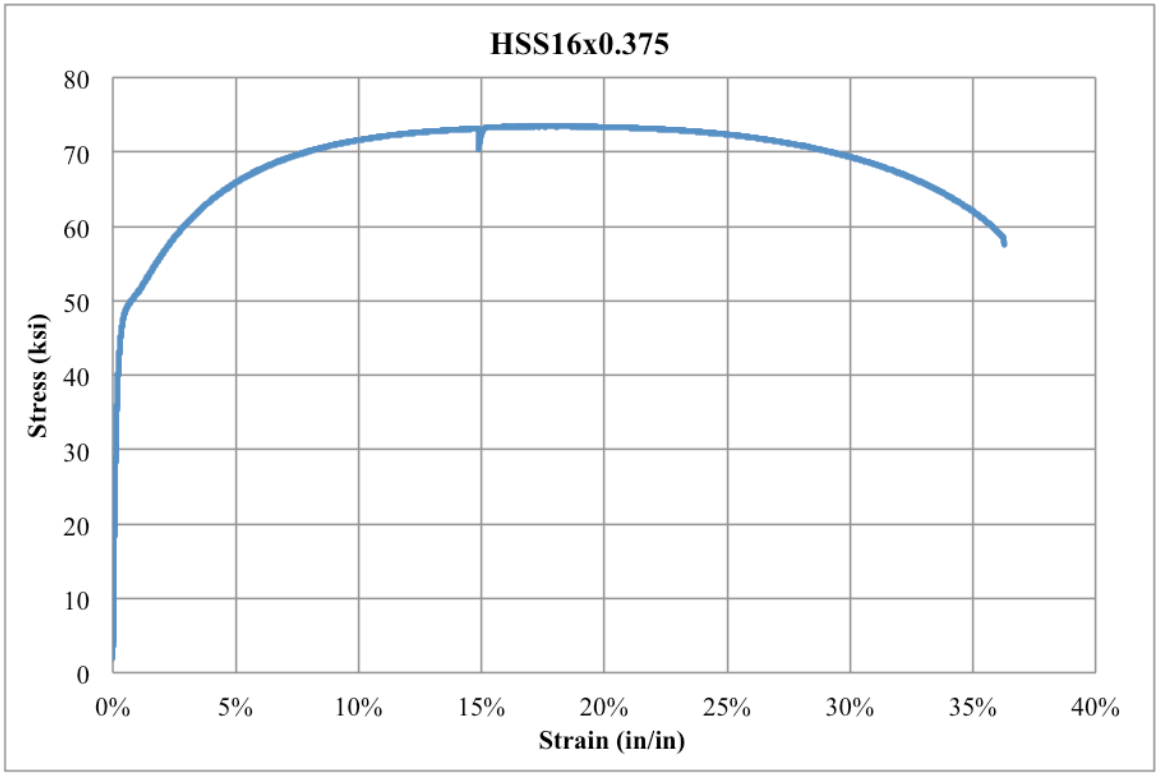
HSS16x0.375
Stress (ksi)
80
70
60
50
40
30
20
10
0
0%
5%
10%
15%
20%
25%
30%
35%
40%
Strain (in/in)

Literature Cited

Alavi Nia, A., & Parsapour, M. (2014). "Comparative analysis of energy absorption capacity of simple and multi-cell thin-walled tubes with triangular, square, hexagonal and octagonal sections." Thin-Walled Structures, 74, 155–165.

Alghamdi, A. A. A. (2001). "Collapsible impact energy absorbers: An overview." Thin-Walled Structures, 39(2), 189–213.

American Institute of Steel Construction. (2010a). "AISC 341-10: Seismic Provisions for Structural Steel Buildings." American Institute of Steel Construction, Chicago, IL.

American Institute of Steel Construction. (2010b). "AISC 360-10: Specifications for Structural Steel Buildings." American Institute of Steel Construction, Chicago, IL.

American Institute of Steel Construction. (2011). "Steel Construction Manual Thirteenth Edition." American Institute of Steel Construction, Chicago, IL.

American Society for Testing and Materials. (2012). "A370-12: Standard Test Methods and Definitions for Mechanical Testing of Steel Products." American Society for Testing and Materials, West Conshohocken, PA.

ANSYS Inc. (2016). "Mechanical APDL Documentation." ANSYS, Inc., Canonsburg, PA.

Eyvazian, A., K. Habibi, M., Hamouda, A. M., & Hedayati, R. (2014). "Axial Crushing Behavior and Energy Absorption Efficiency of Corrugated Tubes." Materials & Design, 54, 1028-1038.

Fadden, M. F. (2013). "Cyclic Bending Behavior of Hollow Structural Sections and their Application in Seismic Moment Frame Systems." University of Michigan, Ann Arbor, MI.

Hanssen, A. G., Langseth, M., & Hopperstad, O. S. (2000). "Static and Dynamic Crushing of Circular Aluminium Extrusions with Aluminium Foam Filler." International Journal of Impact Engineering, 24(5), 475–507.

Kim, H. S. (2002). "New Extruded Multi-Cell Aluminum Profile for Maximum Crash Energy Absorption and Weight Efficiency." Thin-Walled Structures, 40(4), 311–327.

Lavarnway, D. (2013). “Evaluating the Use of Ductile Envelope Connectors for Improved Blast Protection of Buildings.” Case Western Reserve University, Cleveland, OH.

Mamalis, A. G., Johnson, W., & Viegelahn, G. L. (1984). “The Crumpling of Steel Thin-Walled Tubes and Frusta Under Axial Compression at Elevated Strain-Rates: Some Experimental Results.” International Journal of Mechanical Sciences, 26(11–12), 537–547.

Mamalis, A. G., Manolakos, D. E., Saigal, S., Viegelahn, G., & Johnson, W. (1986). “Extensible Plastic Collapse of Thin-Wall Frusta as Energy Absorbers.” International Journal of Mechanical Sciences, 28(4), 219–229.

Parker, J. C. (2008). “Steel Design Guide: Facade Attachments to Steel Buildings.” American Institute of Steel Construction, Chicago, IL.

Salehghaffari, S., Rais-Rohani, M., & Najafi, A. (2011). “Analysis and Optimization of Externally Stiffened Crush Tubes.” Thin-Walled Structures, 49(3), 397–408.

Zhang, X., & Zhang, H. (2014). “Axial Crushing of Circular Multi-Cell Columns.” International Journal of Impact Engineering, 65, 110–125.